

Microglial signaling in Alzheimer's Disease

Hannah Elizabeth Ennerfelt
Charlottesville, VA

A Dissertation

Presented to
the faculty of the School of Medicine of the University of Virginia in candidacy for the degree of
Doctor of Philosophy

Department of Neuroscience

University of Virginia
September 2022

Abstract

The amyloid hypothesis hinges on the predominant clinical role of the amyloid beta (A β) peptide in propagating neurofibrillary tangles and eventual cognitive impairment in Alzheimer's disease (AD). Recent research in the AD field has identified the brain resident macrophages, known as microglia, and their receptors as integral regulators of both the initiation and propagation of inflammation, A β accumulation, neuronal-loss, and memory decline in AD. Emerging studies have also begun to reveal critical roles for distinct innate immune pathways in AD pathogenesis, which has led to great interest in harnessing the innate immune response as a therapeutic strategy to treat AD and other neurodegenerative diseases.

In this dissertation, we highlight recent advances in our understanding of innate immunity and inflammation in AD onset and progression. Additionally, we discuss findings outlining the ability of many AD risk factors to influence disease progression via modulation of microglia and immune responses. Microglia remain a highly targetable cell in neurodegenerative diseases including AD and Multiple Sclerosis (MS). These cells harbor machinery capable of addressing and clearing disease pathology; therefore, enhancement of microglial function is a highly sought-after clinical target. The delineation of specific microglial signaling molecules that modulate cellular response to neurodegenerative pathology is critical for novel treatments that avoid off-target effects during disease.

Utilizing the 5xFAD mouse model of AD, we unearth the mechanisms by which previously under described signaling pathways influence microglial response to A β pathology. We identify SYK as the master coordinator of microglial activation to pathology seen in AD. In fact, SYK is necessary for microglial clearance of A β in 5xFAD mice and damaged myelin pathology in a model of MS. In addition, we find that SYK directs neuroprotective and targetable downstream signaling to promote phagocytosis of A β , including a specific arm of the AKT pathway. These findings uncover a novel microglial signaling molecule that drives cellular function during neurodegeneration and may aid in understanding the continued intricacies of microglial responses during disease.

Additional studies outlined in this dissertation delve into the role of CARD9, a molecule found in microglia and related to fungal response. Using the 5xFAD model, we observe that CARD9 protects against pathology accumulation and regulates microglial cell number and morphological activation. In addition, we observe that the activation of CARD9 drives A β clearance. Altogether, these data indicate a novel role for CARD9 in regulating microglial response and ultimately pathology progression in AD.

In summary, this dissertation emphasizes the critical nature of microglial signaling downstream of several receptors implicated in AD. Our work contributes to a more complete understanding of microglial function and upon further investigation may inform consequential therapeutic targets for neurodegenerative disease.

Acknowledgements

I am incredibly grateful for the opportunity to do my training in the Neuroscience Graduate Program at the University of Virginia (UVA). The support from my fellow members of NGP has been incomparable and I will forever look back fondly on the knowledge and wisdom bestowed on me throughout my time in the department. I want to thank the faculty and trainees within the Brain Immunology and Glia center at UVA which offered daily technical support and constant inspiration on how to sincerely approach a career in science. The incredible insight and encouragement from my thesis committee has also been a key element to my time in NGP; therefore, I want to thank the committee members: Dr. Scott Zeitlin (chair), Dr. Tajie Harris, Dr. Heather Ferris, Dr. Ukpong Eyo, and Dr. Barry Condron for all your support.

A special thanks goes out to my mentor Dr. John Lukens who took a chance on me, entrusted me with a new direction in the lab, and ensured I had every tool imaginable to reach my goals. Thank you for the constant technical and vocational support. Your continued advocacy for my future success opened many doors for me for which I will forever be grateful.

The members of the Lukens Lab have made my graduate school experience immeasurably special. I was lucky enough to spend my working life with two generations of the Lukens lab that made each day amazing. Cat, Elizabeth, and Mariah – your patience, kindness, and limitless knowledge kept me afloat when I joined the lab, thank you for the time you dedicated to my training and for all the laughs we shared during some of those long science days. Ashley – your dedication to science is inspirational and your friendship has been so special to me. I am beyond grateful that I got to be your bench buddy. Thanks for housing me during this last stretch of time in Charlottesville, your daily encouragements kept me going. Gabi, Kate, and Eric - thank you for all your support these last few years, without you there would be no science to show in this dissertation. Katherine and Daniel – thank you for your continual support on all things RNA-seq, I enjoyed getting to know you in lab and am excited for you both as you embark on your clinical adventures. Jess, Ana, Nick, Lexi, Josh, Addie – you all have breathed new life into the second generation of the Lukens lab. I have learned so much from you all during the formation of your new projects! Aman – thanks for always cracking the best jokes. Your sarcasm, resilience, and passion for science make you one of the most genuine lab mates. The rest of the lab is beyond lucky to get to work with you during your PhD, I know I was! Josh Kulas – you walked me through some of the lowest times of my PhD and went above and beyond to make sure I felt supported – I can't thank you enough. Coco – my one and only undergrad, thank you for always taking my frazzled nature in stride, you're exceptional. It has been such an honor getting to see you mature into the amazing scientist and person you have become. Kristine – my work wife, confidant, and the most gracious listener during all my struggles of graduate school – thank you. Our athletic, gastronomic, and in-lab adventures made grad school the best

it could be. As the designated lab mom, you are the glue that keeps everything together. Thank you for being you, doing science without your wisdom, knowledge, and smiles will never be the same.

To my friends and family – thank you for the emotional support and check-ins, grad school had a lot of ups-and-downs, and you were there for all of them. Hanna – you were my very first friend in Charlottesville and your spontaneity and beautiful spirit were the perfect balance for me. All our outdoor adventures kept me sane. Mom, Dad, and Jacob - even though my work during grad school was only circulated in bits and pieces at the dinner table during visits, you were some of my biggest supporters. Mom and Dad – thank you for your constant love and support – you instilled curiosity in me from childhood and I want to thank you for all the opportunities you provided that led me to love to learn. Steven – you are the sole reason I made it through grad school. Thank you for being the best listener, making my side hurt from laughter, and constantly inspiring with your brilliance. You are my number one fan, and I am yours. I am so fortunate that I have you in my life. Thank you, for all of it.

Table of Contents

Chapter 1:	
Introduction	8
1.1 AD pathology	8
1.2 Biomarkers	8
1.3 Innate immunity in AD	10
1.3.1 The role of microglia in homeostasis and AD	12
1.3.2 Microglia receptors implicated in AD	13
1.3.3 Microglial clearance of A β and tau	18
1.3.4 Disease associated microglia	20
1.3.5 Loss of microglial homeostatic function in AD	21
1.3.6 Impact of microglial elimination in AD	21
1.3.7 AD immune cells: microglia or macrophages?	22
1.4 Inflammatory mediation of AD	23
1.4.1 Cytokines in AD	24
1.5 Role of inflammasomes in AD	25
1.6 Role of age, environmental factors, and sex in AD	26
1.7 Concluding Remarks	27

Chapter 2: SYK coordinates neuroprotective microglial responses in neurodegenerative disease **34**

2.1 Abstract	34
2.2 Introduction	36
2.3 Results	37
2.3.1 SYK signaling in microglia limits A β accumulation	37
2.3.2 SYK deletion in microglia leads to worsened neuronal health and memory impairment in 5xFAD mice	42
2.3.3 SYK regulates microglial proliferation and association with A β plaques	44
2.3.4 A β -induced microglial activation is impaired in the absence of SYK	46
2.3.5 A β pathology promotes increased lipid droplet formation and ROS production in SYK-deficient microglia	51
2.3.6 Phagocytosis of A β is coordinated by SYK	52
2.3.7 Exogenous activation of the CLEC7A-SYK signaling pathway promotes improved clearance of A β	55
2.3.8 DAM generation is regulated by SYK in demyelinating neuroinflammatory disease	55
2.3.9 Defective SYK signaling in microglia during demyelinating disease causes damaged myelin debris accumulation and impaired oligodendrocyte proliferation	59
2.4 Discussion	64
2.5 Limitations of the study	67
2.6 Methods	68

Chapter 3: CARD9 attenuates A β pathology and modifies microglial responses in an Alzheimer's disease mouse model **79**

3.1 Abstract	79
3.2 Introduction	79
3.3 Results	81
3.3.1 CARD9 signaling restricts brain amyloidosis in 5xFAD mice	81
3.3.2 The loss of CARD9 exacerbates neuronal loss and memory decline in 5xFAD mice	82
3.3.3 CARD9 deficiency in 5xFAD mice results in altered microglial responses	85

3.3.4 Microglial ROS production and lipid droplet formation are not impacted by CARD9 deletion in 5xFAD mice.....	89
3.3.5 Effects of CARD9 deletion on the microglial transcriptional response in 5xFAD mice..	91
3.3.6 Targeting CARD9 activation limits A β coverage in the hippocampus.....	93
3.4 Discussion.....	95
3.5 Methods.....	96

Chapter 4: Discussion and Future Directions **102**

4.1 Dissertation discussion.....	102
4.1.1 Neuroprotective roles of microglial SYK during neurodegenerative disease.....	102
4.1.2 Pathology regulation by CARD9 in Alzheimer's disease.....	104
4.2 Future Directions.....	105
4.2.1. Determining the role of SYK in generating a microglial response to injury.....	105
4.2.2. Microglial receptors regulating SYK and CARD9 signaling.....	105
4.2.3. Investigating how microglial SYK signaling regulates different cell types (i.e. astrocytes, T cells, OPCs).....	113
4.2.4. Examining the specific role of CARD9 in microglia during AD.....	115
4.3 Concluding Remarks.....	118
4.4 Materials and Methods.....	118

Literature Cited **122**

Table of Figures and Tables

Table 1.1. AD GWAS variants associated with innate immune signaling.....	9
Figure 1.1. The antimicrobial hypothesis of amyloid beta and Alzheimer's disease.....	12
Figure 1.2. Microglial surface receptors that coordinate innate immune responses in AD.....	14
Figure 1.3. The evolving functions of microglia in homeostasis and disease.....	25
Figure 1.4. Immune dysfunction underlies the ability of AD risk factors to impact neurodegeneration....	28
Figure 2.1. Targeted deletion of SYK in tamoxifen-treated <i>Syk^{fl/fl} Cx3cr1^{Ert2Cre}</i> mice.....	38
Figure 2.2. Deletion of <i>Syk</i> in microglia leads to increased A β burden and altered plaque composition in 5xFAD mice.....	40
Figure 2.3. Microglial SYK deletion in the hippocampus and after disease onset significantly alters AD pathology and microgliosis, however, the loss of SYK does not affect microgliosis in the absence of A β	41
Figure 2.4. Loss of <i>Syk</i> in microglia negatively affects neuronal health and exacerbates AD-related behaviors in 5xFAD mice.....	44
Figure 2.5. <i>Syk</i> -deficiency limits microglial proliferation and association with A β plaques.....	45
Figure 2.6. Defective activation of <i>Syk</i> -deficient microglia in 5xFAD mice.....	48
Figure 2.7. Effects of SYK deficiency on microglial gene expression under steady-state conditions and in response to A β pathology.....	50
Figure 2.8. Genetic ablation of SYK in microglia leads to increased levels of microglial lipid droplet accumulation and ROS production in 5xFAD mice.....	52
Figure 2.9. SYK is critical for microglial uptake and phagocytosis of A β	54
Figure 2.10. <i>Syk^{AMG}</i> mice have increased numbers of cytokine producing T cells infiltrating the CNS but have modestly reduced peripheral T cell responses during EAE.....	56
Figure 2.11. <i>Syk</i> -deletion in microglia impedes the formation of DAMs in EAE.....	59
Figure 2.12. Disruption of SYK signaling in microglia during demyelinating disease leads to accumulation of damaged myelin debris and impaired oligodendrogenesis.....	61
Figure 2.13. Disruption of SYK signaling in microglia during demyelinating disease leads to impaired microglial response and reduced OPC proliferation.....	63

Figure 3.1. CARD9 deletion leads to increased A β accumulation in 5xFAD mice.....	82
Figure 3.2. <i>Card9</i> deficiency leads to worsened neuronal health and cognitive impairment in 5xFAD mice.....	84
Figure 3.3. Deletion of <i>Card9</i> in the absence of A β -mediated pathology does not impact learning or memory.....	85
Figure 3.4. CARD9-deficient mice do not display impaired A β clearance <i>in vitro</i> or <i>in vivo</i>	86
Figure 3.5. The loss of <i>Card9</i> leads to altered microgliosis in 5xFAD mice.....	88
Figure 3.6. <i>Card9</i> deficiency in the absence of A β -mediated neuropathology does not affect microglial number or morphology in adult mice.....	89
Figure 3.7. <i>Card9</i> deficiency does not significantly affect microglial ROS production, lipid droplet.....	90
accumulation, or production of inflammatory cytokines associated with microglial activation in 5xFAD mice.....	92
Figure 3.8. <i>Card9</i> -dependent regulation of the microglial transcriptional program in 5xFAD mice.....	93
Figure 3.9. <i>Card9</i> deficiency in the absence of A β does not appreciably affect microglial transcription	
Figure 3.10. Pustulan treatment enhances A β clearance in a CARD9-dependent manner in the hippocampus of 5xFAD mice.....	94
Figure 4.1. Intravital imaging of microglial response to parenchymal laser injury.....	105
Figure 4.2. The loss of CLEC7A increases A β burden and altered plaque composition in 5xFAD mice...	109
Figure 4.3. <i>Syk</i> -deficiency limits microglial morphology and association with A β plaques.....	111
Figure 4.4. Altered transcription and cell signaling in CLEC7A-deficient microglia.....	112
Figure 4.5. Acute CARD9 inhibition in the hippocampus does not affect A β or Iba1 ⁺ cell coverage.....	116
Figure 4.6. Acute KLF4 inhibition in the hippocampus reduces Iba1 ⁺ cell coverage in 5xFAD mice.....	117

Chapter 1

Introduction

1.1 AD pathology:

Alzheimer's disease (AD) is a neurodegenerative disease characterized by neuronal loss, neuroinflammation, and pronounced memory decline (1, 2). Risk factors for developing this neurodegenerative disease include age, genetics, sex, brain injury, and various environmental factors (3). Regardless of origin, neuropathologies consistent among AD patients are amyloid beta ($A\beta$) and neurofibrillary tangle (NFT) deposition (4). $A\beta$ can deposit in the brain decades prior to clinical symptom onset and stimulate other AD pathologies such as hyperphosphorylated tau (p -Tau) aggregation which triggers subsequent NFTs and neuronal death (5-9). These NFTs can mediate neuronal damage that propagates mild cognitive impairment (MCI) and dementia (10). Given that $A\beta$ accumulation precedes NFT formation and memory decline by many years, the focus on $A\beta$ production has dominated AD research (10). $A\beta$ is a cleavage product of amyloid precursor protein (APP) (11). APP cleavage can follow two pathways: amyloidogenic and nonamyloidogenic. The former has a cleavage event spurred by β -secretase and γ -secretase to produce neurotoxic $A\beta$, while the latter undergoes APP cleavage by α -secretase and γ -secretase to generate distinct products, some of which have important neuroprotective functions (11, 12).

The $A\beta$ peptide can act as a building block to produce several distinct higher-order forms of $A\beta$, some of which are more neurotoxic than others (11). For instance, monomers of $A\beta$ peptide can accumulate to form oligomers that can travel throughout the brain and constitute the soluble fraction of $A\beta$ levels in the AD brain (11). $A\beta$ oligomers are the most toxic form of $A\beta$ and have been shown to incite synaptic dysfunction and neuronal cell death signaling (13). $A\beta$ oligomers can seed $A\beta$ fibrils to promote the formation of $A\beta$ aggregates known as "plaques" (14). Monomers of the $A\beta$ peptide can have varying lengths depending on their cleavage (11). However, $A\beta_{42}$ and $A\beta_{40}$ are the most prevalent in AD pathogenesis, with $A\beta_{42}$ being more likely to incorporate into $A\beta$ aggregates (15). AD brains are also marked by dystrophic neurites (16). Dystrophic neurites exhibit axonal transport defects and are often found surrounding $A\beta$ plaques (4). Recent evidence suggests that dystrophic neurites can directly contribute to AD pathology propagation by promoting β -secretase-mediated cleavage of APP and subsequent $A\beta$ peptide generation (17).

1.2 Biomarkers:

The identification of biomarkers relating to AD risk and pathology prior to clinical onset has become an important area of focus in hopes of manipulating AD onset and progression. For decades, the diagnosis of AD relied on post-mortem brain histological assessment to identify A β and NFT pathologies. However, recent technological advancements in genetic testing, PET imaging, and sampling of the cerebrospinal fluid (CSF) and blood have opened doors to the possibility of earlier AD diagnosis. There is great hope that the identification of reliable AD biomarkers will move the field toward preventative medicine; however, continued progress on this front is needed to make this a reality.

There are two classifications of AD based on disease origin and onset: (1) early-onset AD (EOAD) (also known as familial AD or FAD) and (2) late-onset AD (LOAD). EOAD accounts for 5% of all AD cases and is primarily caused by mutations in APP, presenilin-1 (PSEN1), and presenilin-2 (PSEN2), all of which can lead to elevated levels of total A β and increased production of A β 40 and A β 42 (18, 19). EOAD often occurs in individuals younger than 65 years of age (20). In contrast, the origin of LOAD is linked to an interplay between genetic mutations, environment, and neuroinflammatory responses (21). Interestingly, many of the mutations linked to LOAD risk are known to affect innate immune signaling pathways (Table 1.1). The most common variant associated with LOAD risk is apolipoprotein E gene (APOE) ϵ 4 allele (18). APOE has three isoforms which include ϵ 2, ϵ 3, and ϵ 4, with ϵ 4 being the allele exerting the greatest AD risk (22). In homeostasis, APOE is synthesized for lipid transport (23). However, during stress, APOE ϵ 4 is markedly more susceptible to proteolytic cleavage to generate products that promote NFT formation and mitochondrial dysfunction, both of which can contribute to AD progression (23). In addition, APOE has been reported to promote A β aggregation and is often found in large quantities within A β plaques, further implying its role in AD pathogenesis (24, 25). Patients with the APOE ϵ 4 allele are at 3-times higher risk for developing AD (22). The combination of APOE ϵ 4 and chronic inflammation further increases risk for these carriers, emphasizing an important link between genetics and inflammation in AD risk (26). LOAD is also associated with mutations in receptors expressed by microglia, the brain's resident immune cells (27). Recent research shows that multiple microglial receptors are critically involved in A β clearance and that mutations in multiple microglial immune receptors dramatically increases the risk for LOAD (27).

Table 1.1. AD GWAS variants associated with innate immune signaling

Gene	Function	Variant function in AD	References
<i>APOE</i>	Lipid transport	A β aggregation APP transcription Tangle pathology Mitochondrial dysfunction	(23, 24, 28)
<i>TREM2</i>	Inflammatory response Phagocytosis Cellular metabolism	A β accumulation Impaired microglial response	(29-31)
<i>CD33</i>	Cellular activity inhibition	A β accumulation	(32-35)
<i>CLU</i>	Extracellular chaperone Lipid transport Immune modulation Complement	Binding of A β	(36-38)
<i>ABCA7</i>	Lipid homeostasis Cell membrane transport	APP processing regulation A β secretion	(32, 39, 40)

		Impaired phagocytosis	
<i>BIN1</i>	Endocytosis Inflammation Calcium homeostasis	Tau propagation Neuronal degeneration	(41, 42)
<i>CR1</i>	Complement Microglial phagocytosis	A β accumulation Inflammation	(36, 43)
<i>SORL1</i>	Endocytosis Lipid metabolism	APP processing A β accumulation	(44)
<i>IL-34</i>	Survival and differentiation of monocytes	A β neurotoxicity	(45-47)
<i>MS4A gene cluster</i>	Calcium signaling Immunity	Reduced sTREM2 production	(32, 33, 48, 49)
<i>CD2AP</i>	Cytoskeletal dynamics Endocytosis Synapse function	Enhanced A β generation Tau-induced toxicity	(32, 33, 50)
<i>EPHA1</i>	Immunity Endocytosis	Uncharacterized	(32, 33, 51)
<i>INPP5D</i>	Immunity Myeloid cell regulation	Inhibition of TREM2 signaling	(52, 53)
<i>SHARPIN</i>	Inflammation NF- κ B activation	Attenuated inflammatory response	(54)
<i>TREML2</i>	Microglial proliferation	Neuronal degeneration	(55)
<i>SPPL2A</i>	TNF signaling	Immune cell regulation	(38, 56)
<i>HLA-DR</i>	Immunity Antigen presentation	A β accumulation Inflammation	(38, 57)

Diagnosing AD in patients has become amenable with the use of positron emission tomography (PET) imaging of A β and tau in the brain (58). PET imaging is able to detect high levels of A β in the brains of patients with cognitive impairment, allowing for highly sensitive diagnosis of AD (59-61). In addition, the detection of tau using PET has proven to aid in the tracking of AD progression (58, 62). An early diagnosis of AD is also made possible with PET imaging of the initial inflammation of disease, which is often characterized by microglial activation (63). Biomarkers in the CSF and blood are also used to diagnose and detect AD progression (64). CSF markers include levels of A β and tau, with AD patients presenting with a decrease in A β 42 and a significant increase in phosphorylated and total tau (65, 66). Blood is an alternative medium to measure for AD biomarkers, and is especially attractive due to its low invasiveness and medical cost (67). Blood biomarkers for AD include decreased levels of A β 42, a lower A β 42:A β 40 ratio, and increased tau (67). In addition, the level of neurofilament light chains (NfLs) is another blood marker for AD (68). Increased levels of NfLs in the blood is distinct in EOAD patients prior to symptom onset, and changes in NfL levels are often greatest when AD patients transition from the presymptomatic to symptomatic stages of AD (68). Therefore, NfLs can be used to predict AD onset and track its progression in a non-invasive manner.

1.3 Innate immunity in AD:

While numerous physiological functions have been assigned to A β and tau, there is still a general lack of consensus as to what roles these AD-related molecules play in homeostasis. Interestingly, it has

recently been proposed that A β may help provide protection against pathogens by functioning as an antimicrobial peptide (AMP) (Figure 1.1) (69). Such studies demonstrate that A β oligomers are critically involved in limiting both fungal and bacterial infections in cell culture, *C. Elegans*, and mice (70). Additionally, bacterial infections have been shown to incite the seeding of A β in the 5xFAD AD mouse model (70). A β 's AMP function may explain why the peptide has been conserved across a breadth of species for hundreds of millions of years (71). Further implicating A β in the innate immune response is the finding that certain microorganisms' cell membranes are covered with amyloid-like fibrillous structures (72). Bacteria with these amyloid structures, also known as curli fibrils, present a pattern recognized by receptors on immune cells to initiate signaling to remove these invaders (73, 74). A similar response is elicited when A β itself is recognized by microglial pattern recognition receptors (PRRs) in the brain (75). Unfortunately, chronic innate immune activation augmented by sustained A β recognition provokes inflammation that can lead to further propagation of AD pathologies and neurodegeneration (2, 76).

Although the explicit link between A β -seeding and tau accumulation has remained elusive, recent research has begun to shed light on this topic (5). For instance, it has been demonstrated that A β -induced dystrophic neurites accumulate endogenous tau that eventually form into neurofibrillary tangles that correlate with cognitive deficits (5). During homeostasis, endogenous tau participates in the assemblage and stabilization of microtubules in neurons, and, as a result, tau is believed to play functionally important roles in neuronal transport (77). However, the detachment of tau from microtubules and hyperphosphorylation of tau can incite aberrant microglial activation and proinflammatory cytokine production (78). This feedback drives further production of pathogenic tau to enter a cycle that perpetuates its overproduction and neurotoxicity (78). Interestingly, herpes simplex virus (HSV-1), which infects two-thirds of the global population, has been shown to phosphorylate tau (79, 80). In accordance with this finding, antiviral medication has been reported to decrease phosphorylated tau accumulation and A β load (81). A clinical trial is currently investigating the efficacy of the antiviral drug valacyclovir for AD patients with HSV-1 or HSV-2 (82). This further suggests a link between both neuropathologies of AD and the innate immune response that requires further exploration.

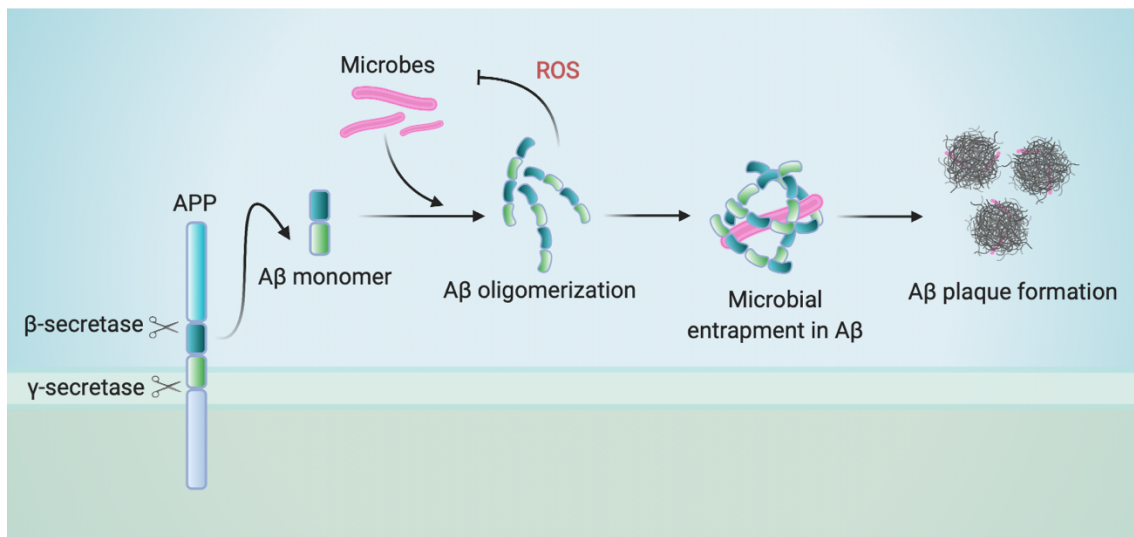


Figure 1.1. The antimicrobial protection hypothesis of amyloid beta and Alzheimer's disease. The cleavage of the amyloid precursor protein (APP) can produce amyloid beta (Aβ) in its monomeric form. The oligomerization of Aβ is thought to help protect the brain against CNS-invading microbes. Aβ oligomers are believed to limit pathogen spread in the brain by promoting the production of reactive oxygen species (ROS) and also by physically encapsulating microbes to limit invasion of host cells. In line with this reasoning, many different microbes have been found to associate with Aβ upon examination of post-mortem AD brains. While the antimicrobial functions of Aβ can potentially play beneficial roles, this process must be tightly controlled as the formation of Aβ aggregates in response to infection can incite the spread of pathological Aβ plaques.

1.3.1 The role of microglia in homeostasis and AD:

As current AD research acknowledges the role of the innate immune response and neuroinflammation in driving neurodegenerative disease, microglia have taken center stage (83). Mounting research suggests that LOAD is, at least in part, mediated by the failure of microglia to properly clear Aβ (84). In fact, frequent variants identified with genome-wide association study (GWAS) in AD patients link mutations in microglia pattern recognition receptors (PRRs) with disease risk (85). Despite microglia being integral for proper phagocytosis and degradation of Aβ, their chronic activation can also provoke maladaptive neuroinflammatory responses with the potential to propagate Aβ production and neuronal distress (86). This has sparked controversy over the enigmatic roles of microglia in AD (86-88), which will be discussed in greater detail throughout this review.

During development, microglia arise from progenitor cells originating in the yolk sac before populating the brain (89). In homeostasis, microglia have been shown to undergo self-renewal to maintain their numbers in the central nervous system (CNS) (89). Microglia act as innate immune sentinels of the brain parenchyma, and perform classical macrophage functions such as coordinating phagocytic disposal of debris and inflammatory cytokine production (90). However, microglia have additional functions in neurogenesis, blood-brain barrier (BBB) permeability, vasculogenesis, myelination, synapse pruning, and neuronal connectivity (90). Microglial morphology transforms during activation, going from a highly branched or "ramified" state during homeostasis to an "ameboid" activated state in response to infection, injury, protein aggregate deposition, and other overt activators of innate immune signaling (91). Microglia express a repertoire of cell surface receptors known as PRRs that enable them to sense and respond to

a diverse array of immunostimulatory triggers in the CNS (92). Microglia associated with disease are commonly found to be in an activated state and upregulate PRR expression (93). Accordingly, microglia are capable of sensing endogenous damage/danger-associated molecular patterns (DAMPs) as well as exogenous pathogen-associated molecular patterns (PAMPs) (92). Microglia can also sense neurodegeneration-associated molecular patterns (NAMPs) that are generated in AD and other forms of neurodegenerative disease (94). In turn, the heterogeneity of microglia populations based on activation state and cell surface receptor expression has piqued interest in their distinct roles in health and disease.

1.3.2 Microglia receptors implicated in AD:

TREM2 -

One of the best-characterized microglia PRRs involved in AD is triggering receptor expressed on myeloid cells 2 (*TREM2*) (Figure 1.2). *TREM2* engages with DAP12 as an adaptor protein, and upon *TREM2* activation, the phosphorylation of the DAP12 immunoreceptor tyrosine-based activation motif (ITAM) is stimulated, leading to the recruitment of spleen tyrosine kinase (SYK) to these sites (29). Engagement of the *TREM2* receptor is believed to stimulate pathways responsible for cytoskeletal reorganization, myeloid cell survival, phagocytosis, and the production of pro-inflammatory cytokines (29). The rare Arginine-47-Histidine (R47H) mutation of *TREM2* significantly increases LOAD risk (95, 96). This R47H mutation is thought to contribute to AD risk by limiting proper *TREM2*-mediated sensing of lipids by microglia (97). *TREM2* recognizes A β , lipids released from damaged neurons, and the A β chaperone APOE in AD (97-99). Activation of *TREM2*/DAP12 signaling limits A β accumulation and other harmful forms of AD pathology, as well as modulates cytokine production (29). Therefore, disruption of *TREM2*/DAP12 signaling can markedly contribute to the progression of A β pathology in AD (29). An additional mechanism by which *TREM2* limits A β pathology is by promoting plaque compaction (100). Plaque morphology is dynamically regulated by microglia, with less-compacted and fibrillous plaques being more neurotoxic than compact plaques (101). Microglia function as a physical barrier to protect neurons from the neurotoxicity of A β plaques and curtail further A β seeding (101, 102). Such studies suggest that the loss of *Trem2* function impairs microglial sensing of A β , leading to defective A β clearance, increased A β plaque toxicity, and neuronal dystrophy in 5xFAD mice (97, 100).

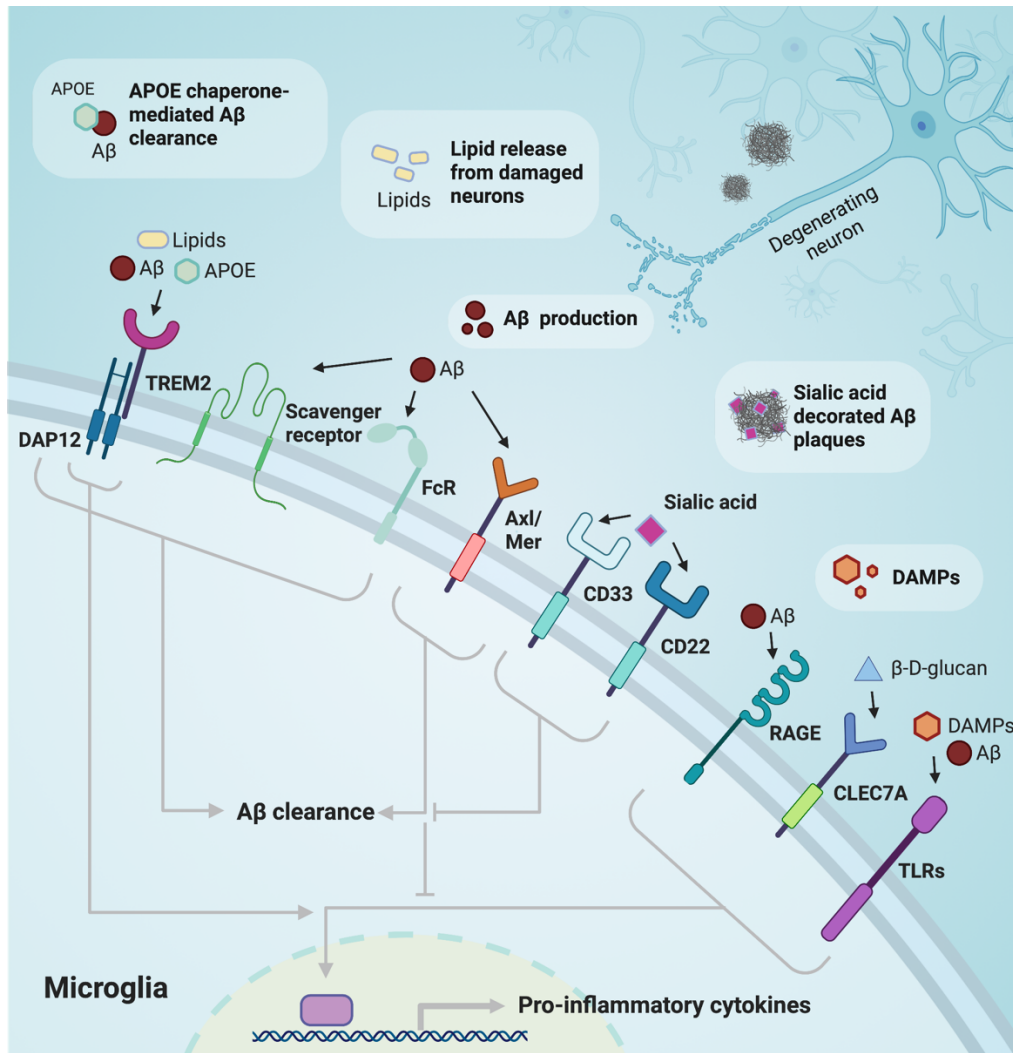


Figure 1.2. Microglial surface receptors that coordinate innate immune responses in AD. TREM2 recognizes Aβ, lipids released from damaged neurons, and the Aβ chaperone APOE in AD. TREM2 activation critically contributes to Aβ clearance and regulates downstream cytokine production. Aβ activation of scavenger and Fc receptors (FcRs) coordinates microglial-mediated Aβ clearance. Axl and Mer receptor activation prompts Aβ clearance while suppressing pro-inflammatory cytokine production. In contrast, CD33 and CD22 bind sialic acid that decorates Aβ plaques, and inhibit downstream signaling events that are required for beneficial microglial responses and Aβ clearance. RAGE, Clec7a, and TLRs are also known to modulate microglial cytokine production in response to Aβ and DAMPs associated with AD.

Patients with the *TREM2* R47H mutation and mice with *Trem2* deficient microglia also present with enhanced autophagy stemming from the dysregulation of the mammalian target of rapamycin (mTOR) signaling (103). This amplification of autophagy impairs microglial response to Aβ and suggests that TREM2 also regulates AD pathology through the maintenance of proper microglial metabolism (103). Recent studies also show that genetic ablation of TREM2 in APPPS1 AD mice (APPPS1;*Trem2*^{-/-}) and loss-of-function *TREM2* mutations in humans both result in reduced association of APOE with Aβ plaques (104). As a result, these APPPS1;*Trem2*^{-/-} mice have increased seeding of Aβ compared with APPPS1 controls (104). Microglia depletion was also found to significantly reduce APOE levels that were associated with Aβ plaques, which further implicates a TREM2-APOE pathway in microglia (104). Interestingly, crosstalk between TREM2 and APOE has also been reported to promote a transcriptional shift in microglia during AD, which can further propagate neuronal loss (105).

Recent studies also suggest the proteolytic cleavage of TREM2 and the subsequent secretion of soluble TREM2 (sTREM2) can ameliorate AD-related disease progression in mouse models. sTREM2 is found at higher levels in the CSF of AD patients, and as such, has been proposed as a potential future biomarker for disease (106). The supplementation of sTREM2 into the brain of 5xFAD mice influences microglia signaling to improve A β clearance preventing further neuritic dystrophy while promoting microglia proliferation and migration (107). Continuation of sTREM2 supplementation, using an adeno-associated virus (AAV) mediated expression technique, was also found to rescue memory and long-term potentiation (LTP) deficits seen in the 5xFAD mice (107). Overall, these studies implicate beneficial roles for TREM2 in the context of proper A β sensing and clearance.

CD33 & CD22 -

Microglial sialic-acid binding immunoglobulin-like lectin (Siglec) receptors have also been shown to play important roles in AD and aging. For instance, CD33, also known as Siglec-3, is another microglial receptor implicated by GWAS in AD risk (32). CD33 binds the sialic acids found ubiquitously on cell membranes (108, 109). In addition, sialic acids are also decorated on the glycoproteins and glycolipids found in A β plaques, and can, therefore, stimulate CD33 signaling in the AD brain (108). However, in contrast to TREM2 which signals utilizing ITAMs, CD33 has intracellular immunoreceptor tyrosine-based inhibitory motifs (ITIMs) (108). The phosphorylation of ITIMs promotes the docking of Src homology 2 domain-containing phosphatases (SHPs) to inhibit downstream microglial signaling mediated by ITAMs that would have otherwise led to the removal of A β in the brain parenchyma (108). The CD33 *rs3865444*^C AD risk allele leads to increased CD33 receptor expression which results in impaired A β 42 phagocytosis (34). Increased expression of *CD33* is significantly associated with a higher clinical score in AD patients and elevated AD pathology (110, 111). Further implicating CD33 in AD risk, 5xFAD mice lacking *Cd33* (5xFAD;*Cd33*^{-/-}) have decreased A β burden and improved memory compared with *Cd33* sufficient 5xFAD mice (112).

More recent studies demonstrate that like CD33, CD22 (also known as Siglec-2), can also hinder microglial phagocytosis in aging and models of AD (113). For instance, *Cd22* is found upregulated in aged microglia, and antibody-mediated blockade was shown to increase A β clearance (113). In addition, microglia in aged mice take on an age-related transcriptional profile that under continued inhibition of *Cd22*, is reverted to a more homeostatic state (113). The inhibition of *Cd22* also ameliorates age-related cognitive decline (113). In summary, both CD33 and CD22 are negative regulators of microglial phagocytic functions in AD that have emerged as attractive therapeutic targets.

CLEC7A -

Recent studies have shown that the receptor CLEC7A, also known as Dectin-1, is dynamically upregulated by microglia in AD, particularly in microglia in intimate contact with A β plaques (105). CLEC7A has been best described in fungal infections where it has been shown to coordinate cytokine production and phagocytosis (114). Similar to TREM2, CLEC7A signals through its intracellular ITAM (114). Although the exact role of CLEC7A in AD remains to be determined, emerging evidence indicates that changes in microglial *Clec7a* expression are associated with AD progression (105). In fact, increased microglial *Clec7a* expression is a hallmark of numerous neurodegenerative disorders and aging (93). Interestingly, multiple human studies have begun to link fungal infections with AD. This work has identified that fungi can be detected in the brains of AD patients (115-117). Levels of chitinase, the enzyme that breaks down chitin found in fungal cell walls, have also been reported to be elevated in the CSF of AD patients (118). This has led to growing speculation that during CNS fungal infections, neuroinflammatory responses and A β production are mounted to protect the brain from the fungal pathogens (119). However, the downside of this is that it may inadvertently set AD pathology in motion. The essential role that CLEC7A is known to play in numerous fungal infections coupled with the pronounced upregulation of microglial CLEC7A expression observed in AD progression, points toward a potentially important role for CLEC7A in AD. However, additional studies probing the specific involvement of CLEC7a in AD pathogenesis are needed.

AXL and MER –

Both *Axl* and *Mer* are TAM receptor tyrosine kinases important for influencing microglial response to AD pathology (120). Foundational work characterizing these receptors establishes *Axl* as an inhibitor of cytokine receptor signaling (121), and *Mer* as a driver of microglial clearance of apoptotic cells (122). Interestingly, *Axl* expression increases in microglia within the AD brain environment, designating *Axl* as an AD-associated gene (123). In fact, recent work describes how the loss of *Axl* and *Mer* impedes microglial clearance of A β plaques in APP/PS1 mice. (120). However, the same study simultaneously observes that APP/PS1 *Axl*^{-/-}*Mer*^{-/-} mouse brains unexpectedly contain less dense core plaques and have worsened fear acquisition compared with APP/PS1 controls (120). These data, along with findings that microglial depletion in 5xFAD mice eliminates A β plaque formation and instead drives alternative A β pathology (124), may suggest an intriguing role for microglia as the constructors of higher-order and less neurotoxic A β architecture.

RAGE –

The binding of A β to the microglial receptor of advanced glycosylation end products (RAGE) stimulates NF- κ B activation resulting in increased production of pro-inflammatory cytokines (125). RAGE is a PRR found on many immune cells that can be upregulated in response to increased ligand production during injury, aging, and neurodegeneration (126, 127). In addition to being a potent inducer of NF- κ B

signaling and downstream inflammation, RAGE has also been shown to promote microglial survival and proliferation in a MAPK-dependent fashion (127, 128). In the context of neurodegenerative disease, overexpression of RAGE in the mAPP AD mouse model triggers IL-1 β and TNF- α production (129). RAGE has also been reported to instigate A β accumulation in the brain by aiding in the transport of A β across the BBB and into the brain (130). Additionally, RAGE signaling in microglia can incite A β accumulation and amplify memory deficits (129). The exaggerated inflammation incited by this A β and RAGE interaction can compromise neuronal health and in turn, negatively affect memory in AD mouse models (125). Despite increased RAGE expression found in the brains of AD patients, clinical trials targeting RAGE have yielded underwhelming results (131, 132).

Complement associated receptors: CR3 and C1qR -

CR3 and C1qR are microglial receptors that can coordinate deleterious synapse pruning in AD (133). The complement receptors CR3 and C1qR are activated by the complement cascade proteins C3 and C1q, respectively (133). In homeostatic neurodevelopment, C3 and C1q contribute to proper synapse pruning and are required to sculpt healthy synaptic connections (134). In contrast, reactivation of C3 and C1q signaling during aging is believed to cause detrimental synapse loss in the hippocampus, the brain structure critical for learning and memory (135, 136). In fact, aged C3-deficient mice exhibit decreased synapse loss, reduced neuronal loss, and improved memory compared with age-matched WT controls (135). In the context of AD, genetic ablation of C3 in APPPS1 AD mice results in reduced synapse loss, lower numbers of microglia interacting with A β plaques, and improved behavior despite increased A β load (137). However, CR3 deficiency in APP AD mice has been shown to limit A β levels by a mechanism involving increased expression of proteolytic enzymes that are known to breakdown A β in the extracellular compartment (138). In turn, the presence of C3 or CR3 in WT mice actually enhances A β 42 fibrillar phagocytosis (139). These findings suggest enigmatic roles for CR3 in modulating the AD brain environment, which are likely impacted by the kinetics and model of disease.

Recent studies demonstrate that microglial-derived C1q is typically found to be elevated in the hippocampus of aged mouse brains and AD human brains (136, 140, 141). C1q tags synapses that are meant to be eliminated by microglia (142). However, C1q-mediated synaptic tagging and subsequent microglial clearance can result in synapse loss in the hippocampus, specifically to the engram cell synapses, which are known to be involved in memory storage (142). Interestingly, the deletion of microglia, impairments in microglial phagocytosis, and inhibition of the complement pathway have all been shown to block this synapse loss and preserve memory in mice (142). Collectively, this illustrates that complement signaling regulated by microglia is needed to ensure proper synapse formation in neurodevelopment. However, unchecked activation of this pathway can propagate aberrant synapse loss and contribute to subsequent aging-induced memory decline and AD-associated phenotypes in mouse models.

1.3.3 Microglial clearance of A β and tau:

Clearance of AD pathology by microglia is executed by several discrete processes. These include receptor-mediated phagocytosis and endocytosis, expression of degradative factors, extracellular chaperone-mediated clearance, and induction of autophagy (143). Each mechanism allows for homeostatic maintenance of the brain parenchyma, and can potentially be targeted to ameliorate A β and tau accumulation in disease.

Clearance by phagocytosis and endocytosis –

Microglial phagocytosis and endocytosis is a critical method of A β clearance, and as a result, there has been tremendous interest in targeting these processes to treat AD. Receptors that mediate this form of clearance include TREM2, toll-like receptors (TLRs), scavenger receptors, and Fc receptors (FcRs) (Figure 1.2) (143). In recent years, TREM2 has emerged as a major mediator of A β endocytosis. Details regarding how TREM2 mechanistically coordinates endocytic clearance of A β can be found earlier in the review. TLRs are highly expressed by microglia in the brain. Microglial TLRs have been reported to bind oligomeric and fibrillar forms A β and this is thought to initiate a signaling cascade that promotes subsequent phagocytic clearance of A β (144). Consistent with this idea, genetic deletion of TLR2 and TLR4 in transgenic mouse models of AD has been shown to promote increased A β deposition and this is generally believed to result from deficits in phagocytosis (145, 146). TLR co-receptors including the TLR4 coreceptor and LPS detector CD14 have also been implicated in AD (147). In a similar fashion to TLRs, CD14 is thought to orchestrate the phagocytosis of fibrillar A β (148). The endocytosis of A β in both fibrillar and oligomeric forms can also be stimulated by class A and class B scavenger receptors. For example, the scavenger receptors CD40 and CD36 have been described to initiate A β endocytosis (143).

Lastly, A β plaques that have been bound by either host-derived or engineered anti-A β antibodies can be phagocytosed following engagement of FcRs on microglia (149). Engineered anti-A β antibodies and vaccine strategies that elicit robust anti-A β antibody production have been shown to promote impressive clearance of A β from the brains of A β -overexpressing AD mouse models (150). FcR-mediated phagocytosis of A β complexes coated with antibodies is thought to be a major mechanism promoting A β reduction following anti-A β antibody infusions and anti-A β vaccination (150). Unfortunately, recent clinical trials in AD patients testing antibody-mediated A β reducing strategies have not been promising (151). Current thinking is that anti-A β antibodies were introduced too late in the disease process to protect neurons that were either already lost or well on their way to neuronal demise. Despite this setback, hope still remains that earlier interventions with anti-A β antibodies may still hold clinical promise. However, for

this to become a reality, improved AD diagnostic biomarkers to identify high-risk patients at earlier stages of disease are required.

Clearance by degradative factors –

In addition to phagocytic pathways, microglia are able to clear AD pathology through their production of degradative factors. These mechanisms include the use of insulin degrading enzyme (IDE), neprilysin, endothelin degrading enzyme (EDE), and the proteasomal degradation pathway (143). IDE, neprilysin, and ECE are all metalloendopeptidases known to degrade A β (143). IDE can be produced by microglia and secreted into the extracellular space to degrade monomeric A β (152). Interestingly, there is a link between taking statins, which lower cholesterol, and a decreased risk for AD (153). One mechanism by which statins are believed to deter AD development is via their promotion of microglial IDE production to degrade A β (153). Neprilysin is another important enzyme in the breakdown of A β (154). In fact, an age-related neprilysin decline in AD brains is thought to contribute to the increased levels of A β that occurs with aging (154). In line with this hypothesis, areas of the brain with high A β plaque load, such as the hippocampus, are known to have decreased neprilysin levels (155). In addition, genetic ablation of neprilysin in APP transgenic AD mice has been reported to cause increased A β deposition in the brain and more severe cognitive decline (156). Similar to IDE and neprilysin, ECE can also promote A β degradation and ECE-deficient mice have increased A β burden in the brain (157). Finally, the proteasomal degradation of AD pathology is regulated by the ubiquitin proteasome system (UPS) (158). This system tags mis-folded proteins with ubiquitin to mark them for proteasomal degradation (66). In AD, this process is believed to be impaired, which in turn leads to increased retention of tau and A β aggregates in the brain (66).

Extracellular chaperone-mediated clearance –

Extracellular chaperone-mediated clearance is another mechanism by which A β can be cleared from the brain. It has been shown that APOE binds to A β and acts as a chaperone to promote its clearance via endosomes (159). The chaperone function of APOE is thought to prompt microglial response to A β plaques, driving A β compaction and in turn, reducing neuronal damage (160). Interestingly, an APOE-TREM2 pathway has emerged in which TREM2 function is shown to be critical for the APOE association with A β plaques to promote plaque compaction (104). The binding of APOE and A β to microglial lipoprotein receptor-related protein 1 (LRP-1) receptor is also thought to initiate signaling through JNK and NF- κ B pathways to promote pro-inflammatory cytokine production (161). The AD risk variant, APOE ϵ 4, is characterized to be less effective at these chaperone-mediated A β clearance duties in addition to inciting an increase in neuroinflammation (159).

Autophagic clearance -

Autophagy acts as an additional mechanism for the clearance of A β . Autophagy is a lysosome-dependent, homeostatic process, whereby organelles and proteins such as A β are broken down and recycled (162). Interestingly, autophagy is linked with many aspects of the innate immune response, including the regulation of pro-inflammatory cytokine production (162). Fibrillar A β can be cleared by microglial autophagy, and the impairment of this process has been shown to propagate NLRP3 inflammasome activation (163). In addition, treatment with trehalose to enhance autophagy markedly decreases tau aggregation in cell culture settings and can reduce neuronal tau inclusions in a tauopathy mouse model (164, 165). Dystrophic neurites are also known to accumulate autophagic vesicles, further supporting a potential role for autophagy in regulating neuronal health (166). In line with a beneficial role for autophagy in AD, boosting autophagic signaling has been shown to ameliorate memory deficits in AD mice (167). Therefore, modulating autophagy presents another potential therapeutic avenue for the treatment of AD that will surely be intensely pursued in future studies.

1.3.4 Disease associated microglia:

The dispute surrounding whether microglia exert beneficial or detrimental roles in AD remains a hotly debated topic. Single-cell RNA-seq recently identified a new subset of microglia known as “disease associated microglia” (DAM) (93). In the past, microglia were largely thought of as a homogenous cell population. However, this diversified transcriptional profile of microglia in the AD, multiple sclerosis, and aging brain environment has prompted many new questions surrounding their role in disease onset and progression. DAMs are classified by two distinct stages: the initial TREM2-independent Stage 1 and TREM2-dependent Stage 2 (93). Stage 1 and 2 DAMs are identified by their downregulation of characteristic homeostatic microglial genes (i.e. *P2ry12*, *Cx3cr1*, and *Tmem119*). Stage 1 DAMs upregulate phagocytic related genes such as *ApoE* and *Dap12* while Stage 2 DAMs upregulate *Clec7A* and *Trem2* (93). As previously discussed in this review, APOE variants are a major risk factor for LOAD, while TREM2, DAP12, and CLEC7A are receptors previously described in phagocytic pathways (23, 29, 114). Initiation of this shift of microglia from a homeostatic phenotype to the DAM signature is believed to be dependent on sensing of NAMPs, engagement of TREM2 signaling, and extended interactions of microglia with A β plaques (94).

The DAM subtype is accepted to serve in a beneficial capacity through their coordination of A β clearance (93). However, this function remains strictly regulated by the inhibitory signaling of CX3CR1, perhaps acting as a harness on DAM function (93). Therefore, future research efforts will likely focus on stimulating the DAM phenotype early on in disease to reduce AD progression. However, the possibility also exists that over-excessive and/or chronic activation of the DAM phenotype may trigger neurotoxic

consequences and propagate AD pathology. This possibility will likely encourage a new AD-microglia field focused on determining how to revert DAM back to their homeostatic microglial state. The multi-faceted roles of microglia underscore the temporal complexities of their function, and will likely keep them in the AD research spotlight for years to come.

1.3.5 Loss of microglial homeostatic function in AD:

Homeostatic microglia possess a signature defined by the expression of receptors such as CX3 chemokine receptor 1 (CX3CR1) and purinergic receptor P2RY12 (27). CX3CR1, which is activated in response to its ligand fractalkine, performs inhibitory duties to sustain a resting-state microglia population (168). Although fractalkine is found at higher levels in the blood of AD patients, *Cx3cr1* is downregulated in DAMs (93, 169). CX3CR1 is thought to have complex roles in AD. For example, deficiency in *Cx3cr1* reduces neuronal loss in the 3xTgAD mouse model, which develop both A β plaques and NFTs (170). In contrast, the loss of *Cx3cr1* in the A β -mediated hAPP-J20 AD mouse model spurs microglial toxicity and intensifies cognitive deficits (171). The presence of A β also downregulates fractalkine in the hAPP-J20 AD mouse model (171). These findings suggest that the role of CX3CR1 is variable depending on the different models of AD being used. Despite these inconsistencies, CX3CR1 appears to be a critical modulator of DAM biology. However, without this CX3CR1 check and balance, excessive microglia activation may contribute to neuronal loss and functional decline, while its overabundance may act to inhibit necessary DAM response to AD pathology. Purinergic receptor P2RY12, on the other hand, is important for microglial migration, and it is highly expressed in homeostatic microglia (172, 173). However, the role of P2RY12 downregulation in plaque-associated DAMs and AD remains unclear and requires further investigation.

1.3.6 Impact of microglial elimination in AD:

The often-contradictory roles of microglia in varying states and stages of neurodegenerative disease has prompted researchers to explore the impact of microglia depletion in AD. In recent years, treatment with the colony stimulating factor 1 receptor (CSF-1R) inhibitor, Plaxxikon, has emerged as a popular approach to study the functional role of microglia in vivo. CSF-1R signaling is required for the survival of microglia and other peripheral macrophages, and as a result, Plaxxikon treatment results in rapid and robust depletion of microglia from the brain (174). Results from recent studies using Plaxxikon indicate a complex role for microglia in mouse models of AD that is greatly influenced by the timing and efficacy of depletion as well as the AD mouse model studied. For example, when 3xTgAD mice were depleted of 30% of their microglia, and aged to have existing A β plaques and tau aggregation, the mice were shown to have improved cognition but this partial deletion of microglia had no effect on A β plaque load or tau aggregation (175). In comparison, a 90% microglial depletion in PS19 AD mice, aged to have tau

aggregation, led to significant reductions in tau propagation (176). Meanwhile, partial depletion of microglia in the APPPS1 mouse model of AD was found to improve memory and ameliorate synaptic degeneration, while having no effect on A β load (177). 5xFAD mice depleted of 80% of their microglia similarly showed improved memory and decreased neuronal damage without modulation of A β levels (178). However, 5xFAD mice depleted of greater than 97% of their microglia prior to A β plaque seeding-onset (i.e. Plexxikon treatment beginning at 1.5 months of age) exhibited reductions in A β load as well as a rescue of anxiety-related behaviors (124). However, the almost complete depletion of microglia in these studies was also found to promote increased numbers of dystrophic neurites, as microglia were no longer present to protect surrounding neurons from the neurotoxicity of the few remaining A β plaques (124). Taken together, current data in mice indicates that partial depletion of microglia does not affect A β plaque and tau load but can result in improved memory and less neuronal damage compared to controls (175, 177, 178). However, near-complete depletion of microglia amid or prior to AD pathology onset attenuates A β and tau load (124, 176). While these studies all point to critical roles of microglia in AD, they also highlight that microglia-targeting therapeutics must carefully take into account the status of disease and desired microglia depletion efficacy to maximize beneficial clinical outcomes and safety.

1.3.7 AD immune cells: microglia or macrophages?

These intriguing findings from Plexxikon depletion studies have prompted speculation over whether microglia or peripheral monocytes repopulate this niche when the depletion drug is removed. As mentioned above, CSF-1R inhibition with Plexxikon treatment can deplete microglia, peripheral macrophages in other tissues, and potentially other cell types reliant on CSF-1R signaling for survival (174). This has led to speculation over the discrete roles of microglia versus other peripherally derived cell types in AD. Plexxikon microglial depletion treatment by itself does not compromise the BBB, and expansion of the few remaining microglia is thought to repopulate the brain following cessation of Plexxikon treatment (179, 180). However, injury models, such as traumatic brain injury (TBI), can cause BBB breakdown and subsequent infiltration of immune cells into the brain (181, 182). Likewise, AD pathology is also thought to propagate the loss of BBB integrity (183). Microglial depletion and repopulation after TBI has been reported to replace chronically activated microglia with resting-state myeloid cells, resulting in decreased neuroinflammation and neuronal loss (181). The neuroprotection conferred by the repopulated myeloid cells post-TBI relies on their induction of IL-6 trans-signaling to enhance learning and memory (184). Therefore, the replacement of activated microglia with more quiescent myeloid cells may underlie neuroprotection. However, while it is speculated that depleted microglia die and are cleared away following Plexxikon treatment, the identity of the repopulating cells in BBB-compromised settings remains poorly understood (179). Multiple myeloid cell types have been proposed to fill this niche including peripheral macrophages and microglia from the small Plexxikon-resistant subset. However, future studies are needed to better understand this process and how it affects

neurological disease. This further illuminates the complexity and heterogeneity of CNS macrophages, and maintains speculation surrounding their capacity to be manipulated during neurodegenerative disease.

Initial studies exploring the ability of CNS-infiltrating monocytes to influence AD-related disease in the APPPS1 AD mouse model initially showed that chemokine receptor *CCR2* deficiency prevents monocytes from entering the brain and that this results in fewer IBA-1⁺ myeloid cells in the brain and impaired A β clearance (185). These data suggest that peripheral monocytes are important for properly controlling AD pathology. In contrast, *CCR2* deficiency in the same mouse model was later shown by a different lab to increase plaque-associated microglia numbers and have minimal impact on A β accumulation (186). What underlies the discrepancies between these two studies remains to be fully resolved. One possibility explaining the divergent outcomes may be related to the latter study's use of irradiation, which can encourage the recruitment and retention of peripherally-derived monocytes in the brain (187). Notably, recent research utilizing an irradiation-independent model has established brain engrafting macrophages that maintain a distinct transcriptional profile from microglia and are able to repopulate the brain following partial microglia depletion (188). Other work also demonstrates that TREM2 can promote peripheral monocytes to enter the brain in APPPS1 mice (189). In contrast to the belief that peripheral myeloid cells are critical for proper AD control, parabiosis studies with WT and 5xFAD mice show minimal infiltration of peripheral monocytes from WT mice into 5xFAD brains (100). Likewise, these parabiosis findings have also been confirmed in the APP/PS1 mouse model (100). In addition, recent research using tdTomato lineage tracing in 5xFAD mice convincingly shows that CX3CR1⁺ microglia comprise virtually all of the myeloid cells surrounding the A β plaques, with virtually no CCR2⁺ peripheral monocytes found in the vicinity of A β in the brain (87). In terms of A β aggregation mouse models, which include 5xFAD and APPPS1 transgenic mice, microglia appear to be the key myeloid cell type responding to A β , with little assistance from infiltrating monocytes. However, this work cannot exclude the potential of peripheral monocyte assistance under all conditions associated with human neurodegenerative disease, especially those that are not fully recapitulated in mouse models. In particular, it will be important for future studies exploring the roles of discrete myeloid cell lineages in AD to assess how combined A β and tau pathology can influence outcomes.

1.4 Inflammatory mediation of AD:

Neuroinflammation centrally contributes to various aspects of AD pathologies and this has led to increasing interest in harnessing inflammatory cytokine signaling to treat AD (2, 190). The role of inflammation in AD remains a hotly debated topic in the field. While on the one hand, chronic inflammation can negatively impact neuronal health, an ever-increasing body of literature also demonstrates that controlled activation of specific inflammatory pathways can help to mobilize beneficial immune functions

to promote A β clearance and neurotrophic factor production (191, 192). In this section, we will discuss the double-edged nature of inflammation in AD.

1.4.1 Cytokines in AD:

Multiple innate immune cytokines including type I interferon (IFN), TNF- α , IL-18, IL-1 β , IL-33, IL-34, IL-12, IL-23, and IL-10 have been described to play important roles in various aspects of AD pathogenesis (47, 193-199). Resting levels of pro-inflammatory cytokines are found to be higher in the blood and cerebrospinal fluid (CSF) of AD patients, suggesting a role for them in disease pathogenesis (200). The deposition of A β , and resultant neuronal damage, provide ligands to activate microglial phagocytosis of A β while also promoting microglia-mediated production of proinflammatory cytokines (88). Acutely, this process can lead to the proper clearance of A β allowing the brain parenchyma to restore homeostasis (Figure 1.3) (201). However, these inflammatory mediators can have complex effects in AD. For example, under chronic inflammation, this process can lose its effectiveness in clearing amyloid beta, while continuing its inflammatory response to further propagate neurotoxicity in a feed-forward mechanism (Figure 1.3) (202). Catalysts for this continued and detrimental response include factors such as age, genetics, injury, and peripheral inflammation (2). The production of specific pro-inflammatory cytokines, such as IFN- γ , also has the potential to encourage further production of A β as well as to recruit microglia activation to respond to neurotoxic A β species (203). Therefore, cytokine production can promote a cycle that is difficult to resolve.

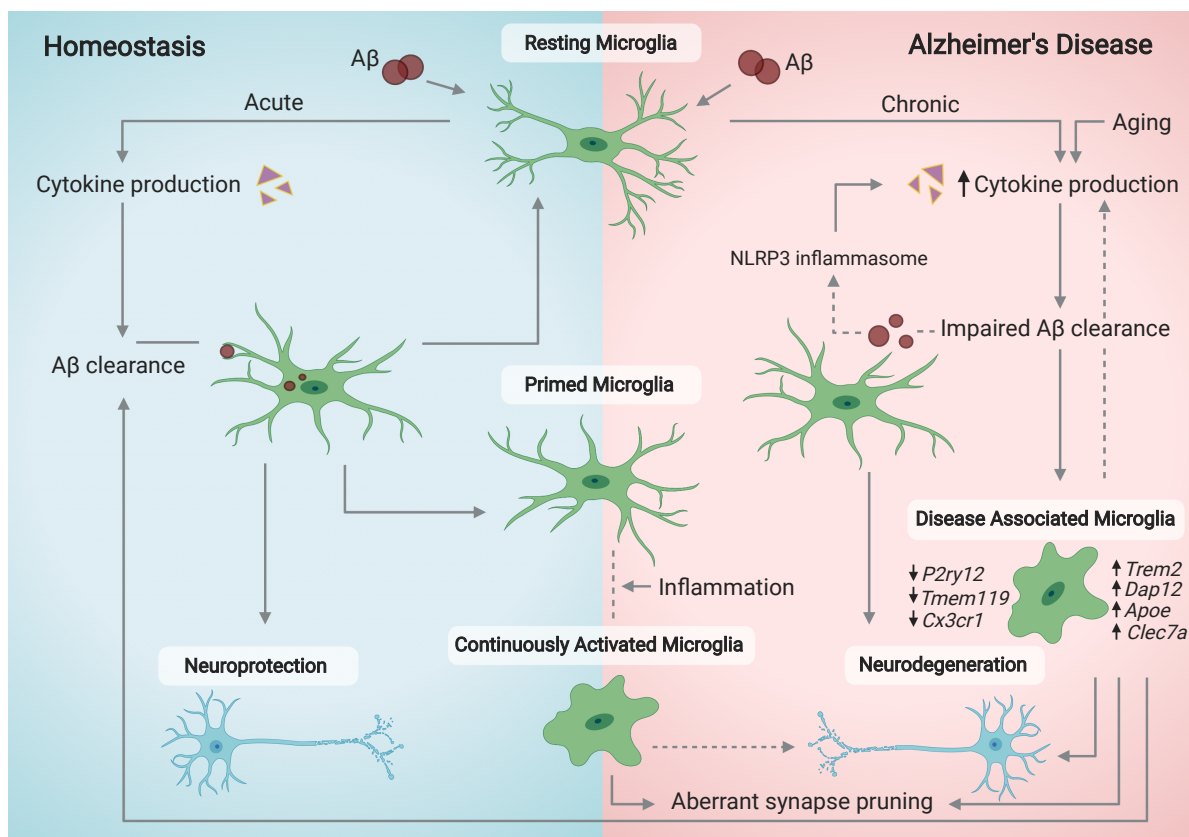


Figure 1.3. The evolving functions of microglia in homeostasis and disease. In homeostasis, acute exposure of microglia to A β initiates a temporary cytokine response that promotes A β clearance. Following proper disposal of A β , microglia typically revert back to a homeostatic resting state. However, this exposure can also prime microglia, and upon secondary or chronic exposure to stress, such as inflammation, this can lead the activated microglia to initiate neurotoxic mechanisms that provoke neuronal loss and excessive synaptic pruning. Upon aging or chronic exposure to A β , as microglia witness in AD, excessive levels of cytokines are produced which can impair proper microglial clearance of A β . Deposition of A β can promote NLRP3 inflammasome activation, which further perpetuates inflammatory cytokine production and subsequent deficits in A β clearance. In both aging and AD, microglial populations are known to take on a transcriptional signature known as “disease associated microglia” or DAM. This change is distinguished by microglial downregulation of homeostatic genes and an upregulation of genes associated with increased microglial activation and inflammatory responses. The role of DAMs in the AD brain are thought to be enigmatic in nature. For instance, DAMs are neurotoxic and lead to neuronal damage and synapse loss. However, DAMs are also able to promote A β clearance.

As was alluded to above, IFN cytokines play significant roles in shaping microglial responses in AD and aging (193, 204). Several AD mouse models show a distinct IFN-stimulated gene (ISG) signature (205). IFN has been described to be expressed by immune cells sensing nucleic acids (206). Of note, fibrillar amyloid beta often contains nucleic acids that can elicit an inflammatory ISG signature in microglia (205). This neurotoxic type of microgliosis has been shown to promote complement-mediated synapse loss that can be curtailed with IFN-receptor blockage (205). Researchers have also shown that knocking out IFN- γ receptor type I in transgenic APP Swedish mutant AD mice leads to a reduction in A β plaque load and reactive microglia (203). In addition, *in vitro* studies indicate that IFN- γ promotes microglial release of TNF- α , and both of these cytokines promote β -secretase cleavage of APP to produce more A β (203). These results strongly suggest that IFN is associated with AD propagation.

The role of TNF- α in AD has remained enigmatic, as some research has focused on the therapeutic benefit of its inhibition, while others show beneficial or benign roles for the cytokine. In support of a detrimental role for TNF- α in AD, it has been shown that higher CSF levels of TNF- α correlate with impaired “functional connectivity,” a measure of the communication between different brain regions underlying various functions such as learning, memory, inhibition, etc. (207). In line with pathologic functions of TNF- α in AD, APPPS1 mice deficient in TNF receptor 1 (TNFR1) have been described to have decreased levels of A β , lower expression of inflammatory factors, improved maintenance of choroid plexus tissue and CSF-blood barrier integrity, and preserved memory compared to TNFR1 sufficient APPPS1 mice (208). In contrast, an injection of murine TNF- α AAV into the hippocampus of APP transgenic mice has been reported to attenuate A β deposition and incite increased microglial responses without increasing APP levels (209). This suggests that under certain spatial and temporal contexts TNF- α may promote plaque clearance. Finally, the proposed causal relationship between TNF- α and AD has recently come into question, as Mendelian randomization modeling of GWAS studies show no causality between peripheral TNF- α expression levels and the risk of developing AD (210).

IL-1 family cytokines, such as pro-inflammatory IL-18, IL-1 β , and IL-33, have also been implicated in modulating AD pathogenesis (197, 211, 212). For example, IL-18 promotes β -secretase mediated cleavage of APP to produce more A β 40 (213). However, loss of *IL-18* in the APPPS1 AD mouse model was found to incite seizure through a proposed mechanism that involves excessive excitatory synapse

activity and impaired dendritic pruning (214). IL-1 β has conflicting roles in AD pathologies. Increased peripheral levels of IL-1 β and its propensity to incite neuroinflammation have led scientists to focus on neutralizing its functions in hopes of therapeutic benefit in AD (200, 215). For instance, IL-1 receptor inhibition in 3xTgAD mice was reported to rescue cognitive deficits, decrease tau phosphorylation, and modestly modulate A β levels (215). Interestingly, conditional overexpression of *IL-1 β* in 3xTgAD mice was conversely found to markedly decrease A β levels while concomitantly leading to increased tau phosphorylation, further highlighting the complex role of neuroinflammation in AD (216). Increased IL-1 production is also known to promote S100B protein release from astrocytes (217). The S100B protein is a neurotrophic cytokine that often acts as a pro-inflammatory cytokine in AD (218). Higher levels of S100B have been documented in AD patients and appears to be associated with increased A β plaque load and gliosis (219-221).

IL-33, an alarmin in the IL-1 cytokine family, has also been implicated in AD. *IL-33* is expressed by oligodendrocytes and its receptor, ST2, is often expressed by microglia (222). *IL-33* expression is reduced in the brains of AD patients, identifying this cytokine as a potential modulator of disease (223). Accordingly, intraperitoneal injection of IL-33 was recently shown to restore LTP deficiency, improve contextual memory, and decrease A β levels in APPPS1 AD mice (197). IL-33 treatment accomplishes this rescue by increasing microglial A β phagocytosis and anti-inflammatory gene expression, while also decreasing microglial pro-inflammatory gene expression (197).

IL-34 and CSF-1 activate the CSF-1 receptor (CSF-1R) to promote microglial population survival and maintenance (179). Interestingly, AD patients have been shown to have increased expression of *IL-34* in the white matter compared with age-matched controls, highlighting its importance in regulating AD pathogenesis (224). More recent work, however, shows reduced expression of *IL-34* in the inferior temporal gyrus (ITG) and an increase in expression of CSF-1 in the ITG and middle temporal gyrus (MTG) of AD patients (225). On one hand, research has found neuroprotective roles for IL-34 in AD. For instance, intracerebroventricular injection of IL-34 into APPPS1 mice promotes improved memory and lower levels of oligomeric A β through a mechanism that involves increased expression of insulin degrading enzyme and heme-oxygenase-1 (47). In contrast, using microglial cultures from AD human brains, researchers show that IL-34 stimulation decreases expression of genes associated with phagocytosis such as CD68, which is a lysosomal marker commonly used to evaluate phagocytic potential in AD mouse models (225). Collectively, these findings highlight the potential temporal and anatomical complexity of IL-34 in the AD brain.

Increasing evidence also supports the role of IL-10, IL-12, and IL-23 in AD pathogenesis. For example, the shared subunit of IL-12 and IL-23 (i.e. p40) and IL-10 are found at elevated levels in the CSF of AD patients (226, 227). A blood biomarker study also found IL-10 and p40 at increased levels in

cognitively normal patients that exhibit abnormally high levels of A β deposition (228). In turn, the ablation of p40 can attenuate cognitive deficits and A β levels in APPPS1 mice (226). Peripheral treatment with anti-p40 antibody in APPPS1 mice is also able to decrease A β levels (226). Interestingly, the loss of IL-12 and IL-23 signaling through p40 genetic ablation has sex-specific effects in which only males exhibit a reduction in A β plaques (229). The silencing of p40 in aged senescence-accelerated mouse prone-8 (SAMP8) mice also mitigates cognitive decline, A β load, and neuronal death (198). Lastly, ablation of *IL-10* in the context of AD is also considered beneficial. In fact, APPPS1 mice lacking *IL-10* show improved synaptic health and cognition compared with APPPS1 controls (199). Therefore, the unchecked functioning of these cytokines during chronic inflammation of AD poses a serious threat to brain health and function.

1.5 Role of inflammasomes in AD:

Recent studies suggest a detrimental role for inflammasomes in AD (230-233). Inflammasomes are multimolecular complexes that form following receptor activation in response to various DAMPs, PAMPs, and NAMPs (234). The formation of these complexes initiates a signaling cascade in which active caspase-1 promotes the cleavage of inflammatory pro-IL-1 β and pro-IL-18 cytokines into their active forms and also incites cell death (234). Inflammasome-mediated cell death is termed “pyroptosis” and is executed by cleaved gasdermin-D (235). Gasdermin-D proteins are cleaved by caspase-1, -4, -5, or -11, and this product comes together to form a pore on the cell membrane to promote cell lysis and the exit of pro-inflammatory cytokines from the cell (236). The NLRP3 inflammasome, in particular, has been identified as an important contributor to AD pathogenesis (214, 230, 231, 237-239). NLRP3 is upregulated and activated in AD, with increased mRNA and protein expression in immune cells (240). The loss of NLRP3 inflammasome in APPPS1 mice attenuates spatial memory and LTP deficits, in addition to decreasing A β burden (230). NLRP3 was also recently shown to promote tau hyperphosphorylation and aggregation (241, 242). Accordingly, inhibitors such as the JC-124 drug or fenamate class NSAIDs have been developed to successfully inhibit the NLRP3 inflammasome to mirror these improvements in a potentially therapeutic format (231, 243). Recent research shows that apoptosis-associated speck-like protein containing CARD (ASC), an adaptor protein critical for the formation of the NLRP3 inflammasome, binds with A β (244). This ASC-A β interaction initiates NLRP3 inflammasome activation and prevents proper clearance of A β (245). In turn, the increased A β levels promote microglial pyroptosis leading to the extracellular release of more ASC that can bind A β to activate the cycle again, generating a chronic neuroinflammatory cascade (245).

The AIM2 inflammasome, which is activated by double-stranded DNA, has also been implicated in AD (233). *Aim2* deficient 5xFAD AD mice have decreased A β plaque load, however, this is not sufficient to rescue memory deficits. Additionally, 5xFAD;*Aim2*^{-/-} mice have increased inflammation mediated by

preserved *IL-1* expression and an increase in the expression of pro-inflammatory cytokines *IL-6* and *IL-18* in the brain (233). This may suggest parallel inflammatory mechanisms to compensate for the loss of *Aim2* in AD mouse models. Interestingly, our lab and others have shown the loss of *Aim2* impacts neuronal morphology and negatively influences several behaviors such as anxiety and memory (246, 247). Furthermore, our recent studies demonstrate that defects in the AIM2 inflammasome can alter neurodevelopment (246). Thus, it is feasible that changes in brain development existing before A β deposition may influence disease outcomes in AD mouse models. Moving forward, it will be interesting to revisit the role of the AIM2 inflammasome in AD using approaches that conditionally ablate AIM2 signaling following neurodevelopment.

1.6 Role of age, environmental factors, and sex in AD:

In recent years, there has been increasing appreciation for the instrumental roles that aging, environmental factors, and lifestyle choices play in AD pathogenesis (Figure 1.4) (248). Interestingly, emerging work has shown that many of these environmental and lifestyle factors influence AD progression by modulating aspects of inflammatory signaling (2). In this section, we will spotlight up-and-coming work describing how changes to inflammatory responses are now believed to underlie the ability of many environmental and lifestyle factors to influence AD.

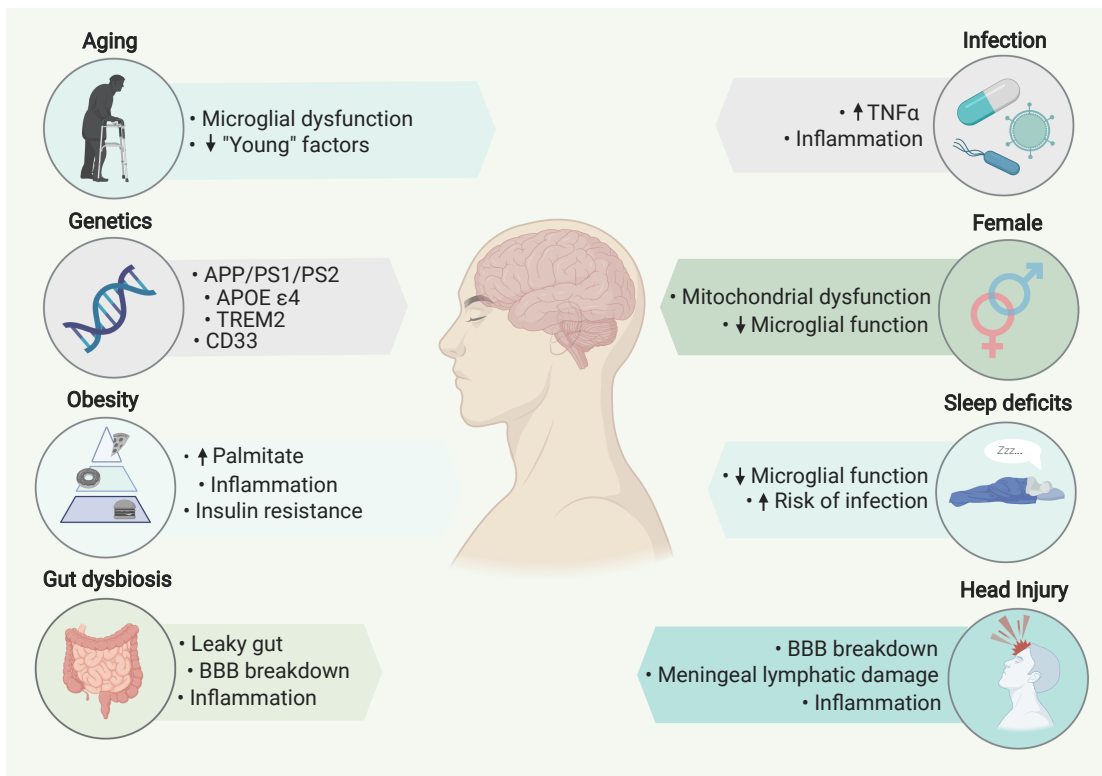


Figure 1.4. Immune dysfunction underlies the ability of AD risk factors to impact neurodegenerative disease development. Several genetic and peripheral factors are known to modulate AD risk. Among these factors, increased AD risk can arise from impaired microglial function amidst aging, genetic variation, sleep deficits, and in females. Additionally, obesity, gut dysbiosis, systemic inflammation, and head injury are known to cause disruptions in blood-brain barrier (BBB) integrity. BBB disruptions can contribute to a heightened risk of disease by means of altered microglial function and impaired removal of AD pathology.

Age is by far the greatest risk factor for developing AD (249). Interestingly, recent studies suggest that aging profoundly impacts microglial biology and that this can hinder their ability to properly handle and dispose of A β (113). Along with their propensity to take on the DAM transcriptional profile, aging also alters microglia morphology, enhances their activation status, limits their motility, and curbs their ability to phagocytose A β (93, 250-252). Unfortunately, all of these age-related microglial changes have the potential to promote AD pathology. The ability of microglia to self-sustain their population is also speculated to make them particularly susceptible to telomeric shortening and cellular senescence, and it has been proposed that the acquisition of this senescence phenotype can cause microglial dysfunction (253). An additional mechanism by which aging contributes to AD is the loss of “youthful” blood-derived factors as one ages. Such studies demonstrate that parabiosis or plasma transfer from young mice to old mice improves learning and memory (254, 255). Two factors shown to be elevated in young blood include thrombospondin-4 and SPARCL1, which support synaptic connectivity (256). It has also been shown that blood from old mice negatively impacts cognition in young mice (257). One factor suggested to contribute to this phenomenon is the chemokine CCL1, as it is elevated in aged-mice plasma levels and directly impairs cognition in recipient young mice (257).

Obesity and exercise have also been implicated in AD prevalence and severity (196, 258-261). Researchers have shown that obese individuals have high levels of the short chain fatty acid known as palmitate in the CSF and that this can lead to impaired neuronal insulin signaling (196). They further report that increased levels of palmitate in the CSF of aged mice provokes pro-inflammatory TNF- α cytokine production and that this can lead to memory deficits (196). Indeed, they showed that TNF- α receptor deficient mice treated with palmitate perform better on memory tests compared with palmitate treated wildtype controls (196). In addition, an intracerebroventricular injection of infliximab, a TNF- α neutralizing antibody, was also found to improve memory and ameliorate microgliosis in mice on a high fat diet (196).

Routine exercise, on the other hand, has been shown to help limit AD development and progression (262). One mechanism that may explain this phenomenon is the release of the myokine FNDC5/irisin from the muscle to the brain during exercise (259). FNDC5/irisin production following exercise increases synaptic plasticity, a critical aspect of memory formation and maintenance (259, 263). A mechanism by which memory formation is promoted by irisin is its ability to activate the memory-associated cAMP–PKA–CREB signaling pathway (264). Frequent exercise is also linked with decreased risk of viral and bacterial infections (265). Therefore, an increased susceptibility to infection as a result of insufficient exercise, which is shown to contribute to neurodegenerative pathology, may account for another mechanism by which exercise is linked with AD pathogenesis (266).

Oral hygiene also appears to play a role in AD risk (267). More specifically, people with the gum disease known as periodontitis have persistent inflammation that is linked with AD (267, 268). For example, it has been demonstrated that serum antibody levels for periodontitis-associated bacteria are increased in AD patients, suggesting a potential link between AD and this peripheral chronic inflammation (269). In addition, levels of the pro-inflammatory cytokine TNF- α are increased in the serum of patients with periodontal disease (270). Accordingly, TNF- α levels are also significantly increased in AD patients, suggesting a potential link between this specific inflammatory cytokine resulting from oral infection and the propagation of AD brain pathology (270-272).

Exposure to pathogens in the environment has also been shown to influence AD risk. Mounting evidence has produced a consequential list of bacteria, viruses, and fungi found in the AD brain, with some even directly associating with A β plaques and influencing tau phosphorylation (117, 273-276). Moreover, it has been reported that AD patients experiencing acute systemic inflammatory responses characterized by increased levels of TNF- α exhibit a two-fold increase in cognitive deficits (277). In fact, patients with sepsis present with long-term cognitive deficits, hippocampal atrophy, and are at a higher risk for developing dementia (278, 279).

TBI has emerged as a major non-genetic risk factor for developing AD and other neurodegenerative disorders later in life. TBI not only significantly increases one's risk of developing AD, but has also been linked to earlier onset and more aggressive disease progression (280-283). More specifically, findings from a number of studies demonstrate that moderate to severe brain injury can increase the risk of developing AD by between 2.3- to 4.5-fold (284-286). These numbers increase exponentially with repetitive brain injuries and interactions with genetic risk factors (287). For instance, possessing one allele of APOE ϵ 4 doubles the risk of developing AD, whereas this risk increases by 10 fold for individuals who carry one copy of the APOE ϵ 4 allele and have a history of brain injury (288). One mechanism thought to underlie the link between TBI and AD is BBB breakdown. TBI-induced vascular shear stress has been shown to appreciably disrupt BBB integrity (289). Cerebrovascular injury induced by TBI and AD has been postulated to be another pathological loop in which BBB breakdown propagates AD pathology and the presence of AD pathology can also incite the loss of BBB integrity (289). For instance, 30% of brains from TBI patients have A β plaques, and TBI can induce tau phosphorylation and A β aggregation (280, 290, 291). The accumulation of A β and tau can then promote BBB breakdown to initiate the cycle once again (289). These findings suggest a link between this inflammatory brain injury and AD progression.

An additional mechanism by which brain injury and neurodegenerative disease interact involves the (re)discovery of the meningeal lymphatics in the CNS (292). In particular, the role of the meningeal lymphatics in neuroinflammation and A β accumulation may provide another compelling angle to the relationship between TBI and AD (293, 294). For instance, TBI has recently been shown to compromise

meningeal lymphatic function, namely its ability to drain inflammatory byproducts to lymph nodes following injury (295). Interestingly, meningeal lymphatic drainage defects are known to significantly increase meningeal A β load and to provoke memory deficits in 5xFAD AD mice (294). Therefore, meningeal lymphatic dysfunction may provide another explanation for the association between AD pathogenesis and brain injury, with promising clinical implications that require further investigation.

BBB permeability is also known to be influenced by gut microbiota composition (296). Indeed, changes in intestinal microbiota landscape have been shown to have prominent effects on the brain either directly via production of microbial products that shape BBB function or indirectly through the modulation of peripheral immune responses (296, 297). Increased gut permeability allows for bacteria, bacterial toxins, and LPS to enter the bloodstream and has been coined “leaky gut” (298, 299). This leakiness is instigated by chronic inflammation and gut dysbiosis, which can contribute to systemic inflammation and the decreased BBB integrity associated with aging and AD (258, 298, 300). BBB breakdown can ultimately lead to impaired removal of toxic species from the CNS and entry of pathogenic mediators from the periphery (298, 300). Interestingly, compared to WT controls, APPPS1 mice have altered bacterial species in the gut, including higher levels of the bacteria *B. thetaiotaomicron* (258). In these studies, it was also shown that modulating the gut microbiota landscape with probiotics and exercise treatment can improve cognitive functions in APPPS1 mice (258).

In addition to rescuing memory, the modulation of microbiota composition upon fecal transfer from WT mice to ADLP^{A β T} AD mice has been shown to attenuate A β load, tau pathology, and microgliosis (301). Antibiotic cocktail treatment to alter microbiota species in the gut of APPPS1-21 AD mice has likewise been reported to reduce A β load and microglial activation in males specifically (302). Accordingly, cognitively impaired patients with high levels of A β also have altered gut microbiota populations. Interestingly, this skew in microbiota composition seen in cognitively impaired individuals is commonly characterized by the outgrowth of commensal microbes that have been linked with enhanced pro-inflammatory cytokine production (303). Dietary changes in patients with MCI also appears to alter the microbiota population and their association with A β and p-Tau levels in the CSF (304). These data convey how peripheral inflammation induced by dysbiosis in the gut can have broad clinical applications for mitigating AD risk and pathology in the future.

Sleep deficits have long been associated with cognitive decline (305). In fact, many AD patients present with shifts in their circadian rhythm (306). However, research also shows that problems with sleep can precede neurodegeneration and increase the risk of developing AD (306, 307). Notably, A β and tau levels are known to be elevated in the CSF and brains of sleep-deprived individuals (308-310). In healthy patients, levels of A β shift, with an increase during the day and a marked decline during sleep (311). However, following A β aggregation, this alignment with the sleep-wake cycle dissipates (311). The half-

life of A β more than doubles with age, likely allowing for improper protein folding and aggregate formation acting as a magnet for extracellular A β and preventing its transport into the CSF (312). Impaired microglial clearance of A β likely contributes to this enhancement in A β half-life. Deficits in sleep itself shift microglia to an activated state and aged phenotype, characterized by impaired A β clearance (313). Additionally, sleep disturbances increase the risk for inflammatory disease, which also has the potential to prime microglia to contribute to their impaired function with aging (253, 314).

The disparity between female and male prevalence of AD has also sparked research to distinguish the pathways underlying this sexual dimorphism. The increase in incidence of AD in females is thought to involve females' dramatic decrease in estrogen levels during menopause, which is known to impact mitochondrial metabolism (315-317). In line with this hypothesis, estrogen replacement therapy (ERT) has been shown to significantly reduce the risk of developing AD (318). The decrease in testosterone in males occurs as a gradual decline, and therefore, it is believed to have a less detrimental effect on mitochondrial function (316). The decrease in sex hormone levels, characteristic during aging, affect mitochondrial metabolism by decreasing mitochondrial energy production and calcium efflux while increasing oxidative stress and reactive oxygen species (ROS) release (316, 319). The surge of oxidative stress and ROS amplifies inflammatory responses (320). Accordingly, the release of ROS can trigger NLRP3 inflammasome activation and lead to downstream proinflammatory cytokine production, pyroptosis, and ASC speck seeding of A β spread (230, 231, 242, 245, 320, 321). Some AD researchers are in favor of a "mitochondrial cascade hypothesis" in which mitochondrial dysfunction precedes AD pathogenesis by stimulating an increase in A β production and leading to the phosphorylation of tau (322). In a feed-forward mechanism, the AD pathologies themselves also propagate mitochondrial dysfunction and inflammatory ROS production which is consistently found at higher levels in AD patients (323, 324). This has led to great interest in AD therapeutics that promote mitophagy to eliminate impaired mitochondria (325). In fact, boosting mitophagy has been shown to attenuate cognitive deficits and promote microglial phagocytosis of A β while decreasing neuroinflammation in APPPS1 AD mice (326).

An additional sex-specific factor involved in AD is the sexual dimorphism of microglia. Female microglia display distinct morphology, decreased density, and altered function (27). It has also been demonstrated that male and female microglia in mice exhibit distinct transcriptional profiles that are retained when transplanted into the opposite sex (327). This suggests that the sex-specific microglia transcriptome does not rely on maintenance by sex-steroids. However, this does not exclude the possibility that the sex-steroids have a permanent effect on microglia during development. In fact, the development of microglia, as measured by gene expression profiles, occurs at disparate paces between the sexes (328). In turn, there is also a sex-specific divergence in the functionality of microglia in mice. For example, using a 5xFAD AD mouse model, it has been shown that female APOE ϵ 4/5xFAD mice exhibit decreased microglia-mediated compaction of A β -plaques, decreased *Trem2* expression, and increased plaque

burden compared with male APOE ϵ 4/5xFAD mice (329). Such studies suggest that sex-based differences in microglial response might help to explain the higher rates of AD in females.

1.7 Concluding Remarks

The role of innate immunity in the modulation of AD pathology and progression poses exciting new avenues for neurodegenerative research. Mounting evidence suggests that microglia and the maintenance of a healthy neuronal environment appear to be inextricably linked. Decades of research have been dedicated to targeting the processing and production of A β , while disappointing clinical results have left researchers to look broader. The new focus on innate immunity, microglia, and neuroinflammation in AD has generated a burgeoning field, and exploring their roles will likely help to identify new and much-needed drug targets to combat this devastating neurodegenerative disease. Recent advancements in AD and neuroimmunology research have begun to uncover critical roles for the innate immune system in AD onset, pathology, and progression. Results from this relatively new area of study suggest that AD treatment is subject to variables such as immune response, environmental factors, and lifestyle choices that are pointing the field to a more individualistic style of therapeutics.

Chapter 2

SYK coordinates neuroprotective microglial responses in neurodegenerative disease

2.1 Abstract

Many neurodegenerative diseases are thought to be caused by impaired containment and/or disposal of neurotoxic material such as amyloid beta (A β) and myelin debris. Indeed, recent human genome-wide association studies (GWAS) and animal model studies have begun to reveal critical roles for the brain's professional phagocytes, microglia, as well as various innate immune receptors expressed by microglia in the control of neurotoxic material and subsequent neurodegenerative disease pathogenesis. Yet, the critical intracellular molecules that orchestrate the neuroprotective functions of microglia in degenerative disorders remain poorly understood. In our studies, we have identified the innate immune signaling molecule spleen tyrosine kinase (SYK) as a key regulator of microglial phagocytosis in neurodegenerative disease. We find that targeted deletion of SYK in microglia leads to exacerbated A β deposition, aggravated neuropathology, and cognitive defects in the 5xFAD mouse model of Alzheimer's disease (AD). Furthermore, disruption of SYK signaling in this AD model was also shown to impede the development of disease-associated microglia (DAMs), alter AKT/GSK3 β -signaling in microglia, and to cause severe deficits in the ability of microglia to phagocytose A β . Importantly, these critical neuroprotective functions of SYK in microglia were not only restricted to A β -driven models of neurodegeneration, as we found that SYK is also a critical regulator of microglial phagocytosis and DAM phenotype acquisition in demyelinating disease. Collectively, these results help to break new ground in our understanding of the key innate immune signaling molecules that instruct beneficial microglial functions in response to neurotoxic material. Moreover, these findings suggest that targeting SYK may offer a therapeutic strategy to treat a spectrum of neurodegenerative disorders.

Hannah Ennerfelt^{1,2,3}, Elizabeth L. Frost¹, Daniel A. Shapiro¹, Coco Holliday¹, Kristine E. Zengeler^{1,2,3}, Gabrielle Voithofer¹, Ashley C. Bolte^{1,4,5}, Catherine R. Lammert^{1,2,6}, Joshua A. Kulas¹, Tyler K. Ulland⁷, and John R. Lukens^{1,2,3,4,5*}

¹Center for Brain Immunology and Glia (BIG), Department of Neuroscience, University of Virginia, Charlottesville, VA 22908, USA, ²Neuroscience Graduate Program, University of Virginia, Charlottesville, VA 22908, USA, ³Cell and Molecular Biology Graduate Training Program, University of Virginia, Charlottesville, VA 22908, USA, ⁴Department of Microbiology, Immunology and Cancer Biology, University of Virginia, Charlottesville, VA 22908, USA. ⁵Medical Scientist Training Program, University of Virginia, Charlottesville, VA, 22908, USA ⁶Department of Neuroscience, Northwestern University, Chicago, IL 60611 ⁷Department of Pathology and Laboratory Medicine, University of Wisconsin, Madison, WI 53705, USA.

Author Contributions:

H.E., E.L.F., T.K.U., and J.R.L. designed the study; H.E., E.L.F., D.A.S., C.H., C.R.L., K.E.Z., and G.V. performed experiments; D.A.S. and A.C.B. performed bioinformatics analysis; H.E., E.L.F., C.H., J.A.K., and D.A.S. analyzed data; H.E. and J.R.L. wrote the manuscript; J.R.L. oversaw the project.

2.2 Introduction

Neurodegenerative disorders, such as Alzheimer's disease (AD), are major public health issues that are likely to increase in prevalence with the aging population. In general terms, neurodegenerative diseases are thought to be driven by the accumulation of neurotoxic material such as amyloid beta ($A\beta$) or myelin debris in the central nervous system (CNS) (1, 330). The buildup of neurotoxic agents is believed to cause neuronal damage and death, which can ultimately lead to various forms of neurological dysfunction that include cognitive decline, motor abnormalities, mental disorders, and loss of inhibition (331-333). Mounting evidence suggests that microglia, which are the professional phagocytes of the CNS, are critically involved in ensuring the proper containment and removal of neurotoxic material in neurodegenerative disease pathogenesis (102, 334, 335). Indeed, human genome-wide association studies (GWAS) have implicated mutations in microglial receptors in the development of several neurodegenerative diseases (51, 52, 105, 336-338).

Most notably, emerging evidence from both AD patients and neurodegenerative mouse models has identified key roles for TREM2, CD33, and CD22 in disease progression (97, 103, 105, 113, 336, 339). While there is growing interest in targeting these receptors to treat neurodegenerative disease, we currently lack knowledge of the major downstream signaling molecules and effector mechanisms employed by these receptors to influence disease pathogenesis. Identification of the intracellular mediators that coordinate neuroprotective microglial functions will help to uncover novel pathways that can be targeted to treat neurodegenerative disease and will also offer new insights into the pathoetiology underlying neurodegeneration. Moreover, targeting major shared intracellular signaling pathways may prove more effective than targeting individual receptors in isolation.

In the studies presented here, we explored whether the intracellular signaling molecule, spleen tyrosine kinase (SYK), is involved in coordinating neuroprotective functions in microglia during neurodegenerative disease. SYK is perhaps best known for the critical role that it plays in mounting protective antifungal immune responses downstream of C-type lectin (CLEC) receptors expressed on innate immune cells (340, 341). In addition to orchestrating immune responses during fungal infections, SYK has been identified as the central kinase that instructs signaling and effector functions downstream of ITAM (immunoreceptor tyrosine-based activation motif)- and ITIM (immunoreceptor tyrosine-based inhibition motif)-containing receptors (30, 342-344). More specifically, SYK activation downstream of ITAM-containing receptor engagement often leads to the induction of inflammatory cytokine production and phagocytosis (345, 346). In contrast, stimulation of ITIM-containing receptors activates the protein tyrosine phosphatase SHP-1 which acts as a brake on SYK-dependent signaling (345, 346). Given that TREM2, CD33, and CD22 are ITAM/ITIM-containing receptors, and that SYK activation is often seen in microglia that surround $A\beta$ and other forms of neurotoxic material (347), we were interested in delineating whether SYK is a critical regulator of microglial responses in neurodegenerative disease. While the ability of SYK to modulate $A\beta$

and tau biology has been explored in previous *in vitro* studies using immortalized CNS lines and pharmacological agents with well-described off-target effects (348, 349), the extent to which SYK influences *in vivo* microglial responses and neurodegenerative disease pathogenesis currently remains poorly understood.

Here, we show that microglia-specific deletion of SYK leads to elevated levels of A β deposition, exacerbated neuropathology, and cognitive impairment in the 5xFAD mouse model of AD. We further demonstrate that SYK is critically involved in both the compaction and phagocytosis of A β by microglia as well as the regulation AKT/GSK3 β -signaling. Recent studies have shown that microglia transition from a homeostatic state to a disease-associated microglia (DAM) phenotype during neurodegenerative disease, and it is widely thought that this transformation is required for microglia to exert their optimal neuroprotective functions in degenerative disease (93). Interestingly, we identify SYK as a key intracellular regulator of DAM phenotype acquisition and further show that CLEC7A-induced activation of SYK in 5xFAD mice promotes improved clearance of A β . Moreover, we show that the neuroprotective effects of SYK on microglia are not confined to A β -driven models of degenerative disease, but rather that DAM induction and microglial phagocytosis are also dependent on SYK signaling in the context of demyelinating disease. Collectively, these findings define SYK as a central regulator of neuroprotective microglial responses in neurodegenerative disease.

2.3 Results

2.3.1 SYK signaling in microglia limits A β accumulation

To interrogate how SYK signaling in microglia impacts A β -mediated neurodegenerative disease, we first generated *Syk^{fl/fl} Cx3cr1^{ERT2Cre}* mice (hereafter referred to as *Syk^{AMG}* mice) as a genetic tool to delete SYK from microglia. We then crossed *Syk^{AMG}* mice with 5xFAD mice which is an AD mouse model that develops aggressive A β pathology starting at 1.5 months of age (350). Importantly, SYK expression is unchanged between 5xFAD and non-5xFAD immune cells that have been described to modulate AD pathogenesis (Figures 2.1A and 2.1B) (334, 351-354). 5xFAD *Syk^{AMG}* mice were given tamoxifen food for 2 weeks after weaning to induce deletion of SYK and then returned to normal chow to allow for peripheral *Cx3cr1*-expressing immune cells to turn over and regain *Syk* expression, while permitting long-lived microglia to remain SYK-deficient (Figures 2.1C-2.1H). As controls, Cre-negative *Syk^{fl/fl}* 5xFAD littermates (hereafter referred to as 5xFAD mice) were similarly fed tamoxifen for 2 weeks at weaning and then returned to normal chow for the remainder of the experiment. It is important to note that this genetic targeting strategy may also induce deletion of SYK in *Cx3cr1*-expressing CNS border-associated macrophages (BAMs), which do not undergo the frequent turnover characteristic of *Cx3cr1*-expressing peripheral immune cells (355). Therefore, SYK deletion in *Syk^{AMG}* mice is likely not limited to microglia found in the brain

parenchyma, but may also encompass self-renewing BAMs found in CNS border regions such as the meninges and choroid plexus (356).

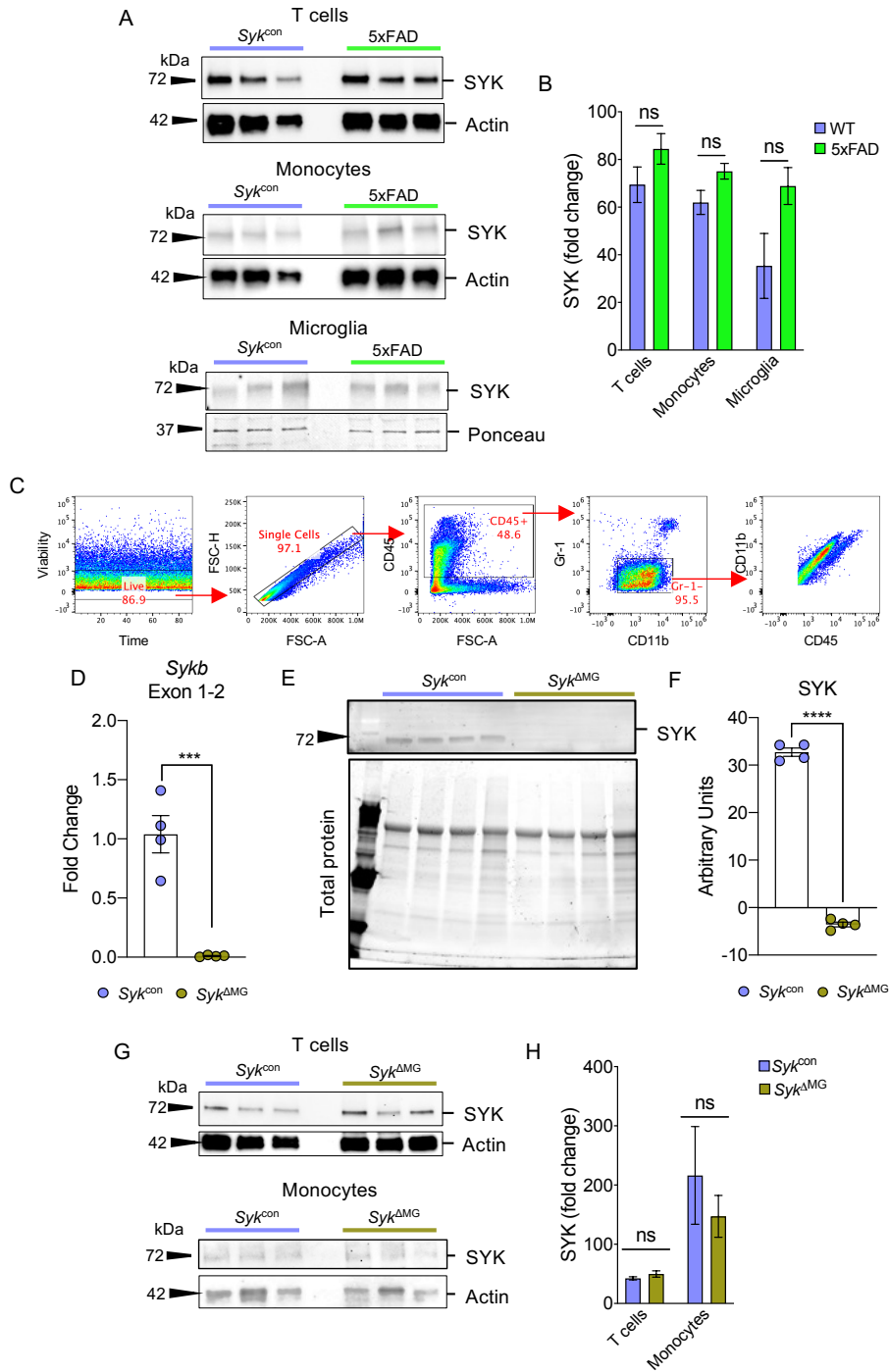


Figure 2.1. Targeted deletion of SYK in tamoxifen-treated *Syk^{fl/fl} Cx3cr1^{Ert2Cre}* mice, related to Figure 1 (A-B) Cre-negative 5xFAD *Syk^{fl/fl}* littermate controls (5xFAD mice) and Cre-negative *Syk^{fl/fl}* littermate controls (*Syk^{con}* mice) received tamoxifen food for 2 weeks starting at 3 weeks of age and then mice were returned to regular food for the remainder of the experiment. Spleens and brains were harvested at 5 months of age to evaluate SYK expression in T cells, monocytes, and microglia. T cells, monocytes, and microglia were sorted from single-cell suspensions using respective anti-CD90.2⁺, anti-CD11b⁺, anti-CD11b⁺(microglia) -coated magnetic beads and magnetic column sorting. (A) MACS-sorted splenic T cells and monocytes and MACS-sorted brain microglia were harvested from 5-month-old *Syk^{con}* and 5xFAD mice, and levels of SYK protein (top panel) and Actin or Ponceau-stained protein (bottom panel) were measured by Western blotting. (B) Quantification of intensity of SYK protein bands normalized to total Actin in sorted splenic T cells and monocytes, and intensity of SYK protein bands normalized to Ponceau staining in brain microglia from *Syk^{con}* and 5xFAD mice. (C-F) *Syk^{fl/fl} Cx3cr1^{Ert2Cre}* (*Syk^{ΔMG}* mice) and Cre-negative *Syk^{fl/fl}* littermate controls (*Syk^{con}* mice) received tamoxifen food for 2 weeks starting at 3 weeks of age and then mice were returned to regular food for the remainder of the experiment. Brains and spinal cords were later harvested to evaluate SYK deletion. Microglia were sorted from single-cell suspensions using anti-CD11b⁺-coated magnetic beads and magnetic column sorting. (C) Representative flow cytometry gating strategy used to validate purity of MACS-sorted microglia from naïve *Syk^{con}* and *Syk^{ΔMG}* combined brain and spinal cord samples. (D) Expression levels of *Sykb* mRNA from MACS-sorted microglia quantified by qPCR. (E) Levels of SYK protein (top panel) and total protein loaded (bottom panel) from MACS-sorted microglia determined by Western blotting and SDS-PAGE with a stain-free gel, respectively. (F) Quantification of intensity of SYK protein bands normalized to intensity of bands from total protein loaded. (G-H) *Syk^{con}* and *Syk^{ΔMG}* mice received tamoxifen food for 2 weeks starting at 3 weeks of age and then mice were returned to regular food for the remainder of the experiment. Spleens were harvested at 5 months of age to evaluate SYK expression in T cells and monocytes. (G) Levels of SYK protein (top panel) and Actin protein (bottom panel) from MACS-sorted splenic T cells and monocytes determined by Western blotting. (H) Quantification of intensity of SYK protein bands normalized to total Actin in sorted splenic T cells and monocytes from *Syk^{con}* and *Syk^{ΔMG}* mice. Statistical significance between experimental groups was calculated by unpaired Student's *t*-test. ****p* < 0.001, *****p* < 0.0001. (B, D, F, H). Error bars represent mean ± S.E.M. and each data point represents an individual mouse.

Using these newly generated transgenic mouse lines, we found that SYK-deletion in 5xFAD *Syk^{ΔMG}* mice leads to significantly elevated accumulation of Aβ in the cortex, hippocampus, and thalamus at 5 months of age (Figures 2.2A and 2.2B). Microglia help to limit the spread of pathological Aβ in the brain parenchyma by forming a barrier around Aβ deposits and promoting the physical compaction of Aβ into dense spherical plaques, which ultimately decreases Aβ interaction with susceptible neurons (102). Therefore, the lack of Aβ plaque sphericity is often used to identify potentially neurotoxic Aβ aggregates and to provide insights into the efficacy of microglial compaction (100, 101). In addition to higher amounts of Aβ load, we observed that Aβ plaques in the cortex and hippocampus of 5xFAD *Syk^{ΔMG}* mice exhibited lower sphericity than the plaques found in 5xFAD littermate controls (Figures 2.2C, 2.2D, 2.3A, and 2.3B). Importantly, delayed deletion of SYK in 4-month-old 5xFAD mice yields similarly increased plaque load in the hippocampus and decreased plaque sphericity in the cortex when harvested at 8 months of age (Figure 2.3H-2.3K). This suggests that microglial SYK remains influential in attenuating pathology after disease-onset in 5xFAD mice. In further support of there being less efficient compaction of Aβ into plaques by SYK-deficient microglia, we observed that Aβ aggregates in 5xFAD *Syk^{ΔMG}* mice were more filamentous (increased 6E10 antibody labeling that detects filamentous Aβ (357)) and less compact (decreased staining of Thioflavin S (ThioS) that detects inert plaques (357)) than the Aβ deposits found in 5xFAD littermate controls (Figures 2.2E and 2.2F). Taken together, these findings suggest that SYK signaling in microglia plays a critical role in the control of Aβ accumulation and compaction.

Microglia are required for the consolidation of soluble Aβ oligomers into insoluble fibrils and the construction of these fibrils into compact plaques (120, 358, 359). Aβ40 and Aβ42 are the predominant isoforms that make up plaques, with soluble Aβ42 being one of the most highly pathological forms of Aβ, especially in comparison to the more inert insoluble forms of Aβ42 (15, 360, 361). To evaluate whether the absence of SYK in microglia also affects the levels of both soluble and insoluble Aβ in 5xFAD mice, we next evaluated Aβ load using ELISA and various extraction techniques to isolate Aβ based on solubility.

From these studies, we saw that the levels of soluble A β 40 and A β 42 were considerably higher in 5xFAD *Syk*^{ΔMG} mice than in 5xFAD littermate controls (Figure 2.2G). Although we did not detect any appreciable differences in A β ELISA levels between experimental groups in the Triton X-100 extraction samples, we did observe reduced levels of insoluble A β 42 in the guanidine fractions isolated from 5xFAD *Syk*^{ΔMG} mice (Figures 2.2H and 2.2I), indicating that SYK centrally contributes to the ability of microglia to construct more inert A β structures. Altogether, these data indicate that SYK is critical for A β consolidation and plaque compaction by microglia in 5xFAD mice.

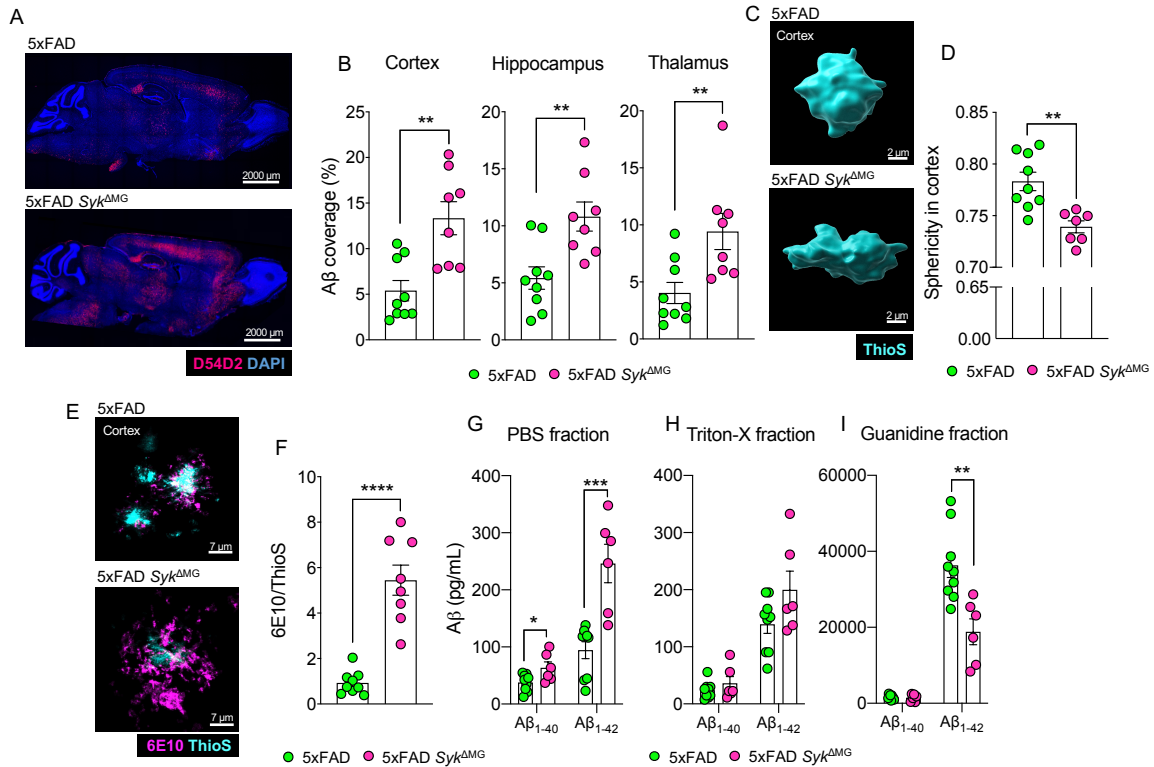


Figure 2.2. Deletion of *Syk* in microglia leads to increased A β burden and altered plaque composition in 5xFAD mice (A-I) 5xFAD *Syk*^{fl/fl}*Cx3cr1*^{ERT2Cre} (5xFAD *Syk*^{ΔMG} mice) and Cre-negative 5xFAD *Syk*^{fl/fl} littermate controls (5xFAD mice) received tamoxifen food for 2 weeks starting at 3 weeks of age and then mice were returned to regular food for the remainder of the experiment. Mice were later harvested at 5 months of age to evaluate amyloid beta (A β) load in the brain. (A-B) Immunofluorescence staining of A β (D54D2, red; DAPI, blue) was performed on sagittal sections and the percent area covered by A β in the cortex, hippocampus, and thalamus was quantified. Original magnification: 10x; scale bar = 2000 μ m. (C) Sphericity of ThioflavinS (ThioS)-labeled and Imaris-rendered A β plaques in the cortex of matched sagittal sections. Original magnification: 63x; scale bar = 2 μ m. (D) Quantification of sphericity with 1.00 being the most spherical, combined data from a total of 50-100 plaques from 3 matching brain sections per mouse. (E-F) Representative images and quantification of A β plaque composition labeling 6E10 (purple) for filamentous forms of A β and ThioS (blue) for more compact or inert forms of A β in the cortex of matched sagittal brain sections. Original magnification: 63x; scale bar = 7 μ m. (F) Quantification represents the percent volume of the 6E10/ThioS ratio per field of view from a total of 10-15 plaques from 3 brain sections per mouse. (G-I) Soluble (PBS) and insoluble (Triton-X and Guanidine) fractions of A β ₁₋₄₀ and A β ₁₋₄₂ measured in the right hemisphere of the brain by ELISA. Statistical significance between experimental groups was calculated by unpaired Student's t-test. *p < 0.05, **p < 0.01, ***p < 0.001, ****p < 0.0001 (B, D, F-I). Error bars represent mean \pm S.E.M. and each data point represents an individual mouse.

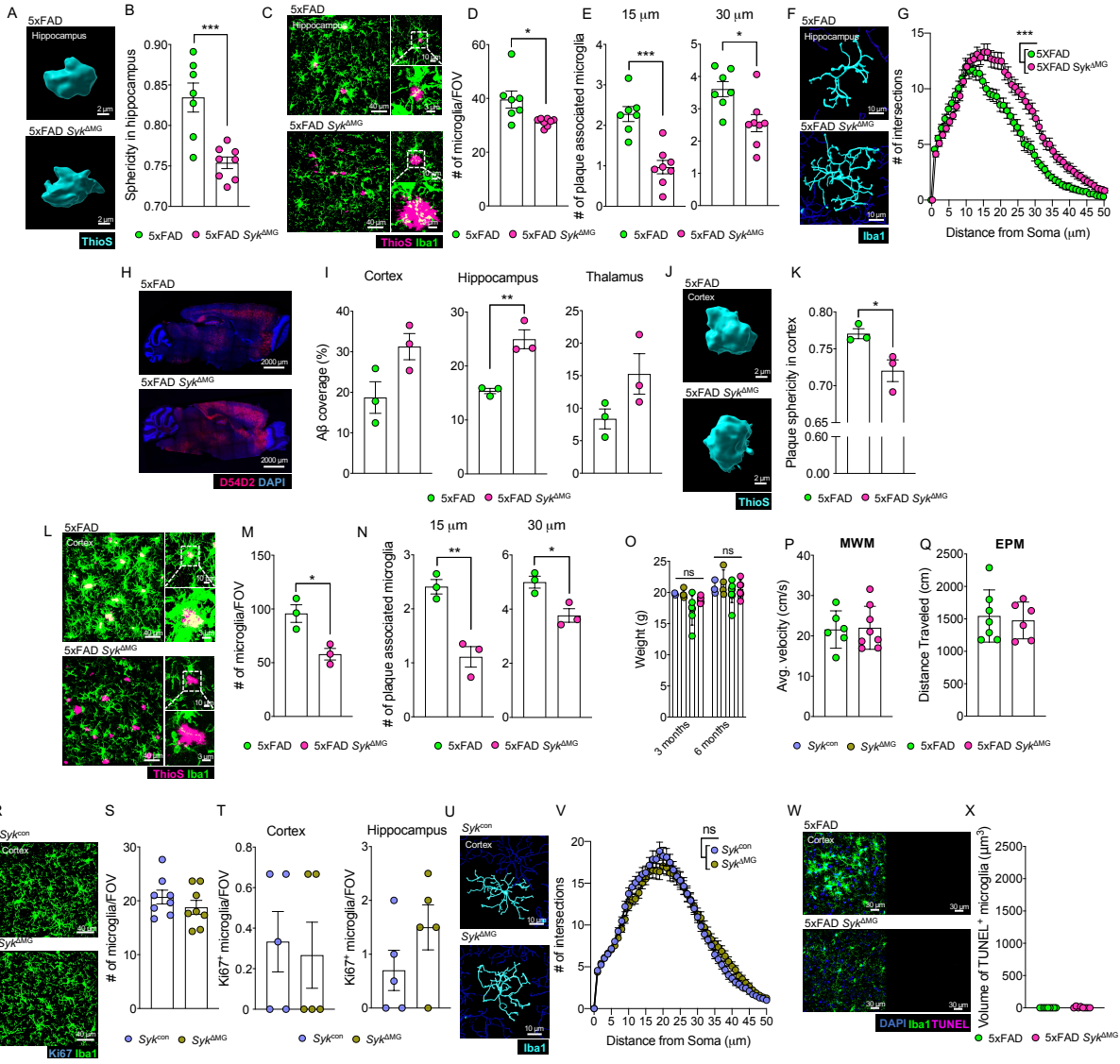


Figure 2.3. Microglial SYK deletion in the hippocampus and after disease onset significantly alters AD pathology and microgliosis, however, the loss of SYK does not affect microgliosis in the absence of A β , related to Figure 1, 2, and 3 (A-G) 5xFAD *Syk^{fl/fl}Cx3cr1^{ERT2Cre}* (5xFAD *Syk^{ΔMG}* mice) and Cre-negative 5xFAD *Syk^{fl/fl}* littermate controls (5xFAD mice) received tamoxifen food for 2 weeks starting at 3 weeks of age and then mice were returned to regular food for the remainder of the experiment. Brains were then harvested at 5 months of age to evaluate plaque sphericity and microgliosis in the hippocampus. (A-B) Microglial response to plaques measured by (A) the sphericity of ThioS labeled and Imaris-rendered A β plaques in the hippocampus of matched sagittal sections. Original magnification: 63x; scale bar = 2 μ m. (B) Quantification of sphericity with 1.00 being the most spherical, combined data from a total of 50-100 plaques from 3 matching brain sections per mouse. (C-E) Microglia were imaged by labeling with Iba1 (green) surrounding A β plaques labelled with ThioS (pink) to assess microglial coverage and proximity to plaques. (C) Representative images of Iba1 and ThioS staining in the hippocampus of matching sagittal brain sections. Original magnification: 63x; scale bar = 40 μ m, 10 μ m, and insets at 3 μ m. (D) Quantification of microglial numbers in the field of view (FOV) in 40 μ m images. (E) Quantification of the number of microglia within a 15 and 30 μ m radius surrounding ThioS-labelled A β plaques. (F) Representative Imaris rendering of Iba1+ microglia in the hippocampus of 5xFAD and 5xFAD *Syk^{ΔMG}* mice. Original magnification: 63x; scale bar = 10 μ m. (G) Sholl analysis quantification from a total of 12 microglia from 3 matching brain sections per mouse (5xFAD n=7, 5xFAD *Syk^{ΔMG}* n=7). (H-N) 5xFAD *Syk^{ΔMG}* mice and 5xFAD mice received tamoxifen food for 2 weeks starting at 4 months of age and then mice were returned to regular food for the remainder of the experiment. Brains were then harvested at 8 months of age in this delayed deletion model to evaluate amyloid beta (A β) load in the brain. (H-I) Immunofluorescence staining of A β (D54D2, red; DAPI, blue) was performed on sagittal sections and the percent area covered by A β in the cortex, hippocampus, and thalamus was quantified. Original magnification: 10x; scale bar = 2000 μ m. (J) Sphericity of ThioflavinS (ThioS)-labeled and Imaris-rendered A β plaques in the cortex of matched sagittal sections. Original magnification: 63x; scale bar = 2 μ m. (K) Quantification of sphericity with 1.00 being the most spherical, combined data from a total of 50-100 plaques from 3 matching brain sections per mouse. (L-N) Microglia were imaged by labeling with Iba1 (green) surrounding A β plaques labelled with ThioS (pink) to assess microglial coverage and proximity to plaques. (L) Representative images of Iba1 and ThioS staining in the cortex of matching sagittal brain sections. Original magnification: 63x; scale bar = 40 μ m, 10 μ m, and insets at 3 μ m. (M) Quantification of microglial numbers in the field of view (FOV) in 40 μ m images. (N) Quantification of the number of microglia within a 15 and 30 μ m radius surrounding ThioS-labelled A β plaques. (O-X) 5xFAD *Syk^{ΔMG}* mice, 5xFAD mice, *Syk^{fl/fl}Cx3cr1^{ERT2Cre}* (*Syk^{ΔMG}* mice), and Cre-negative *Syk^{fl/fl}* littermate controls (*Syk^{con}* mice) received tamoxifen food for 2 weeks starting at 3 weeks of age and then mice were returned to regular food for the remainder of the experiment. (O-Q) Mouse body weight was measured at 3 and 6 months of age, while memory and anxiety-related behaviors were evaluated in the Morris water maze (MWM) and elevated plus maze (EPM) at 4 months of age. (O) Mouse body weight recorded in grams (g) across experimental groups. (P) Distance traveled in the MWM on day 4 of the acquisition phase of the test. (Q) Distance traveled in the EPM. (R-V) Brains from *Syk^{ΔMG}* and *Syk^{con}* mice were harvested at 5 months of age to evaluate microgliosis in the absence of A β . (R) Iba1 (green) and Ki67 (blue) staining was performed on sagittal sections to evaluate *Syk^{ΔMG}* and *Syk^{con}* microglial numbers and proliferation. Original magnification: 63x; scale bar = 40 μ m. (S) Quantification of microglial numbers in the field of view (FOV) averaged from 3 matching cortical sections per mouse. (T) Quantification of Ki67+ microglia in the field of view (FOV) of the cortex and hippocampus of mice averaged from 3 matching brain sections per mouse. (U) Representative Imaris rendering of Iba1+ microglia in the cortex of *Syk^{con}* and *Syk^{ΔMG}* mice. Original magnification: 63x; scale bar = 10 μ m. (V) Sholl analysis quantification from a total of 12 microglia from 3 matching brain sections per mouse (*Syk^{con}* n=5, *Syk^{ΔMG}* n=5). (W-X) Brains were harvested from 5xFAD *Syk^{ΔMG}* and 5xFAD mice at 5 months of age to evaluate microglial apoptosis by TUNEL staining. (W) 5xFAD *Syk^{ΔMG}* and 5xFAD microglia labeled with Iba1 (green) and TUNEL (pink) surrounding A β plaques. Original magnification: 63x; scale bar = 30 μ m. (X) Quantification of TUNEL volume within Iba1+ microglia as a measure of apoptosis. Statistical significance between experimental groups was calculated by an unpaired Student's t-test (B, D-E, I, K, M-N, P-Q, S-T, X), two-way ANOVA with a Bonferroni post-hoc test (G, V), and one-way ANOVA with multiple comparisons (O). ns = not significant, *p < 0.05, **p < 0.01, ***p < 0.001. Error bars represent mean \pm S.E.M.

2.3.2 SYK deletion in microglia leads to worsened neuronal health and memory impairment in 5xFAD mice

Due to the influence of SYK signaling in microglia on A β accumulation and composition, and the propensity of A β to impair neuronal function (362, 363), we next assessed neuronal health in 5xFAD and 5xFAD *Syk^{ΔMG}* mice. We found that 5-month-old 5xFAD *Syk^{ΔMG}* mice had a ~1.5-fold increase in plaque-associated dystrophic neurites in the cortex compared with 5xFAD controls (Figures 2.4A and 2.4B). Heightened accumulation of hyperphosphorylated tau, labeled with the AT8 antibody, was also observed around plaques in the cortex of 5xFAD *Syk^{ΔMG}* mice (Figures 2.4C and 2.4D). This increase in hyperphosphorylated tau is likely indicative of neuronal debilitation (364, 365) that has culminated from the accumulation of neurotoxic A β . 5xFAD *Syk^{ΔMG}* mouse neurons in the CA1 region of the hippocampus also displayed increased levels of cell death, as visualized by TUNEL staining (Figures 2.4E and 2.4F). These collective findings suggest that SYK activity in microglia helps to preserve neuronal health in 5xFAD mice.

To better understand how *Syk*-deficiency in microglia impacts brain function, we evaluated the performance of 4-month-old 5xFAD and 5xFAD *Syk^{ΔMG}* mice in the Morris water maze (MWM), which is commonly used to assess spatial learning and memory. In parallel with increased A β plaque load and neuronal death, we found that 5xFAD *Syk^{ΔMG}* mice also displayed more severe cognitive impairments than

5xFAD littermate controls. Specifically, we found that it took markedly longer for 5xFAD *Syk*^{ΔMG} mice to find the hidden platform in comparison to 5xFAD littermate controls on day 4 of the MWM test (Figure 2.4G), which suggests that there is impaired spatial learning in 5xFAD *Syk*^{ΔMG} mice. Importantly, these differences in performance were not due to altered bodyweight or defects in locomotor activity in 5xFAD *Syk*^{ΔMG} mice, as we observed that body weight and travel velocities in the MWM were similar between the experimental mouse groups (Figure 2.3O and 2.3P). Moreover, when the platform was removed for a probe trial on day 5 of the MWM test, 5xFAD *Syk*^{ΔMG} mice spent significantly less time than 5xFAD mice in the quadrant of the pool where the hidden platform had previously been located (Figure 2.4H), which is indicative of impaired spatial memory in 5xFAD *Syk*^{ΔMG} mice. These MWM findings suggest that disruption of microglial SYK signaling in 5xFAD mice leads to defective spatial learning and memory.

A β deposition in 5xFAD mice has also been shown to spur the development of risk-taking and exploratory behaviors, as can be observed in some AD patients (363, 366). Therefore, to explore if targeted ablation of SYK in microglia also influences risk-taking and exploratory behaviors, we evaluated the performance of 4-month-old 5xFAD *Syk*^{ΔMG} mice and 5xFAD littermate controls in the elevated plus maze (EPM). In these studies, we observed that 5xFAD *Syk*^{ΔMG} mice spent more time exploring the open arm of the maze compared to 5xFAD controls (Figures 2.4I and 2.3Q), which suggests that SYK deletion in microglia on the 5xFAD background also leads to greater levels of risk-taking and exploratory behaviors. Taken together, these data demonstrate a critical role for microglial SYK in preventing neuronal loss as well as limiting the development of memory impairment and risk-taking-related behaviors in A β -mediated neurodegenerative disease.

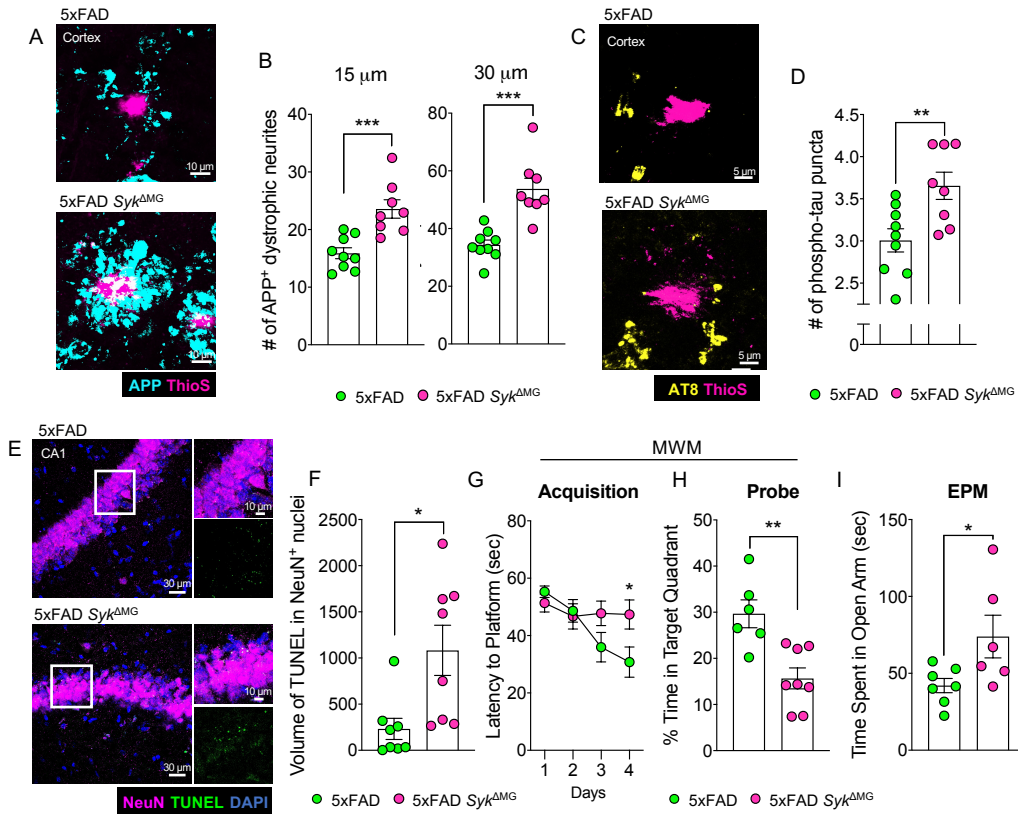


Figure 2.4. Loss of Syk in microglia negatively affects neuronal health and exacerbates AD-related behaviors in 5xFAD mice (A-I) 5xFAD $Syk^{fl/fl}Cx3cr1^{ERT2Cre}$ (5xFAD $Syk^{\Delta MG}$ mice) and Cre-negative 5xFAD $Syk^{fl/fl}$ littermate controls (5xFAD mice) received tamoxifen food for 2 weeks starting at 3 weeks of age and then mice were returned to regular food for the remainder of the experiment. (A-F) Brains were later harvested at 5 months of age to evaluate neuronal health and cell death. (A-B) The formation of dystrophic neurites surrounding plaques in the cortex was determined by staining for APP (blue) and Aβ using ThioS (pink). Original magnification: 63x; scale bar = 10 μm. (B) Quantification of APP+ puncta found within 15 and 30 μm of Aβ plaques from a total of ~40 plaques from 3 matching brain sections per mouse. (C-D) Cortical sections were stained with AT8 (yellow) for phosphorylated tau puncta found within 15 μm of ThioS (pink) stained Aβ plaques. Original magnification: 63x; scale bar = 5 μm. (D) Quantification of phosphorylated tau from a total of ~40 plaques from 3 matching brain sections per mouse. (E-F) Neuronal cell death in the CA1 region of the hippocampus was evaluated by TUNEL assay (green) and NeuN staining (pink). Original magnification: 63x; scale bars = 30 μm and 10 μm for image insets. (F) Quantification of volume of TUNEL+ stain found in NeuN+ nuclei from 2 corresponding brain sections per mouse. (G-H) 4-month-old 5xFAD (n=6) and 5xFAD $Syk^{\Delta MG}$ (n=8) mice were evaluated in the Morris water maze (MWM) to assess spatial learning and memory. Statistics for MWM acquisition were calculated on day 4. Combined data from 3 independent experiments. (I) Performance in the elevated plus maze (EPM) was measured to evaluate anxiety-related behaviors in 4-month-old 5xFAD and 5xFAD $Syk^{\Delta MG}$ mice. Combined data from 2 independent experiments. Statistical significance between experimental groups was calculated by unpaired Student's t-test (B, D, F-I). *p < 0.05, **p < 0.01, ***p < 0.001. Error bars represent mean ± S.E.M. and each data point represents an individual mouse.

2.3.3 SYK regulates microglial proliferation and association with Aβ plaques

To gain insights into how SYK influences microglial biology in response to Aβ pathology, we next explored the impact of SYK deletion on microgliosis. Here, we found that 5xFAD littermate controls have significantly more cortical and hippocampal microglia than 5xFAD $Syk^{\Delta MG}$ mice (Figures 2.5A, 2.5B, 2.3C, and 2.3D). We also observed impaired microglia clustering to Aβ plaques in the cortex and hippocampus of 5xFAD $Syk^{\Delta MG}$ mice, with the number of plaque-associated microglia being 2-fold lower in 5xFAD $Syk^{\Delta MG}$ mice than 5xFAD littermate controls (Figures 2.5C, 2.5D, 2.3C, and 2.3E). Interestingly, the reduction in microglia numbers observed in 5xFAD $Syk^{\Delta MG}$ mice appears to be specific to Aβ-mediated pathology, as we did not observe any appreciable differences in microglia numbers between $Syk^{\Delta MG}$ mice and Cre-negative $Cx3cr1^{ERT2Cre} Syk^{fl/fl}$ mice (Syk^{con}) which do not express the 5xFAD transgenes (Figures 2.3R and 2.3S). In addition, 5xFAD mice that underwent delayed deletion of SYK at 4 months of age

displayed a corresponding decrease in microglial number and association with A β plaques at 8 months of age compared with 5xFAD controls (Figures 2.3L-2.3N). Thus, the criticality of SYK driving microglial responses exists during both disease-onset and disease-progression in 5xFAD mice. To distinguish what might contribute to the reduced numbers of microglia in 5xFAD *Syk* ^{Δ MG} mice, we evaluated the proliferative capacity of SYK-deficient microglia. We found that SYK deficiency in 5xFAD mice leads to reduced microglial proliferation, as illustrated by the ~3-fold decrease in Ki67⁺ microglia seen in the cortex and hippocampus of 5xFAD *Syk* ^{Δ MG} mice (Figures 2.5E and 2.5F). In contrast, in the absence of A β accumulation in mice that lack the 5xFAD transgenes, we did not detect any appreciable differences in microglial Ki67 staining between *Syk*^{con} and *Syk* ^{Δ MG} mice (Figure 2.3R and 2.3T).

The possibility also exists that increased microglial death could be contributing at some level to reduced numbers of microglia seen in the brains of in 5xFAD *Syk* ^{Δ MG} mice (Figures 2.5A and 2.5B). Therefore, to interrogate if deletion of SYK in microglia leads to increased levels of microglial cell death in the 5xFAD model, we performed TUNEL staining in the cortex of 5-month-old 5xFAD and 5xFAD *Syk* ^{Δ MG} mice. We did not, however, detect appreciable numbers of Iba1⁺ microglial cells that stained positive for TUNEL in either 5xFAD or 5xFAD *Syk* ^{Δ MG} mice (Figure 2.3W and 2.3X). This suggests that apoptosis is likely not a major driver of decreased microglial cell numbers in 5xFAD *Syk* ^{Δ MG} mice at this time point. In summary, these results suggest that SYK is critically involved in coordinating microgliosis in response to A β pathology.

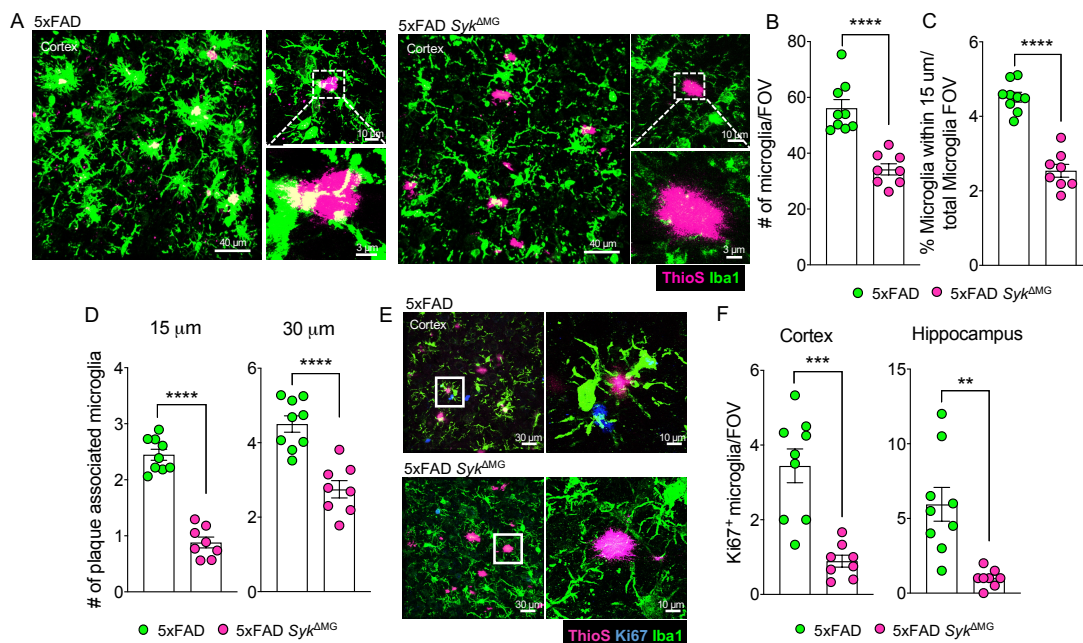


Figure 2.5. Syk-deficiency limits microglial proliferation and association with A β plaques (A-F) 5xFAD *Syk^{fl/fl}Cx3cr1^{ERT2Cre}* (5xFAD *Syk^{ΔMG}* mice) and Cre-negative 5xFAD *Syk^{fl/fl}* littermate controls (5xFAD mice) received tamoxifen food for 2 weeks starting at 3 weeks of age and then mice were returned to regular food for the remainder of the experiment. Brains were later harvested at 5 months of age to evaluate microgliosis. (A-C) Microglia were imaged by labeling with Iba1 (green) surrounding A β plaques labelled with ThioS (pink) to assess microglial coverage and proximity to plaques. (A) Representative images of Iba1 and ThioS staining in the cortex of matching sagittal brain sections. Original magnification: 63x; scale bar = 40 μ m, 10 μ m, and insets at 3 μ m. (B) Quantification of microglial numbers in the field of view (FOV) in 40 μ m images. (C) Quantification of microglial association with plaques as the percent of microglia within 15 μ m of a plaque normalized to the total number of plaques in 40 μ m field of view (FOV). (D) Quantification of the number of microglia within a 15 and 30 μ m radius surrounding ThioS-labelled A β plaques. Each point represents an individual mouse with an average of 50-100 plaques from 3 matching brain sections per mouse. (E) Representative images of microglial proliferation measured by evaluating Ki67 (blue) colocalization with Iba1+ (green) microglia in the cortex of matched sagittal sections. Original magnification: 63x; scale bar = 30 μ m and 10 μ m for image insets. (F) Quantification of Ki67+ microglia in the field of view (FOV) at 30 μ m scale in the cortex and hippocampus of mice averaged from 3 matching brain sections per mouse. Statistical significance between experimental groups was calculated by an unpaired Student's t-test. **p < 0.01, ***p < 0.001, ****p < 0.0001. (B-D, F). Error bars represent mean \pm S.E.M. and each data point represents an individual mouse.

2.3.4 A β -induced microglial activation is impaired in the absence of SYK

To ascertain whether SYK signaling also impacts microglia activation in response to A β , we first evaluated differences in microglia morphology using Sholl analysis. Microglia morphology is widely used to offer insights into their activation status. For instance, homeostatic/resting microglia typically exhibit highly ramified processes, whereas activated microglia tend to retract these processes and acquire an amoeboid morphology (91). Using Sholl analysis to decipher morphological changes, we observed that non-plaque-associated microglia in the cortex and hippocampus of 5xFAD *Syk^{ΔMG}* mice had significantly more ramified processes compared with 5xFAD controls (Figures 2.6A, 2.6B, 2.3F, and 2.3G). In contrast, resting morphological differences were not seen between *Syk^{con}* and *Syk^{ΔMG}* mice in the absence of A β (Figures 2.3U and 2.3V), which suggests that the morphological differences observed between 5xFAD *Syk^{ΔMG}* and 5xFAD controls is specific to A β -driven neurological disease. Taken together, these Sholl analysis results suggest that microglia-intrinsic SYK signaling plays a central role in coordinating the ability of microglia to take on a morphologically activated state in response to A β pathology.

Recent studies have also shown that microglia upregulate a unique transcriptional program in neurodegenerative disease. This activation-induced transition into diseased-associated microglia (DAM) is thought to endow microglia with key neuroprotective functions (93). This progressive shift from resting-state microglia to DAMs involves the coordinated downregulation of many homeostatic markers in stage 1, followed by an upregulation of genes related to microglial response to neurodegenerative pathology in stage 2. Therefore, we next aimed to elucidate whether SYK affects DAM acquisition in response to A β -driven neuropathology. To answer this question, and gain a comprehensive and unbiased picture of how SYK modulates microglial biology in 5xFAD mice, we performed bulk RNA sequencing (RNA-seq) on magnetic bead-sorted CD11b+ cells isolated from the brains of 5-month-old *Syk^{con}*, *Syk^{ΔMG}*, 5xFAD, and 5xFAD *Syk^{ΔMG}* mice (Figure 2.7A). Importantly, these brains were cleared of their meninges and choroid

plexus to eliminate contamination of potential SYK-deficient BAMs. Principal component (PC) analysis revealed, as expected, that 5xFAD microglia form a distinct cluster from control microglia (Figure 2.6C),

which is indicative of the altered transcriptional profile microglia take on in the presence of A β . In contrast, the loss of SYK in microglia blocked this transformation, as 5xFAD *Syk*^{ΔMG} microglia clustered with unperturbed *Syk*^{con} and *Syk*^{ΔMG} microglia, suggesting that 5xFAD *Syk*^{ΔMG} are more similar to homeostatic microglia than those isolated from the 5xFAD mouse model of AD. Upon further inspection, we observed 2769 downregulated and 2668 upregulated genes (FDR<0.1) when comparing microglia isolated from 5xFAD *Syk*^{ΔMG} and 5xFAD mice (Figures 2.6D and 2.7D). Moreover, KEGG analysis revealed that many of the repressed genes in 5xFAD *Syk*^{ΔMG} microglia were related to neurodegeneration (Figure 2.6E). In contrast to the numerous transcriptional differences seen between 5xFAD and 5xFAD *Syk*^{ΔMG} microglia, we only observed a marginal effect of SYK deletion between *Syk*^{ΔMG} and *Syk*^{con} microglia, with 37 downregulated and 7 upregulated genes (FDR<0.1) (Figures 2.7B and 2.7C). These findings suggest that SYK acts as a critical regulator of the transcriptional shift that microglia undergo in response to A β -associated neuropathology in 5xFAD mice.

Notably, we also found that a large number of genes were markedly repressed in 5xFAD *Syk*^{ΔMG} microglia (Figure 2.6D). More specifically, upon *Syk* deletion we observed a significant downregulation of stage 1 DAM genes between 5xFAD *Syk*^{ΔMG} and 5xFAD microglia (Figure 2.6F). However, an even more striking downregulation of stage 2 DAM genes (i.e. *Lpl*, *Cst7*, *Itgax*, *Axl*, *Clec7a*, *Csf1*, and *Ccl6*) was observed in 5xFAD *Syk*^{ΔMG} microglia relative to 5xFAD microglia (Figures 2.6F and 2.7D). Therefore, SYK appears to be especially critical for the ability of microglia to acquire the more activated stage 2 DAM transcriptional phenotype in 5xFAD mice. To validate this transcriptional block in DAM generation seen in SYK-deficient microglia at the protein level, we next performed immunofluorescence staining to evaluate the expression levels of the signature microglial homeostatic marker, Tmem119. As DAMs undergo transcriptional activation, homeostatic Tmem119 expression canonically decreases in stage 1 DAMs (105). However, we observed that 5xFAD *Syk*^{ΔMG} microglia retained significantly higher Tmem119 expression compared to 5xFAD microglia (Figures 2.7E and 2.7F), suggesting their retention of a homeostatic state. In addition, we investigated the expression of stage-2 DAM marker, CLEC7A (105), on Iba1⁺ microglia surrounding A β plaques in 5xFAD and 5xFAD *Syk*^{ΔMG} mice. These imaging studies revealed significantly reduced expression of CLEC7A on Iba1⁺ microglia surrounding plaques in 5xFAD *Syk*^{ΔMG} mice (Figures 2.7G-2.7I), suggesting that SYK is required for the optimal upregulation of this DAM protein. Altogether, these findings reveal that SYK centrally contributes to the critical transformation of homeostatic microglia into DAMs following exposure to A β .

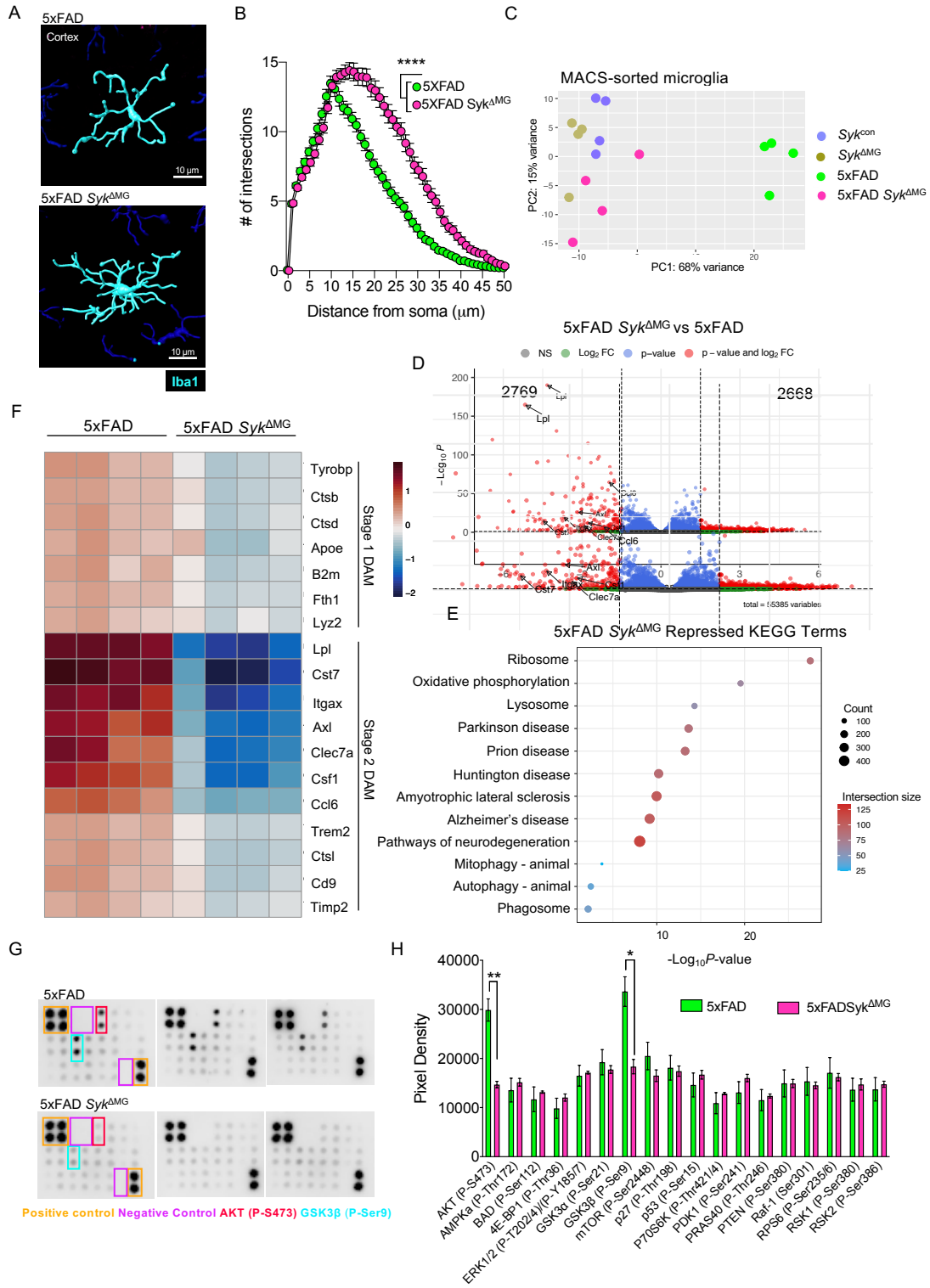


Figure 2.6. Defective activation of *Syk*-deficient microglia in 5xFAD mice (A-H) 5xFAD *Syk^{fl/fl}Cx3cr1^{ERT2Cre}* (5xFAD *Syk^{ΔMG}* mice), Cre-negative 5xFAD *Syk^{fl/fl}* littermate controls (5xFAD mice), *Syk^{fl/fl}Cx3cr1^{ERT2Cre}* (*Syk^{ΔMG}* mice), and Cre-negative *Syk^{fl/fl}* littermate controls (*Syk^{con}* mice) received tamoxifen food for 2 weeks starting at 3 weeks of age and then mice were returned to regular food for the remainder of the experiment. Brains were later harvested at 5 months of age to evaluate microglial activation. (A) Imaris-rendered microglia morphology labeled with Iba1 (blue) in the cortex. Original magnification: 63x; scale bar = 10 μm. (B) Sholl analysis quantification from a total of 12 microglia from 3 matching brain sections per mouse (5xFAD n=9, 5xFAD *Syk^{ΔMG}* n=8). (C-F) Microglia from 5-month-old 5xFAD *Syk^{ΔMG}*, 5xFAD, *Syk^{ΔMG}*, and *Syk^{con}* mice were sorted from single-cell brain suspensions using anti-CD11b⁺-coated magnetic beads and magnetic column sorting, finally, RNA-Seq was performed. (C) Principal component (PC) analysis of sample clustering. (D) Volcano plots depicting differentially expressed genes (FDR<0.1) where 2769 genes are downregulated, and 2668 genes are upregulated in 5xFAD *Syk^{ΔMG}* compared to 5xFAD control microglia. (E) KEGG term enrichment scatter plot highlighting major pathways that are repressed in 5xFAD *Syk^{ΔMG}* microglia in comparison to 5xFAD microglia. (F) Heatmap representation of significantly downregulated (FDR<0.1) stage 1 & 2 disease-associated microglia (DAM) genes between 5xFAD *Syk^{ΔMG}* and 5xFAD groups. (G-H) Mouse AKT pathway phosphorylation array conducted on microglia from 5-month-old 5xFAD *Syk^{ΔMG}* and 5xFAD mice that were sorted from single-cell brain suspensions using anti-CD11b⁺-coated magnetic beads and magnetic columns. (G) Membranes incubated with 5xFAD and 5xFAD *Syk^{ΔMG}* microglia measuring 18 different AKT phosphorylation targets. Positive control dots highlighted in yellow, negative control dots highlighted in magenta, AKT (P-S473) denoted in red, and GSK3β (P-Ser9) denoted in cyan. (H) Quantification of dot pixel density normalized with respective positive and negative control sample dot pixel density. Data are plotted in membrane order of phosphorylated protein probes; n of 3 for each group. Statistical significance between experimental groups was calculated by a two-way ANOVA with a Bonferroni post-hoc test (B) and an unpaired Student's t-test (H). *p < 0.05, **p < 0.01, ****p < 0.0001. Error bars represent mean ± S.E.M.

The downstream signaling that coordinates DAM acquisition has remained poorly described, although, it has been suggested that PI3K/AKT signaling can regulate many of the processes and pathways linked to microglial activation in AD (103, 367-369). Therefore, we chose to interrogate how the loss of SYK in microglia regulates PI3K/AKT signaling in response to Aβ pathology. Utilizing magnetic bead-sorted CD11b⁺ microglia isolated from the brains of 5-month-old 5xFAD and 5xFAD *Syk^{ΔMG}* mice that were stripped of their meninges and choroid plexus, we evaluated the phosphorylation status of 18 proteins that have been shown to be centrally involved in the PI3K/AKT signaling pathway. In these studies, we found that one particular arm of the AKT signaling pathway was differentially regulated between 5xFAD and 5xFAD *Syk^{ΔMG}* microglia. More specifically, we observed that phosphorylation levels of both AKT (P-S473) and GSK3β (P-Ser9) were reduced in 5xFAD *Syk^{ΔMG}* microglia compared with 5xFAD control microglia (Figures 2.6G and 2.6H). These findings are notable as decreased phosphorylation of AKT (P-S473) and GSK3β (P-Ser9) have been observed in the brains of AD patients in comparison to age-matched controls (370, 371). Moreover, mutations in *GSK3B* have also been linked to both familial and sporadic forms of AD in humans (372). Our data indicate that 5xFAD *Syk^{ΔMG}* microglia exhibit decreased AKT activation as well as diminished phosphorylation of GSK3β at Ser9 (Figures 2.6G and 2.6H). Phosphorylation of GSK3β at Ser9 leads to its potent inactivation (370, 373), which ultimately indicates that there is increased activation of GSK3β in 5xFAD *Syk^{ΔMG}* microglia. Given that GSK3β activation has been shown to contribute to Aβ accumulation, tau phosphorylation, and neuronal damage in models of AD (374-377), SYK-related modulation of the GSK3β pathway may contribute to the exacerbation of disease seen in 5xFAD *Syk^{ΔMG}* mice.

The extent to which SYK regulates microglial transcriptional transition into DAMs prompted an investigation into what upstream receptor SYK signaling relies on to enact Aβ pathology-induced microglial response. Extensive work has characterized microglial receptor TREM2 as influential in driving microglial acquisition of the DAM transcriptome (93, 97, 105). Based on these findings, we wanted to determine if the impaired transcriptional shift we observed in our SYK-deficient 5xFAD microglia phenocopies the previously described deficiency in microglial transcriptional activation seen in TREM2-deficient 5xFAD

microglia. To better understand the extent to which SYK regulates transcriptional DAM acquisition and to identify if TREM2 regulates SYK function, we compared our RNA-seq dataset with a previously published dataset analyzing 5xFAD *Trem2*^{-/-} microglia (112). We found that 25% of genes upregulated and ~60% of genes downregulated in 5xFAD *Trem2*^{-/-} microglia were shared with 5xFAD *Syk*^{ΔMG} microglia (FDR<0.05) (Figure 2.7J). In addition, the genes downregulated by 5xFAD *Trem2*^{-/-} and 5xFAD *Syk*^{ΔMG} microglia share molecular function terms such as “signaling receptor binding” and “protein binding” (Figure 2.7K). These data suggest an important shared signaling axis between TREM2 and SYK. However, the transcriptional shift upon SYK deletion in 5xFAD *Syk*^{ΔMG} microglia encompasses a substantial population of uniquely upregulated (>97%) and downregulated (>63%) differentially expressed genes not observed in 5xFAD mice that lack TREM2 (FDR<0.05) (Figure 2.7J). Therefore, it is likely that TREM2 signaling through SYK is only partially regulating microglial DAM transition, and that SYK conceivably transmits signals from multiple receptors in addition to TREM2 in the 5xFAD mouse model.

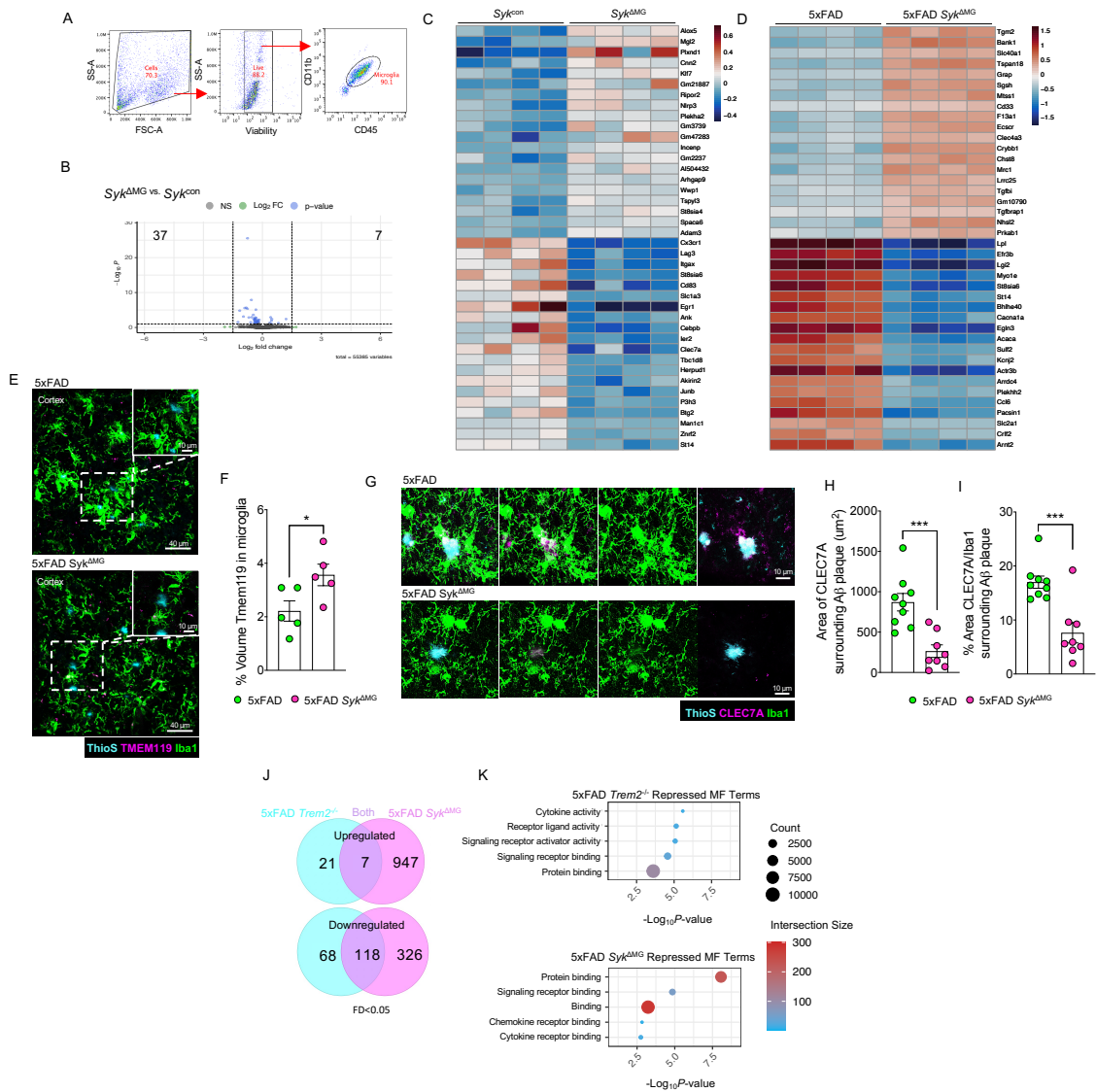


Figure 2.7. Effects of SYK deficiency on microglial gene expression under steady-state conditions and in response to A β pathology, related to Figure 4 (A-K) 5xFAD *Syk^{fl/fl}Cx3cr1^{ERT2Cre}* (5xFAD *Syk^{ΔMG}* mice), Cre-negative 5xFAD *Syk^{fl/fl}* littermate controls (5xFAD mice), *Syk^{fl/fl}Cx3cr1^{ERT2Cre}* (*Syk^{ΔMG}* mice), and Cre-negative *Syk^{fl/fl}* littermate controls (*Syk^{con}* mice) received tamoxifen food for 2 weeks starting at 3 weeks of age and then mice were returned to regular food for the remainder of the experiment. Brains were later harvested at 5 months of age to evaluate microglial activation. (A-D) Microglia from 5-month-old 5xFAD *Syk^{ΔMG}*, 5xFAD, *Syk^{ΔMG}*, and *Syk^{con}* mice were sorted from single-cell brain suspensions using anti-CD11b⁺-coated magnetic beads and magnetic column sorting, finally, RNA-Seq was performed. (A) Representative flow cytometry gating strategy used to validate purity of MACS-sorted microglia from 5xFAD *Syk^{ΔMG}*, 5xFAD, *Syk^{ΔMG}*, and *Syk^{con}* brain samples. (B) Volcano plots depicting differentially expressed genes (FDR<0.1) where 37 genes are downregulated, and 7 genes are upregulated in *Syk^{ΔMG}* microglia compared to *Syk^{con}* microglia. (C) Heatmap representation of the 20 most significantly upregulated and downregulated (FDR<0.1) genes between *Syk^{ΔMG}* and *Syk^{con}* mice. (D) Heatmap representation of the 20 most significantly upregulated and downregulated (FDR<0.1) genes between 5xFAD *Syk^{ΔMG}* and 5xFAD mice. (E-I) Immunohistochemistry validation of RNA-Seq findings in 5-month-old 5xFAD *Syk^{ΔMG}* and 5xFAD mice. (E) 5xFAD *Syk^{ΔMG}* and 5xFAD microglia labeled with Iba1 (green) and Tmem119 (pink) surrounding A β plaques labelled with ThioS (blue). Original magnification: 63x; scale bar = 40 μ m and 10 μ m for image insets. (F) Quantification of Tmem119 volume colocalized with Iba1. (G) 5xFAD *Syk^{ΔMG}* and 5xFAD microglia labeled with Iba1 (green) and CLEC7A (pink) surrounding A β plaques labelled with ThioS (blue). Original magnification: 63x; scale bar = 10 μ m. (H-I) Quantification of total area of CLEC7A surrounding individual A β plaques and percent area of CLEC7A normalized to the area of Iba1⁺ cells per A β plaque, respectively. Quantification was determined by averaging the Iba1 and CLEC7A area found surrounding ~30 plaques from 3 matching brain sections per mouse. (J-K) Comparison of the transcriptional changes that arise in microglia with the loss of either SYK or TREM2 in 5xFAD mice. 5xFAD *Syk^{ΔMG}* and 5xFAD brains were harvested at 5 months of age and their microglia were sorted from single-cell brain suspensions using anti-CD11b⁺-coated magnetic beads and magnetic column sorting to perform RNA-Seq. 8-month-old 5xFAD *Trem2^{-/-}* and littermate 5xFAD microglia were FACS-sorted and analyzed by RNA-Seq in (Griciuc et al. 2019). (J) Venn diagram of significantly upregulated and downregulated genes in 5xFAD *Trem2^{-/-}* and 5xFAD *Syk^{ΔMG}* microglia compared with their respective littermate 5xFAD controls (FD<0.05). (K) Molecular function (MF) term enrichment scatter plot highlighting major functions that are repressed in 5xFAD *Trem2^{-/-}* and 5xFAD *Syk^{ΔMG}* microglia in comparison to littermate 5xFAD microglia. Statistical significance between experimental groups was calculated by unpaired Student's *t*-test. **p* < 0.05, ****p* < 0.001 (F, H-I). Error bars represent mean \pm S.E.M. and each data point represents an individual mouse.

2.3.5 A β pathology promotes increased lipid droplet formation and ROS production in SYK-deficient microglia

Our RNA-seq findings revealed that 5xFAD *Syk^{ΔMG}* microglia exhibit a prominent reduction in lipoprotein lipase (*Lpl*) expression (Figure 2.6F), a DAM-marker known to be critical for regulating cellular lipid homeostasis and lipid droplet accumulation (378). Interestingly, recent work in microglial biology during aging and neurodegeneration has identified a population of lipid-droplet-accumulating microglia (LDAMs), which display impaired phagocytosis and increased reactive oxygen species (ROS) production (379). Therefore, to further understand how SYK may regulate microglial responses in the AD-brain environment, we chose to evaluate lipid homeostasis in SYK-deficient microglia using BODIPY which is a fluorescent dye that detects lipid droplets (379). In these studies, we observed a significant increase in BODIPY fluorescence in 5xFAD *Syk^{ΔMG}* CD11b⁺CD45^{int} microglia, indicating an increase in lipid droplet accumulation in SYK-deficient microglia (Figures 2.8A and 2.8B). Previous work has defined several dysfunctions in LDAMs, including their increased production of reactive oxygen species (ROS) in the aged brain. Indeed, 5xFAD *Syk^{ΔMG}* CD11b⁺CD45^{int} microglia displayed an increase in CellROX fluorescence, a cell-permeant dye that fluoresces when oxidized by ROS, compared with control 5xFAD microglia (Figures 2.8C and 2.8D). These collective findings suggest that SYK may act to partially limit microglial transition to an LDAM-like state.

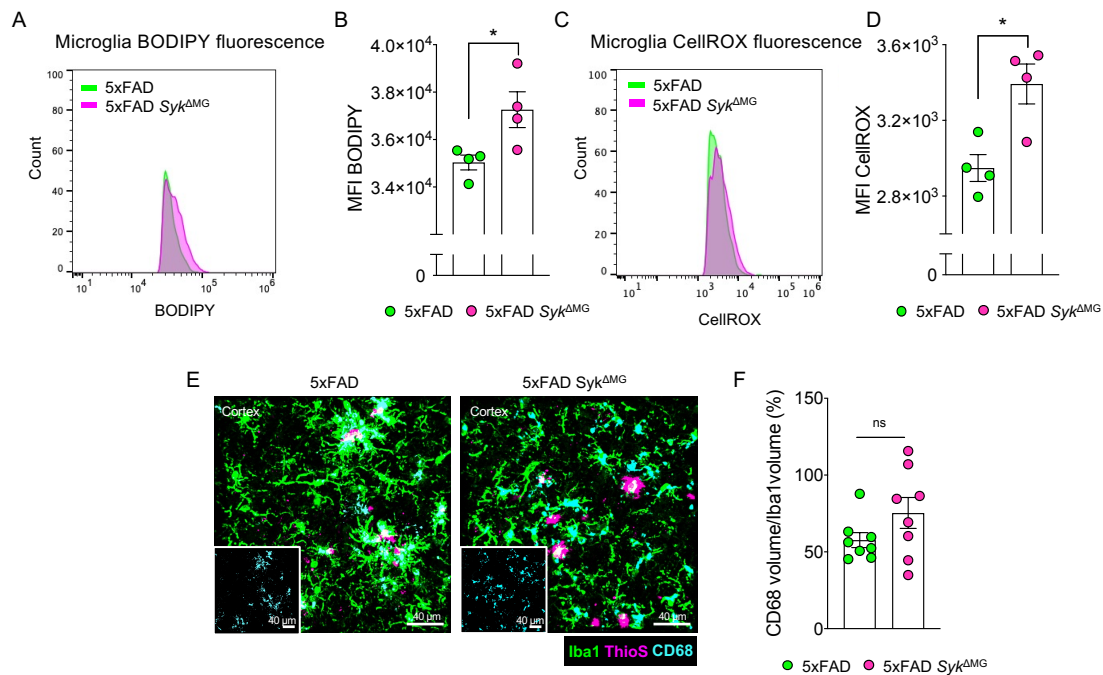


Figure 2.8. Genetic ablation of SYK in microglia leads to increased levels of microglial lipid droplet accumulation and ROS production in 5xFAD mice, related to Figure 5 (A-D) 5xFAD *Syk^{fl/fl}Cx3cr1^{ERT2Cre}* (5xFAD *Syk^{ΔMG}* mice) and Cre-negative 5xFAD *Syk^{fl/fl}* littermate controls (5xFAD mice) received tamoxifen food for 2 weeks starting at 4 months of age and then mice were returned to regular food for the remainder of the experiment. Microglia from 8-month-old 5xFAD *Syk^{ΔMG}* and 5xFAD mice were sorted from single-cell brain suspensions using flow-cytometry. (A) Representative histograms of BODIPY-labeled lipid-droplet accumulation in CD11b⁺CD45^{int} microglia. (B) Mean Fluorescence Intensity (MFI) quantification of BODIPY in 5xFAD and 5xFAD *Syk^{ΔMG}* microglia. (C) Representative histograms of CellROX-labeled reactive oxygen species (ROS) in CD11b⁺CD45^{int} microglia. (D) MFI quantification of CellROX in 5xFAD and 5xFAD *Syk^{ΔMG}* microglia. (E-F) 5xFAD *Syk^{ΔMG}* mice and Cre-negative 5xFAD mice received tamoxifen food for 2 weeks starting at 3 weeks of age and then mice were returned to regular food for the remainder of the experiment. Brains were later harvested and Iba1 staining was performed at 5 months of age to evaluate microglial activation. (E) 5xFAD *Syk^{ΔMG}* and 5xFAD microglia labeled with Iba1 (green) and CD68 (blue) surrounding Aβ plaques labelled with ThioS (pink). Original magnification: 63x; scale bar = 40 μm and 40 μm for image insets. (F) Volumetric quantification of CD68 normalized to Iba1 volume. Statistical significance between experimental groups was calculated by unpaired Student's *t*-test (B, D, F). ns = not significant, *p < 0.05. (B, D, F) Error bars represent mean ± S.E.M. and each data point represents an individual mouse.

2.3.6 Phagocytosis of Aβ is coordinated by SYK

DAMs have been shown to highly express multiple genes that are involved in phagocytosis, and this upregulation of phagocytic machinery is thought to be one of the ways in which DAMs can exert neuroprotective clearance of neurotoxic material in degenerative disease (93). Given that the loss of *Syk* limits microglia DAM marker expression and augments Aβ accumulation, we hypothesized that SYK may also play critical roles in microglial phagocytosis of Aβ in 5xFAD mice, which could help to explain the elevated deposition of Aβ seen in 5xFAD *Syk^{ΔMG}* mice (Figure 2.2). To investigate this possibility, we measured Aβ engulfment by microglia using immunohistochemistry and saw that 5xFAD microglia engulfed more than twice the amount of Aβ than 5xFAD *Syk^{ΔMG}* microglia (Figures 2.9A and 2.9B). Similarly, approximately twice the volume of Aβ was engulfed within CD68, a well-described marker of microglial phagolysosomes (380-382), in 5xFAD microglia compared with 5xFAD *Syk^{ΔMG}* microglia (Figures 2.9C and 2.9D). Notably, we noticed that 5xFAD *Syk^{ΔMG}* and 5xFAD microglia upregulated CD68 to comparable total levels across the cortex (Figures 2.8E and 2.8F). However, while much of the engulfed

A β detected in 5xFAD microglia colocalized with CD68, there was far less A β engulfed within CD68 in SYK-deficient 5xFAD microglia (Figure 2.9C and 2.9D).

These imaging data indicate that SYK is a pivotal regulator of A β phagocytosis in microglia. To further substantiate a role for microglial SYK in A β phagocytosis, we next explored this in a secondary experimental system. In these studies, 5-month-old 5xFAD *Syk* ^{Δ MG} mice and 5xFAD littermate controls received an intraperitoneal (i.p.) injection of Methoxy-X04 which is a brain penetrant dye that labels fibrillar A β . After 3 hours, we harvested brains from these mice to quantify the percentage of microglia that had taken up Methoxy-X04-labelled A β using flow cytometry. Approximately 20% of 5xFAD microglia had ingested A β (Methoxy-X04⁺) while almost none of the 5xFAD *Syk* ^{Δ MG} microglia contained Methoxy-X04-stained A β (Figures 2.9E and 2.9F). In total, these combined results provide evidence that SYK promotes the phagocytic capacity of microglia in response to A β .

We next explored what contributes to defective A β phagocytosis in 5xFAD *Syk* ^{Δ MG} mice. We turned our attention to GSK3 β signaling as this was found to be profoundly affected in 5xFAD *Syk* ^{Δ MG} microglia (Figure 2.6G and 2.6H). To this end, we pretreated WT and SYK-deficient bone marrow-derived macrophages (BMDMS) with the GSK3 β inhibitor Tideglusib and then evaluated phagocytosis of CypHer5E-tagged A β oligomers. CypHer5E fluoresces in a low pH environment such as the phagolysosome; therefore, we analyzed CypHer5E fluorescence by flow cytometry as a readout for A β phagocytosis. In these studies, we found that GSK3 β inhibition with Tideglusib treatment significantly increased A β phagocytosis in SYK-deficient macrophages (Figure 2.9G and 2.9H). This suggests that the dysregulated GSK3 β signaling that unfolds in the absence of SYK can contribute to defective phagocytosis of A β by macrophages.

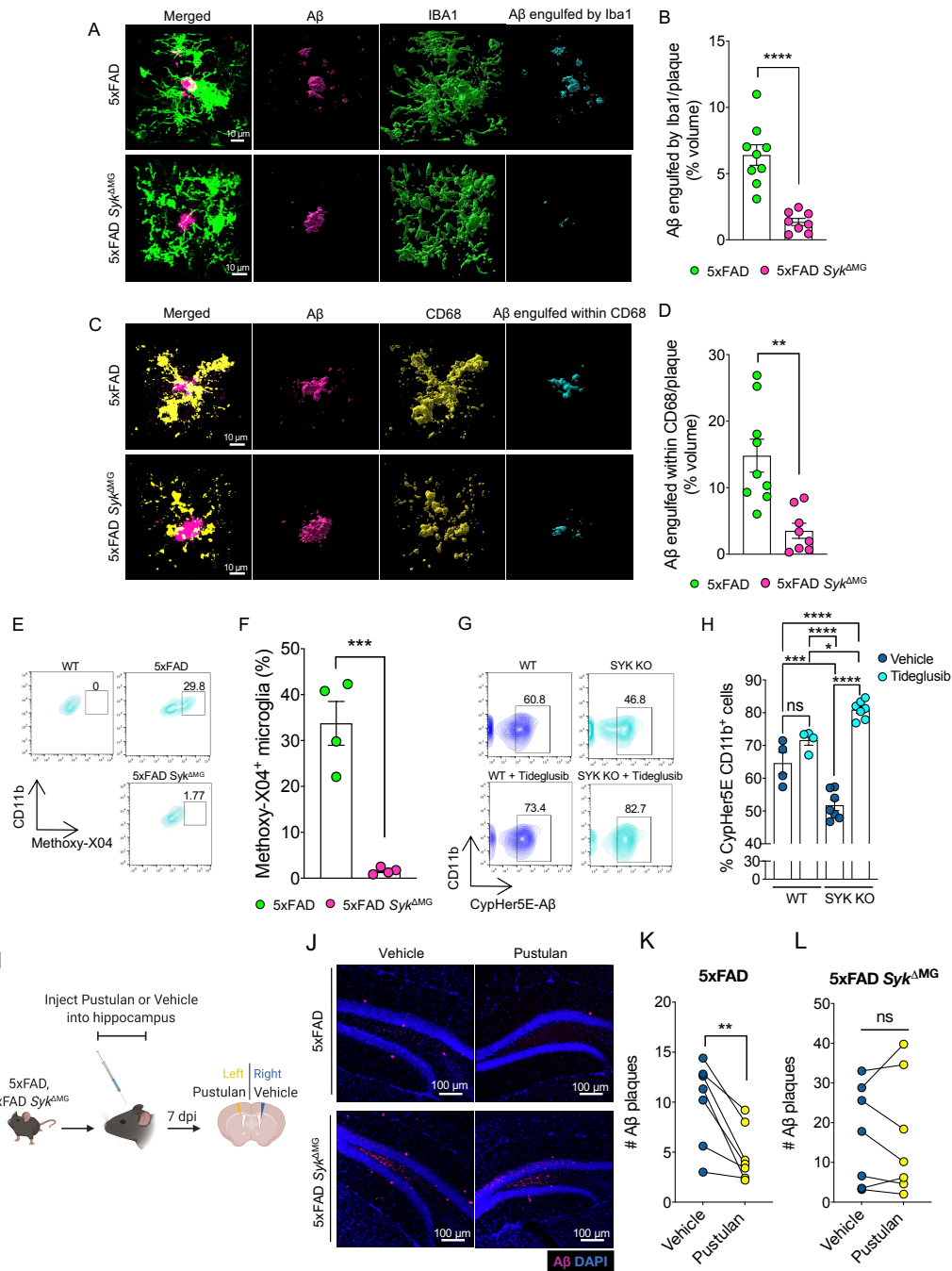


Figure 2.9. SYK is critical for microglial uptake and phagocytosis of Aβ (A-F) 5xFAD *Syk*^{fl/fl}*Cx3cr1*^{ERT2Cre} (5xFAD *Syk*^{ΔMG} mice) and Cre-negative 5xFAD *Syk*^{fl/fl} littermate controls (5xFAD mice) received tamoxifen food for 2 weeks starting at 3 weeks of age and then mice were returned to regular food for the remainder of the experiment. Brains were then harvested at 5 months of age to evaluate microglial phagocytosis. (A) Imaris-rendered Aβ plaques (ThioS, pink) and Iba1+ cells (green) with the completely localized Aβ-microglia (engulfed) channel in blue. Original magnification: 63x; scale bar = 10 μm. (B) Percent area of engulfment quantification from a total of ~20 plaques from 3 matching brain sections per mouse. (C) Imaris-rendered Aβ plaques (ThioS, pink) and CD68 (yellow) with the completely localized Aβ-CD68 (engulfed) channel in blue. Original magnification: 63x; scale bar = 10 μm. (D) Percent area of engulfment quantification from a total of ~20 plaques from 3 matching brain sections per mouse. (E-F) Mice received intraperitoneal injections of methoxy-X04 (labels fibrillar Aβ) and then microglial phagocytosis of Aβ was determined 3 hours later by performing flow cytometry staining to evaluate the uptake of methoxy-X04+ labeled Aβ. (E-F) Representative flow cytometry plots and quantification of the percentage of CD45^{int}CD11b^{hi} cells that had taken up methoxy-X04+ labelled Aβ. (G-H) WT and *Syk*^{fl/fl} *LysM*^{Cre} bone marrow-derived macrophages (BMDMs) pre-treated with vehicle or 10 μM Tideglusib, a GSK3β inhibitor, for 1 hour prior to treatment with 10 μM CypHer5E-tagged Aβ oligomers. Aβ phagocytosis by BMDMs was determined 24 hours later by measuring CypHer5E fluorescence by flow cytometry. (G-H) Representative flow cytometry plots and quantification of percent CypHer5E CD11b^{hi}F4/80^{hi} cells. (I-L) 10-week-old 5xFAD and 5xFAD *Syk*^{ΔMG} mice received bilateral intrahippocampal injections of vehicle and CLEC7A agonist pustulan. Seven days post injection (dpi) brains were harvested to measure Aβ load between matched vehicle and pustulan injected hippocampal hemispheres. (J) Representative immunofluorescence staining of D54D2-labeled Aβ (pink) in 5xFAD and 5xFAD *Syk*^{ΔMG} mouse hippocampal sections. (K-L) Mouse-matched quantification of Aβ in vehicle and pustulan injected hippocampal hemispheres, where each mouse is represented by two dots connected by a line. Statistical significance between experimental groups was calculated by unpaired Student's t-test (B, D, F), one-way ANOVA with multiple comparisons (H), and paired Student's t-test (K-L). *p < 0.05, **p < 0.01, ***p < 0.001, ****p < 0.0001. Error bars represent mean ± S.E.M. and each data point represents an individual mouse.

2.3.7 Exogenous activation of the CLEC7A-SYK signaling pathway promotes improved clearance of A β

Thus far, we have demonstrated that SYK-deficiency impairs microglial responses to A β pathology in 5xFAD mice. However, to reinforce the integral role for SYK in driving microglial response in this environment, we investigated if the reciprocal activation of SYK signaling would enhance protective microglial activities in the AD brain. To achieve this, we chose to induce SYK activation through CLEC7A, a receptor shown to be important for microglial activation in response to AD pathology. CLEC7A is a canonical fungal pathogen receptor that signals through SYK in the periphery and has recently been identified to be upregulated in Stage 2 DAMs (93, 383). In our studies presented here, we have identified SYK as critical for A β phagocytosis (Figures 2.9A-H); therefore, we aimed to determine if CLEC7A-stimulated SYK signaling could enhance microglial phagocytic response. Thus, we injected pustulan, a β -D-glucan and ligand for CLEC7A, into the hippocampus of 2-month-old 5xFAD and 5xFAD *Syk*^{ΔMG} mice. We chose the hippocampus due to its reliable accumulation of A β in 5xFAD mice. As an internal control, one hemisphere of the hippocampus received a vehicle injection, while the other hippocampal hemisphere received a pustulan injection. After 7 days, we harvested the brains from the injected mice and investigated levels of A β between the vehicle and pustulan-injected hippocampal hemispheres using immunofluorescence (Figure 2.9I). Strikingly, 5xFAD mice displayed decreased A β load in the pustulan-injected hippocampal hemisphere compared to the vehicle-injected hippocampal hemisphere (Figures 2.9J and 2.9K), indicating that pustulan-induced microglial CLEC7A activation is sufficient in stimulating A β clearance in the 5xFAD brain. In contrast, pustulan treatment in 5xFAD *Syk*^{ΔMG} mice did not promote A β clearance in the hippocampus (Figures 2.9J and 2.9L), suggesting that SYK is necessary for the protective CLEC7A-driven phagocytic response by microglia. Altogether, our data suggests that CLEC7A signals through SYK to promote protective microglial phagocytic response to A β .

2.3.8 DAM generation is regulated by SYK in demyelinating neuroinflammatory disease

Next, we investigated whether SYK also influences DAM generation and microglial biology in other models of neurological disease. As a first approach, we explored the impact of SYK deletion in microglia on demyelinating neuroinflammatory disease progression in the experimental autoimmune encephalomyelitis (EAE) mouse model of multiple sclerosis (MS). Importantly, microglia have previously been described to play pivotal roles in EAE disease progression (384). In particular, the clearance of myelin debris by microglia is believed to be critically required to limit neuronal damage in EAE (385-387). In our studies, we found that *Syk*^{ΔMG} mice develop exacerbated paralyzing disease and more severe demyelination in comparison to *Syk*^{con} littermate controls (Figures 2.11A-C). Interestingly, ablation of SYK in *Syk*^{ΔMG} mice was also found to have an effect on T cell responses in the EAE disease model. More specifically, we observed a modest, albeit statistically significant, increase in total T cell numbers, and more T cells producing GM-CSF, IFN- γ , and IL-17 in the spinal cords of *Syk*^{ΔMG} EAE mice relative to *Syk*^{con} EAE

controls during the effector phase of EAE disease (>30 days post-immunization) (Figure 2.10A-2.10E). Moreover, we detected less splenic CD4⁺ T cells making GM-CSF, IFN γ , and IL-17 in *Syk*^{ΔMG} EAE mice compared to *Syk*^{con} EAE controls when mice were harvested during the EAE effector phase (Figure 2.10F-2.10H). These collective findings point toward key neuroprotective roles for SYK in microglia during demyelinating neuroinflammatory disease.

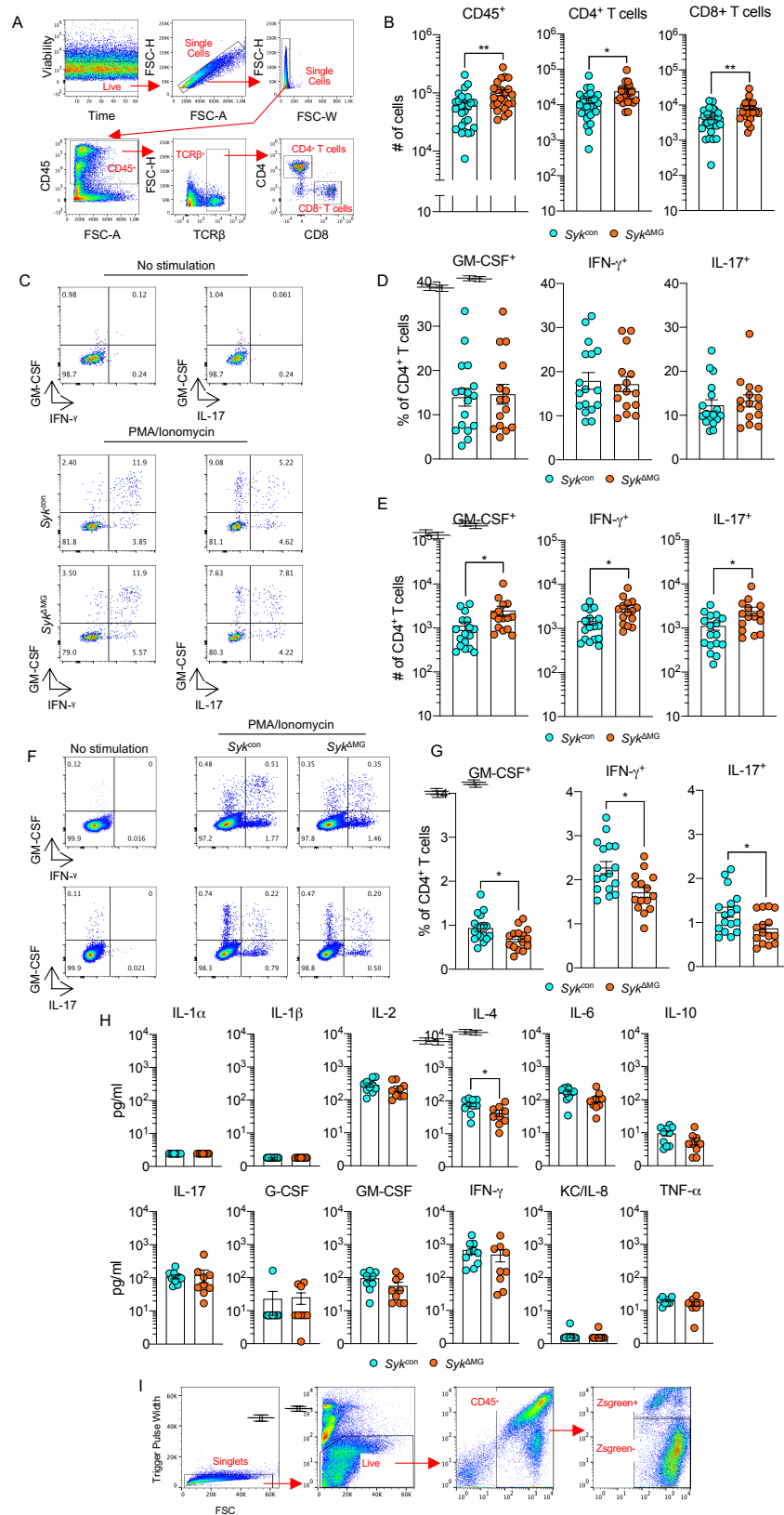


Figure 2.10. *Syk*^{ΔMG} mice have increased numbers of cytokine producing T cells infiltrating the CNS but have modestly reduced peripheral T cell responses during EAE, related to Figure 6 (A-H) *Syk*^{fl/fl} *Cx3cr1*^{ERT2Cre} (*Syk*^{ΔMG} mice) and Cre-negative *Syk*^{fl/fl} littermate controls (*Syk*^{con} mice) received tamoxifen food for 2 weeks starting at 3 weeks of age and then mice were returned to regular food for the remainder of the experiment. Mice were later immunized with MOG+CFA and pertussis toxin at 8-14 weeks of age to induce experimental autoimmune encephalomyelitis (EAE). (A-E) Spinal cords were then harvested from mice during the effector phase of clinical disease (at least 30 days post-immunization) to evaluate immune cell responses by flow cytometry. (A) Representative flow cytometry gating strategy. (B) Quantification of immune cell populations. (C) Representative dot plots of effector cytokine-producing CD4⁺ T cells after no stimulation or 5-hour *ex vivo* stimulation with PMA and ionomycin in the presence of monensin. (D) Quantification of the frequencies of effector cytokine producing CD4⁺ T cells. (E) Quantification of the total numbers of effector cytokine producing-CD4⁺ T cells. (F-H) Spleens were harvested from mice during the effector phase of clinical disease (at least 30 days post-immunization) to evaluate immune cell responses by flow cytometry. (F) Representative dot plots of EAE effector-cytokine producing CD4⁺ T cells from EAE effector phase spleens after no stimulation or 5-hour *ex vivo* stimulation with PMA and ionomycin in the presence of monensin. (G) Quantification of effector cytokine production by CD4⁺ T cells. Data are combined from 2 independent experiments. (H) Quantification of secreted cytokine levels in culture media from *Syk*^{con} and *Syk*^{ΔMG} EAE effector phase splenocytes stimulated *ex vivo* with MOG₃₅₋₅₅ peptide for 48 hours. Levels of indicated analytes were measured by multiplex cytokine assay. (I) Flow cytometry-based sorting of ZsGreen⁺ microglia from *Syk*^{ΔMG-Ai6} and *Syk*^{con-Ai6} mice. *Syk*^{ΔMG} and *Syk*^{con} mice were crossed onto the Ai6-ZsGreen reporter background (denoted as *Syk*^{ΔMG-Ai6} and *Syk*^{con-Ai6} mice) to isolate microglia in the EAE disease model. Spinal cords were harvested from mice on day 35 post-immunization and single-cell RNA-sequencing was performed on FACS-sorted ZsGreen⁺ microglia. Statistical significance between experimental groups was calculated by unpaired Student's *t*-test (B, D-E, G-H). **p* < 0.05, ***p* < 0.01. Error bars represent mean ± S.E.M. and each data point represents an individual mouse.

Having seen that SYK ablation in *Syk*^{ΔMG} mice leads to more severe demyelinating neuroinflammatory disease, we next wanted to better understand how SYK influences microglial responses in EAE. Given our results in the 5xFAD model, we were particularly interested in interrogating whether SYK also instructs DAM generation and modulates microglial transcriptional expression of phagocytic machinery in this separate model of neurodegenerative disease. To accomplish this in a comprehensive and unbiased fashion, we conducted single-cell RNA-sequencing (scRNA-seq) on sorted spinal cord macrophages. In comparison to the 5xFAD AD mouse model, where it has been shown that there is negligible recruitment of peripherally-derived myeloid cells into the CNS (87, 100), disease progression in EAE is characterized by massive infiltration of various circulating myeloid cell types into the spinal cord (388). This ultimately makes it challenging to unequivocally differentiate between bona fide microglia and CNS-infiltrating myeloid cells using traditional cell sorting techniques (e.g. flow cytometric sorting on CD11b⁺ cells). Therefore, to circumvent this technical limitation associated with the EAE model, we crossed *Syk*^{+/+} *Cx3cr1*^{ERT2Cre} and *Syk*^{fl/fl} *Cx3cr1*^{ERT2Cre} mice with the Ai6-ZsGreen reporter mouse line to target Ai6-ZsGreen expression to *Cx3cr1*-expressing cells. The Ai6-ZsGreen model has been adopted by others in the field to purify CNS-resident macrophages in settings where peripheral-derived myeloid cells are expected to infiltrate the CNS (389, 390). Ai6-ZsGreen reporter mice possess a LoxP-flanked STOP cassette that prevents the expression of green fluorescent protein variant ZsGreen1 until the stop site is excised after tamoxifen induction of Cre-recombinase activity. Following the withdrawal of tamoxifen, short-lived Ai6-ZsGreen expressing cells in the periphery are promptly replaced by newly derived cells that lack Ai6-ZsGreen expression. In contrast, the long-lived nature of microglia allows them retain their Ai6-ZsGreen signal for months post-tamoxifen withdrawal (391).

In our studies, we purified ZsGreen⁺ cells from the spinal cords of Ai6-ZsGreen *Syk*^{+/+} *Cx3cr1*^{ERT2Cre} (*Syk*^{con-Ai6}) and Ai6-ZsGreen *Syk*^{fl/fl} *Cx3cr1*^{ERT2Cre} (*Syk*^{ΔMG-Ai6}) mice at day 35 post-EAE induction using flow cytometry-based cell sorting (Figure 2.10I). Utilizing scRNA-seq, we uncovered 6 unique microglia populations, including homeostatic microglia, highly metabolic microglia, M1-like microglia, and M2-like

microglia (Figure 2.11D). We also identified a unique population of microglia that we denoted as CD36hi microglia, as *Cd36* was one of the top-defining genes of this cluster and it failed to conform with other known microglia types (Figures 2.11D and 2.11E). The final microglia cluster highly expressed the canonical genes of DAMs, including *Cst7*, *Lpl*, *Spp1*, *Tyrobp*, and *Itgax* (Figures 2.11D and 2.11E).

To understand if microglia followed a trajectory in their maturation state during EAE and if this was influenced by SYK, we performed a pseudotime analysis of the microglia transcriptional data. After establishing homeostatic microglia as the earliest point in pseudotime, three potential pathways were revealed: a homeostatic to highly metabolic and M1-like microglia pathway, a homeostatic to CD36hi pathway, and a homeostatic to DAM and M2-like pathway (Figure 2.11F). When comparing the distribution of cells in each cluster by *Syk*^{con-Ai6} vs. *Syk*^{ΔMG-Ai6}, we observed that *Syk*^{con-Ai6} microglia tend to follow the homeostatic to DAM and M2-like pathways more than *Syk*^{ΔMG-Ai6} microglia (Figures 2.11F and 2.11G). In contrast, *Syk*^{ΔMG-Ai6} microglia, when compared to *Syk*^{con-Ai6} microglia, more commonly followed the homeostatic to CD36hi trajectory (Figures 2.11F and 2.11G). These pathway biases are confirmed by the proportion of cells in each cluster by sample, where the *Syk*^{con-Ai6} samples have a higher proportion of DAM microglia and the *Syk*^{ΔMG-Ai6} samples have a higher proportion of CD36hi microglia and few DAMs (Figure 2.11H). Therefore, *Syk*^{ΔMG-Ai6} microglia appear to be less apt to acquire DAM transcriptional status in the EAE model of demyelinating neuroinflammatory disease.

Interestingly, the *Syk*^{ΔMG-Ai6} samples also have a higher proportion of homeostatic microglia when compared to microglia isolated from *Syk*^{con-Ai6} mice (Figure 2.11H). To further examine the failure of *Syk*^{ΔMG-Ai6} microglia to take on a DAM transcriptional signature, we generated feature plots to visualize gene expression of DAM markers: *Cst7*, *Lpl*, *Itgax*, and *Spp1* by cluster (Figure 2.11I). We observed that *Syk*^{ΔMG} microglia in the DAM cluster had much lower average expression of these DAM genes compared with microglia obtained from *Syk*^{con-Ai6} mice (Figure 2.11I). Finally, to better understand the biological processes potentially being driven by the DAM cluster, we used DAM-defining genes to plot KEGG and GO terms related to phagocytosis. These shared terms included “phagosome,” “abnormal phagocyte morphology,” and “microglia pathogen phagocytosis pathway,” and shared phagocytosis genes such as *Trem2*, *Tyrobp*, *C1qa*, *Lamp1*, *Cd68*, and *Cd22* (Figure 2.11J). In summary, our collective EAE findings corroborate our 5xFAD data characterizing SYK as a pivotal intracellular regulator of DAM generation and promoter of neuroprotective functions in microglia during neurodegenerative disease.

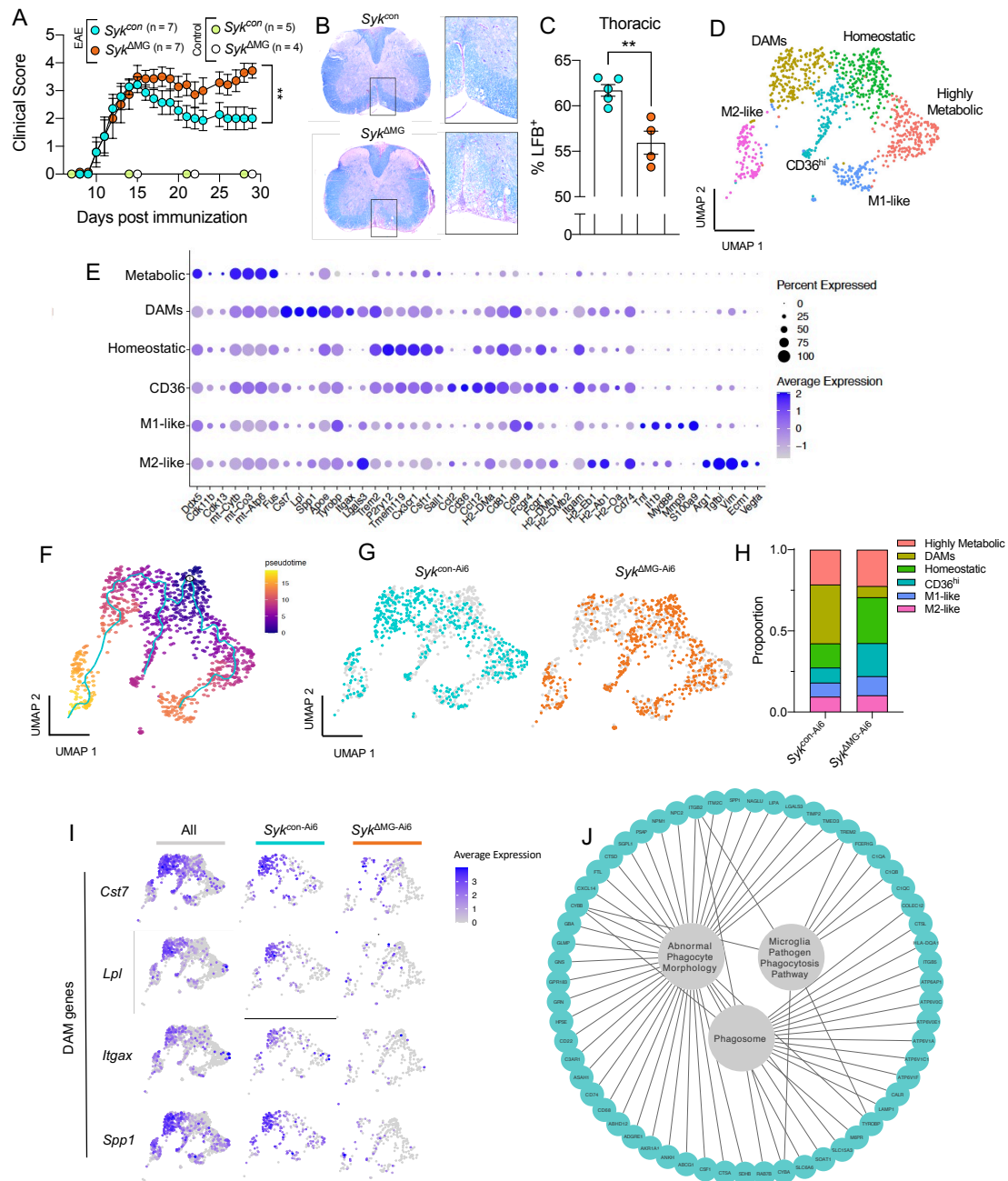


Figure 2.11. Syk-deletion in microglia impedes the formation of DAMs in EAE (A-C) *Syk^{fl/fl} Cx3cr1^{ERT2Cre} (Syk^{ΔMG} mice)* and Cre-negative *Syk^{fl/fl}* littermate controls (*Syk^{con}* mice) received tamoxifen food for 2 weeks starting at 3 weeks of age and then mice were returned to regular food for the remainder of the experiment. Mice were then immunized with MOG+CFA and pertussis toxin at 8-14 weeks of age to induce experimental autoimmune encephalomyelitis (EAE). Control mice did not receive EAE induction. (A) Severity of hind-limb paralysis was assessed using a 5-point clinical scoring system. (B-C) Representative images and quantification of spinal cords stained with Luxol fast blue (LFB) to evaluate demyelination. (D-J) *Syk^{+/+} Cx3cr1^{ERT2Cre}* and *Syk^{fl/fl} Cx3cr1^{ERT2Cre}* were crossed onto the Ai6-ZsGreen reporter background (denoted as *Syk^{con-Ai6}* and *Syk^{ΔMG-Ai6}* mice) to isolate microglia in the EAE disease model. *Syk^{con-Ai6}* and *Syk^{ΔMG-Ai6}* mice received tamoxifen food for 2 weeks starting at 3 weeks of age and then mice were returned to regular food for the remainder of the experiment. Mice were then immunized with MOG+CFA and pertussis toxin at 8-14 weeks of age to induce EAE. Spinal cords were harvested from mice on day 35 post-immunization and single-cell RNA-sequencing was performed on FACS-sorted ZsGreen⁺ microglia. (D) Uniform Manifold Approximation and Projection (UMAP) representation of combined *Syk^{con-Ai6}* and *Syk^{ΔMG-Ai6}* microglia cell populations. (E) A dot plot representation of cluster defining genes for each cell population, where the genes represent some of the most significant cluster-defining markers for each cluster. (F) UMAP representation of pseudotime cellular trajectory profiles showing microglia maturation trajectories. (G) UMAP representation of the cell populations present in each of the clusters. (H) Breakdown of cluster proportions. (I) Feature plots depicting several DAM genes. (J) Plotted KEGG and GO terms related to phagocytosis using defining genes of the DAM cluster. Statistical significance between experimental groups was calculated by non-parametric Mann-Whitney U-test (A) and unpaired Student's t-test (C). **p < 0.01. Error bars represent mean ± S.E.M. and each data point represents an individual mouse (C).

2.3.9 Defective SYK signaling in microglia during demyelinating disease causes damaged myelin debris accumulation and impaired oligodendrocyte proliferation

To further validate the ability of SYK to modulate microglial responses in a separate model of demyelinating disease that does not involve autoimmune attack, we explored the effects of cuprizone intoxication on neurological disease in *Syk*^{ΔMG} mice and *Syk*^{con} littermate controls. Cuprizone is toxic to myelinating oligodendrocytes, including those found in the corpus callosum, thus 5 continuous weeks of feeding cuprizone to mice leads to a localized areas of demyelination (392). Importantly, we observed no appreciable changes in myelin basic protein (MBP) levels in the corpus callosum of *Syk*^{ΔMG} and *Syk*^{con} mice, indicating that myelination at steady-state is not affected in SYK-deficient mice (Figures 2.13A and 2.13B). However, we noticed that the corpus callosum of *Syk*^{ΔMG} mice had significantly fewer microglia than *Syk*^{con} controls during both cuprizone-induced demyelination and remyelination (Figures 2.13C and 2.13D). We determined that the decreased number of microglia in *Syk*^{ΔMG} mice is likely not due to differential apoptosis using TUNEL staining (Figures 2.13E and 2.13F). Consistent with previous studies, we found that feeding wild-type *Syk*^{con} mice cuprizone diet leads to increased staining of the phagocytic marker CD68 in Iba1⁺ cells (Figures 2.13G and 2.13H) (387). In contrast, CD68 positivity was substantially decreased in Iba1⁺ cells found in the corpus callosum of cuprizone-fed *Syk*^{ΔMG} mice during the demyelinating phase (Figures 2.13G and 2.13H), suggesting impaired phagocytic microglial response compared to *Syk*^{con} mice. Indeed, increased damaged myelin basic protein (dMBP) accumulation was evident during both demyelination and remyelination in the *Syk*^{ΔMG} corpus callosum compared with *Syk*^{con} mice (Figures 2.12A and 2.12B). Microglia are established to phagocytose damaged myelin in the cuprizone model of demyelination; therefore, this accumulation is likely due to a microglial phagocytic deficit (393). These results provide evidence that SYK signaling in microglia is critically involved in the clearance of myelin debris independent of the robust autoimmune response associated with EAE.

The inability to phagocytose myelin debris in the cuprizone model is known to obstruct aspects of oligodendrocyte biology including the differentiation of oligodendrocyte precursor cells (OPCs) into myelin-producing oligodendrocytes (394). Therefore, we hypothesized that any phagocytic deficits seen in *Syk*^{ΔMG} mice in the cuprizone model would subsequently manifest as impaired OPC proliferation and/or differentiation into mature oligodendrocytes during the remyelination phase that follows cuprizone cessation. Consistent with this hypothesis, we found that SYK deficiency in cuprizone-treated *Syk*^{ΔMG} mice leads to greatly reduced numbers of OPCs (Olig2⁺Pdgfra⁺ cells) and oligodendrocytes (Olig2⁺CC1⁺ cells) during the remyelination phase of the cuprizone model (Figures 2.12C-2.12E). We also noted that OPCs in cuprizone-treated *Syk*^{ΔMG} mice had severely impaired proliferation during demyelination (Figures 2.13I and 2.13J), which likely accounts for the decreased numbers of OPCs and oligodendrocytes seen in *Syk*^{ΔMG} mice following cuprizone treatment. In comparison, we observed comparable numbers of OPCs and oligodendrocytes in *Syk*^{ΔMG} mice and *Syk*^{con} littermate controls that were fed normal chow (Figures 2.12C-2.12E), suggesting that SYK deficiency in microglia does not appreciably affect oligodendrocyte-lineage cell numbers under homeostatic conditions. Our findings indicate that disruption of SYK signaling

in microglia causes prominent defects in the clearance of damaged myelin in the cuprizone model of demyelinating disease. Moreover, they suggest that the lack of neuroprotective functions in SYK-deficient microglia can ultimately lead to impaired oligodendrocyte generation during remyelination. Altogether, these cuprizone data support our 5xFAD and EAE findings that define a critical role for SYK in promoting protective microglial responses that limit neurodegenerative disease progression.

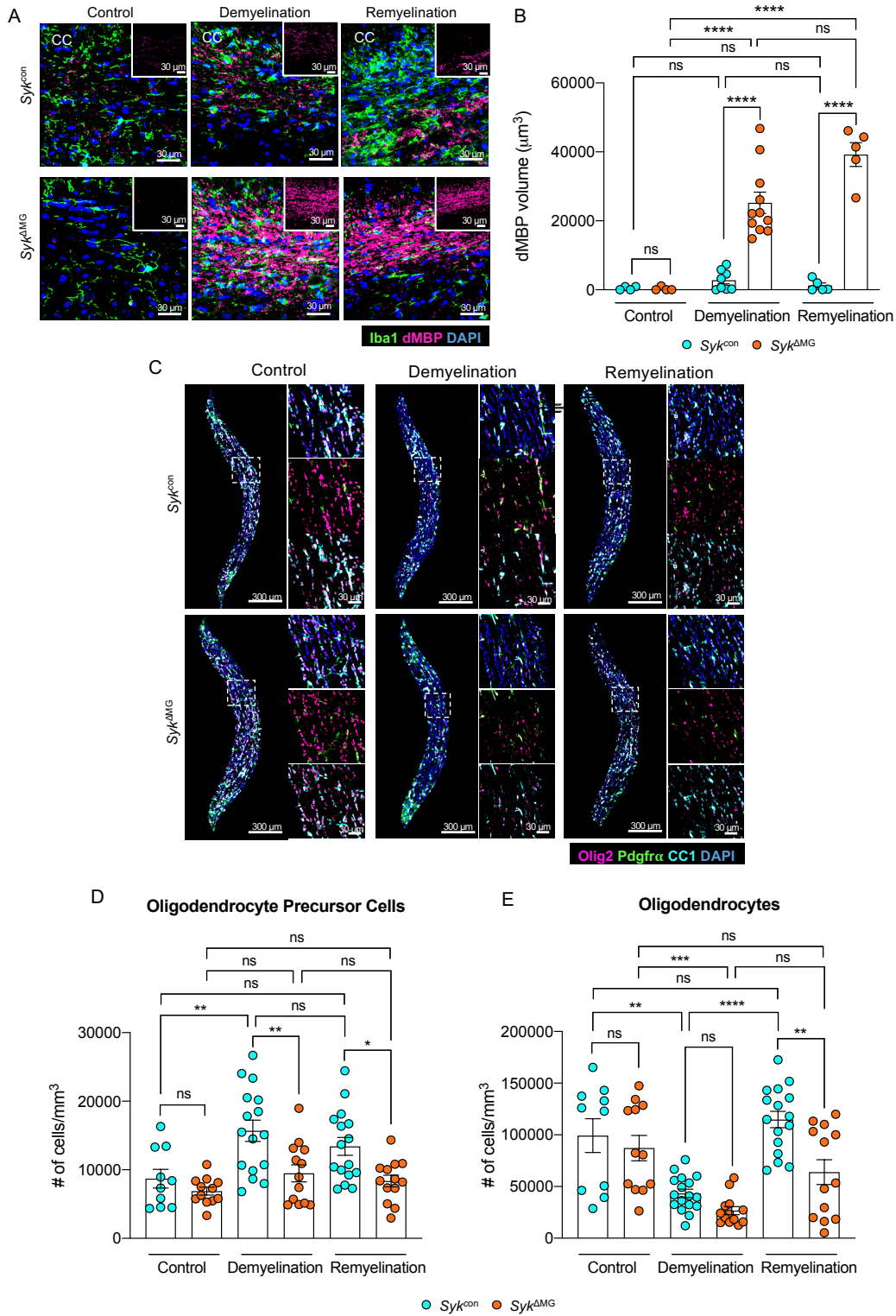


Figure 2.12. Disruption of SYK signaling in microglia during demyelinating disease leads to accumulation of damaged myelin debris and impaired oligodendrogenesis (A-E) *Syk^{fl/fl} Cx3cr1^{ERT2Cre}* (*Syk^{ΔMG}* mice) and Cre-negative *Syk^{fl/fl}* littermate controls (*Syk^{con}* mice) received tamoxifen food for 2 weeks starting at 3 weeks of age and then mice were returned to regular food for the remainder of the experiment. Adult (8–12-month-old) mice were later fed a diet consisting of 0.3% cuprizone for 5 weeks to induce demyelination. Mice were then either harvested after 5 weeks of cuprizone treatment (demyelination group) or returned to normal chow for one additional week before being harvesting (remyelination group). Control mice were not introduced to the cuprizone diet. (A) Representative images of microglia labeled with Iba1 (green) and damaged myelin basic protein (MBP; pink) expression in the corpus callosum. Original magnification: 40x; scale bar = 30 μm and 30 μm for image insets. (B) Quantification of dMBP volume in the corpus callosum. (C) Representative images of oligodendrocyte lineage markers in the corpus callosum. Original magnification: 40x; scale bar = 300 μm and 30 μm for image insets. (D-E) Quantification of the number of Pdgfra⁺ Olig2⁺ oligodendrocyte precursor cells (D) and number of CC1⁺ Olig2⁺ mature oligodendrocytes (E) in the corpus callosum. Statistical significance between experimental groups was calculated by one-way ANOVA with multiple comparisons (B, D, E). ns = not significant, *p < 0.05, **p < 0.01, ***p < 0.001, ****p < 0.0001. Data are mean ± S.E.M and combined from two independent experiments and each data point represents an individual mouse.

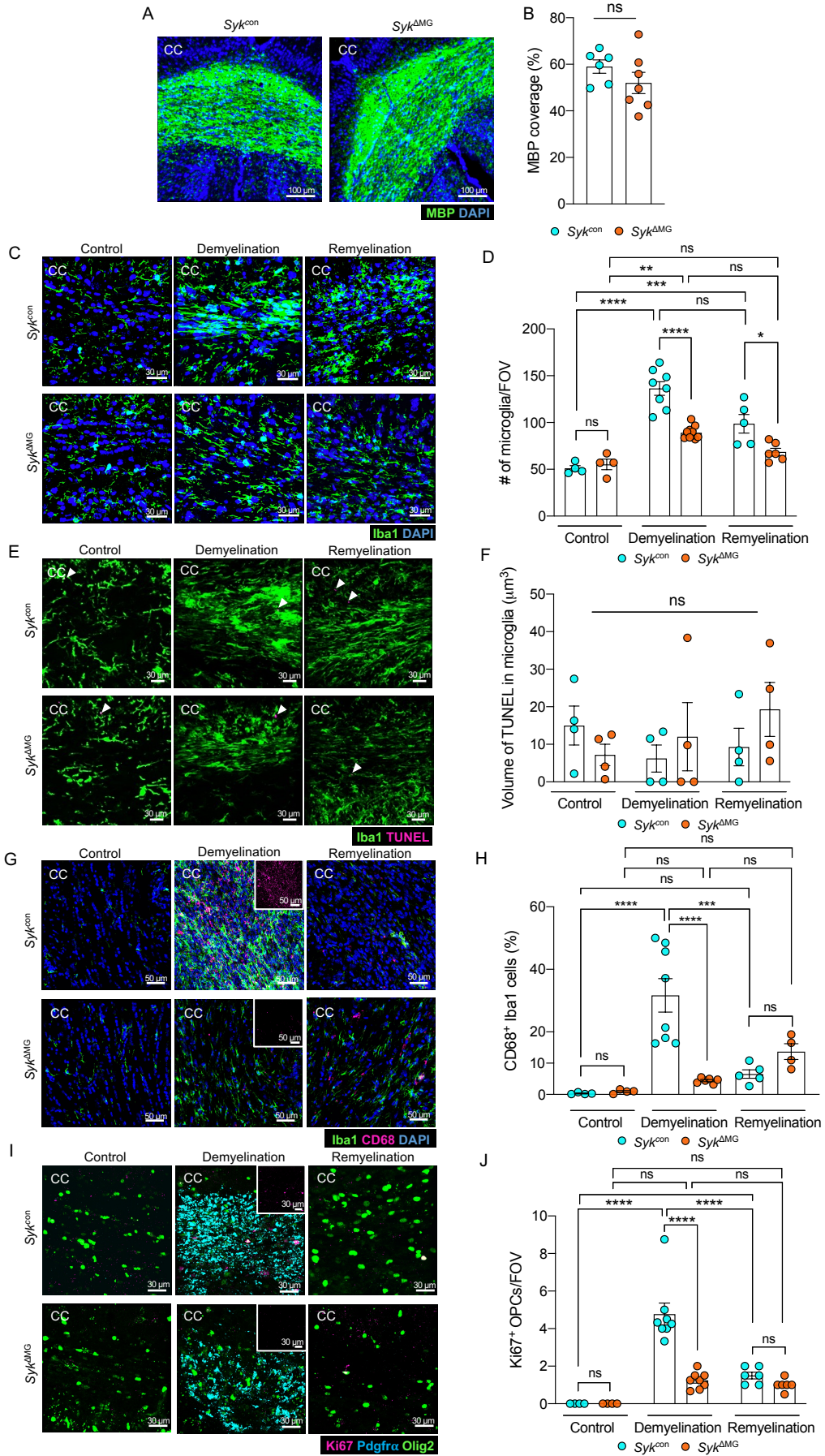


Figure 2.13. Disruption of SYK signaling in microglia during demyelinating disease leads to impaired microglial response and reduced OPC proliferation, related to Figure 7 (A-B) *Syk^{fl/fl} Cx3cr1^{ERT2Cre}* (*Syk^{ΔMG}* mice) and Cre-negative *Syk^{fl/fl}* littermate controls (*Syk^{con}* mice) received tamoxifen food for 2 weeks starting at 3 weeks of age and then mice were returned to regular food for the remainder of the experiment. Mice were harvested at 8 months of age and total myelin levels were evaluated in the corpus callosum. (A) *Syk^{ΔMG}* mice and *Syk^{con}* corpus callosum labeled with myelin basic protein (MBP; green) and DAPI (blue). Original magnification: 20x; scale bar = 1000 μm. (B) Quantification of percent area covered by MBP in the corpus callosum at baseline. (C-J) *Syk^{ΔMG}* mice and *Syk^{con}* mice received tamoxifen food for 2 weeks starting at 3 weeks of age and then mice were returned to regular food for the remainder of the experiment. Adult (8–12-month-old) mice were later fed a diet consisting of 0.3% cuprizone for 5 weeks to induce demyelination. Mice were then either harvested after 5 weeks of cuprizone treatment (demyelination group) or returned to normal chow for one additional week before being harvested (remyelination group). Control mice were not introduced to the cuprizone diet. (C-D) Representative images and quantification of the number of Iba1⁺ cells (green) in the corpus callosum. Original magnification: 63x; scale bar = 30 μm. (E-F) Representative images and quantification of microglial apoptosis measured by TUNEL⁺ volume (pink) in Iba1⁺ microglia (green) in the corpus callosum. Original magnification: 63x; scale bar = 30 μm. (G) Representative images of Iba1⁺ microglia (green) and CD68 (pink) expression in the corpus callosum. Original magnification: 40x; scale bar = 50 μm and 50 μm for image insets. (H) Volume of CD68 colocalized to the volume of Iba1 in the corpus callosum. (I) Representative images of proliferating Ki67⁺ (pink) Pdgfra⁺ Olig2⁺ (blue; green) oligodendrocyte precursor cells (OPCs) in the corpus callosum. Original magnification: 63x; scale bar = 30 μm and 30 μm for image insets. (J) Quantification of Ki67⁺ OPCs in the corpus callosum. Statistical significance between experimental groups was calculated by unpaired Student's *t*-test (B) and one-way ANOVA with multiple comparisons (D, F, H, J). ns = not significant, **p* < 0.05, ***p* < 0.01, ****p* < 0.001, *****p* < 0.0001. Data are mean ± S.E.M and combined from two independent experiments and each data point represents an individual mouse.

2.4 Discussion

Human GWAS and sequencing studies conducted over the last few years have helped to uncover an ever-increasing link between microglial dysfunction and various neurodegenerative disorders (93, 95, 96, 395). This has spurred tremendous recent efforts to reveal how microglial biology contributes to degenerative disease. For instance, the identification of the link between mutations in *Trem2* and *Cd33* in human AD has led to breakthroughs in our understanding of how these microglial receptors affect neurobiology in multiple neurodegenerative disease models (34, 97, 100, 385). Emerging from this collective work is the idea that microglia can play both neuroprotective and deleterious roles in neurological disease pathogenesis (86, 100, 102, 230, 242, 244, 384, 396-399). However, what accounts for the acquisition of damaging versus beneficial functions by microglia is still a matter of great debate in the field. Despite this, recent advances have begun to uncover some of the major transcriptional networks and effector mechanisms that underpin the ability of microglia to impact neurodegenerative disease susceptibility and progression.

While numerous mechanisms have been proposed to date, it has become increasingly clear that the ability of microglia to corral and phagocytose neurotoxic material is essential for them to exert their neuroprotective effects in degenerative disease (100, 102, 120, 396). Consistent with this idea, recent studies demonstrate that TREM2 is deployed by microglia to coordinate both the containment and phagocytosis of Aβ and dead cells in an effort to limit Aβ-driven neurodegenerative disease (97, 400). CD33, on the other hand, has been shown to inhibit the ability of microglia to phagocytose Aβ (35). In line with this, gain-of-function mutations in CD33 have been strongly linked with AD risk in humans (34). It has also been proposed that aging-related defects in phagocytosis contribute to the increased risk of developing neurodegenerative disease later in life (401). This has motivated many groups to perform screens in search of the molecular players that underlie age-associated decline in microglial phagocytosis. In one such study, it was shown that the receptor CD22 hinders microglial phagocytic capacity during aging (113). Furthermore, this study reported that antibody-based blockade of CD22 provides an effective

strategy to boost the phagocytosis of both A β and myelin debris. While great strides have been made in recent years in defining some of the surface receptors that modulate microglial biology in neurodegenerative disease, the identity of the key intracellular signaling molecules exploited by microglia to regulate their neuroprotective functions is currently less well understood.

In the studies presented here, we have identified SYK as a pivotal intracellular regulator of neuroprotective microglial responses in mouse models of both AD and MS. We demonstrate that SYK is critically involved in the acquisition of a DAM phenotype in neurodegenerative disease and that disruption of this key signaling hub in microglia causes pronounced deficits in microglial activation, including defective A β phagocytosis and stunted proliferation in response to AD-associated neuropathology. These defects in SYK-coordinated microglial responses were further shown to cause exacerbated neuritic dystrophy, neuronal cell death, and cognitive impairment in the 5xFAD mouse model of AD. It is important to note that replacing one allele of *Cx3cr1* with Cre-recombinase in *Cx3cr1*^{ERT2cre} mice may potentially affect aspects of microglial biology. However, in a recent study it was shown that targeting microglia with this strategy actually leads to improved clearance of A β and ameliorated disease progression in the APP/PS1 mouse model of AD (402). Therefore, our observation of worsened disease status in 5xFAD *Syk*^{AMG} is likely not explained by this variable. In addition, future studies are also needed to ascertain whether SYK deletion in long-lived BAMs contributes at any level to the phenotypes seen in our *Syk*^{AMG} studies. Nevertheless, we found that the loss of SYK in microglia leads to more severe demyelinating neuroinflammatory disease in the EAE model of MS. Using scRNA-seq we revealed that SYK is centrally involved in microglial acquisition of a DAM signature during EAE. Finally, by adopting cuprizone as an alternative model of demyelinating disease, we observed that disruption of SYK signaling in microglia also leads to defects in microglial phagocytosis and subsequent impairments in oligodendrocyte lineage cell repopulation. Taken together, our findings suggest that SYK is a key regulator of microglial activation and phagocytosis in response to both A β - and myelin-driven neurodegenerative disease.

Tremendous efforts in recent years have also been paid to defining how microglial responses evolve during the course of neurodegenerative disease in hopes of unearthing key transcriptional signatures and molecular players that influence disease progression. Emerging from these collective studies is the notion that microglia take on a neuroprotective DAM phenotype during neurodegenerative disease progression, and that this transformation is meant to equip them with the machinery needed to properly contain and dispose of neurotoxic material (93). This transition is characterized by the downregulation of homeostatic genes such as *Tmem119* and *P2ry12*, and the concomitant upregulation of DAM and neurodegenerative disease-associated microglia (MGnDs) factors that include *Lpl*, *Ccl6*, *Clec7a*, and *Cst7* (93, 94). While this paradigm of microglial activation has been extensively studied and adopted in multiple models of neurological disease, we currently lack knowledge of the key signaling molecules that instruct this important transformation in microglia. From the studies presented here, we have identified SYK as a novel

intracellular coordinator of microglia transition from a resting state to a DAM phenotype in mouse models of both AD and MS.

SYK is perhaps best known for its essential roles in the generation of protective immunity against many fungal infections as well as in the regulation of T cell and B cell receptor signaling (403-405). However, in recent years there has been growing appreciation for the critical involvement of SYK in models of sterile inflammation that do not involve microbes (406). In particular, it has been shown that SYK activation occurs following stimulation with various damage-associated molecular patterns (DAMPs) released from damaged or dying cells and that SYK-directed signaling in these scenarios induces robust immune responses (340, 407). While there has been some initial progress made in identifying key roles for SYK in sterile inflammatory disorders that affect peripheral organs, far less is known in regards to how SYK signaling affects neurological health and disease. That being said, the SYK homolog in *Drosophila*, known as Shark, was shown to be critical for glial phagocytosis of axonal debris (408). In addition, there have been a handful of recent studies that have used pharmacological inhibitors and *in vitro* cell culture systems to begin to explore how SYK affects CNS biology (348). For instance, it has been demonstrated that SYK activation, as indicated by phospho-SYK staining, is highly upregulated in plaque- and tau-associated microglia (347), and that SYK inhibitors can lead to phagocytic impairments in immortalized cells (409). It was also recently shown that systemic treatment with the SYK inhibitor piceatannol limits neurological disease progression in a mouse model of ischemia stroke (410). However, the specific cell types in which SYK acts to affect ischemic stroke still remain to be determined. Given the important roles for both peripheral immune cells and CNS-resident cells in ischemic stroke, it is possible that SYK could be functioning in multiple cell types to influence neurological disease progression in this model.

Older studies have also reported that treatment with the blood pressure-lowering drug, Nilvadipine, is effective in attenuating tau hyperphosphorylation and A β production both in cell culture studies and mouse models of AD (348). Nilvadipine was originally developed to be a calcium channel blocker (411); however, it was later found to also limit SYK activity to some degree (348, 412). This led Paris et al. to conclude that the beneficial effects that they saw with Nilvadipine treatment in AD models were likely due to its ability to modulate SYK (348). These Nilvadipine findings are contrary to our results demonstrating that disruption of SYK in microglia leads to exacerbated A β pathology and neuropathology in the 5xFAD mouse model of AD. Moreover, our findings suggest that SYK agonists, and not inhibitors as suggested in the Nilvadipine studies, would be most effective in the treatment of AD. The discrepancies between our findings and the previous Nilvadipine work could be explained by various reasons. For one, the ability of Nilvadipine to dampen AD-related pathology could be related to its potent blockade of calcium channels (413) and have little to do with its secondary effects on SYK. Or, considering the fact that Nilvadipine treatment targeted all cells and not just microglia in these previously published studies (Paris et al., 2014), the possibility also exists that SYK can impact disease through its actions in other CNS-resident cells

and/or peripheral cells. Regardless, these previous Nivradipine studies and the findings presented here highlight the need for additional studies to dissect the effects of SYK in neurodegenerative disease, and to also test the efficacy of other SYK targeting approaches to treat neurodegenerative disease.

The role of SYK in demyelinating neuroinflammatory disease also currently remains poorly described. This is surprising given that mutations in various SYK-related molecules have been identified as prominent MS genetic risk factors (414, 415). For instance, mutations in multiple upstream activators of SYK including CD37, TREM2, numerous C-type lectin receptors (e.g., CLEC16A, CLECL1, and CLEC2D), and Fc receptor-like proteins (i.e., FCRL2 and FCRL3) have been strongly linked to MS in GWAS studies (337, 415). Likewise, mutations in downstream molecules involved in SYK signaling including BCL10 and MALT1 have also been associated with MS risk (416, 417). It should, however, be noted that one recent study has provided some initial insights into how SYK can potentially impact EAE disease progression (418). Here it was shown that pharmacological inhibition of SYK in bone marrow-derived neutrophils abrogates the expression of oncostatin M, a neuroprotective molecule that was identified by this group as a novel attenuator of demyelinating neuroinflammatory disease progression (418).

In summary, while pivotal roles for microglia have recently been uncovered in AD, MS, and many other neurodegenerative disorders (51, 97, 105, 107, 113, 336), the key signaling pathways that microglia leverage to instruct neuroprotective functions remain poorly defined. Through the studies presented here, we have identified SYK as an instrumental regulator of neuroprotective responses in mouse models of AD and MS. Moreover, our studies suggest that targeting SYK may offer novel strategies to boost microglial protective responses, including phagocytosis of neurotoxic material, to treat neurodegenerative disease.

2.5 Limitations of the study

Future studies are needed to fully define all of the key microglial receptors that rely on SYK to influence neurodegenerative disease progression. Based on receptor structure alone, there are a wide-range of microglial receptors that could potentially leverage SYK to coordinate their effects on neuropathogenesis. Most notably, and of relevance to neurodegenerative disease research, this list includes TREM2, CLEC7A, CD33, CD22, Fc γ R, and complement receptor 3 (CR3) (113, 410, 419-422). However, various other CLEC receptors, SIGLEC receptors, and integrin receptors could also potentially leverage SYK signaling to influence neurological disease. Importantly, targeting a major shared intracellular signaling pathway, such as SYK, may prove more effective than targeting individual receptors in isolation.

While previous *in vitro* studies have shown that TREM2 activation can provoke SYK signaling (419), it still remains to be seen whether TREM2 relies exclusively on SYK to coordinate its effects on *in vivo* Alzheimer's-related disease progression. Therefore, additional *in vivo* studies in relevant disease models are needed to address this. Likewise, even though our studies provide promising early evidence that

promoting SYK activation via CLEC7A engagement can boost the clearance of A β , future studies are needed to better characterize the role of CLEC7A in AD-related disease. In particular, it still remains to be seen why CLEC7A is so highly expressed by microglia in response to neurodegenerative disease pathology in mice (93, 94, 105). The possibility exists that CLEC7A could have differential downstream effects on microglial responses and neurological disease pathogenesis depending on the source (fungal-versus -endogenously derived) and avidity of the CLEC7A agonist. Therefore, while our early studies suggest the SYK is a major regulator of neuroprotective microglial responses in models of AD and MS, future studies are needed to better characterize both the upstream and downstream players that coordinate the effects of SYK on neurodegenerative disease progression.

2.6 Methods

Mice

All mouse experiments were performed in accordance with the relevant guidelines and regulations of the University of Virginia and approved by the University of Virginia Animal Care and Use Committee. 5xFAD mice (Stock # 34848-JAX), *Syk*^{fl/fl} mice (Stock #028652), and *Cx3cr1*^{ERT2cre} mice (Stock # 020940) were obtained from The Jackson Laboratory and were crossed to generate *Syk*^{fl/fl} (denoted as *Syk*^{con}), *Syk*^{fl/fl} *Cx3cr1*^{ERT2cre} (denoted as *Syk* ^{Δ MG}), 5xFAD *Syk*^{fl/fl} (denoted as 5xFAD), and 5xFAD *Syk*^{fl/fl} *Cx3cr1*^{ERT2cre} (denoted as 5xFAD *Syk* ^{Δ MG}) experimental mice. Upon weaning, female *Syk*^{con} and *Syk* ^{Δ MG}, 5xFAD, and 5xFAD *Syk* ^{Δ MG} littermates were fed tamoxifen diet (Envigo Teklad #TD.130858) *ad libitum* for two weeks and then returned to normal chow. Ai6-ZsGreen reporter mice were generously provided by Dr. Tajie Harris and crossed with *Syk*^{+/+} *Cx3cr1*^{ERT2Cre} and *Syk*^{fl/fl} *Cx3cr1*^{ERT2Cre} mice. In EAE experiments, *Syk*^{con}, *Syk* ^{Δ MG}, *Syk*^{con-Ai6}, and *Syk* ^{Δ MG-Ai6} mice were fed tamoxifen diet for two weeks upon weaning and then returned to normal chow. In cuprizone experiments, *Syk*^{con} and *Syk* ^{Δ MG} were fed tamoxifen diet for two weeks upon weaning and then returned to normal chow. Mice were housed for AD and demyelinating experiments in specific pathogen-free conditions under standard 12-hour light/dark cycle conditions in rooms equipped with control for temperature (21 \pm 1.5° C) and humidity (50 \pm 10%).

Experimental autoimmune encephalomyelitis (EAE) Induction and Scoring

On the day of immunization (Day 0), mice were injected subcutaneously over each shoulder with 100 μ l of an emulsion containing 0.5 mg/ml MOG₃₅₋₅₅ peptide (Bio-Synthesis, 12668-01) and 1.25 mg/ml heat-killed *Mycobacterium tuberculosis* (Becton, Dickinson, & Company, 231141) in Complete Freund's Adjuvant (Sigma Aldrich, F5881). Mice were intraperitoneally injected with 200 ng of *Pertussis* toxin (List Biological Laboratories, 180) on days 0 and 2 post-immunization.

Beginning at approximately day 7 post-immunization, mice were monitored daily for onset of hind-limb paralysis and scored for EAE severity using the following 5-point clinical scoring system: 0=normal tail;

0.5=limp at tip of tail; 1=completely limp tail; 1.5=partial hind limb weakness/mouse can be flipped onto its back; 2=complete hindlimb weakness with abnormal gait; 3=partial hind-limb paralysis; 3.5=complete hind-limb paralysis in both legs; 4=hind- and fore-limb paralysis; 5=moribund/dead.

Cuprizone model

For the cuprizone model, adult mice were fed regular chow mixed with 0.3% cuprizone (Sigma, 14690) *ad libitum* for 5 weeks to induce demyelination.

Western blotting

MACS-sorted microglia were resuspended in Western blot lysis buffer [dH₂O, RIPA, cOmplete Protease Inhibitor Cocktail (Roche), and PhosSTOP (Roche)]. Protein concentration was measured using Pierce 660 nm Protein Assay Reagent (Thermo Scientific, 22660). 4X SDS loading dye was added to protein lysates and incubated at 95°C for 3 minutes. For each sample, 25 ug of protein was loaded per lane of a 4-20% Mini-PROTEAN TGX Stain-Free Protein Gel (BioRad, 4568093) and run at 120 volts for 1.5 hours using Mini-PROTEAN Tetra Cell (BioRad, 1658004). Proteins were transferred to an Immun-Blot Low Fluorescence PVDF membrane (BioRad, 1620264) using Trans-Blot Turbo transfer system (BioRad, 1704150) set to 2 mini gels and mixed MW for 21 minutes. SYK protein was probed using anti-SYK (D3Z1E) XP Rabbit mAb (Cell Signaling Technologies, 13198, 1:1000 overnight at 4° C) and goat anti-rabbit IgG StarBright Blue 700 secondary antibody (BioRad, 12004161, 1:1000 for 2 hours at room temperature). The stain-free gel and blotted membrane were imaged using ChemiDoc MP Imaging System (BioRad, 12003154). Total protein loaded was quantified using Image lab touch software (BioRad), Beta-Actin (Cell Signaling, 12620S), Ponceau S stain (Sigma-Aldrich, P7170) and SYK protein were quantified using Fiji. Samples underwent the same preparation for the AKT pathway phosphorylation pathway kit (RayBiotech, AAH-AKT-1-8). The AKT assay was performed in accordance to manual instructions and pixel density was analyzed using Adobe Photoshop.

Brain sample preparation

Mice were euthanized using CO₂ asphyxiation and transcardially perfused with 20 ml of 1xPBS. For AD experiments, brains were dissected out with the left hemisphere drop-fixed in 4% paraformaldehyde overnight at 4°C and the right hemisphere flash-frozen and stored at -80°C. Drop-fixed samples were transferred to 30% sucrose for 48 hours and then mounted and frozen in Tissue-Plus OCT compound (Thermo Fisher). These brains were then sectioned at 50 µm in thickness using a cryostat (Leica) and stored in PBS + 0.05% sodium azide at 4°C for downstream staining and imaging. The flash-frozen brains were thawed for RNA and protein extraction and mechanically homogenized in 500 µl of Tissue Protein Extraction Reagent T-PER (Thermo Fisher, 78510) containing phosphatase inhibitor cocktail PhosSTOP

(Roche, 04906845001) and protease inhibitor cocktail cOmplete (Roche, 11873580001). Following homogenization, 50 μ l of the brain sample was diluted in 500 μ l Trizol for future RNA extraction and stored at -80°C . The stock brain samples were then spun down at 16,000 rpm for 10 minutes and the supernatant and pellet were isolated for soluble and insoluble amyloid beta analyses, respectively. For EAE experiments, brain tissue was dissected and immersion fixed in 4% paraformaldehyde for 48 hours, followed by dehydration in 30% sucrose and freezing in OCT. Free-floating cryosections were cut (40 μ m) and collected in PBS containing 0.02% sodium azide and stored at 4°C until further analysis using the methods outlined above.

ELISA

Brain samples underwent guanidine-extraction in which pelleted brain samples were incubated 1:6 in 5 M guanidine HCL/50 mM tris, pH = 8.0 at room temperature for 3 hours, then diluted 1:5 in PBS containing protease inhibitor cocktail cOmplete (Roche, 11873580001), centrifuged at 16,000 g for 20 minutes at 4°C , and the supernatant was collected and stored at -80°C pending ELISA. Triton-X extraction was performed by diluting the pelleted brain samples 1:5 in 1% Triton-X-100 in T-PER buffer and sonicating the samples for 30 minutes at room temperature, then spun down at 16,000 g for 20 minutes at 4°C and the supernatant stored at -80°C until used for A β measurement by ELISA. Amyloid beta 40 or 42 Mouse ELISA kits were utilized (Thermo Fisher, KMB3481, KMB3441) on samples obtained with the soluble fraction (T-PER extracted supernatant) diluted 1:10, Triton-X fraction diluted 1:40, and the guanidine fraction diluted 1:200 following manufacturer's instructions.

Immunofluorescence microscopy

Floating brains sectioned stored in PBS + 0.05% sodium azide were blocked with 2% donkey serum, 1% bovine serum albumin, 0.1% triton, 0.05% tween in PBS for 1 hour at room temperature before applying the primary antibody master mix diluted in this block overnight at 4°C . Samples were stained with anti-A β (D54D2, Cell Signaling, 1:300; or 6e10, BioLegend, 1:1000) to label plaques. To study microglial morphology and numbers, sections were stained with Iba1 (ab5076, Abcam, 1:300). To further characterize microglia, we labeled with Ki67-EF660 (SoIA15, Thermo Fisher, 1:100), anti-Clec7a (R1-8g7, Invivogen, 1:30), Tmem119 (ab209064, Abcam, 1:300), and anti-CD68 (FA-11, BioRad, 1:1000). Neuronal health was probed by staining for anti-APP (Y188, ab32136, Abcam, 1:750), anti-phospho-tau (AT8, Thermo Fisher, 1:500), and anti-NeuN (MAB377, Millipore Sigma, 1:500). For cuprizone experiments, sections were stained with PDGFR α (AF1062, 1:200, R&D Systems), CC1 (OP80, 1:200, Millipore), Olig2 (AB9610, 1:500, Millipore), dMBP (AB5864, Millipore Sigma, 1:2000), and MBP (ab7349, Abcam, 1:1000). Sections were then washed 3 times for 10 minutes at room temperature in PBS and 0.05% tween-20, then incubated in matched donkey Alexa Fluor 488, 594, 647 anti-rabbit, -goat, -rat, -

streptavidin, and -mouse (Thermo Fisher, 1:1000 dilution) at room temperature for 2 hours. Samples were washed again 3 times for 10 minutes at room temperature and incubated with DAPI (1:1000) for 10 minutes at room temperature, or stained for plaques with ThioflavinS (Sigma-Aldrich, 2 mg/10ml) for 8 minutes followed by three 2-minute washes with 50% ethanol at room temperature. To investigate cell death, sections were stained by TUNEL (Millipore Sigma, 11684795910) following the manufacturer's protocol. All tissue sections were then transferred to wells containing PBS before being mounted to glass slides with ProLongGold antifade reagent (Invitrogen, P36930) and coverslips. Mounted slides were stored at 4°C until imaged using LAS AF software (Leica Microsystems) on a Leica TCS SP8 confocal microscope. Quantification of images were performed using FIJI software or Imaris software (9.5.1).

Behavior

All behavior experiments were performed between 8 am and 12 pm in a blinded fashion. All mice were 4 months old at the time of the assay. Mice were transported from their home vivarium room to the behavior core and allowed 30 minutes to habituate before beginning each test.

Morris Water Maze

The MWM was done as described previously (294). In brief, the test involved four days of training consisting of four trials, one day of probe consisting of one trial, and two days of reversal consisting of four trials per mouse. Mice were alternately placed facing different visual cues for each trial in a 23°C pool made opaque with white paint. The hidden platform was placed 1 cm below the water surface. Each trial lasted 60 seconds, and the mouse was placed on the hidden platform for 5 seconds if unable to locate it within the 60 second trial. All trials were tracked and scored using video tracking software (Noldus Ethovision XT).

Elevated Plus Maze

EPM was used to investigate anxiety in mice and was performed as described previously (Lammert et al., 2020). The maze has two open arms (35 x 6 cm²) and two closed arms (35 x 6 cm²) with 20 cm-tall black plexiglass walls elevated 121 cm from the floor. The mice were placed in the center square connecting the open and closed arms and allowed to explore during a 5 minute trial. Activity was monitored and scored using video tracking software (Noldus Ethovision XT).

In vivo A β phagocytosis assay

5xFAD, 5xFAD *Syk*^{ΔMG}, and littermate controls were intraperitoneally injected with 10 mg/kg methoxy-X04 (ApexBio, B5769) in a 1:1 ratio of PBS and DMSO. A brain harvest was completed 3 hours after injection in which mice were euthanized using CO₂ asphyxiation before being intracardially perfused with 20 mL of PBS + Na heparin (5 units/mL). The brains were placed in a Hanks buffer saline solution (HBSS) (Gibco, 14025092) with DNase I (50 U/mL) (Sigma-Aldrich, 10104159001) and papain (2 mg/mL) (LS003124, Worthington) and homogenized using a 10 mL serological pipette. The brain homogenates were then incubated at 37°C for 15 minutes. This process was repeated for a total of 3 times with the final two homogenizations accomplished using a 5 mL serological pipette. The brain homogenates were then passed through a 70 μm strainer to create a single-cell suspension. The cell suspension was then placed in 20 mL of DMEM/F12 buffer (21331020, Thermo Fisher) with 10% fetal bovine serum (FBS), 1% Anti-anti, and 1% Glutamax and spun down with a slow brake at 300 g for 10 minutes. The cell pellet was then resuspended in 13 mL of 37% Percoll (Cytiva, 17-0891-02) and spun down with no brake at 2000 rpm for 12 minutes. Myelin was removed and cells were resuspended in MACS buffer (Miltenyi Biotec, 130-0910376) to wash. Flow cytometry for microglia was then performed (as described below) with additional gating for methoxy-X04.

CypHer5E-Aβ preparation

Monomerization of Aβ (1-42) (641-15, California peptide) was achieved using a previously published protocol (423), using hexafluoroisopropanol (HFIP) (52517, Sigma-Aldrich). 5mM monomeric Aβ samples were incubated for 24 hours at 4°C in F12 media to make a 200 μM stock of oligomeric Aβ. Samples were then incubated with CypHer5E-NHS ester (PA15401, GE Healthcare) diluted in 0.1 M sodium bicarbonate for 30 minutes covered and at room temperature. Following incubation, Biospin columns (7326227, Bio-Rad) were used to quench unbound dye. CypHer5E-tagged Aβ oligomers were stored at 4°C prior to BMDM treatment.

In vitro Aβ phagocytosis assay

Bone marrow-derived macrophages (BMDMs) were isolated from the hindlimbs of WT and *Syk*^{fl/fl} *LysM*^{Cre} mice. Marrow-containing bones were sprayed with 70% ethanol before being placed in IMDM (12440-053, Gibco) containing penicillin/streptomycin (P/S) (15140-122, Gibco). A 25-gauge needle was used to flush marrow from the bones using 20 ml of IMDM containing P/S. An 18-gauge needle was then used to triturate flushed bone marrow 5 times to make a single-cell suspension. Samples were spun down at 1500 rpm for 5 minutes at 4°C. Cell pellets were resuspended BMDM media containing IMDM, 10% FBS, 1% non-essential amino acids, 1% P/S, and 50 ng/ml M-CSF. Cell plating was performed using 150 X 25 mm culture dishes (430597, Thomas Scientific). After three days, 5 ml of BMDM media was added to each dish. Six days post initial cell plating, media was aspirated from dishes and 10 ml of PBS was added to

each plate and incubated for 10 minutes at 4°C. BMDMs were removed from the dish using a scraper and transferred to a conical tube, spun down, and resuspended in BMDM media. 100,000 cells/well were pipetted in into a flat bottom 96 well plate. The next day, BMDMs were treated with vehicle or 10 µM of Tideglusib 1 hour prior to treatment with 10 µM of oligomeric Aβ tagged with CypHer5E. 24 hours post Aβ treatment, BMDMs were then collected and flow cytometry was used to assess CypHer5E fluorescence.

Intrahippocampal injection

5xFAD and 5xFAD *Syk*^{ΔMG} mice were anesthetized before receiving a bilateral hippocampal injection of 2 µl of vehicle or 2 µg pustulan into the right and left hemisphere of the hippocampus (at ±2 mm lateral, -2 mm posterior, and -2 mm ventral relative to the intersection of the coronal and sagittal suture (bregma) at a rate of 200 nl/min) using a stereotaxic frame (51730U, Stoelting) and nanoliter injector (NL2010MC2T, World Precision Instruments). Seven days post injection, mice were euthanized using CO₂ and transcardially perfused before preparing brains for immunofluorescent staining to evaluate Aβ clearance in the hippocampus. Images were analyzed using FIJI software and Imaris software (9.5.1).

MACS isolation of microglia, T cells, and monocytes

Mice were euthanized with CO₂ and immediately transcardially perfused with 20 ml 1X PBS. For AD experiments, brains were collected and their meninges and choroid plexus removed then the MACS-sorting protocol was used to isolate microglia as described (424). For EAE experiments, spinal cords were dissected and kept on ice in DMEM (Gibco, 11885-084,) with penicillin/streptomycin (Gibco, 15140-122). Tissues were homogenized by gently mashing through a 70 µm cell strainer. Homogenates were centrifuged at 1500 rpm for 5 minutes then resuspended in 13 ml 37% isotonic Percoll (GE Healthcare, 17-0891-01) in 1X PBS. Samples were centrifuged at 2000 rpm for 12 minutes at room temperature with no brake. After centrifugation, the top myelin layer and supernatant were aspirated and the cell pellet was resuspended in MACS buffer (Miltenyi Biotec, 130-0910376) to proceed with column purification of microglia using CD11b microbeads (Miltenyi, 130-093-634), purification of T cells using CD90.2 microbeads (Miltenyi, 130-121,278), and purification of monocytes using CD11b microbeads (Miltenyi, 130-049,601). We then performed sorting utilizing LS columns and a QuadroMACS magnet (Miltenyi, 130-042-401 and 130-091-051) according to manufacturer's instructions. Column-bound cells were analyzed for purity by flow cytometry, probed for SYK expression by qPCR and Western blotting, or submitted for RNA-seq.

Flow cytometry

For MACS-sort validation, an aliquot of the microglia-positive and -negative fractions were transferred to a 96-well round bottom plate, then washed with 1X PBS and spun down at 1600 rpm for 5 minutes. The cells were then stained with fixable viability dye (eBioscience, 65-0866-14) at 1:1000 for 30 minutes at 4°C. Following incubation, cells were then washed with FACS buffer (pH 7.4; 0.1 M PBS; 1 mM EDTA, and 1% BSA). Cells were then stained 1:200 with CD11b (APC), CD45 (PE-Cy7), and TCR β chain (Brilliant Violet 510) flow antibodies (all from eBioscience) in FACS buffer for 15 minutes at 4°C. The cell pellets were then washed with FACS buffer then resuspended in 100 μ l of FACS buffer. Microglia were identified as the CD45^{int} and CD11b^{hi} after gating for single and live cells.

For lipid-droplet-accumulation and reactive oxygen species (ROS) assessment in microglia, mice were euthanized with CO₂ at 8 months of age and immediately transcardially perfused with 20 ml 1X PBS. Brains were collected and their meninges and choroid plexus removed and prepped as a single cell suspension as described in (424). Brain homogenates were centrifuged at 1500 rpm for 5 minutes then resuspended in 13 ml 37% isotonic Percoll (GE Healthcare, 17-0891-01) in 1X PBS. Samples were centrifuged at 2000 rpm for 12 minutes at room temperature with no brake. After centrifugation, the top myelin layer and supernatant were aspirated and the cell pellet was washed with PBS. Cells were then stained either 1:500 with CellROX (Thermo Fisher, C10491) for 30 minutes or 1:2000 with BODIPY (Invitrogen, D3861) for 10 minutes diluted in PBS at 37°C. Cells were spun down and washed with FACS buffer (pH 7.4; 0.1 M PBS; 1 mM EDTA, and 1% BSA). Cells were then stained 1:200 with CD11b (APC), CD45 (PE-Cy7), and TCR β chain (Brilliant Violet 510) flow antibodies (all from eBioscience) in FACS buffer for 15 minutes at 4°C. The cell pellets were then washed with FACS buffer then resuspended 1:5000 with DAPI in 100 μ l of FACS buffer. Microglia were identified as the CD45^{int} and CD11b^{hi} after gating for single and live cells.

For flow cytometry staining of BMDMs, cells were washed with FACS buffer and centrifuged at 1500 rpm for 5 min, and resuspended in 100 μ l of FACS buffer with fluorescently labeled antibodies (all from eBioscience) specific for CD11b (clone M1/70) and F4/80 (clone BM8) diluted 1:200. Cells were incubated in the dark for 20 minutes at room temperature, washed with FACS buffer, and resuspended 1:5000 with DAPI in 100 μ l of FACS buffer. BMDMs were identified as the CD11b^{hi} and F4/80^{hi} after gating for single and live cells.

For flow cytometry staining in EAE experiments, cells were plated (100 μ l of resuspended spinal cord or 1x10⁶ splenocytes) in a 96-well plate and washed with FACS buffer. After centrifugation at 1500 rpm for 5 minutes and removal of supernatants, cells were resuspended in 100 μ l 1X PBS with 1:1000 fixable viability dye (eBioscience, 65-0866-14) and 1:1000 Fc Block (eBioscience, 14-0161-86). Cells were incubated at 4°C for 30 min. Cells were then washed with FACS buffer, centrifuged at 1500 rpm for 5 min, and resuspended in 100 μ l of FACS buffer with fluorescently labeled antibodies (all from eBioscience)

specific for CD45 (clone 30-F11), CD11b (clone M1/70), Gr-1 (clone RB6-8C5), MHC-II (clone M5/114.15.2), TCR β (clone H57-597), CD4 (clone RM4-5), CD8 (clone 53-6.7), CD11c (clone N418), and CD80 (clone 16-10A1) diluted 1:200. Cells were incubated in the dark for 20 minutes at room temperature, washed twice with FACS buffer, and fixed with 1% paraformaldehyde in FACS buffer.

For intracellular cytokine staining, cells were plated (100 μ l of resuspended spinal cord or draining lymph node cells or 1×10^6 splenocytes) in a 96-well plate in IMDM stimulation media [Iscove's Modified Dulbecco's Media (Gibco, 12440-053), penicillin/streptomycin (Gibco, 15140-122), 10% heat-inactivated fetal bovine serum (Gibco, 16000-044), 1% L-glutamine (Gibco, 25030-081), and 50 μ M beta-mercaptoethanol (Gibco, 21985-023)] with 20 ng/ml PMA (Sigma Aldrich, P1585), 1 μ g/ml ionomycin (Sigma Aldrich, I9657), and 1:1000 monensin (eBioscience, 00-4505-51). Cells were incubated for 5 hours at 37°C with 5% CO₂, then washed with 1X PBS prior to proceeding with surface staining for flow cytometry as described above. Cells were fixed and permeabilized using IC fixation buffer (eBioscience, 00-8222-49) and permeabilization buffer (eBioscience, 00-8333-56) following manufacturer's instructions. Cells were then stained with 100 μ l fluorescently labeled antibodies (all from eBioscience) for GM-CSF (clone MP1-22E9), IFN- γ (clone XMG1.2), and IL-17A (clone eBio17B7) diluted 1:200 in 1X permeabilization buffer for 20 min at room temperature. Cells were washed twice with 1X permeabilization buffer, then twice with FACS buffer.

Sample data were acquired within a few days of fixation using a Gallios flow cytometer (10 colors, 3 lasers, B5-R1-V2 Configuration with Kaluza Acquisition; Beckman Coulter) and analyzed using FlowJo software (Becton, Dickinson, & Company).

Multiplex Cytokine Assay

Immune cells isolated from spinal cords or spleens were plated in a 96-well plate at up to 2×10^5 cells/well and stimulated with 30 μ g/ml MOG₃₅₋₅₅ peptide in IMDM stimulation media for 48 hours at 37°C with 5% CO₂. After incubation, cells were centrifuged at 1600 rpm for 5 minutes and supernatants were collected for storage at -80°C.

Supernatants were assayed for concentrations of various cytokines using Bio-Rad Bio-Plex Pro reagent kit (Bio-Rad, 171-304070M) and Bio-Plex Pro Mouse Cytokine 23-Plex Group I magnetic beads and detection antibodies for IL-1 α , IL-1 β , IL-2, IL-4, IL-6, IL-17A, G-CSF, GM-CSF, IFN- γ , KC, and TNF- α according to manufacturers' instructions. Sample data for Bio-Plex Pro assays were acquired with a Bio-Plex 200 System (Bio-Rad) or Luminex MAGPIX and analyzed using Bio-Plex Manager software (Bio-Rad).

Histopathological Analysis of EAE Spinal Cords

Mice were euthanized with CO₂ and immediately transcardially perfused with 20 ml 1X PBS followed by 20 ml 10% neutral buffered formalin (NBF; Azer Scientific). Spinal columns were dissected and immersion fixed in 10% NBF for at least 48 hours. Spinal columns were cut into cervical, thoracic, and lumbar pieces. Spinal cords from each piece were carefully dissected from the column, embedded in paraffin, sectioned coronally from the rostral end of each piece, and mounted on slides. Sections were stained with Luxol Fast Blue (LFB; Acros Organics, 212170250) to label myelin. In brief, after deparaffinization, sections were incubated at 60°C for 16-24 hours in 0.1% Luxol Fast Blue in 95% ethanol + 0.05% acetic acid. Excess stain was removed with 95% ethanol and slides were dipped in 0.05% lithium carbonate (Acros Organics, 446322500) in dH₂O for 10-20 seconds then in 70% ethanol to remove LFB staining from gray matter but not from myelinated white matter. Slides were washed with dH₂O then counterstained with hematoxylin (Sigma Aldrich, HHS128) to label nuclei. Brightfield images were acquired on a Keyence BZ-X810 microscope at 4X and 40X magnification.

Isolation of Immune Cells

Mice were euthanized with CO₂ and immediately transcardially perfused with 20 ml 1X PBS. Spinal cords and spleens were dissected and kept on ice in DMEM (Gibco, 11885-084) with penicillin/streptomycin (Gibco, 15140-122). Tissues were homogenized by gently mashing through a 70 µm cell strainer. For spinal cords, homogenates were centrifuged at 1500 rpm for 5 minutes then resuspended in 13 ml 37% isotonic Percoll (GE Healthcare, 17-0891-01) in 1X PBS. Samples were centrifuged at 2000 rpm for 12 minutes at room temperature with no brake. After centrifugation, the top myelin layer and supernatant were aspirated and the cell pellet was resuspended in 500 µl DMEM with penicillin/streptomycin. For spleens, homogenates were centrifuged at 1500 rpm for 5 minutes then resuspended in 2 ml ACK lysis buffer (Quality Biological, 118-156-101) and incubated at room temperature for 3 minutes to lyse red blood cells. Cells were washed and resuspended in DMEM with penicillin/streptomycin. Cells were counted using a Cellometer Auto 2000 (Nexcelcom Bioscience).

RNA isolation, cDNA synthesis, qPCR

RNA was isolated from the left hemisphere of the brain of 5xFAD and 5xFAD *Syk*^{AMG} mice. 50 µl of brain homogenate (described in the brain sample preparation section) was added to 500 µl of TRIzol (Life Technologies, 15596018). Following vortexing of these samples, 200 µl of chloroform (Fisher Scientific, BP1145-1) was added and incubated for 5 minutes before being spun down at 14,000 rpm at 4°C for 15 minutes. The top aqueous fraction was transferred to a new tube and an equal volume of isopropanol (Sigma, I9516) was added then vortexed. The samples were incubated at room temperature for 10

minutes and then spun down at 12,000 rpm at 4°C for 5 minutes. The pellet was then washed with 1 mL 70% ethanol 2 times, then allowed to air dry for 15 minutes before resuspending the RNA pellet in 100 µl of DNase/RNase free water. RNA was isolated from MACS-sorted microglia in the spinal cord using an RNeasy Micro kit (Qiagen, 74004) according to manufacturer's instructions. Sample quality and quantity for AD and EAE samples was evaluated using NanoDrop 2000 Spectrophotometer (Thermo Scientific). The RNA was then converted to cDNA using a Sensifast cDNA Synthesis kit (Bioline, BIO-65054). Levels of *Sykb* (Mm01333035_m1) and *Gapdh* (Mm99999915_g1) mRNA were determined using Taqman Gene Expression Assay primer/probe mix (Thermo Fisher), Sensifast Probe No-ROX kit (Bioline, BIO-86005), and a CFX384 Real-Time PCR System (BioRad, 1855484). All reagents were used according to manufacturer's instructions.

FACS sorting for RNA sequencing

Syk^{con-Ai6} and *Syk*^{ΔMG-Ai6} mice were euthanized on EAE Day 35 with CO₂ and immediately transcardially perfused with 20 ml ice cold 1X PBS. Spinal cords were dissected and placed on ice in DMEM + 10% FBS. Tissues were gently homogenized by mashing through a cell strainer then centrifuged at 1500 rpm for 5 min. Pellets were resuspended in 13 ml 37% isotonic Percoll (GE Healthcare, 17-0891-01) in 1X PBS. Samples were centrifuged at 2000 rpm for 12 minutes at room temperature with no brake. After centrifugation, the top myelin layer and supernatant were aspirated and the cell pellet was resuspended in FACS buffer. Cell suspensions were incubated with Fc Block and antibodies for CD45, CD11b, and Gr-1. After two washes with FACS buffer, cells were resuspended in FACS buffer + 0.2 mg/ml DAPI and sorted on DAPI⁻ CD45⁺ ZsGreen⁺ cells using an Influx Cell Sorter (Becton, Dickinson & Company) in the University of Virginia Flow Cytometry Core Facility.

RNA sequencing data analysis

AD microglia RNA-Seq

MACS-sorted microglia were sent to GENEWIZ Next Generation Sequencing. The raw sequencing reads (FASTQ files) were aligned to the UCSC mm10 mouse genome build using the splice-aware read aligner HISAT2. Samtools was used for quality control filtering. Reads were sorted into feature counts with HTSeq. DESeq2 (v1.30.0) was used to normalize the raw counts based on read depth, perform principal component analysis, and conduct differential expression analysis. The p-values were corrected with the Benjamini-Hochberg procedure to limit false positives arising from multiple testing. The significantly repressed and enhanced genes were put into GProfiler to gather the KEGG terms. The analysis itself was performed using the Seq2Pathway, fgsea, tidyverse, and dplyr software packages. Heatmaps were generated using the pheatmap R package [<https://github.com/raivokolde/pheatmap>] while other plots were

made with the lattice (<http://lattice.r-forge.r-project.org/>) or ggplot2 [<https://ggplot2.tidyverse.org>] packages.

EAE microglia scRNA-Seq

FACS-sorted single cell suspensions were submitted to the University of Virginia Genome Analysis and Technology Core for single-cell RNA sequencing library preparation. The raw sequencing reads (FASTQ files) were aligned to the UCSC mm10 mouse genome build using Cell Ranger (v1.3.1) which performs alignment, filtering, barcode counting and unique molecular identifier (UMI) counting. R studio (v4.0.5) was used for all downstream analyses and Seurat (v4.0.2) was used for filtering out low-quality cells, normalization of the data, determination of cluster defining markers and graphing of the data on UMAP. Low-quality cells were excluded in an initial quality-control (QC) step by removing genes expressed in fewer than three cells, cells with fewer than 150 genes expressed, and cells expressing more than 5000 genes. Cells with more than 20% of mitochondrial-associated genes and cells with more than 5% hemoglobin among their expressed genes were also removed. Genes with high variance were selected using the FindVariableGenes function, then the dimensionality of the data was reduced by principal component analysis (PCA) and identified by random sampling 20 significant principal components (PCs) for each sample with the PCElbowPlot function. Cells were clustered with Seurat's FindClusters function. Differential gene expression analysis was performed within clusters using the ZinBWave function and DESeq2 (v1.32.0). ToppCluster (Cincinnati Children's) was used for network analyses to identify KEGG and GO terms in the DAM cluster. Data was organized and graphs were created using patchwork, dplyr, tidyverse, and Seurat. The frequency plot was created using Prism GraphPad. Pseudotime analysis was conducted using Monocle (v0.2.3.0).

Statistics

Mean values, SEM values, Student's t test (unpaired), and one-way ANOVA were calculated using Prism software (GraphPad). Significance for pooled EAE experiments was performed by a Mann-Whitney test. *P* values less than 0.05 were considered significant. **p* < 0.05, ***p* < 0.01, ****p* < 0.001, *****p* < 0.0001.

Chapter 3

CARD9 attenuates A β pathology and modifies microglial responses in an Alzheimer's disease mouse model

3.1 Abstract

Recent advances have highlighted the importance of several innate immune receptors expressed by microglia in Alzheimer's disease (AD). In particular, mounting evidence from AD patients and experimental models indicates pivotal roles for TREM2, CD33, and CD22 in neurodegenerative disease progression. While there is growing interest in targeting these microglial receptors to treat AD, we still lack knowledge of the downstream signaling molecules used by these receptors to orchestrate immune responses in AD. Notably, TREM2, CD33, and CD22 have been described to rely on signaling through the intracellular adaptor molecule CARD9 to mount downstream immune responses outside of the brain. However, the role of CARD9 in AD remains poorly understood. Here, we show that genetic ablation of CARD9 in the 5xFAD mouse model of AD results in exacerbated amyloid beta (A β) deposition, increased neuronal loss, worsened cognitive deficits, and alterations in microglial responses. We further show that pharmacological activation of CARD9 promotes improved clearance of A β deposits from the brains of 5xFAD mice. These results help to establish CARD9 as a key intracellular innate immune signaling molecule that regulates A β -mediated disease and microglial responses. Moreover, these findings suggest that targeting CARD9 might offer a novel strategy to improve A β clearance in AD.

Hannah Ennerfelt^{1,2,3*}, Coco Holliday¹, Daniel A. Shapiro¹, Kristine E. Zengeler^{1,2,3}, Ashley C. Bolte^{1,4,5}, Tyler K. Ulland⁶, and John R. Lukens^{1,2,3,4,5*}

¹Center for Brain Immunology and Glia (BIG), Department of Neuroscience, University of Virginia, Charlottesville, VA 22908, USA, ²Neuroscience Graduate Program, University of Virginia, Charlottesville, VA 22908, USA, ³Cell and Molecular Biology Graduate Training Program, University of Virginia, Charlottesville, VA 22908, USA, ⁴Department of Microbiology, Immunology and Cancer Biology, University of Virginia, Charlottesville, VA 22908, USA. ⁵Medical Scientist Training Program, University of Virginia, Charlottesville, VA, 22908, USA. ⁶Department of Pathology and Laboratory Medicine, University of Wisconsin, Madison, WI 53705, USA.

Author Contributions:

H.E., T.K.U., and J.R.L. designed the study; H.E., D.A.S., C.H., and K.E.Z. performed experiments; D.A.S. and A.C.B. performed bioinformatics analyses; H.E., C.H., and D.A.S. analyzed data; H.E. and J.R.L. wrote the manuscript; J.R.L. oversaw the project.

3.2 Introduction

Alzheimer's disease (AD) is a neurodegenerative disorder characterized by amyloid beta (A β) accumulation, the seeding of neurofibrillary tangles (NFTs), and neuroinflammation (425, 426). The culmination of these

pathologies leads to neuronal loss and memory decline in patients (427). Microglia, the resident immune cells of the brain, have been heavily implicated in AD pathogenesis. More specifically, genome wide association studies (GWAS) have identified that a large percentage of late-onset AD risk loci affect genes involved in microglial biology and function (e.g., *TREM2* and *CD33*) (85). Importantly, recent findings from AD mouse models have further solidified pivotal roles for microglia in Alzheimer's-related disease pathogenesis (86, 87, 102, 124, 178, 428, 429). It is currently thought that microglia affect AD progression through various mechanisms that include cytokine production, phagocytosis of A β and other neurotoxic agents, and compaction/containment of A β plaques. While these studies clearly define microglia as important players in AD, we are only just beginning to appreciate the molecular and effector mechanisms that microglia employ to influence neurodegenerative disease. For instance, despite our ample understanding of which microglial receptors are involved in modulating AD progression, much of the intracellular signaling employed by microglia in the AD brain environment remains poorly described.

Notably, both human genetics studies and work in AD animal models have begun to uncover pivotal roles for a number of ITAM (immunoreceptor tyrosine-based activation motif)- and ITIM (immunoreceptor tyrosine-based inhibition motif)-containing receptors in AD pathogenesis. For example, emerging evidence indicates critical roles for the ITAM-containing receptor *TREM2*, as well as the ITIM-containing receptors *CD33* and *CD22* in AD (34, 35, 97, 98, 100, 101, 103, 105, 112, 113, 189, 339, 398, 399, 430-439). In the context of peripheral infection models, engagement of ITAM-containing receptors has been shown to promote the activation of *CARD9* signaling and subsequent upregulation of cytokine production (345, 346, 440). In contrast, stimulation of ITIM-containing receptors provokes *SHP-1* activation which potentially inhibits downstream *CARD9* signaling and consequently results in the dampening of cytokine production and phagocytosis (345, 346). While increasing evidence indicates that ITAM/ITIM-containing immune receptors (i.e. *TREM2*, *CD33*, and *CD22*) are critically involved in AD progression, we still lack in-depth knowledge of the intracellular signaling molecules employed by these immune receptors to influence neurodegenerative disease. *CARD9* has been shown to control immune responses downstream of *TREM2*, *CD33*, and *CD22* in other models of disease (345, 346, 440), although the involvement of *CARD9* in AD and most other neurodegenerative disorders remains to be determined.

To explore a potential role for *CARD9* in Alzheimer's-related disease we crossed *CARD9*-deficient mice with 5xFAD mice, a well-described mouse model of A β -mediated neurological disease. Here we find that genetic ablation of *Card9* in 5xFAD mice leads to increased A β accumulation in the brain, exacerbated neuronal loss, and worsened memory decline compared with 5xFAD littermate controls. Given that *CARD9* is nearly exclusively expressed by microglia in the central nervous system (CNS) (441), we observed that microglia in *Card9*^{-/-} 5xFAD mice display dramatically increased proliferation while they simultaneously exhibit impaired morphological activation in response to A β plaques. We further show that treating 5xFAD mice with a potent exogenous trigger of *CARD9* signaling leads to improved control of A β

in the hippocampus. Taken together, these findings indicate that the innate immune signaling molecule CARD9 is a novel regulator of A β -mediated neurological disease and further suggest that targeting CARD9 activation may offer a therapeutic strategy to promote A β clearance.

3.3 Results

3.3.1 CARD9 signaling restricts brain amyloidosis in 5xFAD mice

To investigate how CARD9 influences the development of A β pathology, we introduced a germline deletion of *Card9* into 5xFAD mice, an AD mouse model characterized by early A β accumulation (350, 442). At 5 months of age, *Card9*^{-/-}5xFAD mice had significantly greater A β burden in the cortex, hippocampus, and thalamus in comparison to *Card9*^{+/-}5xFAD and *Card9*^{+/+}5xFAD (referred to as 5xFAD mice) littermate controls (Figures 3.1A and 3.1B). Consistent with the increased levels of A β staining observed in 5xFAD mice that lack CARD9, we likewise detected increased amounts of A β 42, the most deleterious isoform of A β (360, 443), in both the soluble (PBS-extracted) and insoluble (guanidine-extracted) brain fractions obtained from *Card9*^{-/-}5xFAD mice (Figures 3.1C and 3.1D). The soluble fraction of A β is thought to contain the most neurotoxic oligomers of A β (444), whereas the insoluble fraction consists of higher-order A β forms found in amyloid plaques (445). In alignment with the increase of A β in the insoluble fraction, the cortex in *Card9*^{-/-}5xFAD also contain approximately double the number of individual plaques in comparison to 5xFAD littermate control mice (Figures 3.1E and 3.1F). These data suggest that CARD9 plays an important role in limiting A β accumulation in 5xFAD mice.

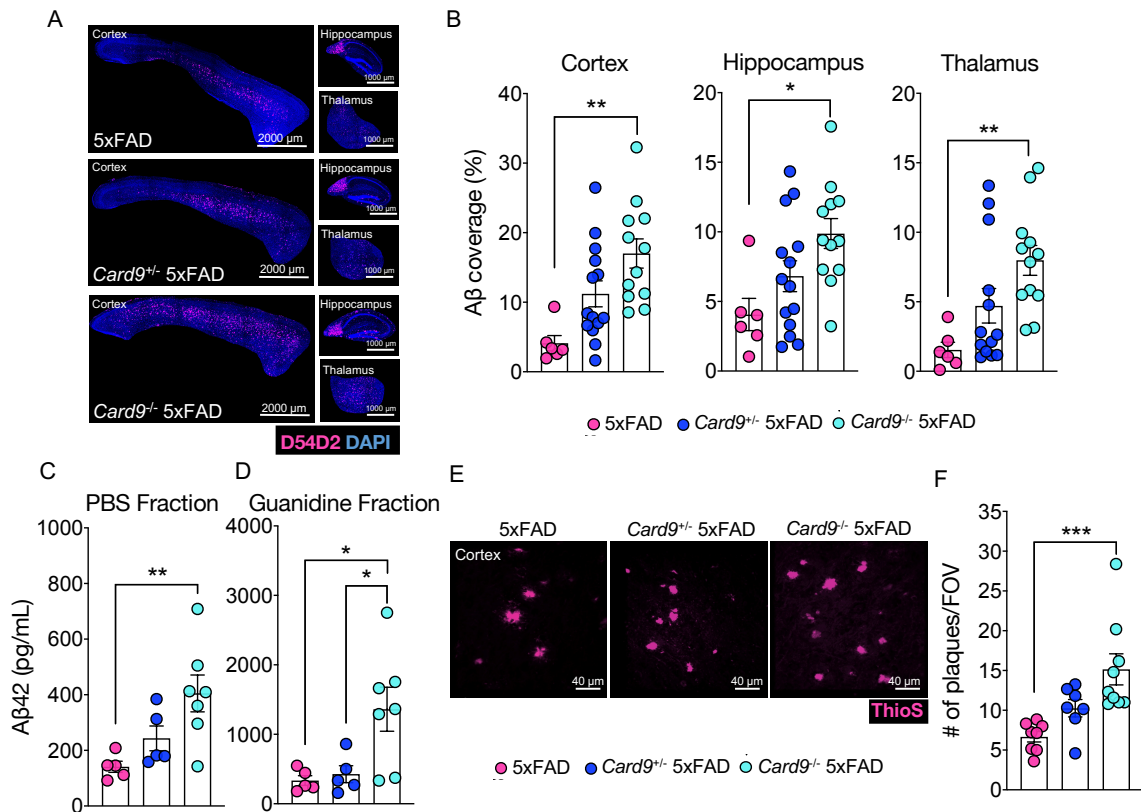


Figure 3.1. CARD9 deletion leads to increased A β accumulation in 5xFAD mice. (A-F) Brains were harvested from 5-month-old 5xFAD, *Card9*^{+/-} 5xFAD, and *Card9*^{-/-} 5xFAD mice to evaluate A β load. (A) Representative images from sagittal sections of A β (D54D2, red; DAPI, blue) staining in the cortex, hippocampus, and thalamus. Original magnification: 10x; scale bar = 2000 μ m and 10000 μ m. (B) Quantification of percent area covered by A β in the cortex, hippocampus, and thalamus. Combined data from three independent experiments. (C-D) A β levels detected by A β -42 ELISA. (C) Soluble (PBS buffer extraction) and (D) insoluble (guanidine extraction) fractions from 5-month-old 5xFAD, *Card9*^{+/-} 5xFAD, and *Card9*^{-/-} 5xFAD half-brain hemispheres. (E-F) Representative images and quantification of A β plaques measuring ThioS⁺ (pink) plaque numbers in the cortex field of view (FOV), with combined data from a total of 50-100 plaques from 3 matching brain sections per mouse. Original magnification: 63x; scale bar = 40 μ m. Statistical significance between experimental groups was calculated by one-way ANOVA with Tukey's post hoc test (B-D, F). **P* < 0.05, ***P* < 0.01, ****P* < 0.001. Error bars represent mean \pm S.E.M. and each data point represents an individual mouse (B-D, F).

3.3.2 The loss of CARD9 exacerbates neuronal loss and memory decline in 5xFAD mice

Continual accumulation of A β can cause appreciable neuronal damage in the AD brain (426, 446, 447) and the deleterious effects of A β deposition on neuronal health is thought to drive behavioral changes and pronounced learning and memory decline (363, 448-450). To determine if the increase in A β accumulation seen in *Card9*^{-/-} 5xFAD mice is accompanied by heightened neuronal loss, we first evaluated neuronal cell death by performing TUNEL staining on the CA1 region of hippocampal samples from 5xFAD, *Card9*^{+/-} 5xFAD, and *Card9*^{-/-} 5xFAD mice. The CA1 region of the hippocampus is densely packed with neurons forming circuits responsible for the consolidation and retrieval of memory (451). Initial seeding of A β often originates in the hippocampus; therefore, neuronal damage is often seen in this region, and this is thought to explain some of the learning and memory behavioral deficits commonly observed in A β -driven mouse models of AD (452-454). Although 5xFAD mice do not characteristically display marked neuronal loss until later stages of disease (455), 5-month-old *Card9*^{-/-} 5xFAD mice were found to have pronounced levels of TUNEL⁺ NeuN⁺ cells in the CA1, indicative of neuronal death (Figures 3.2A and 3.2B). Taken together,

these data suggest that impaired control of A β in CARD9-deficient 5xFAD mice is associated with increased levels of neuronal cell death in the CA1 region of the hippocampus.

Given the increased neuronal loss and amyloidosis observed in CARD9-deficient 5xFAD mice, we next sought to determine if *Card9*^{-/-}5xFAD mice also display deficits in learning and memory. To this end, we employed the Morris water maze (MWM) behavioral test to probe spatial learning and memory (456). Over the first four days of MWM, 5xFAD control mice exhibited a substantial decrease in latency to find the hidden platform which is indicative of intact spatial learning (Figure 3.2C). In comparison, *Card9*^{-/-}5xFAD mice spent more time searching for the hidden platform over the four acquisition days, demonstrating significantly impaired spatial learning in comparison to 5xFAD littermate controls (Figure 3.2C). The navigation path used by mice to find the platform can also provide insights into the degree of cognitive dysfunction. Allocentric movement, for example, is defined by the ability of the mouse to find the hidden platform within 3 navigational turns and is dependent on hippocampal spatial memory (457). Interestingly, *Card9*^{-/-}5xFAD mice displayed significantly decreased hippocampal-based allocentric spatial memory when searching for the hidden platform compared with 5xFAD and *Card9*^{+/-}5xFAD littermate control mice (Figures 3.2D and 3.2E). Moreover, *Card9*^{-/-}5xFAD mice also covered a significantly larger distance in search of the hidden platform on the fourth day of the MWM test (Figure 3.2F), suggesting a less targeted platform search in comparison to 5xFAD controls. Locomotor deficits did not contribute to any differences seen between groups in the MWM acquisition days, as comparable speeds were measured between 5xFAD, *Card9*^{+/-}5xFAD, and *Card9*^{-/-}5xFAD mice (Figure 3.2G). Impaired spatial memory was also displayed by *Card9*^{-/-}5xFAD mice during probe day, as they spent significantly less time than 5xFAD and *Card9*^{+/-}5xFAD mice in the MWM pool target quadrant that had contained the hidden platform during the first four days of acquisition (Figure 3.2H). Importantly, CARD9 deletion alone in the absence of A β amyloidosis was not found to appreciably impact performance in the MWM test and we observed comparable spatial learning and memory in *Card9*^{+/+}, *Card9*^{+/-}, *Card9*^{-/-} mice (Figure 3.3). These findings suggest that absence of CARD9 in 5xFAD mice leads to increased levels of neuronal cell death in the hippocampus and accelerated cognitive impairments.

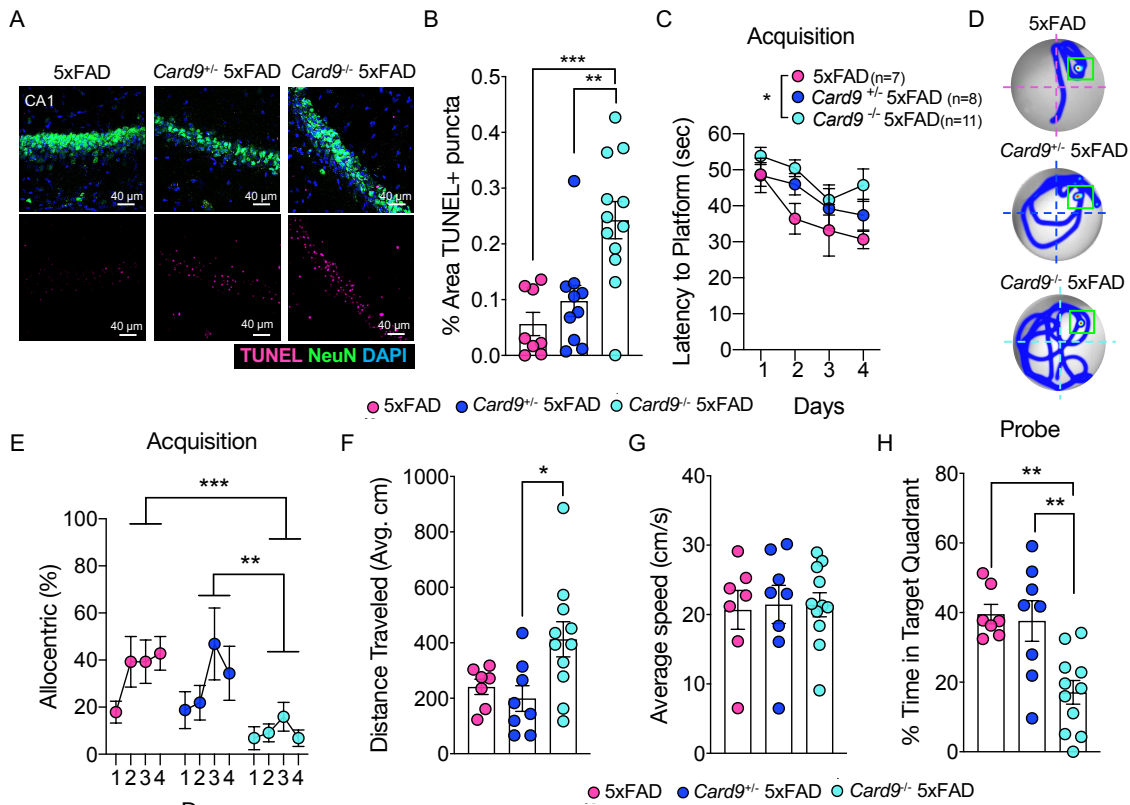


Figure 3.2. *Card9* deficiency leads to worsened neuronal health and cognitive impairment in 5xFAD mice. (A-B) Brains were harvested from 5-month-old 5xFAD, *Card9*^{+/-}5xFAD, and *Card9*^{-/-}5xFAD mice to evaluate neuronal death. The CA1 region of the hippocampus was evaluated for neuronal cell death by the TUNEL assay (pink), NeuN staining (green) and DAPI (blue). Original magnification: 63x; scale bars = 40 μm. (C-H) The Morris water maze (MWM) test was used to assess spatial learning and memory in 4-month-old 5xFAD, *Card9*^{+/-} 5xFAD, and *Card9*^{-/-} 5xFAD mice. (C-G) Acquisition stage of learning in the MWM. (C) Latency to platform (acquisition). (D) Representative heatmaps of mouse trajectory on day 4 of acquisition and (E) plotted percentage of allocentric navigation strategy during MWM acquisition. (F) Distance traveled averaged from all four trials in maze (cm) and (G) average speed of travel (cm/s) on day 4 of acquisition. (H) Percentage of time spent in the target quadrant (probe). Statistical significance between experimental groups was calculated by repeated-measures two-way ANOVA with Bonferroni's post hoc test (C, E) or one-way ANOVA with Tukey's post hoc test (B, F-H) from three independent experiments. **P* < 0.05, ***P* < 0.01, ****P* < 0.001. Error bars represent mean ± S.E.M. (B, C, E-H) and each data point represents an individual mouse (B, F-H), or the average of experimental mice per group (C,E).

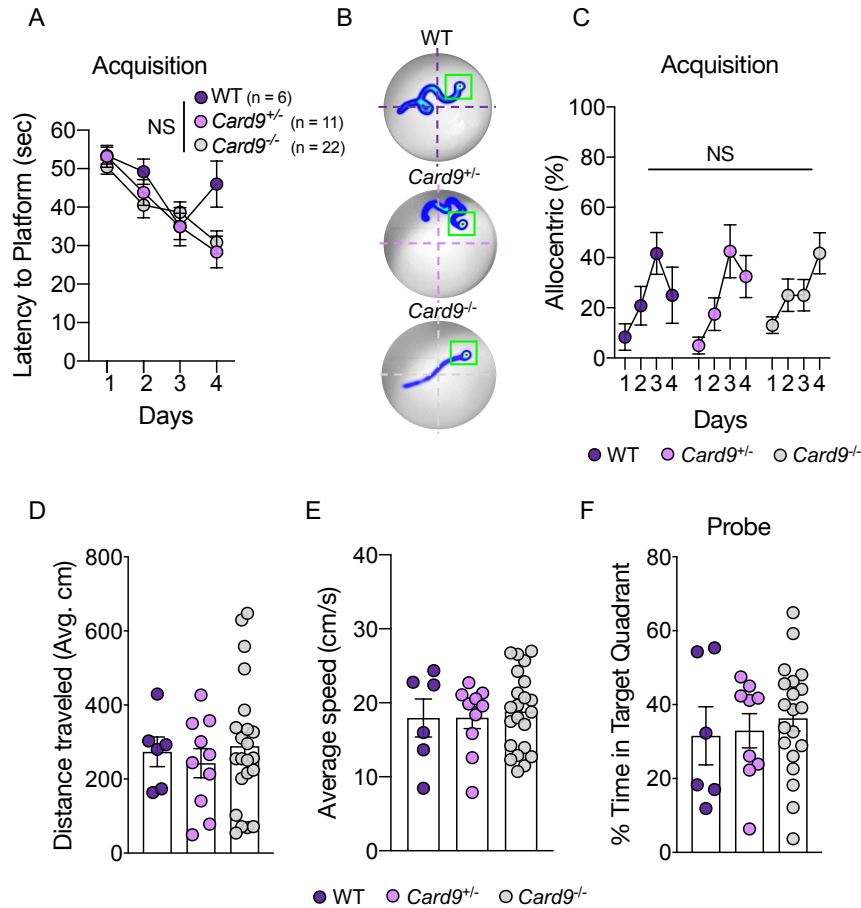


Figure 3.3. Deletion of *Card9* in the absence of A β -mediated pathology does not impact learning or memory. (A-F) The Morris water maze (MWM) test was used to assess spatial learning and memory in 4-month-old *Card9*^{+/+} (denoted as WT), *Card9*^{+/-}, and *Card9*^{-/-} mice. (A-E) Acquisition stage of learning in the MWM. (A) Latency to platform (acquisition). (B) Representative heatmaps of mouse trajectory on day 4 of acquisition and (C) plotted percentage of allocentric navigation strategies during MWM acquisition. (D) Distance traveled in maze (cm) and (E) average speed of travel (cm/s) on day 4 of acquisition. (F) Percentage of time spent in the target quadrant (probe). Statistical significance between experimental groups was calculated by repeated-measures two-way ANOVA with Bonferroni's post hoc test (A, C) or one-way ANOVA with Tukey's post hoc test (D-F) from three independent experiments. NS = not significant, **P* < 0.05. Error bars represent mean \pm S.E.M. (A, C-F) and each data point represents an individual mouse (D-F).

3.3.3 *CARD9* deficiency in 5xFAD mice results in altered microglial responses

In recent years there has been ever-growing interest in the roles that microglia play in AD. This was initially sparked by results obtained in human genetics studies linking mutations in multiple microglial genes to late onset AD (85). Follow-up studies in AD mouse models have largely confirmed that microglia can influence various aspects of AD related pathology (97, 100, 105, 112, 113). Notably, mounting evidence suggests that microglia are critically involved in both the phagocytosis and compaction of A β , and that this subsequently helps to protect neurons from interacting with neurotoxic species of A β (101, 396). Therefore, given our findings demonstrating increased levels of A β and neuronal loss in *CARD9*-deficient 5xFAD mice, paired with the knowledge that *Card9* is primarily expressed by microglia in the brain, we were interested in how *CARD9* deletion affects the mobilization of microglial responses to A β -driven pathology.

The observed increase in A β load in the *Card9*^{-/-}5xFAD brain prompted us to investigate potential differences in the phagocytic capacity of macrophages in *Card9*-deficient mice. To begin, we generated bone marrow-derived macrophages (BMDMs) from *Card9*^{+/+} (referred to as WT) and *Card9*^{-/-} mice. WT and *Card9*^{-/-} BMDMs were stimulated with oligomeric A β tagged with CyPher5E, a pH sensitive dye. CypHer5E fluoresces when brought into the low-pH environment of the phagolysosome; consequently, an increased staining of CypHer5E signal suggests elevated phagocytosis of A β by BMDMs. In these studies, we found that CARD9 deletion did not appreciably impact A β uptake by BMDMs (Figure 3.4). To discern whether *Card9*-deficiency affects A β clearance *in vivo*, we next injected CypHer5E-tagged A β into the cortex of WT and *Card9*^{-/-} mice and compared the presence of CypHer5E relative to total A β in the injection site. Similar to our *in vitro* macrophage findings, we did not observe substantial differences in the clearance of A β by IBA1⁺ cells between WT and *Card9*^{-/-} mice at 48 hours post intracortical injection of CypHer5E-tagged A β (Figure 3.4). Collectively, these results suggest that *Card9*-deficiency does not appreciably affect the phagocytosis of A β by BMDMs or CNS-resident cells.

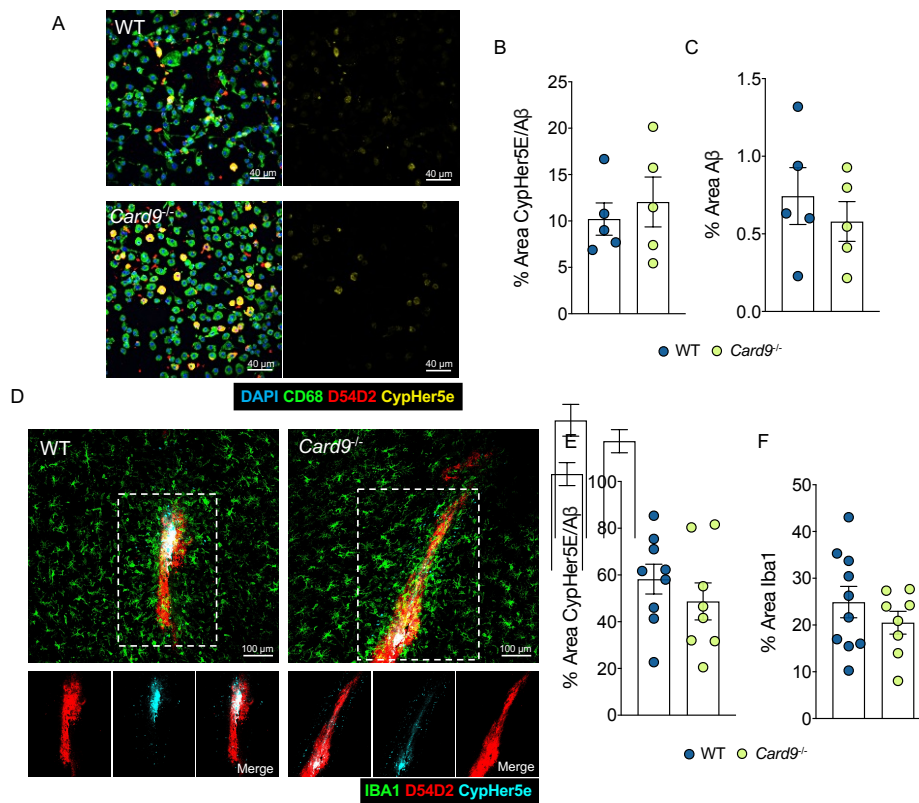


Figure 3.4. CARD9-deficient mice do not display impaired A β clearance *in vitro* or *in vivo*. (A-C) Bone marrow-derived macrophages (BMDMs) from C57BL/6J or *Card9*-deficient mice were stimulated with 10 μ m oligomeric A β (D54D2, red) tagged with pH-sensitive CypHer5e dye (yellow) for 24 hours. (A) Representative images of stimulated BMDMs. (B) The percent area of CypHer5e dye relative to A β and (C) percent area of A β . Original magnification: 40x; scale bar = 40 μ m. (D-F) Brains harvested from C57BL/6J or *Card9*-deficient mice stereotaxically injected with A β (D54D2, red) tagged with pH-sensitive CypHer5e dye (blue) in the cortex and harvested 48 hours post injection. (D) Representative images of the A β -CypHer5E injection site in the cortex of C57BL/6J and *Card9*-deficient mice. (E) The percentage of the ratio of CypHer5e dye and residual A β and (F) the percent area of IBA1⁺ cells at the site of injection. Consecutive sections, spaced 40 μ m apart, were quantified and averaged for each mouse in a blinded fashion to assess total clearance of CypHer5E-labelled A β oligomers over the entire area of the injection site. Original magnification: 40x; scale bar = 100 μ m. Statistical significance between experimental groups was calculated by unpaired two-tailed Student's *t*-test from two independent experiments. Error bars represent mean \pm S.E.M. and each data point represents an individual mouse (B-C, E-F).

To our surprise, we found that the loss of *Card9* results in a step-wise increase in the number of IBA1-labeled microglia within the cortex of 5xFAD mice (Figures 3.5A and 3.5B). This progressive increase in microglia between 5xFAD, *Card9*^{+/-}5xFAD, and *Card9*^{-/-}5xFAD mice is suggestive of a gene-dosage effect for the *Card9* allele (Figures 3.5A and 3.5B). The approximate doubling of microglial numbers in the cortex of *Card9*^{-/-}5xFAD mice compared with 5xFAD controls is likely explained by a similar magnitude increase in the number of proliferating microglia (Figures 3.5C and 3.5D). More specifically, *Card9*^{-/-}5xFAD mice have approximately twice the number of Ki67⁺ microglia in their cortex compared with 5xFAD mice (Figures 3.5C and 3.5D). In contrast, we did not observe any appreciable differences in microglial numbers or Ki67 expression between CARD9-deficient and wild-type mice that lacked the 5xFAD transgenes (Figure 3.6), suggesting that the increased numbers of microglia seen in *Card9*^{-/-}5xFAD mice was likely driven by A β -associated pathology.

The stimulation of microglial recruitment and proliferation in response to AD pathology is well characterized (100, 458), however, the loss of CARD9 appears to significantly enhance microglial mobilization to A β plaques while concurrently exacerbating A β load in the cortex of 5xFAD mice. One potential explanation for these somewhat paradoxical findings of increased numbers of both microglia and A β load in *Card9*^{-/-}5xFAD mice is that the microglia recruited to A β in CARD9-deficient 5xFAD mice are less effective in influencing A β compaction. To test this, we evaluated both A β plaque volume and sphericity as a readout of the ability of CARD9-sufficient and -deficient microglia to shape A β plaque compaction (100, 102, 396). For instance, more compact plaques are believed to indicate the formation of a functional microglial barrier in which microglia physically interact with the plaque to decrease the A β footprint in the brain parenchyma (100, 459). While we did not observe any notable differences in A β plaque sphericity between 5xFAD and *Card9*^{-/-}5xFAD mice (Figures 3.5E and 3.5F), we did, however, observe that CARD9 deficiency in 5xFAD mice leads to increased plaque volume when compared to 5xFAD littermate controls (Figures 3.5E and 3.5G). Therefore, despite the increase in microglia numbers in *Card9*^{-/-}5xFAD mice, *Card9*-deficient microglia failed to reduce the extent of A β plaque volume, suggesting that CARD9 is critical for microglial containment of A β .

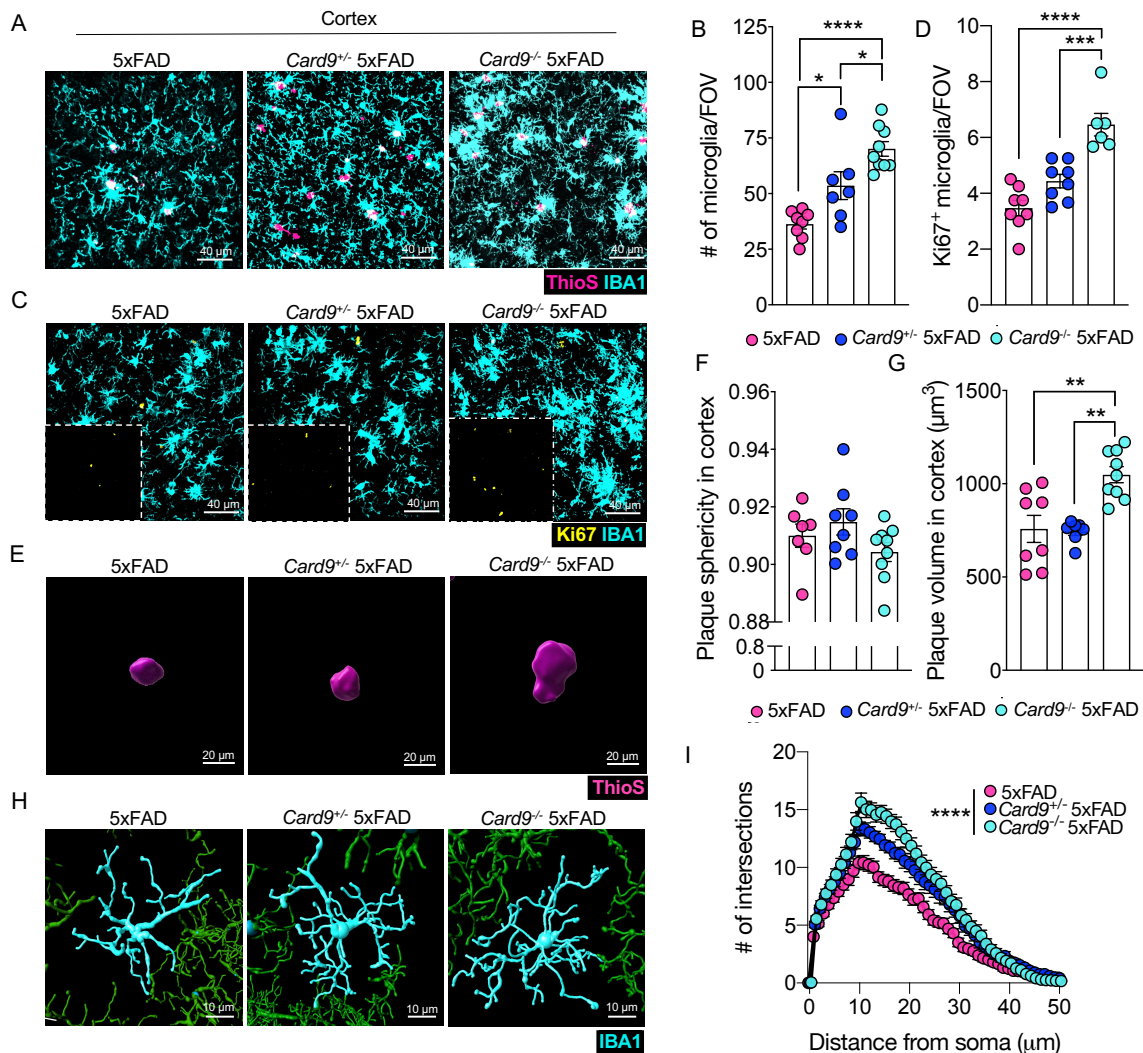


Figure 3.5. The loss of *Card9* leads to altered microgliosis in 5xFAD mice. (A-I) Brains were harvested from 5-month-old 5xFAD, *Card9*^{+/+}5xFAD, and *Card9*^{-/-}5xFAD mice to assess microglial activity and A β plaque volume. (A-B) Representative images and quantification of microglia numbers (IBA1, cyan) surrounding ThioS⁺ plaques (pink) in the field of view (FOV) of the frontal cortex of 5xFAD, *Card9*^{+/+}5xFAD, and *Card9*^{-/-}5xFAD mice. Original magnification: 63x; scale bar = 40 μ m. (C-D) Representative images of microglial proliferation measured by evaluating Ki67 (yellow) colocalization with IBA1+ (cyan) microglia in the cortex of matched sagittal sections. Original magnification: 63x; scale bar = 40 μ m. (E-G) Representative images and quantification of ThioS-labeled (pink) plaque sphericity and volume in the cortex. Original magnification: 63x; scale bar = 20 μ m. (H-I) Microglial morphology calculated by Sholl analysis from a total of 12 microglia from 3 matching brain sections per mouse (n=5 mice per group). (H) Representative microglia renderings and (I) Sholl analysis. Original magnification: 63x; scale bar = 10 μ m. Statistical significance between experimental groups was calculated by one-way ANOVA with Tukey's post hoc test (B-D, F-G) or repeated-measures two-way ANOVA with Bonferroni's post hoc test (I). * P < 0.05, ** P < 0.01, *** P < 0.001, **** P < 0.0001. Error bars represent mean \pm S.E.M. (B-D, F-G, I). Each data point represents an individual mouse (B-D, F-G) or the average of 5 mice (I). Data was collected from 6 fields of view (FOV) from a total of 3 matched sagittal sections (B, D) or 50-100 plaques from the cortex of each mouse (F, G).

It has been extensively shown that microglia become less ramified and more amoeboid in morphology in response to A β , and this is thought to affect the ability of microglia to handle and shape A β load (91). Because *Card9*^{-/-}5xFAD microglia exhibit increased proliferation without curbing A β load, we were thus also interested in investigating whether *Card9*-deficiency also impacts the ability of microglia to undergo morphological changes in response to A β -associated pathology. To explore this in greater detail, we focused on the A β -rich cortex and identified progressive microglial morphological differences between 5xFAD, *Card9*^{+/+}5xFAD, and *Card9*^{-/-}5xFAD mice (Figures 3.5H and 3.5I). For instance, *Card9*^{+/+}5xFAD and *Card9*^{-/-}5xFAD microglia displayed significantly more complex morphology as measured by Sholl analysis compared with 5xFAD microglia (Figures 3.5H and 3.5I). In contrast, *Card9*^{+/+}, *Card9*^{+/+}, *Card9*^{-/-}

microglia did not exhibit morphological changes in the absence of A β (Figure S6). Therefore, CARD9 is critical in driving microglial morphological activation upon A β stimulation. Collectively our findings suggest that CARD9 regulates microglial proliferation and morphological activation as well as A β compaction in the 5xFAD brain.

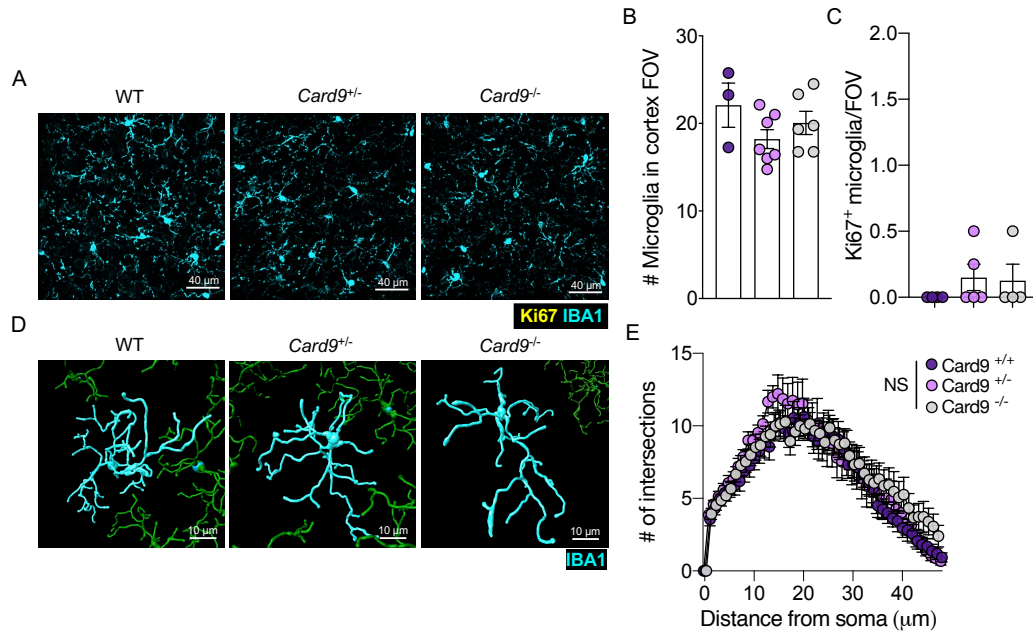


Figure 3.6. *Card9* deficiency in the absence of A β -mediated neuropathology does not affect microglial number or morphology in adult mice. Brains were harvested from 5-month-old *Card9*^{+/+} (denoted as WT), *Card9*^{+/-}, and *Card9*^{-/-} mice to assess microglial activity. (A-B) Representative images and quantification of microglia numbers (IBA1, cyan) in the field of view (FOV) of the frontal cortex. Original magnification: 63x; scale bar = 40 μm. (C) Quantification of microglial proliferation measured by evaluating Ki67 (yellow) colocalization with IBA1+ (cyan) microglia in the cortex of matched sagittal sections. (D-E) Microglial morphology calculated by Sholl analysis from a total of 12 microglia from 3 matching brain sections per mouse (n=4 mice per group). (D) Representative microglia renderings and (E) Sholl analysis quantification. Original magnification: 63x; scale bar = 10 μm. Statistical significance between experimental groups was calculated by one-way ANOVA with Tukey's post hoc tests from two independent experiments. Error bars represent mean \pm S.E.M. and each data point represents an individual mouse (B-C) or represents an average of 4 mice per group (E). Data was collected from 6 fields of view (FOV) from a total of 3 matched sagittal sections (B-C).

3.3.4 Microglial ROS production and lipid droplet formation are not impacted by CARD9 deletion in 5xFAD mice

While microglia can play beneficial roles in AD-related disease through their critical involvement in A β containment and disposal, unchecked activation of microglial inflammatory responses can also have deleterious effects and perpetuate further AD pathogenesis (86, 446). To gain a deeper understanding of how CARD9 may impact microglial-induced inflammation, we began by investigating whether *Card9*^{-/-} 5xFAD microglia take on lipid-droplet-accumulating microglia (LDAM) properties. LDAMs have been previously described in the aged brain as pro-inflammatory, with increased reactive oxygen species (ROS) and cytokine production (379). To determine if CARD9-deficient microglia in the 5xFAD brain exhibit LDAM-related dysregulation, we harvested brains from 5xFAD and *Card9*^{-/-}5xFAD mice and measured levels of BODIPY, a dye that labels lipid-droplets, and CellROX, a dye that fluoresces when oxidized by ROS, in CD11b^{hi}CD45^{int} cells. However, flow cytometric analysis revealed no appreciable differences in

BODIPY or CellROX staining in *Card9*^{-/-}5xFAD microglia when compared to 5xFAD control microglia (Figure S7). Thus, *Card9*-deficiency does not significantly increase the prevalence of LDAMs or ROS production by microglia in the 5xFAD brain.

Aberrant production of proinflammatory cytokine production by microglia is also believed to contribute to the propagation of AD pathology and memory deficits. For instance, the cytokines IL-6, IL-1 β , and IL-18 are often elevated in AD and have been reported to provoke A β accumulation and cognitive decline (460-463). CARD9 is known to regulate NF-kB activation, a transcription factor that coordinates the production of several pro-inflammatory cytokines including IL-6, pro-IL-1 β , and pro-IL-18 (464). Therefore, we investigated the levels of key pro and anti-inflammatory cytokines in the whole brain of 5xFAD, *Card9*^{+/-}5xFAD, and *Card9*^{-/-}5xFAD mice. However, we did not observe altered levels of IL-1 α , IL-1 β , IL-4, IL-6, IL-10, IL-17, IFN- γ , TNF- α by a multiplex ELISA (Figure S7). Altogether, these findings suggest that CARD9 deletion in 5xFAD mice does not substantially influence proinflammatory cytokine levels, production of ROS, or lipid droplet accumulation by microglia.

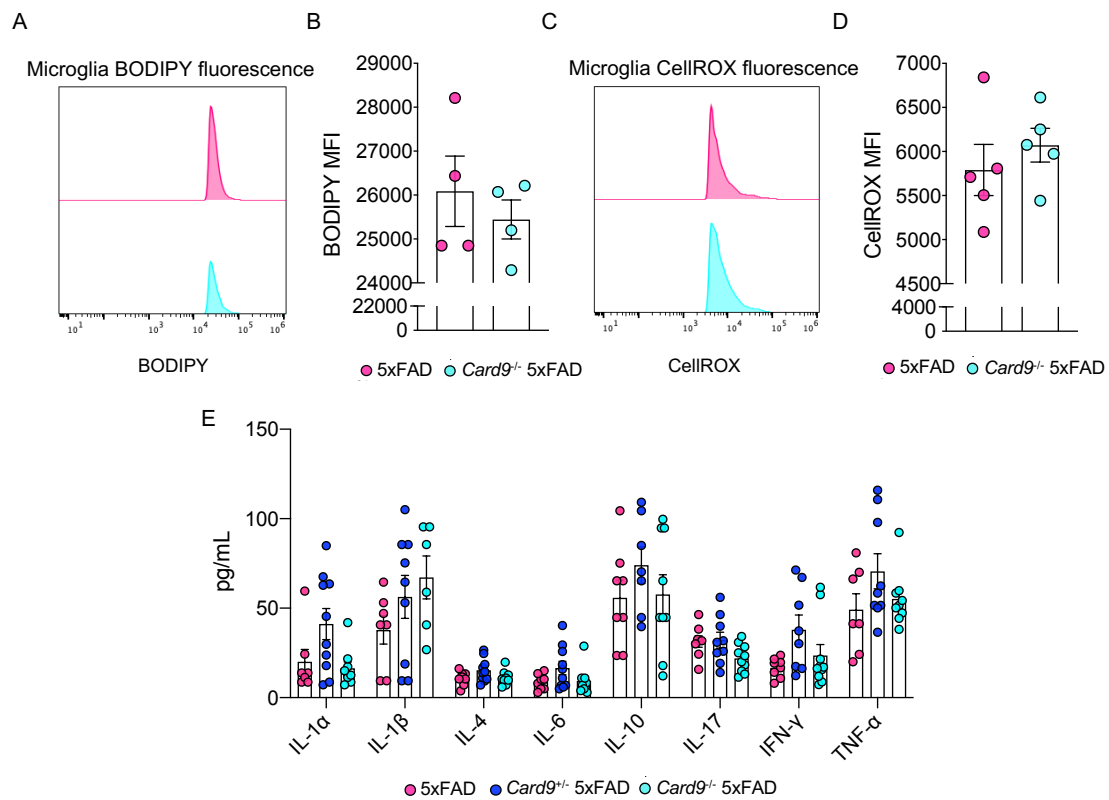


Figure 3.7. *Card9* deficiency does not significantly affect microglial ROS production, lipid droplet accumulation, or production of inflammatory cytokines associated with microglial activation in 5xFAD mice. (A-D) CD11b^{hi}CD45^{int} cells were gated from the brains of 5-month-old 5xFAD and *Card9*^{-/-}5xFAD mice and probed for reactive oxygen species (ROS) production and lipid droplet accumulation in microglia by flow cytometry. (A-B) Representative flow-cytometry histograms and mean fluorescence intensity (MFI) quantification of BODIPY labeled lipid droplets in sorted CD11b^{hi}CD45^{int} cells. (C-D) Representative flow-cytometry histograms and MFI quantification of CellROX labeled ROS in sorted CD11b^{hi}CD45^{int} cells. (E) Brain homogenate supernatants from 5-month-old 5xFAD, *Card9*^{+/-}5xFAD, and *Card9*^{-/-}5xFAD mice were analyzed for cytokine levels using a multiplex immunoassay. Statistical significance between experimental groups was calculated by unpaired two-tailed Student's *t*-test (B, D) and one-way ANOVA with Tukey's post hoc tests (E). Error bars represent mean \pm S.E.M. and each data point represents an individual mouse.

3.3.5 Effects of CARD9 deletion on the microglial transcriptional response in 5xFAD mice

Microglia exposed to AD-associated pathology are thought to undergo a transcriptional shift to become disease associated microglia (DAMs) (93). Upon stimulation, DAMs downregulate their homeostatic markers and subsequently upregulate several activation markers in a biphasic manner (94). This process of DAM acquisition is thought to supply microglia with an increased capacity to respond to and eliminate AD pathology (168). Given that *Card9*-deficiency exacerbates disease progression in 5xFAD mice, we hypothesized that the microglia of *Card9*^{-/-}5xFAD mice would be unable to undergo the transcriptional evolution seen in DAMs. Thus, to evaluate how CARD9 may affect microglia activity in an unbiased and comprehensive manner, we performed bulk RNA sequencing (RNA-Seq) on magnetic bead-sorted CD11b⁺ cells from the brains of *Card9*^{+/+} (WT), *Card9*^{-/-}, 5xFAD, and *Card9*^{-/-}5xFAD mice. Principal component (PC) analysis uncovered a prominent separation between homeostatic (WT and *Card9*^{-/-}) and 5xFAD (5xFAD and *Card9*^{-/-}5xFAD) microglia (Figure 3.8A). More specifically, when comparing 5xFAD and WT microglia, we identified 156 downregulated and 510 upregulated genes (FDR<0.1) (Figure 3.8B). As expected, several of the top upregulated genes in 5xFAD microglia were DAM-defining genes, including: *Cst7*, *Lpl*, and *Itgax* (Figure 3.8B).

pathology (465, 466). Although we did not observe overt changes in inflammatory signaling or oxidative stress between 5xFAD and *Card9*^{-/-}5xFAD mice (Figures 3.8 and 3.7) which have previously been described to be regulated by KLF4, we did observe a significant increase in neuronal cell death in the CA1 region of the hippocampus (Figures 3.2A and 3.2B). Neuronal cell loss is a key element contributing to AD progression that is reported to be propagated by KLF4 (465-468). Interestingly, KLF4 is believed to contribute to microglial iron dyshomeostasis that promotes impaired microglial response to A β (466). In fact, iron-laden microglia have been identified in the AD brain (469). Therefore, we looked at ferritin heavy chain accumulation in microglia, a subunit of ferritin critical for iron sequestration (470). We took into account the increase in microglial coverage in the cortex of *Card9*^{-/-}5xFAD mice by normalizing the volume of ferritin heavy chain to the total volume of IBA1⁺ cells, therefore reflecting the ferritin heavy chain level per microglia, and observed a striking increase in ferritin heavy chain staining within *Card9*^{-/-}5xFAD microglia compared with 5xFAD controls (Figures 3.8F and 3.8G). Thus, CARD9 likely regulates iron homeostasis in 5xFAD microglia. It is important to note that *Card9*-deletion at steady-state in the absence of 5xFAD transgene did not cause a major transcriptional shift in microglia, with a unique 4 downregulated (*Ly6i*, *Hebp1*, *Tppp3*, and *Cd300e*) and 4 upregulated (*Cacnb2*, *Prkcq*, *Ppfia4*, *Mrc2*) genes compared with WT microglia (FDR<0.1) (Figure 3.9). These findings indicate that CARD9 deletion in 5xFAD mice leads to elevated expression of KLF4 in the brain and that this is associated with increased production of ferritin heavy chain by IBA1⁺ cells.

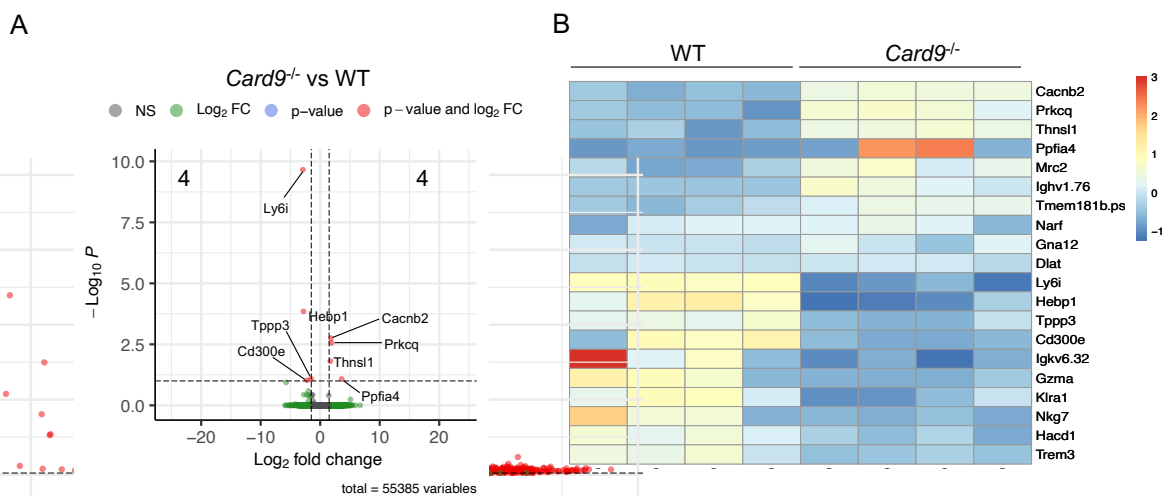


Figure 3.9. *Card9* deficiency in the absence of A β does not appreciably affect microglial transcription. (A-B) RNA-Seq was performed on microglia from 5-month-old *Card9*^{+/+} (denoted as WT) and *Card9*^{-/-} mice sorted from single-cell brain suspensions using anti-CD11b⁺-coated magnetic beads and magnetic column sorting. (A) Volcano plot comparing significantly differentially expressed genes (FDR<0.1) between *Card9*^{-/-} and WT microglia, where 4 genes are downregulated, and 4 genes are upregulated. (B) Heatmap representation of the top overall 10 upregulated and downregulated genes between *Card9*^{-/-} and WT microglia.

3.3.6 Targeting CARD9 activation limits A β coverage in the hippocampus

Thus far, we have demonstrated that CARD9 deletion is detrimental for microglial activation and pathology progression in the 5xFAD mouse model. These findings suggest that CARD9 activity plays a protective

role in response to A β pathology, thus, we sought to explore whether CARD9 stimulation can reduce A β load in the brain. We chose to enhance CARD9 signaling by targeting the activation of CLEC7A, a receptor that has been extensively reported to promote CARD9 activation in response to fungal triggers (471, 472). CLEC7A initiates downstream CARD9 signaling following its binding to β -D-glucans, a component of yeast cell walls (383). We injected pustulan, a β -D-glucan, into the A β -laden hippocampus of 5xFAD mice to evaluate how the activation of the CLEC7A-CARD9 pathway affected A β load. 2-month-old 5xFAD mice were injected with vehicle or 2 μ g of pustulan into the right and left hemisphere of the hippocampus (at \pm 2 mm lateral, -2 mm posterior, and -2 mm ventral relative to the intersection of the coronal and sagittal suture (bregma) at a rate of 200 nl/min), respectively. Brains were then harvested at 7 days post-injection and A β plaque load was compared between the vehicle- and pustulan-treated hemispheres of the hippocampus (Figure 3.10A). In 5xFAD mice, the hippocampal hemisphere treated with pustulan had significantly reduced A β coverage compared to the vehicle-treated hippocampal hemisphere (Figures 3.10B and 3.10C). In contrast, the hippocampi of *Card9*^{-/-}5xFAD mice had comparable levels of A β regardless of treatment (Figures 3.10B and 3.10D), suggesting that pustulan promotes A β control in a CARD9-dependent fashion. Altogether, these data indicate that CARD9 signaling contributes to the restriction of A β -driven pathology in the 5xFAD mouse model of AD.

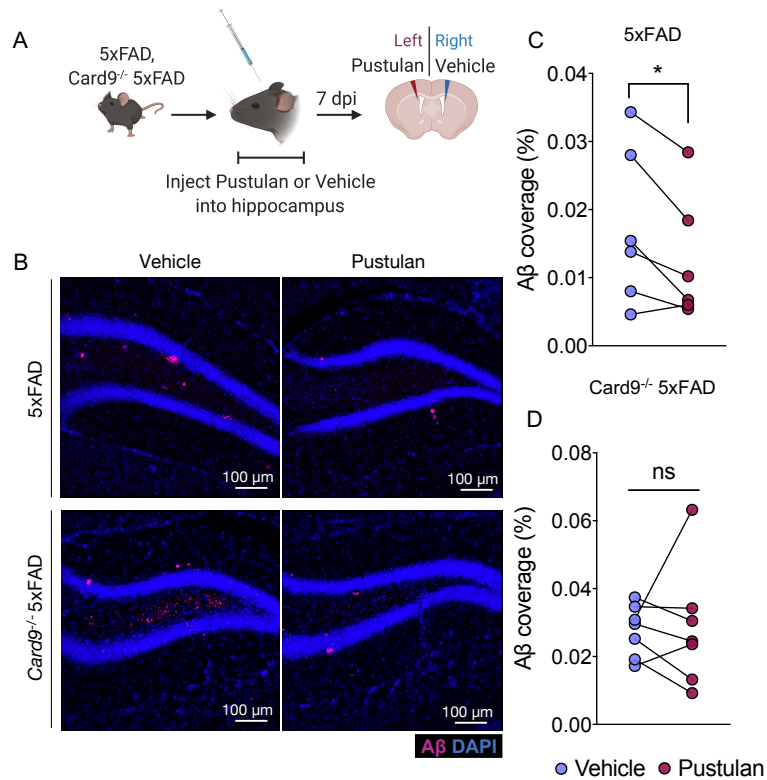


Figure 3.10. Pustulan treatment enhances A β clearance in a CARD9-dependent manner in the hippocampus of 5xFAD mice. (A-D) Right and left hippocampal injection of vehicle or pustulan, respectively, into 2-month-old 5xFAD and *Card9*^{-/-} 5xFAD mice. Brains were then harvested 7 days post injection (dpi). (A) Experimental design schematic. (B) Representative images of A β (pink) coverage in 2-month-old 5xFAD and *Card9*^{-/-} 5xFAD mice 7 days following intrahippocampal injection of vehicle or 2 μ g of pustulan. (C-D) Quantification of A β (D54D2, pink) in the hippocampus of (C) 5xFAD and (D) *Card9*^{-/-} 5xFAD mice. Statistical significance between experimental groups was calculated by paired Student's t-test (C-D). ns = nonsignificant, **P* < 0.05. Representative data from 3 independent experiments (C-D). Error bars represent mean \pm S.E.M. and each data point represents an individual mouse.

3.4 Discussion

The identification of microglial AD risk genes from GWAS studies has implicated several receptors in both aberrant and protective microglial responses (85, 94, 473). The characterization of these microglial receptors in mice and humans has uncovered several potential therapeutic targets (474-476); the activation or inhibition of these receptors has dominated microglia-targeted AD therapy as they extensively influence microglial response to AD pathology (100, 103, 105, 112, 113, 124, 396). In particular, activation of the TREM2 receptor has been demonstrated to exert neuroprotective effects and has advanced to phase 2 clinical trials for AD treatment (474). However, much of the microglial downstream signaling in AD remains poorly defined, potentially leaving a stone unturned for additional and more precise interventions. The intricacies of microglial function in AD, and how best to target them, are more likely to be uncovered by elucidating the unique and shared downstream molecular underpinnings of these receptors.

In our studies presented here, we identify CARD9, an immune molecule downstream of several microglial receptors implicated in AD, as an important regulator of microglial activation in the context of A β -driven pathology in 5xFAD mice. We demonstrate that CARD9 regulates the microglial response to A β in the 5xFAD brain, ultimately impacting A β load and neuronal loss. In addition, we find that CARD9 protects against cognitive impairment in 5xFAD mice. A transcriptional comparison between 5xFAD and *Card9*^{-/-} 5xFAD microglia uncovered increased expression of *Klf4* in CARD9-deficient microglia, a transcription factor linked with increased neuronal loss and iron dyshomeostasis (465, 466, 468). Interestingly, in addition to increased neuronal loss seen in the hippocampus, CARD9-deficient 5xFAD mice also display significantly higher iron retention in their microglia, a phenotype emblematic of microglial dysfunction (477, 478). Furthermore, we demonstrate that pustulan-induced activation of CARD9 drives a reduction in A β plaque load in the hippocampus of 5xFAD mice. Together, our studies suggest an important role for CARD9 in regulating microglial activation and A β load in 5xFAD mice.

CARD9 has classically been defined for its roles in driving myeloid cell inflammatory responses in the context of peripheral fungal infection (383, 403, 464, 479). The ability of microglia to function in the context of infection has long been known (480-483), but whether this mirrors microglial responses to AD pathology remains ill-defined. Interestingly, artifacts of fungal pathogens adjacent to A β plaques have been found in the brains of AD patients (117, 484), and although it remains controversial whether fungal infection precedes or follows AD onset (119), microglia are well-equipped to recognize and respond to this pathogen in the brain (480). Thus, microglia contain sophisticated machinery that responds to both infectious triggers and AD pathology (86, 429, 482, 485); in turn, microglia have the potential to act as a critical bridge between immune activation and AD pathogenesis. For example, CLEC7A, a receptor upstream of CARD9, is upregulated by microglia surrounding fungal aggregates and A β plaques (105,

485). Interestingly, fungal pathogens contain an amyloid-like structure on their cell surface that allows for pathogen adhesion and biofilm formation (486, 487), which may explain the multi-modal upregulation of a fungal receptor such as CLEC7A. Altogether, the characterization of this innate immune response in both modalities of brain infection and neurodegeneration may uncover enigmatic etiologies of AD.

Targeting microglia in AD has become increasingly more complex as scientists gain a more complete understanding of the pleiotropic roles that microglia play in the evolution of disease. Just as AD can be stimulated by vastly heterogeneous triggers involving a combination of aging, environmental factors, and genetics (249, 473, 488-490), microglial functions can also be significantly affected by these same contributing factors. Importantly, the progression of microglial transcription throughout AD pathogenesis has the capacity to significantly alter microglial responses and subsequent AD progression (93, 94, 105, 438, 491). Recent work has described the importance of these innate myeloid cells taking on a DAM signature during AD, promoting enhanced phagocytic and inflammatory function (93). However, more recent work has demonstrated that microglia undergo a phasic shift from phagocytic and proliferative to anti-viral and apoptotic in the context of tauopathy (491). In the latter phase, microglia are immunosuppressed, but also contribute to chronic inflammation, a pathogenic hallmark in the AD brain (491). Ultimately, effectively targeting microglia in AD, either through the enhancement or diminution of microglial function, may largely depend on the prevailing pathology, stage of disease, and the delineation of influential microglial signaling.

Altogether, differential microglial responses in AD, including proliferation, activation, and pathology clearance, involve critical downstream signaling that have remained poorly described to date. In the studies presented here, we have demonstrated that CARD9 functions to impede AD pathology progression and acts as a relevant intracellular mediator of microglial response to A β in 5xFAD mice. Our findings highlight the important nature of CARD9, a shared downstream molecule of several AD-associated microglial receptors, in protecting against A β -mediated neurodegeneration.

3.5 Methods

Mice

All mouse experiments were performed in accordance with the relevant guidelines and regulations of the University of Virginia and approved by the University of Virginia Animal Care and Use Committee. Female 5xFAD mice (Stock # 34848-JAX), *Card9*^{-/-} mice (Stock # 017309), and C57BL/6J mice (Stock # 000664) were obtained from The Jackson Laboratory and were crossed to generate *Card9*^{+/+} (denoted as WT), *Card9*^{+/-}, *Card9*^{-/-}, *Card9*^{+/+}5xFAD (denoted as 5xFAD), *Card9*^{+/-}5xFAD, and *Card9*^{-/-}5xFAD experimental

mice. Mice underwent a 12-hour light/dark cycle, were housed in specific pathogen-free conditions and kept at a standardized temperature ($21 \pm 1.5^\circ \text{C}$) and humidity ($50 \pm 10\%$).

Brain tissue harvest

Experimental mice underwent euthanasia by means of CO_2 asphyxiation and were transcardially perfused with 20 ml of 1xPBS. Brains were then harvested and bisected. The left hemisphere was drop-fixed in 4% paraformaldehyde over night at 4°C and the right hemisphere flash-frozen and stored at -80°C . Fixed samples were placed in 30% sucrose until sunken in solution and then frozen in Tissue-Plus OCT compound (Thermo Fisher). Using a cryostat (Leica), brains were sectioned at $50 \mu\text{m}$ in thickness and stored in PBS + 0.05% sodium azide at 4°C until stained for imaging. For RNA extraction and protein extraction, the flash-frozen brains were thawed on ice and mechanically homogenized in 500 μl of Tissue Protein Extraction Reagent T-PER (Thermo Fisher, 78510) containing protease inhibitor cocktail cOmplete (Roche, 11873580001) and phosphatase inhibitor cocktail PhosSTOP (Roche, 04906845001). For RNA extraction, 50 μl of brain homogenate was diluted in 500 μl Trizol and stored at -80°C . The remaining brain homogenates were then spun down at 16,000 rpm for 10 minutes and the supernatant was collected for soluble amyloid beta analysis and pellet were isolated for insoluble amyloid beta analysis by ELISA.

Immunofluorescence microscopy

Brain sections were blocked for 1 hour at room temperature with 2% donkey serum, 1% bovine serum albumin, 0.1% triton, 0.05% tween in PBS prior to incubation with primary antibodies. The primary antibodies were then diluted in this block overnight at 4°C . Brain sections were stained with anti-A β (D54D2, Cell Signaling, 1:300 dilution) to label plaques. To assess neuronal cell death, sections were stained with anti-NeuN (MAB377, Millipore Sigma, 1:500 dilution) and TUNEL (Millipore Sigma, 11684795910, according to the manufacturer's instructions). In order to analyze microglia, sections were stained with IBA1 (ab5076, Abcam, 1:300 dilution). Microglial proliferation was assessed using Ki67-EF660 (SoIA15, Thermo Fisher, 1:100 dilution). Microglial iron accumulation was measured using Ferritin Heavy Chain (PA5-27500, Thermo Fisher, 1:500). Following primary antibody incubation, sections were then washed 3 times for 10 minutes at room temperature in PBS and 0.05% tween-20. After washing, the brain sections were incubated in respective donkey Alexa Fluor 488, 594, 647 anti-rabbit, -goat, -rat, -streptavidin, and -mouse (Thermo Fisher, 1:1000 dilution) for 2 hours at room temperature. Once again, brain sections were washed 3 times for 10 minutes at room temperature. Following washing, sections were stained with DAPI (1:1000) for 10 minutes at room temperature to label nuclei, or stained with ThioflavinS (Sigma-Aldrich, 2 mg/10ml) for 8 minutes followed by three 2-minute washes with 50% ethanol at room temperature to label plaques. Brain sections were then transferred to PBS before being mounted to glass microscope slides with 50 μl of ProLongGold antifade reagent (P36930, Invitrogen) and

coverslips. For storage, mounted brain sections were kept at 4°C and were imaged using LAS AF software (Leica Microsystems) on a Leica TCS SP8 confocal microscope. Images were analyzed using FIJI software or Imaris software (9.5.1).

ELISA

To assess amyloid beta composition in the brain, A β was measured in brain homogenates supernatants for soluble A β analysis, or brain homogenate pellets that underwent guanidine extraction by incubating the pellets 1:6 in 5 M guanidine HCL/50 mM tris, pH = 8.0 at room temperature for 3 hours for insoluble A β analysis. The guanidine-extracted samples were then diluted 1:5 in PBS containing protease inhibitor cocktail cOmplete (11873580001, Roche) then centrifuged at 16,000 g for 20 minutes at 4°C. The brain homogenate supernatant was diluted 1:10 and the guanidine-extraction supernatant was diluted 1:200 and quantified by Amyloid beta 42 Mouse ELISA kit (KMB3441, Thermo Fisher).

Mouse behavior

The Morris water maze (MWM) was completed on 4-month-old mice and was performed as outlined in (294). The first four days of acquisition had four 60-second trials and the fifth day (probe) had one 60-second trial in which the hidden platform was removed. Mice were gently placed in an opaque 23°C pool filled with white paint and a hidden platform 1 cm below water level. The pool contained 4 different visual cues with varying shapes and colors and mice were placed in alternate places in the pool for each trial. Mice were given 60 seconds to find the hidden platform during each trial, however, if the mouse was unable to find the platform, they were placed on the platform for 5 seconds at the end of the trial. Tracking and scoring of all behavioral trials was accomplished using video tracking software (Noldus Ethovision XT).

A β oligomer preparation

A β (1-42) (641-15, California peptide) was monomerized using a previously published protocol (423), using hexafluoroisopropanol (HFIP) (52517, Sigma-Aldrich). 5mM monomeric A β samples were incubated for 24 hours at 4°C in F12 media to make a 200 μ M stock of oligomeric A β . Samples were then incubated with CypHer5E-NHS ester (PA15401, GE Healthcare) diluted in 0.1 M sodium bicarbonate for 30 minutes covered and at room temperature. Following incubation, Biospin columns (7326227, Bio-Rad) were used to quench unbound dye. CypHer5E-tagged A β oligomers were stored at 4°C prior to cell culture treatment or injection.

In vitro phagocytosis

Bone marrow-derived macrophages (BMDMs) were harvested from the hind limbs of WT and *Card9*^{-/-} mice. Collected bones were sprayed with 70% ethanol before being placed in IMDM (12440-053, Gibco) containing penicillin/streptomycin (P/S) (15140-122, Gibco). Using a 25-gauge needle, marrow was flushed through bones using 20 ml of IMDM containing P/S. Using an 18-gauge needle, the flushed bone marrow was triturated 5 times to make a single-cell suspension. Samples were spun down at 1500 rpm for 5 minutes at 4°C. Cell pellets were resuspended in bone marrow macrophages differentiation media (BMDM media) containing IMDM, 10% FBS, 1% non-essential amino acids, 1% P/S, and 50 ng/ml M-CSF. Cells were then plated on 150 X 25 mm culture dishes (430597, Thomas Scientific). Three days after plating, 5 ml of BMDM media was added to each dish. On day 6, media was aspirated from dishes and 10 ml of PBS was added to each plate and incubated for 10 minutes at 4°C. Using a scraper, BMDMs were removed from the dish and transferred to a conical tube, spun down, and resuspended in BMDM media. 2 million cells/well were pipetted in 6 well plates containing glass coverslips. The next day, BMDMs were treated with 10 μM of oligomeric Aβ tagged with CypHer5E for 24 hours. BMDM-coated glass coverslips were fixed for 10 minutes at room temperature in 4% PFA. Following fixation, coverslips were washed 3 times with cold PBS. The cells were then permeabilized using 0.25% Triton X-100 diluted in PBS for 10 minutes at room temperature. Cells were washed 3 times with cold PBS. The coverslips containing BMDMs were then blocked in 2% donkey serum, 1% bovine serum albumin, 0.1% triton, 0.05% tween in PBS for 1 hour prior to incubation with primary antibodies for CD68 (MCA1957, Bio-Rad, 1:1000 dilution) and anti-Aβ (D54D2, Cell Signaling, 1:300 dilution) diluted in blocking buffer overnight at 4°C. Cells were then washed 3 times with PBS and stained with Alexa Fluor secondary antibodies (Thermo Fisher, 1:1000 dilution) for 1 hour at room temperature. Finally, cells were washed 3 times with PBS and stained with DAPI (1:1000) for 10 minutes at room temperature before mounting the coverslips onto microscope slides to assess Aβ phagocytosis.

In vivo phagocytosis

WT and *Card9*^{-/-} mice received a 1 μl injection of CypHer5E-tagged Aβ oligomers (1 mg/ml) into the right-hemisphere cortex (at ±2 mm lateral, 0 mm anterior-posterior, and -1.5 mm ventral relative to the intersection of the coronal and sagittal suture (bregma) at a rate of 200 nl/min) using a stereotaxic frame (51730U, Stoelting) and nanoliter injector (NL2010MC2T, World Precision Instruments). 48 hours post injection, mice were euthanized using CO₂ and transcardially perfused before processing the brains to be imaged to assess Aβ phagocytosis.

Flow cytometry

To assess BODIPY and ROS in gated microglia, mice were euthanized using CO₂ and transcardially perfused using 20 ml of PBS. After removing the meninges and choroid plexus, the brains were processed

into a single cell suspension as described in (424). Cell pellets were then resuspended in 13 ml of 37% isotonic Percoll (17-0891-01, GE Healthcare) to remove myelin. Samples were spun down with no brake and the myelin layer was removed. The remaining cell pellet was transferred to a 96 well V-bottom plate and washed with 1X PBS. The assessment of lipid droplet accumulation in cells was accomplished by staining the cells with BODIPY (D3861, Invitrogen, 1:2000) diluted in PBS at 37°C for 10 minutes. To label reactive oxygen species, cells were stained with CellROX (C10491, Thermo Fisher, 1:500) diluted in PBS at 37°C for 30 minutes. Following BODIPY and CellROX staining, cells were spun down 1500 rpm for 5 minutes at 4°C and washed with FACS buffer (pH 7.4, 0.1 M PBS; 1 mM EDTA, and 1% BSA). To label microglia, cells were stained with flow antibodies for CD11b, and CD45 (eBioscience) diluted 1:200 in FACS buffer for 20 minutes at 4°C. Cells were spun down and washed with FACS buffer. Prior to running samples on the cytometer, cells were resuspended in 100 µl FACS buffer containing DAPI 1:5000. Microglia were gated as live cells (DAPI negative), single cells, and as CD11b^{hi}CD45^{int} cells. BODIPY and CellROX mean fluorescence intensity (MFI) was measured in these gated microglia.

MACS isolation of microglia for RNA-sequencing

Euthanasia of mice was performed using CO₂ followed by transcardial perfusion using 20 ml of 1X PBS with heparin. The meninges and choroid plexus were removed from the brain before beginning the magnetic-activated cell sorting (MACS)-sorting protocol. Microglia were isolated using the methods described in (424). In brief, brains were placed in 5 ml of HBSS (with Mg and Ca) (14025092, Gibco) with papain 4U/ml (LS003126, Worthington) and 50 U/ml DNase I (10104159001, Sigma-Aldrich). Following 3 triturations of the samples using a 5 ml serological pipette over 45 minutes at 37°C, the brain homogenates were transferred to a conical tube containing a 70-µm cell strainer and topped with 20 ml of DMEM/F12 (21331020, Gibco) containing 10% FBS, 1x antibiotic-antimycotic (15240096, Thermo Fisher), and 1x GlutaMAX (35050061, Invitrogen). Strained samples were then spun down with slow brake (3 on a 0-10 scale) for 10 minutes at 300 G, resuspended in 160 µl MACS buffer (130-091-376, Miltenyi Biotec), and then incubated with 20 µl MACS CD11b (microglia) microbeads (130-093-634, Miltenyi Biotec) for 15 min at 4°C. Sorting was performed using LS columns and a QuadroMACS magnet (Miltenyi, 130-042-401 and 130-091-051) according to the product instructions. The protocol efficiency was validated using flow cytometry (>90% CD11b^{hi}CD45^{int}) before submitting for RNA-sequencing.

RNA-sequencing analysis

Microglia sorted using MACS isolation were sent to Azenta Next Generation Sequencing. Using splice-aware read aligner HISAT2, FASTQ files were aligned with the UCSC mm10 mouse genome. Quality control filtering was applied using Samtools. Next, HTSeq was used to sort reads into feature counts. DESeq2 (v1.30.0) was utilized to normalize raw counts to read depth, perform principal component

analysis, and carry out differential expression analysis. The Benjamini-Hochberg procedure was used to correct p-values and limit false positives arising from multiple testing. RNA-seq analyses were performed using Seq2Pathway, fgsea, tidyverse, and dplyr software packages. Heatmaps were produced using the pheatmap R package (<https://github.com/raivokolde/pheatmap>), lattice (<http://lattice.r-forge.r-project.org/>) or ggplot2 (<https://ggplot2.tidyverse.org>) packages. Volcano plots were produced using the EnhancedVolcano R package (<https://github.com/kevinblighe/EnhancedVolcano>).

Intrahippocampal injection procedure

5xFAD and *Card9*^{-/-}5xFAD mice were anesthetized with a ketamine/xylazine cocktail before receiving a bilateral hippocampal injection of 2 μ l of vehicle or 2 μ g pustulan into the right and left hemisphere of the hippocampus (at ± 2 mm lateral, -2 mm posterior, and -2 mm ventral relative to the intersection of the coronal and sagittal suture (bregma) at a rate of 200 nl/min) using a stereotaxic frame (51730U, Stoelting) and nanoliter injector (NL2010MC2T, World Precision Instruments). Seven days post injection, mice were euthanized using CO₂ and transcardially perfused before preparing brains for immunofluorescent staining to evaluate A β clearance in the hippocampus. Images were analyzed using FIJI software or Imaris software (9.5.1).

Statistics

All statistical analyses were performed using Prism software (GraphPad). Statistical tests include Student's t test (paired and unpaired), one-way ANOVA, and two-way ANOVA. *P* values less than 0.05 were deemed significant: **p* < 0.05, ***p* < 0.01, ****p* < 0.001, *****p* < 0.0001. All data are represented as mean \pm SEM.

Chapter 4

Discussion and Future Directions

4.1 Dissertation discussion

This dissertation focused on the signaling mechanisms by which the resident innate immune cells of the brain, microglia, modulate Alzheimer's disease pathology progression. We presented novel data outlining the critical role spleen tyrosine kinase (SYK) plays in driving protective microglial mobilization and proliferation in response to A β pathology (Chapter 2). In addition, we showed that SYK regulates microglial morphological activation, AKT/GSK3 β -signaling, and disease-associated microglia (DAM) phenotype acquisition (Chapter 2). Finally, we demonstrated that SYK drives microglial phagocytosis of multiple neurodegenerative pathologies including A β in a mouse model of AD and damaged myelin in a mouse model of demyelination (Chapter 2). We then described how another critical intracellular signaling molecule further downstream of SYK, known as caspase recruitment domain-containing protein 9 (CARD9), regulates microglial response to A β (Chapter 3). We observed CARD9-dependent protection against A β accumulation, neuronal loss, and memory decline (Chapter 3). Finally, we showed that pharmacological boosting of CARD9 signaling drives clearance of A β plaques (Chapter 3). Initial work characterizing important intracellular signaling in microglia during neurodegeneration have begun to unravel some immunological mysteries of the brain during aging and disease. Therefore, the molecular underpinnings of microglial response to AD pathology require further investigation to identify novel therapeutic targets in lieu of unsuccessful A β drug targets. In this discussion, I will feature future directions to further uncover the significant mechanisms by which microglial SYK and CARD9 signaling pathways may regulate microglial response to neurodegenerative pathology.

4.1.1 Neuroprotective roles of microglial SYK during neurodegenerative disease

Although several microglial receptors have been described to influence cellular responses to neurodegenerative pathology, the intracellular signaling specifically directing microglial aptitude during neurodegeneration has remained relatively unexplored. It is apparent that microglia critically regulate pathology accumulation and disease progression during AD and demyelinating disease (88, 202, 384, 446, 492). Targeting downstream signaling molecules has the potential to produce more precise interventions while allowing other cellular processes to remain unperturbed. In our studies, we find that SYK instructs signaling downstream of several microglial receptors during AD and demyelination. Our data also suggest that SYK drives neuroprotective and more targetable downstream signaling, such as AKT phosphorylation, driving a shift away from detrimental GSK3 β signaling. These findings, along with future analysis of additional SYK-dependent alterations in microglial downstream signaling during neurodegeneration, may guide novel targets for disease.

Microglia remain a double-edged sword during neurodegeneration. Specifically in AD, activation of machinery, such as the TREM2 and SYK signaling, protects against disease progression (97, 100, 103, 339, 357, 387, 400, 431, 493). However, continual microglial exposure to plaque pathology, and resultant microglial activation, provokes a detrimental shift in function. For instance, microglia deviate from cells capable of regulating cellular debris and offering trophic support to other cells in the brain, instead becoming chronically activated cells that instigate neuroinflammation and drive heightened AD pathology accumulation (133, 494-496). AD cases are vastly heterogeneous due to their varying root causes, and similarly, the kinetics by which microglia transform from protective surveillance cells to propagators of disease likely remains variable in patients (497, 498). This underscores the importance of calibrating the timing of pharmacologically targeting microglial populations. It is imperative that we further elucidate microglial signaling, including SYK and its downstream mediators, throughout the timeline of disease so that we may gain a broader understanding of when and how to target these immune cells.

The protective nature of homeostatic microglia undergoing transcriptional activation into DAMs during AD remains contested (93, 94, 499). The loss of homeostatic expression in DAMs is countered with upregulation of genes associated with machinery particularly apt at phagocytosing AD pathology (93, 94). Therefore, this shift is likely beneficial in the short term. For instance, we demonstrate that SYK-deficient microglia are unable to take on the DAM transcriptional signature and this exacerbates A β pathology accumulation. However, previous or continual exposure to stressors or neurodegenerative pathology can make this microglial shift permanently inflammatory and propagative of more pathology and neuronal damage (248, 496, 500, 501). Therefore, many studies are now focusing on the complete removal of microglia following disease onset (124, 175, 178, 502). In the context of AD, these studies indicate that microglia are necessary for amyloid plaque formation by building higher-order A β structure from more neurotoxic lower-order A β oligomers (120). However, A β plaques themselves damage surrounding neurons, and are therefore not harmless. Following plaque formation, microglia form a critical barrier to protect the surrounding neurons, and when this capacity is lost, neuronal loss and subsequent memory decline is exacerbated, as seen in the SYK-deficient mice (101, 102, 396, 503). Interestingly, during a “sledgehammer approach,” in which near complete removal of microglia is achieved, A β plaque load is diminished, further demonstrating their role in building A β plaques (120, 124). However, the loss of microglia disturbs additional protective responses, such as the microglial maintenance of the brain vasculature (504). This loss of function can lead to different, but equally harmful, pathology accumulation such as vascular amyloidosis that spurs intracranial hemorrhage and premature death (504).

Collectively, defining microglial signaling in the context of neurodegeneration will allow us to comprehensively understand microglial biology during disease to support more informed targeting of microglial responses. Defining the role of microglial SYK in driving protective signaling and responses

during AD and demyelination is the tip of the proverbial iceberg for microglial signaling. Much of microglial signaling in these disease contexts rely on upstream SYK (340, 505), leaving the role of many downstream molecules undescribed. By understanding the nuances of microglial signaling during different stages of disease, more individualistic therapies can be achieved. Although straightforward, the complete elimination of microglia is likely too simplistic and dangerous to treat AD patients due to the intricacies of microglial function throughout the brain. Embracing the complex nature of microglia and investigating the molecular underpinnings of their responses may alleviate the burden of off-target effects and may unearth a deeper understanding of how to address microglia during neurodegeneration.

4.1.2 Pathology regulation by *CARD9* in Alzheimer's disease

Microglial signaling encompasses many parallels with its peripheral counterparts. As the resident immune cells of the brain, microglia possess machinery that responds to neurodegenerative and, similar to peripheral macrophages, infectious triggers (506, 507). The shared nature and evolutionary roots of these microglial signaling axes during both neurodegeneration and infection remains to be fully understood. One such signaling arm abundantly described in peripheral macrophages during infection is the CLEC7A-SYK-CARD9 fungal pathway (342, 383, 508). The downstream molecule, *CARD9*, is a critical mediator of fungal response, however, its role in the brain has gone underappreciated until now. In our studies, we define a role for *CARD9* in driving protective microglial responses to A β pathology and dampening disease progression in AD mice. The further delineation of the mechanisms by which *CARD9* is protective in the context of AD is necessary for potential intervention.

Our studies indicate only a slight transcriptional shift between *CARD9*-sufficient and -deficient 5xFAD microglia. This finding is surprising due to the appreciable differences in A β pathology accumulation seen between genotypes. However, increased A β load and exacerbated neuronal loss and memory decline in *Card9*^{-/-}5xFAD mice is complimented with an increase in microglial transcription of *Klf4*. *KLF4* levels are appreciably increased in the AD brain and correspond with heightened levels of reactive oxygen species, neuronal loss, and iron dyshomeostasis (465, 466). The loss of *CARD9* does indeed exacerbate neuronal loss in 5xFAD mice and interestingly leads to iron retention in *Card9*^{-/-}5xFAD microglia. Iron dyshomeostasis in microglia causes the cells to become susceptible to a type of cell death known as ferroptosis (509). The role of ferroptosis in regulating microglial viability and response to AD pathology remains an important area of interest.

The utilization of a germline deletion of *Card9* in 5xFAD mice introduces several caveats to our experimental conclusions. In addition to the loss of *CARD9* in microglia, we can assume there is a loss of *CARD9* in other peripheral and CNS border-associated myeloid cells (510). The loss of *CARD9* across a vast population of immune cells, coupled with the limited transcriptional changes observed in *CARD9*-

deficient 5xFAD microglia, suggests a potential role for peripheral cells driving differential pathology accumulation in the brain. The description of peripheral perturbations affecting the brain is not a novel concept, however, the mechanisms by which this occurs remains enigmatic and a burgeoning field of study. Derivations of the exclusive role CARD9 plays in microglia requires the tandem use of our current model and an alternative inducible deletion of *Card9* in microglia.

4.2 Future Directions

4.2.1. Determining the role of SYK in generating a microglial response to injury

This dissertation work describes a striking regulation of microglial response to neurodegenerative pathologies by SYK. However, the inability of microglia to associate with A β and their “resting” state in 5xFAD *Syk* ^{Δ MG} mice led us to question the role of SYK in driving microglial sensing of disease and damage. To ascertain whether SYK drives microglial “sensing” of damage, we chose to induce neuronal injury in the brains of Ai6-ZsGreen *Syk*^{+/+} *Cx3cr1*^{ERT2Cre} (*Syk*^{con-Ai6}) and Ai6-ZsGreen *Syk*^{fl/fl} *Cx3cr1*^{ERT2Cre} (*Syk* ^{Δ MG-Ai6}) mice. To begin, we inserted cranial windows in the skull of *Syk*^{con-Ai6} and *Syk* ^{Δ MG-Ai6} mice 2 weeks prior to inducing a laser injury using a 2-photon microscope. We will perform live imaging of the Ai6-labeled microglia in *Syk*^{con-Ai6} and *Syk* ^{Δ MG-Ai6} mice immediately after injury. Under normal conditions, microglia sense the insult and extend their processes out toward the area of injury, as measured by velocity of the targeted response (511). Additionally, imaging will be performed 24 hours post injury to analyze microglial recruitment to injury through the measurement of microglial cell body migration to the site. These studies will aid in our understanding of what microglial responses are controlled by SYK and which ligands (i.e. A β or other disease-associated molecular patterns) critically inform these functions.

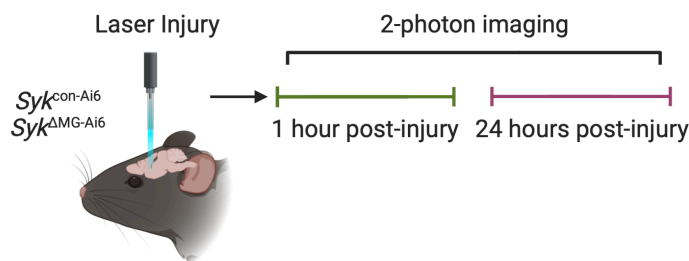


Figure 4.1. Intravital imaging of microglial response to parenchymal laser injury. Experimental schematic to study the role of SYK in regulating microglial response following laser injury to the brains of *Syk*^{con-Ai6} and *Syk* ^{Δ MG-Ai6} mice.

4.2.2. Microglial receptors regulating SYK and CARD9 signaling

The comprehensive understanding by which SYK signaling regulates microglial response during neurodegeneration requires the identification of upstream and downstream mediators of the molecule. The further investigation of downstream signaling pathways activated by SYK following exposure to neurodegenerative ligands is a continued area of interest for our research. We will achieve this aim by first utilizing a combination of techniques investigating the phosphorylation of several key SYK targets including: PLC γ , ERK, NF κ B, and VAV (340). Other potential downstream components include microglial receptors. For instance, our RNA-sequencing of SYK-deficient microglia in both AD and demyelination

models indicates increased expression of CD36, a scavenger receptor implicated in AD (492, 512-514). CD36 responds to A β and damaged myelin ligands (492, 514), and the potential upregulation of this receptor upon the loss of SYK may uncover additional molecular mediators of microglial function during neurodegeneration. However, continual interest remains in determining which receptor predominantly affects SYK activity during disease. For example, we describe TREM2, a receptor known to signal through SYK (29), as a probable component of SYK signaling in 5xFAD microglia (Chapter 2, Figure 2.7). However, an expansion beyond transcriptional similarities between 5xFAD *Syk*^{AMG} and 5xFAD *Trem2*^{-/-} microglia must be achieved to draw these conclusions. In addition, the role of CLEC7A, the fungal receptor known to signal through both SYK and CARD9 in peripheral macrophages (114, 383), is a likely contributor to SYK engagement in the AD brain (105). In this future direction, we intend to uncover and define critical signaling receptors responsible for regulating SYK activation in response to both AD and demyelination pathologies.

CD36 is a scavenger receptor characterized in microglia to respond to A β , apoptotic cells, myelin, and oxidized low-density lipoproteins (513). Previous studies suggest that the TREM2 receptor relies on CD36 upregulation to promote A β phagocytosis (400). However, CD36 is also propagative of a pro-inflammatory state following exposure to A β (514). This phenomenon draws parallels with the ambiguity of DAMs across different disease stages. In our studies, we observe an upregulation of CD36 upon the loss of SYK in 5xFAD and EAE microglia. This finding may suggest a compensatory upregulation of CD36 by SYK-deficient microglia to counterbalance defective SYK-dependent phagocytic pathways.

To study the potential regulation of CD36 expression and engagement by SYK, we will confirm increased microglial CD36 protein levels by imaging SYK-sufficient and -deficient microglia from 5xFAD or cuprizone-treated mice. Upon verification of differential CD36 expression at the protein level, we will test the critical nature by which CD36 activation may influence SYK-deficient microglia. Utilizing a previously described CD36 inhibitor (492), we can assess pathology accumulation between treated and non-treated *Syk*^{AMG} mice both in the 5xFAD and cuprizone models. If 5xFAD *Syk*^{AMG} mice or *Syk*^{AMG} mice undergoing demyelination are treated with a CD36 inhibitor and have worsened A β and myelin debris accumulation compared with vehicle-treated 5xFAD *Syk*^{AMG} controls, we can infer that upregulation of CD36 by SYK-deficient microglia acts in a protective manner. However, if 5xFAD *Syk*^{AMG} mice or *Syk*^{AMG} mice undergoing demyelination are treated with a CD36 inhibitor and have diminished A β and myelin debris accumulation compared with vehicle-treated 5xFAD *Syk*^{AMG} controls, we can assume that the upregulation of CD36 by SYK-deficient microglia acts in a detrimental manner for pathology accumulation.

Using this experimental model of CD36 inhibition in AD, we can also gain valuable information on the role CD36 plays in driving differential microglial response to pathology in the context of neurodegeneration. The study of microglial morphology and association with pathology may offer a broad understanding of

how CD36 may regulate microglial behavior. Based on past characterization of CD36 as a critical receptor for oxidized lipids (515, 516), we will also aim to uncover any potential links with increased CD36 expression and the increased levels of reactive oxygen species observed in 5xFAD *Syk*^{ΔMG} microglia. Outside of promoting TREM2-driven phagocytosis (400), CD36 signaling in AD microglia is not wholly established, and the objective of our future studies involves the establishment of its potential role in other processes during neurodegeneration.

Impaired TREM2 receptor function can negatively impact microglial response to AD pathology (97, 100, 101, 396, 431, 435). Several years of work has described the involved microglial signaling orchestrated by TREM2 activation in neurodegenerative disease (29, 30, 103). The activation of SYK following the stimulation of TREM2 is well documented (29), however the receptor specificity by which SYK relies on TREM2 to direct its downstream signaling is not wholly described. Data presented in this dissertation indicate that SYK signaling does not completely rely on TREM2 activation, but instead likely involves additional receptor activation such as CLEC7A. This conclusion was drawn from an RNA-sequencing comparison in which 5xFAD *Syk*^{ΔMG} microglia have vastly more differentially expressed genes than 5xFAD *Trem2*^{-/-} microglia when each are compared with 5xFAD microglia (Figure 2.7). To further elucidate TREM2-independent workings of microglial SYK signaling during AD, we will compare pathology accumulation and microglial activation between 5xFAD *Syk*^{ΔMG} and 5xFAD *Trem2*^{-/-}. More specifically, we can delve into altered microglial signaling between groups to uncover unique pathway alterations upon the loss of SYK or TREM2 in 5xFAD microglia. These studies will further specify the cellular mechanisms, including relevant receptors, by which SYK directs microglial responses in AD.

CLEC7A is a fungal receptor primarily characterized on peripheral myeloid cells (114, 517). However, recent work has uncovered a potential role for the receptor in microglia during AD (105, 439). In addition to RNA-sequencing data illustrating the upregulation of *Clec7a* in DAMs, plaque-associated microglia also strongly upregulate the receptor at points of interaction between microglia and Aβ species (105). This observation has spurred our interest in understanding the role of CLEC7A in driving microglial responses during AD. Interestingly, upon activation CLEC7A can signal through both SYK and CARD9 (383, 518), and based on our previous findings outlining protective SYK and CARD9 signaling in microglia, we assumed a similar role for the CLEC7A receptor. However, our preliminary findings suggest that CLEC7A signaling in 5xFAD mice is detrimental. Therefore, we aim to understand the mechanisms by which CLEC7A may drive worsened disease progression in AD mice.

To begin to ask how CLEC7A may influence AD progression, we used mice with a germline deletion of CLEC7A crossed with 5xFAD mice. Antithetical to our original hypothesis, we found that 5-month-old *Clec7a*^{-/-} 5xFAD mice exhibit markedly less Aβ plaque load in the cortex of the brain compared with 5xFAD controls (Figures 4.2A and 4.2B). Furthermore, we observed a slight reduction in the quantity of ThioS-labeled Aβ plaques (Figures 4.2C and 4.2D) in the *Clec7a*^{-/-} 5xFAD mouse cortex compared with controls.

Of the remaining plaques found within the *Clec7a*^{-/-} 5xFAD cortex, the plaques displayed significantly higher intensity (Figure 4.2E), indicating increased plaque density compared with 5xFAD mice. The density and composition of A β plaques are often indicative of microglial formation and compaction of plaques into more inert structures (100). Interestingly, soluble oligomeric levels of A β remain unchanged between groups, whereas insoluble A β levels were diminished in the *Clec7a*^{-/-} 5xFAD brain compared with 5xFAD mice (Figure 4.2F). This reduction in insoluble A β levels suggests that upon the loss of CLEC7A, there are fewer A β fibrils that make up the higher-order ThioS-labeled plaque architecture. In fact, plaque composition within the cortex of *Clec7a*^{-/-} 5xFAD mice is shifted away from ThioS and predominantly composed of lower-order 6E10 labeled A β (Figures 4.2G and 4.2H). However, the neurons surrounding the modified A β plaques in both *Clec7a*^{+/-} 5xFAD and *Clec7a*^{-/-} 5xFAD structures undergo reduced damage compared with 5xFAD controls as measured by APP⁺ dystrophic neurite frequency (Figures 4.2I and 4.2J) (100). Therefore, CLEC7A-deficient 5xFAD mice display reduced A β levels coupled with altered A β composition in the cortex, which ultimately protects surrounding neurons from A β -induced neuronal toxicity.

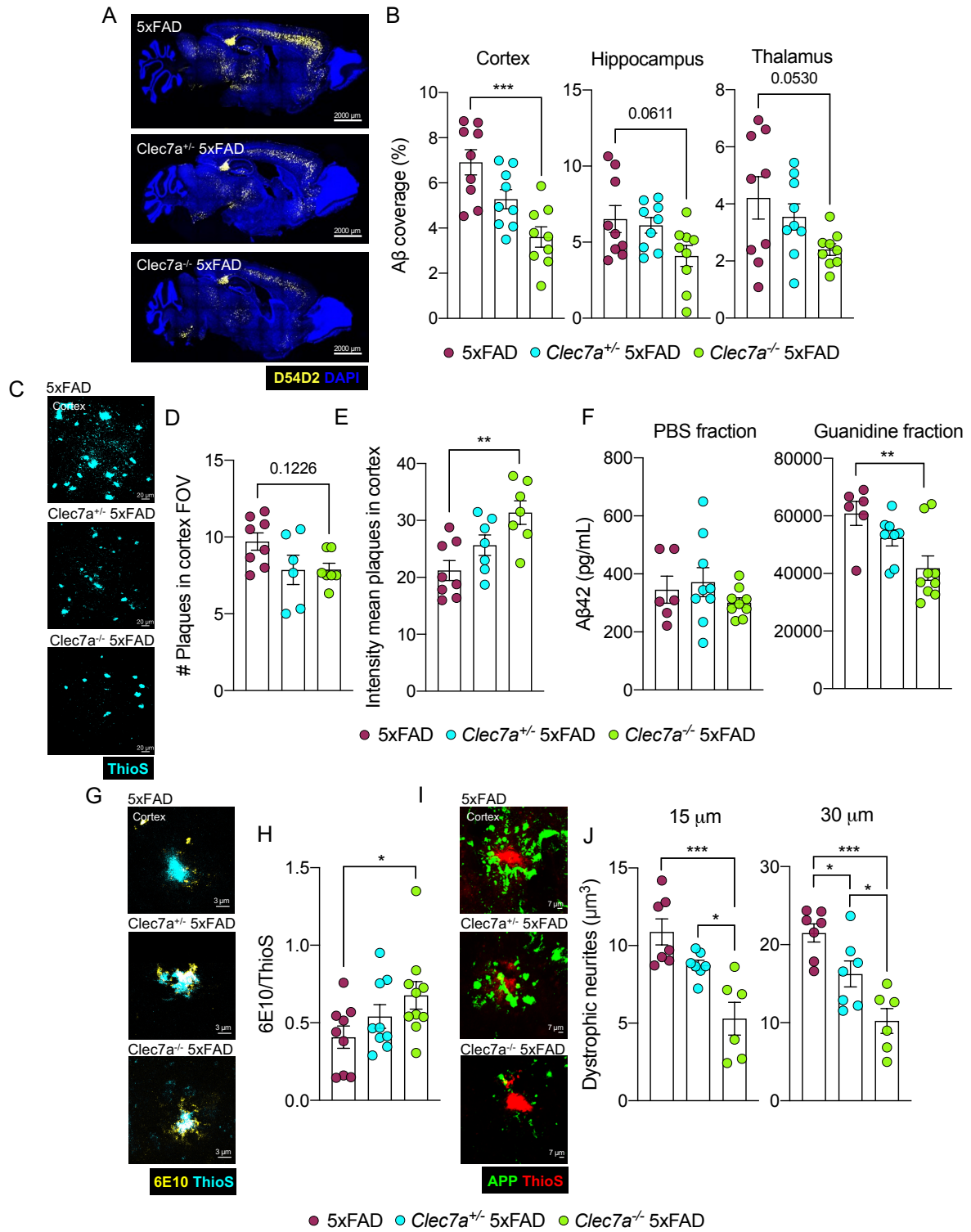


Figure 4.2. The loss of CLEC7A increases Aβ burden and alters plaque composition in 5xFAD mice. (A-J) 5-month-old 5xFAD, *Clec7a*^{+/+} 5xFAD, and *Clec7a*^{-/-} 5xFAD were harvested to evaluate amyloid beta (Aβ) load in the brain. (A-B) Immunofluorescence staining of Aβ (D54D2, yellow; DAPI, blue) was performed on sagittal sections and the percent area covered by Aβ in the cortex, hippocampus, and thalamus was quantified. Original magnification: 10x; scale bar = 2000 μm. (C-E) Aβ load and intensity in the cortex labeled with ThioflavinS (ThioS, cyan). Original magnification: 63x; scale bar = 20 μm. (F) Soluble (PBS) and insoluble (Guanidine) fractions of Aβ₁₋₄₂ measured in the right hemisphere of the brain by ELISA. (G-H) Representative images and quantification of Aβ plaque composition labeling 6E10 (yellow) for filamentous forms of Aβ and ThioS (cyan) for more compact or inert forms of Aβ in the cortex of matched sagittal brain sections. Original magnification: 63x; scale bar = 3 μm. (H) Quantification represents the percent volume of the 6E10/ThioS ratio per field of view from a total of 10-15 plaques from 3 brain sections per mouse. (I-J) The formation of dystrophic neurites surrounding plaques in the cortex was determined by staining for APP (green) and Aβ using ThioS (red). Original magnification: 63x; scale bar = 7 μm. (J) Quantification of APP⁺ puncta found within 15 and 30 μm of Aβ plaques from a total of ~40 plaques from 3 matching brain sections per mouse. Statistical significance between experimental groups was calculated by one-way ANOVA with Tukey's post hoc test. *p < 0.05, **p < 0.01, ***p < 0.001 (B, D-F, H, J). Error bars represent mean ± S.E.M. and each data point represents an individual mouse.

The predominance of CLEC7A expression by microglia in the brain prompted our query into how CLEC7A may regulate microglial response to A β pathology in 5xFAD mice (441). We observed increased numbers of microglia within the *Clec7a*^{-/-} 5xFAD cortex compared with 5xFAD controls (Figures 4.3A and 4.3B). In addition, the cortex of *Clec7a*^{-/-} 5xFAD possess more microglia directly surrounding the A β plaques, suggesting a heightened microglial response to AD pathology upon the loss of CLEC7A (Figures 4.3A and 4.3C). However, we did not detect an increase in microglial proliferation in the *Clec7a*^{-/-} 5xFAD brain (Figures 4.3A and 4.3D), leaving open the possibility of potential infiltration of peripheral macrophages or altered microglial turnover in disease. To further elucidate what may cause increased Iba1⁺ cell numbers in the cortex *Clec7a*^{-/-} 5xFAD mice, we will begin by utilizing a co-labeling system to differentiate potential macrophages from brain-resident microglia. Iba1 can label both microglia and macrophages, however P2Y12 is a microglia-specific marker (519). The colocalization of Iba1 and P2Y12 indicates microglia, while Iba1-only cell labeling identifies infiltrating macrophages. If we determine there are macrophages in the *Clec7a*^{-/-} 5xFAD brain using this system, we can analyze the microglia to macrophage ratio to decipher whether CLEC7A deficiency accounts for increased Iba1⁺ cell numbers through means of altered microglial cell number or alternative macrophage infiltration.

Microglial activation and phagocytic responses to A β are critical for pathology clearance and subsequent neuronal protection (397, 401, 520). Interestingly, microglia undergo a morphological shift upon stimulation with A β (91). Following activation, microglia become more ameboid-like in structure while losing their cellular ramifications (91). Surprisingly, *Clec7a*^{-/-} 5xFAD microglia are more morphologically at-rest and retain more ramifications compared to 5xFAD microglia (Figures 4.3E and 4.3F). *Clec7a*^{-/-} 5xFAD and *Clec7a*^{+/-} 5xFAD microglia also appear to have less A β engulfed within microglia despite having reduced levels of A β overall (Figures 4.3G and 4.3H). Although surprising, the decreased microglial uptake of A β in CLEC7A-deficient microglia coupled with the observed reduction in A β levels (Figure 4.2) may be explained by efficient A β uptake not captured at this timepoint. Alternatively, the increased number of Iba1⁺ cells in the *Clec7a*^{-/-} 5xFAD brain may be able to “divide and conquer,” leaving less A β to be engulfed by neighboring cells. To determine if the phagocytic capacity of CLEC7A-deficient microglia is truly impaired, we will employ a Methoxy-X04 experiment in which we will inject this BBB-permeable dye that labels A β and study A β uptake by microglia using flow cytometry. We anticipate that *Clec7a*^{-/-} 5xFAD microglia do not have impaired phagocytosis, however, if they display reduced A β engulfment it may lead us to uncover if CLEC7A regulates phagocytosis of differential forms of A β .

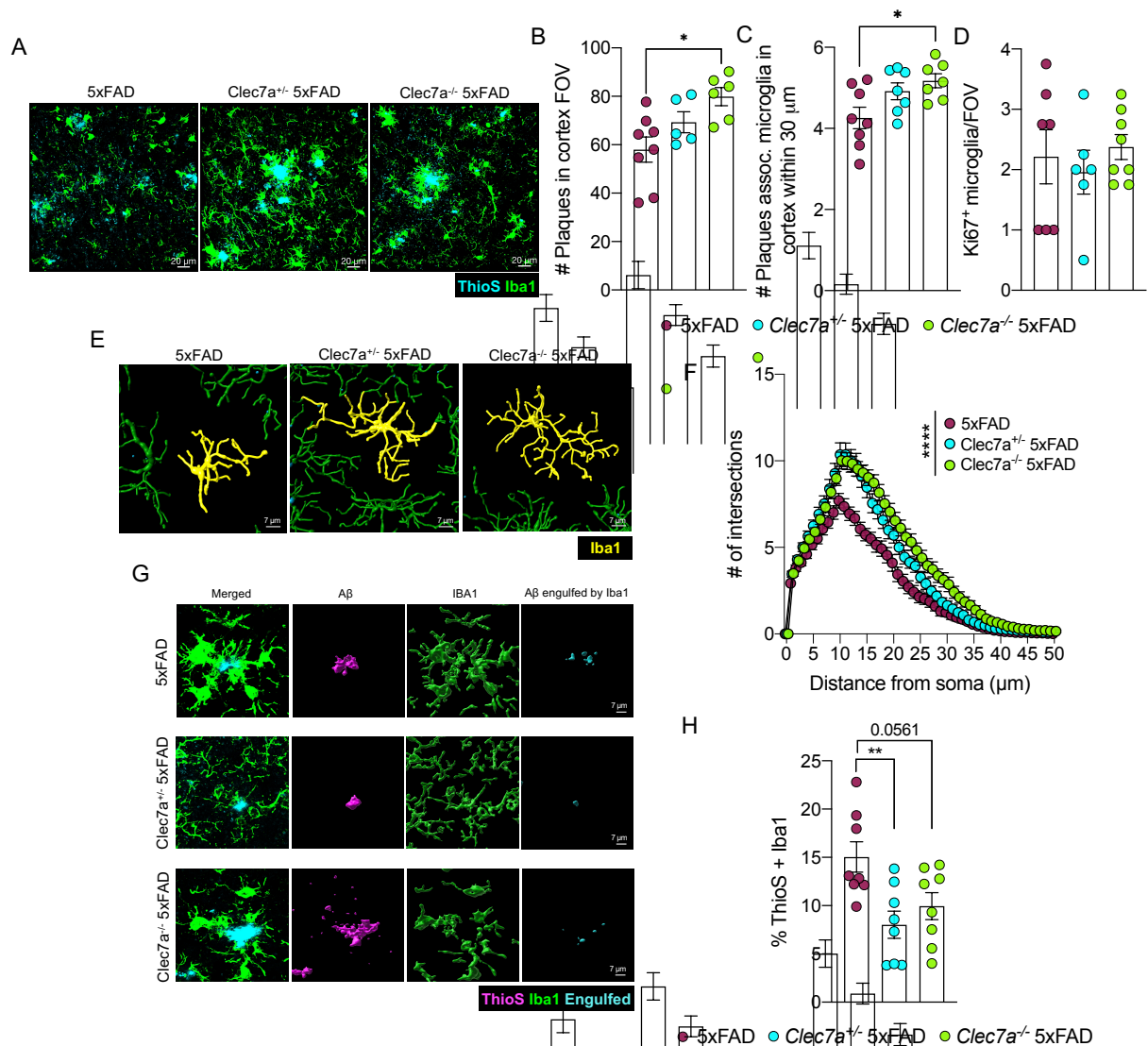


Figure 4.3. *Clec7a*-deficiency alters microglial response to Aβ pathology in 5xFAD mice. (A-H) 5-month-old 5xFAD, *Clec7a*^{+/-} 5xFAD, and *Clec7a*^{-/-} 5xFAD were harvested to evaluate microglial response in the brain. (A-C) Microglia were imaged by labeling with Iba1 (green) surrounding Aβ plaques labelled with ThioS (cyan) to assess microglial coverage and proximity to plaques. (A) Representative images of Iba1 and ThioS staining in the cortex of matching sagittal brain sections. Original magnification: 63x; scale bar = 20 μm. (B) Quantification of microglial numbers in the field of view (FOV). (C) Quantification of the number of microglia within a 30 μm radius surrounding ThioS-labelled Aβ plaques. Each point represents an individual mouse with an average of 50-100 plaques from 3 matching brain sections per mouse. (D) Quantification of Ki67⁺ microglia in the field of view (FOV) in the cortex of mice averaged from 3 matching brain sections per mouse. (E) Imaparis-rendered microglia morphology labeled with Iba1 (yellow) in the cortex. Original magnification: 63x; scale bar = 7 μm. (F) Sholl analysis quantification from a total of 12 microglia from 3 matching brain sections per mouse (5xFAD n=7, *Clec7a*^{+/-} 5xFAD, n=7, *Clec7a*^{-/-} 5xFAD n=8). (G) Imaparis-rendered Aβ plaques (ThioS, pink) and Iba1+ cells (green) with the completely localized Aβ-microglia (engulfed) channel in cyan. Original magnification: 63x; scale bar = 7 μm. (H) Percent area of engulfment quantification from a total of ~20 plaques from 3 matching brain sections per mouse. Statistical significance between experimental groups was calculated by one-way ANOVA with Tukey's post hoc test (B-D, H) or a repeated-measures two-way ANOVA with Bonferroni's post hoc test (F). *p < 0.05 **p < 0.01, ****p < 0.0001. Error bars represent mean ± S.E.M. and each data point represents an individual mouse (B-D, H).

Finally, to study CLE7A regulation of microglial activation in AD, we chose an unbiased approach in which we performed bulk RNA-sequencing on MACS-isolated 5xFAD and *Clec7a*^{-/-} 5xFAD microglia. Firstly, we observed the downregulation of many immune-related genes in *Clec7a*^{-/-} 5xFAD microglia, including: *Ccl24*, *Cxcl1*, and *Ccl7* (Figures 4.4A and 4.4B). Additionally, several differentially expressed genes implicate NK cells and neutrophils which we will examine using both flow cytometry and imaging to determine potential infiltration of these cells into the brain of *Clec7a*^{-/-} 5xFAD mice. In addition to gene expression, we were also interested in defining key cellular signaling pathways potentially altered upon the loss of CLE7A in 5xFAD microglia. To this end, we used a Luminex assay to study the

phosphorylation of AKT and its downstream phosphorylated targets. AKT regulates many neuroprotective microglial activities, including cell survival, mobilization, and metabolism (367, 521). We observed increased phosphorylation of PTEN and GSK3 β in *Clec7a*^{-/-} 5xFAD microglia (Figure 4.4C). PTEN has been shown to drive microglial phagocytic capacity (522). Interestingly, the increased Ser9 phosphorylation of GSK3 β seen in *Clec7a*^{-/-} 5xFAD microglia leads to protective inhibition of GSK3 β . It has been demonstrated that GSK3 β contributes to A β and tau accumulation; thus, the inhibition of GSK3 β activity through increased Ser9 phosphorylation likely contributes to reduced disease severity in *Clec7a*^{-/-} 5xFAD mice (371-373, 376, 377). Therefore, the altered AKT signaling found in *Clec7a*^{-/-} 5xFAD microglia likely drives some of the protective phenotypes observed following the loss of CLEC7A in 5xFAD mice.

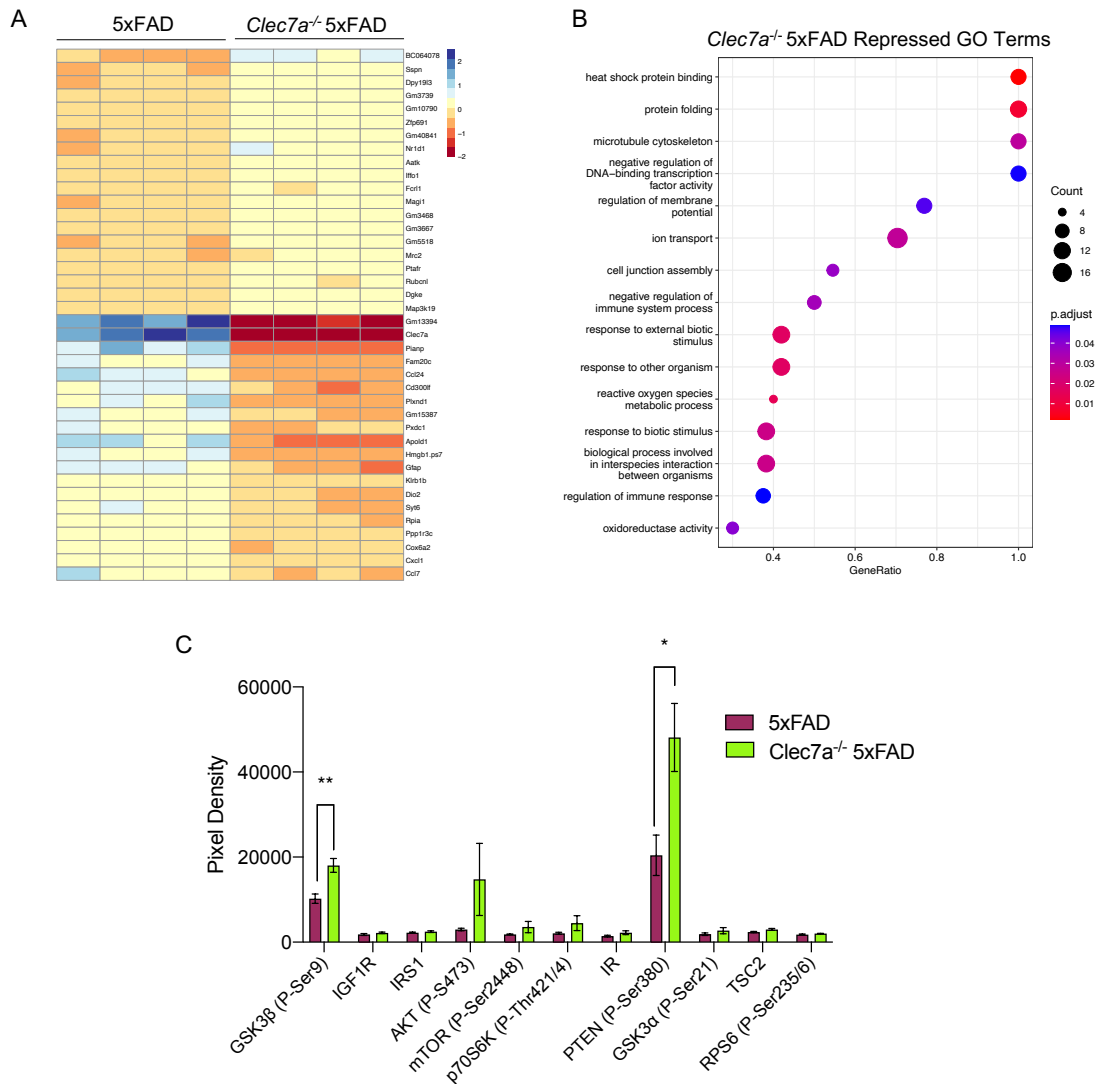


Figure 4.4. Altered transcription and cell signaling in CLEC7A-deficient microglia. (A-B) Microglia from 5-month-old 5xFAD and *Clec7a*^{-/-} 5xFAD mice were sorted from single-cell brain suspensions using anti-CD11b⁺-coated magnetic beads and magnetic column sorting, finally, RNA-Seq was performed. (A) Heatmap representation of the top significantly upregulated and downregulated genes (FDR<0.1) between 5xFAD and *Clec7a*^{-/-} 5xFAD microglia. (B) GO term enrichment scatter plot highlighting major pathways that are repressed in *Clec7a*^{-/-} 5xFAD microglia in comparison to 5xFAD microglia. (C) Mouse AKT pathway phosphorylation array conducted on microglia from 5-month-old 5xFAD and *Clec7a*^{-/-} 5xFAD mice that were sorted from single-cell brain suspensions using anti-CD11b⁺-coated magnetic beads and magnetic columns; n of 4 for each group. Statistical significance between experimental groups was calculated by an unpaired Student's t-test (C). *p < 0.05, **p < 0.01. Error bars represent mean \pm S.E.M.

To further delineate the root mechanisms by which CLEC7A may drive harmful microglial responses to A β pathology, we will begin by defining the importance of the ligands in driving alternative CLEC7A receptor activity. Our previous work describes that the hippocampal treatment of the CLEC7A ligand β -D-glucan (pustulan) is protective for driving microglial clearance of A β . These data indicate the protective nature of CLEC7A in the context of AD. However, contrary to our pustulan data, we observe that the presence of CLEC7A worsens disease pathology in 5xFAD mice. Thus, the distinction between endogenous versus exogenous ligands may be required to understand the full complexity of CLEC7A signaling during AD. Endogenous ligands such as those found within A β plaques, vimentin, annexins, galectin-9, N-glycans, etc., versus exogenous ligands such as pustulan may differentially drive non-protective and protective microglial response to A β (517). This reasoning may explain the contrasting phenotypes during the exogenous hippocampal pustulan injections and the loss of CLEC7A in the context of endogenous A β . To test this hypothesis, we will inject alternative endogenous ligands (such as galectin-9) into the hippocampus of 5xFAD and *Clec7a*^{-/-} 5xFAD mice followed by an evaluation of A β clearance by microglia. These studies may uncover the nuances of CLEC7A signaling in regulating microglial response during AD and identify novel targets for modulating receptor signaling.

4.2.3. Investigating how microglial SYK signaling regulates different cell types (i.e. astrocytes, T cells, OPCs)

In Chapter 2 of this dissertation, we observe that the loss of SYK in microglia can affect the activity of other cell types. For instance, the T cell response is altered in *Syk*^{AMG} during EAE, with increased CD45⁺, CD4⁺, and CD8⁺ T cell numbers and increased cytokine expressing CD4⁺ T cells (Figure 2.10). In addition, OPC proliferation is decreased in the *Syk*^{AMG} corpus collosum following cuprizone-induced demyelination, ultimately affecting oligodendrocyte numbers during remyelination (Figure 2.12). These observations may be an artifact of increased pathology accumulation within the area of disease. However, these findings may also be explained by microglial SYK signaling driving microglial activities to shape the cellular milieu during disease. To further investigate how microglial SYK signaling may influence alternative cell types during neurodegeneration, we aim to identify potential signals produced by microglia to drive cellular responses outside of microglia themselves.

The role of astrocytes, T cells, and OPCs in neurodegeneration is vast (351, 352, 523-528). The contribution of these cells in addressing AD pathology remains almost completely ignored in the studies outlined in this dissertation. However, the communication of all cell types during neurodegeneration is the preeminent goal for understanding the full picture of disease onset and progression. To begin to interrogate the ability of microglial SYK to impact alternate cell types and disease severity, we will first turn to studying microglial interaction with astrocytes. The roles astrocytes play in AD are numerable, and include the regulation of the BBB, neuronal activity, and A β clearance (523). To begin to study how SYK in microglia may alter astrocytic response, we will examine astrocytic numbers and activation between

Syk^{con}, *Syk*^{ΔMG}, 5xFAD *Syk*^{con}, and 5xFAD *Syk*^{ΔMG} mice. Understanding how microglial SYK regulates astrocytic activity at homeostasis is necessary to draw conclusions from potential differences we may observe between 5xFAD and 5xFAD *Syk*^{ΔMG} mice. Based on the inability of SYK-deficient microglia to activate both transcriptionally and morphologically, we hypothesize that the *Syk*^{ΔMG} brain may have diminished signals from microglia to promote astrocytic activation (529). Studying the transcriptional and morphological activation of astrocytes using RNA-sequencing and imaging may begin to answer how the presence of SYK signaling in microglia influences astrocytic responses in the 5xFAD brain environment. Comparing the transcriptional shifts in astrocytes between 5xFAD and 5xFAD *Syk*^{ΔMG} mice may uncover potential SYK-modulated signaling pathways to follow up with using both *in vitro* and *in vivo* methods. Altogether, the ability of microglia to regulate astrocytic activation and the capacity of astrocytes to regulate AD pathology may expose novel mechanisms by which microglial SYK influences other cellular responses in the context of AD.

SYK signaling in microglia also affects CD4⁺ T cell response in EAE-induced neurodegeneration (Figure 2.10). For instance, in Chapter 2 of this dissertation we find that the spinal cords of *Syk*^{ΔMG} mice contain increased numbers of CD4⁺ T cells and increased numbers of cytokine producing CD4⁺ T cells compared with *Syk*^{con} mice. Unchecked CD4⁺ T cell response during EAE is harmful and contributes to heightened disease (530, 531). However, the induction of regulatory T cells can curb the pro-inflammatory CD4⁺ T cell response, and under certain contexts, microglia can act as antigen-presenting cells to prompt the induction of regulatory T cells (530). Therefore, we will investigate whether microglial SYK affects regulatory T cell induction and if this may explain the heightened CD4⁺ T cell response observed in the spinal cords of *Syk*^{ΔMG} mice during EAE. These studies may further expound the importance of microglial signaling through SYK to impact neurodegenerative disease severity.

The induction of demyelination using cuprizone granted us a unique opportunity to study if SYK signaling in microglia influences the OPC response to demyelinating conditions in the corpus collosum. In Chapter 2 of this dissertation, we observed a reduced population of OPCs during demyelination and remyelination in *Syk*^{ΔMG} mice, which likely contributes to the reduced oligodendrocyte number seen in the corpus collosum of *Syk*^{ΔMG} mice during remyelination. OPCs play a vital role during demyelination, and their recruitment to areas of demyelination and subsequent proliferation and maturation into myelinating oligodendrocytes promotes neuronal repair (532). The impaired OPC response we observed in *Syk*^{ΔMG} mice may reinforce the worsened damaged myelin accumulation in the cuprizone treated mice. To uncover what SYK-regulated microglial signaling molecule(s) drive OPC response during demyelination we will employ an alternative model of demyelination using lysolecithin to induce demyelination in a defined temporal and spatial area (533). Using this method, we will harvest *Syk*^{con} and *Syk*^{ΔMG} microglia and OPCs for RNA-sequencing from the area of demyelination in the corpus collosum. Differential transcription between *Syk*^{con} and *Syk*^{ΔMG} microglia and OPCs at 6 days post-demyelination induction may uncover altered signaling pathways that will require *in vitro* validation and subsequent *in vivo* studies utilizing the

supplementation or inhibition of the altered signaling in *Syk*^{AMG} microglia and OPCs. The identification of microglia-OPC crosstalk has the potential to unearth previously underappreciated SYK-dependent microglial signaling that can alter multicellular responses during neurodegeneration.

4.2.4. Examining the specific role of *CARD9* in microglia during AD

Previous work describes that the stimulation of CLEC7A-SYK signaling can lead to the activation of *CARD9* (383). Our work demonstrates critical and varying roles for CLEC7A, SYK, and *CARD9* in regulating microglial response and AD pathology accumulation. More specifically, our experiments define a protective role for *CARD9* in 5xFAD mice, however, our model does not specifically target *CARD9* within microglia. Although microglia are the predominant expressors of *CARD9* in the brain (441), peripheral myeloid cells and other brain-resident cells also possess *CARD9* (464, 472, 510). Therefore, the distinction between protective *CARD9* signaling in microglia or alternate cells remains to be realized. Thus, we intend to tease out potential cellular mechanisms by which *CARD9* may alter AD progression.

To begin to understand how *CARD9* specifically affects microglial responses in the context of AD, we began by injecting a newly developed *CARD9* inhibitor directly into the hippocampus of 5xFAD and *Card9*^{-/-} 5xFAD mice (534). We performed this experiment on 3-month-old mice and waited seven days post injection to harvest the right hippocampus (vehicle injected) and left hippocampus (*CARD9* inhibitor injected) to analyze A β and Iba1⁺ cell coverage (Figure 4.5A). Importantly, off-target effects were not observed, as we did not detect differences in A β load or Iba1⁺ cell level measures between the treated and non-treated hippocampal hemispheres of *Card9*^{-/-} 5xFAD mice (Figure 4.5B and 4.5D). In addition, we did not find a difference in A β load or Iba1⁺ cell coverage between the vehicle or *CARD9* inhibitor-treated 5xFAD hippocampus (Figure 4.5B and 4.5C), indicating that the acute inhibition of *CARD9* in the hippocampus does not alter A β plaque accumulation or Iba1⁺ cell coverage. This finding may support the potential significance of peripheral *CARD9* or that chronic inhibition of *CARD9* is necessary to see significant changes in A β levels.

Outside of generating a novel mouse line in which we would flox *CARD9* specifically out of *Cx3cr1*-expressing cells, we can further demonstrate the role of *CARD9* independent of microglia by depleting microglia in 5xFAD and *Card9*^{-/-} 5xFAD mice to examine if there are apparent differences in disease progression upon the absence of these cells. Therefore, we will expose 2-month-old 5xFAD and *Card9*^{-/-} 5xFAD mice to PLX5622 to eliminate microglia and examine A β accumulation following 2 months of microglial depletion. If *Card9*^{-/-} 5xFAD mice that receive PLX5622 continue to have significantly worsened A β compared with 5xFAD mice, we can assume that *CARD9* may play an important role in regulating AD pathology peripherally. If this is the case, the reframing of this project would be significant and require entirely new experiments investigating the peripheral cell type responsible for this affect. In addition,

follow-up studies would need to determine the potential cellular or peripheral factor infiltration into the CNS of 5xFAD mice.

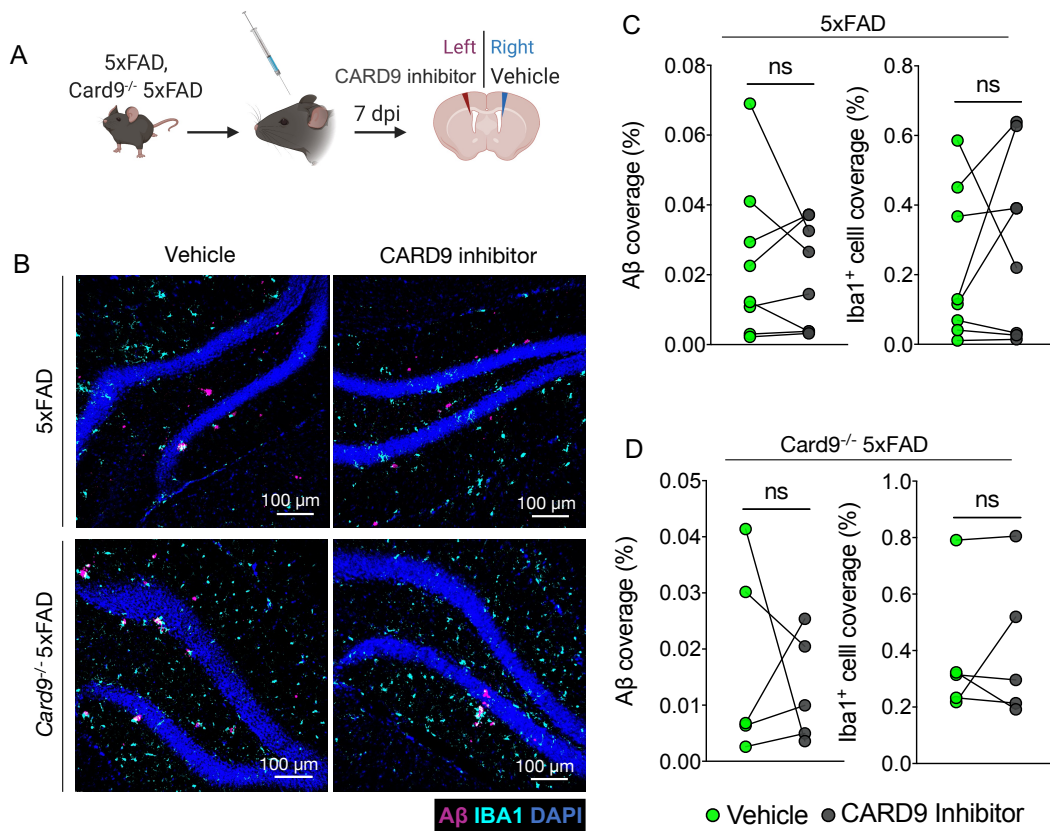


Figure 4.5. Acute CARD9 inhibition in the hippocampus does not affect A β or Iba1⁺ cell coverage. (A-D) Right and left hippocampal injection of vehicle or CARD9 inhibitor (BRD5529), respectively, into 3-month-old 5xFAD and *Card9*^{-/-} 5xFAD mice. Brains were then harvested 7 days post injection (dpi). (A) Experimental design schematic. (B) Representative images of A β (pink) and Iba1 (cyan) coverage in 3-month-old 5xFAD and *Card9*^{-/-} 5xFAD mice 7 days following intrahippocampal injection of vehicle or 200 μ mol of the CARD9 inhibitor. (C-D) Quantification of A β (D54D2, pink) and Iba1⁺ cells (cyan) in the hippocampus of (C) 5xFAD and (D) *Card9*^{-/-} 5xFAD mice. Statistical significance between experimental groups was calculated by paired Student's t-test (C-D). ns = nonsignificant. Representative data from 2 independent experiments (C-D).

However, if *Card9*^{-/-} 5xFAD mice that receive PLX5622 no longer have increased A β accumulation compared with 5xFAD mice, we can assume that microglial CARD9 may play an important role in regulating AD pathology. The continuation in understanding of how microglial CARD9 staves off disease progression requires additional mechanistic insight. As an extension of our current dataset, we asked how increased expression of KLF4 in *Card9*^{-/-} 5xFAD microglia may drive any detrimental effects. Increased KLF4 expression is a marker for AD and contributes to neuronal loss and iron dyshomeostasis (465, 466). To determine if KLF4 may contribute to the worsened disease state observed in *Card9*^{-/-} 5xFAD mice, we injected a KLF4 inhibitor (Kenpaullone) into the hippocampus of 5xFAD and *Card9*^{-/-} 5xFAD mice (535).

As internal controls, the opposing side of the hippocampus was injected with vehicle. Seven days post-injection, we analyzed A β and Iba1⁺ cell coverage in the injected right and left hippocampus of 5xFAD and *Card9*^{-/-} 5xFAD mice (Figure 4.6A). We did not observe a difference in A β load between the inhibitor- and vehicle-injected hippocampus of 5xFAD mice (Figure 4.6B and 4.6C). However, we did find significantly less Iba1⁺ cell coverage in the KLF4 inhibitor-injected side of the hippocampus (Figure 4.6B and 4.6C). Thus, KLF4 may regulate microglial response to AD pathology. In addition, although not statistically significant, the KLF4 inhibitor-injected hippocampal hemisphere of *Card9*^{-/-} 5xFAD mice had slightly reduced A β coverage with no change in Iba1⁺ cell coverage (Figure 4.6B and 4.6D). Therefore, KLF4 may be partially responsible for driving alternate and harmful microglial responses upon the loss of CARD9 in 5xFAD mice.

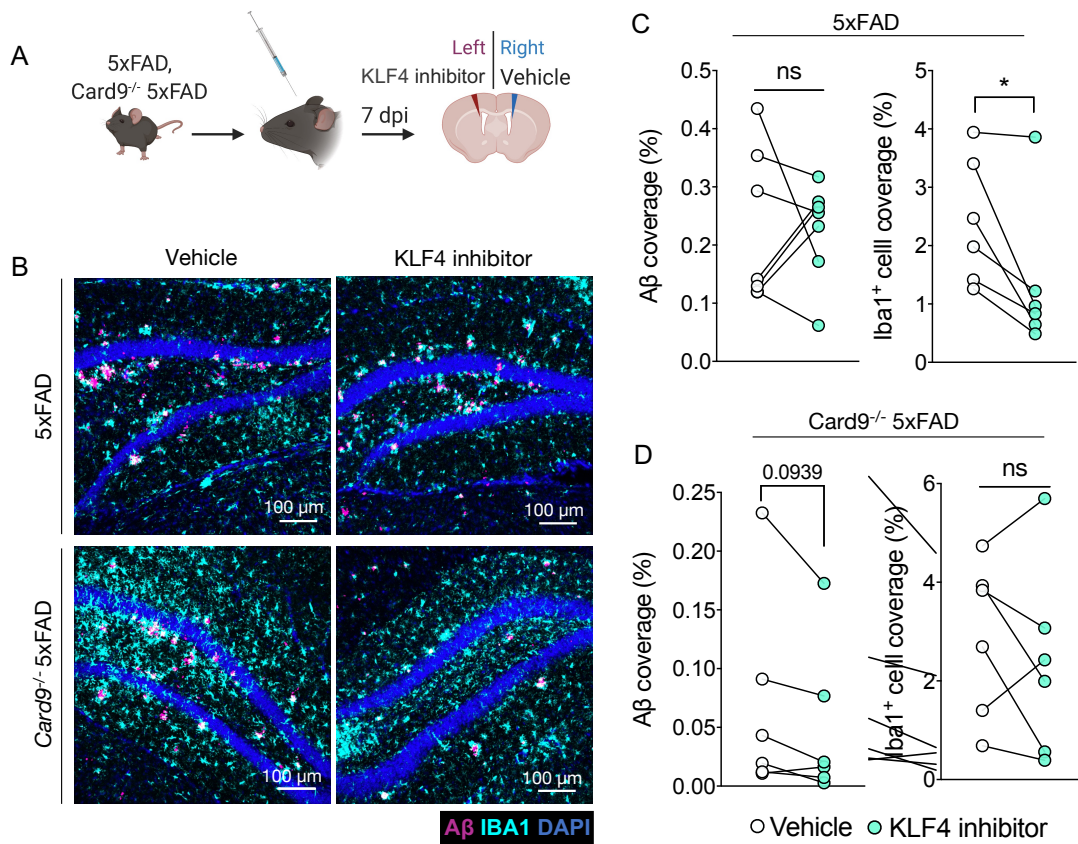


Figure 4.6. Acute KLF4 inhibition in the hippocampus reduces Iba1⁺ cell coverage in 5xFAD mice. (A-D) Right and left hippocampal injection of vehicle or KLF4 inhibitor (Kenpaullone), respectively, into 4-month-old 5xFAD and *Card9*^{-/-} 5xFAD mice. Brains were then harvested 7 days post injection (dpi). (A) Experimental design schematic. (B) Representative images of A β (pink) and Iba1 (cyan) coverage in 4-month-old 5xFAD and *Card9*^{-/-} 5xFAD mice 7 days following intrahippocampal injection of vehicle or 5 μ mol of the KLF4 inhibitor. (C-D) Quantification of A β (D54D2, pink) and Iba1⁺ cells (cyan) in the hippocampus of (C) 5xFAD and (D) *Card9*^{-/-} 5xFAD mice. Statistical significance between experimental groups was calculated by paired Student's t-test (C-D). ns = nonsignificant, * $P < 0.05$. Representative data from 2 independent experiments (C-D).

Overall, the delineation of cell specific CARD9 activation may provide a novel understanding by which microglia or the peripheral immune system impacts AD progression. The interplay between immune and AD signaling pathways has become increasingly apparent. The further characterization of these

independent or shared pathways may uncover highly specific treatments through the modulation of CNS-resident or non-resident immune cells. Added understanding of spatially and temporally affected microglial intracellular signaling in disease will continue to provide a necessary and informed approach to intervention during neurodegeneration.

4.3 Concluding Remarks

The increasing prevalence of Alzheimer's disease has resulted in a collective dedication by multiple scientific disciplines to uncover methods to prevent disease onset and progression. This collective mission has brought about a growing appreciation for the interplay between the immune system and the brain during disease. More specifically, the resident immune cells of the brain, microglia, have received a decade of limelight due to their ability to proficiently respond to AD pathology. The continued probing of microglial function during AD has unmasked a rather complicated role for these cells throughout varying stages of disease. In addition, microglial responses during demyelination-related neurodegeneration also indicate a nuanced but critical role for these immune cells during disease. In turn, interventional approaches resulting in massive alterations of microglial function have proved ineffectual, steering future work to focus on the manipulatable "understory" of microglial signaling. This dissertation work reveals a pivotal role for microglial SYK in regulating numerous microglial responses that are critically relevant in the context of AD and demyelinating disease. Indeed, we found that SYK modulates downstream microglial signaling necessary for phagocytosis and both morphological and transcriptional activation. An additional chapter of this dissertation describes the ability of CARD9, a downstream molecule activated in the context of fungal infection, to curb AD pathology progression in 5xFAD mice. Therefore, our work identified two microglial intracellular signaling molecules that can massively and/or specifically impact microglial function during neurodegeneration. Work from this dissertation delves into previously undescribed microglial biology during neurodegeneration which can lead to increasingly informed modulation of microglial activity for therapeutic intervention.

4.4 Materials and Methods

Mice

All mouse experiments were performed in accordance with the relevant guidelines and regulations of the University of Virginia and approved by the University of Virginia Animal Care and Use Committee. Female 5xFAD mice (Stock # 34848), *Syk*^{fl/fl} mice (Stock #028652), and *Cx3cr1*^{ERT2cre} mice (Stock # 020940) were obtained from The Jackson Laboratory and were crossed to generate *Syk*^{fl/fl} (denoted as *Syk*^{con}), *Syk*^{fl/fl} *Cx3cr1*^{ERT2cre} (denoted as *Syk*^{ΔMG}), 5xFAD *Syk*^{fl/fl} (denoted as 5xFAD), and 5xFAD *Syk*^{fl/fl} *Cx3cr1*^{ERT2cre} (denoted as 5xFAD *Syk*^{ΔMG}) experimental mice. Female 5xFAD mice (Stock # 34848), *Clec7a*^{-/-} (Stock # 12337), *Card9*^{-/-} mice (Stock # 017309), and C57BL/6J mice (Stock # 000664) were obtained from The Jackson Laboratory and were crossed to generate *Clec7a*^{+/+} (denoted as WT), *Clec7a*^{+/-}, *Clec7a*^{-/-}, 5xFAD,

Clec7a^{+/-}5xFAD, *Clec7a*^{-/-}5xFAD, *Card9*^{+/+} (denoted as WT), *Card9*^{+/-}, *Card9*^{-/-}, *Card9*^{+/+}5xFAD (denoted as 5xFAD), *Card9*^{+/-}5xFAD, and *Card9*^{-/-}5xFAD experimental mice. Mice underwent a 12-hour light/dark cycle, were housed in specific pathogen-free conditions and kept at a standardized temperature ($21 \pm 1.5^\circ$ C) and humidity ($50 \pm 10\%$).

Brain tissue harvest

Experimental mice underwent euthanasia by means of CO₂ asphyxiation and were transcardially perfused with 20 ml of 1xPBS. Brains were then harvested and bisected. The left hemisphere was drop-fixed in 4% paraformaldehyde over night at 4°C and the right hemisphere flash-frozen and stored at -80°C. Fixed samples were placed in 30% sucrose until sunken in solution and then frozen in Tissue-Plus OCT compound (Thermo Fisher). Using a cryostat (Leica), brains were sectioned at 50 µm in thickness and stored in PBS + 0.05% sodium azide at 4°C until stained for imaging. For RNA extraction and protein extraction, the flash-frozen brains were thawed on ice and mechanically homogenized in 500 µl of Tissue Protein Extraction Reagent T-PER (Thermo Fisher, 78510) containing protease inhibitor cocktail cOmplete (Roche, 11873580001) and phosphatase inhibitor cocktail PhosSTOP (Roche, 04906845001). For RNA extraction, 50 µl of brain homogenate was diluted in 500 µl Trizol and stored at -80°C. The remaining brain homogenates were then spun down at 16,000 rpm for 10 minutes and the supernatant was collected for soluble amyloid beta analysis and pellet were isolated for insoluble amyloid beta analysis by ELISA.

Immunofluorescence microscopy

Brain sections were blocked for 1 hour at room temperature with 2% donkey serum, 1% bovine serum albumin, 0.1% triton, 0.05% tween in PBS prior to incubation with primary antibodies. The primary antibodies were then diluted in this block overnight at 4°C. Brain sections were stained with anti-Aβ (D54D2, Cell Signaling, 1:300 dilution) to label plaques. Neuronal health was probed by staining for anti-APP (Y188, ab32136, Abcam, 1:750). In order to analyze microglia, sections were stained with IBA1 (ab5076, Abcam, 1:300 dilution). Microglial proliferation was assessed using Ki67-EF660 (SoIA15, Thermo Fisher, 1:100 dilution). Following primary antibody incubation, sections were then washed 3 times for 10 minutes at room temperature in PBS and 0.05% tween-20. After washing, the brain sections were incubated in respective donkey Alexa Fluor 488, 594, 647 anti-rabbit, -goat, -rat, -streptavidin, and -mouse (Thermo Fisher, 1:1000 dilution) for 2 hours at room temperature. Once again, brain sections were washed 3 times for 10 minutes at room temperature. Following washing, sections were stained with DAPI (1:1000) for 10 minutes at room temperature to label nuclei, or stained with ThioflavinS (Sigma-Aldrich, 2 mg/10ml) for 8 minutes followed by three 2-minute washes with 50% ethanol at room temperature to label plaques. Brain sections were then transferred to PBS before being mounted to glass microscope slides with 50 µl of ProLongGold antifade reagent (P36930, Invitrogen) and coverslips. For storage, mounted brain

sections were kept at 4°C and were imaged using LAS AF software (Leica Microsystems) on a Leica TCS SP8 confocal microscope. Images were analyzed using FIJI software or Imaris software (9.5.1).

ELISA

To assess amyloid beta composition in the brain, A β was measured in brain homogenate supernatants for soluble A β analysis, or brain homogenate pellets that underwent guanidine extraction by incubating the pellets 1:6 in 5 M guanidine HCL/50 mM tris, pH = 8.0 at room temperature for 3 hours for insoluble A β analysis. The guanidine-extracted samples were then diluted 1:5 in PBS containing protease inhibitor cocktail cOmplete (11873580001, Roche) then centrifuged at 16,000 g for 20 minutes at 4°C. The brain homogenate supernatant was diluted 1:10 and the guanidine-extraction supernatant was diluted 1:200 and quantified by Amyloid beta 42 Mouse ELISA kit (KMB3441, Thermo Fisher).

MACS isolation of microglia for RNA-sequencing

Euthanasia of mice was performed using CO₂ followed by transcardial perfusion using 20 ml of 1X PBS with heparin. The meninges and choroid plexus were removed from the brain before beginning the magnetic-activated cell sorting (MACS) protocol. Microglia were isolated using the methods described in (424). In brief, brains were placed in 5 ml of HBSS (with Mg and Ca) (14025092, Gibco) with papain 4U/ml (LS003126, Worthington) and 50 U/ml DNase I (10104159001, Sigma-Aldrich). Following 3 triturations of the samples using a 5 ml serological pipette over 45 minutes at 37°C, the brain homogenates were transferred to a conical tube containing a 70- μ m cell strainer and topped with 20 ml of DMEM/F12 (21331020, Gibco) containing 10% FBS, 1x antibiotic-antimycotic (15240096, Thermo Fisher), and 1x GlutaMAX (35050061, Invitrogen). Strained samples were then spun down with slow brake (3 on a 0-10 scale) for 10 minutes at 300 G, resuspended in 160 μ l MACS buffer (130-091-376, Miltenyi Biotec), and then incubated with 20 μ l MACS CD11b (microglia) microbeads (130-093-634, Miltenyi Biotec) for 15 min at 4°C. Sorting was performed using LS columns and a QuadroMACS magnet (Miltenyi, 130-042-401 and 130-091-051) according to the product instructions. The protocol efficiency was validated using flow cytometry (>90% CD11b^{hi}CD45^{int}) before submitting for RNA-sequencing.

Flow cytometry

To label microglia, cells were stained with flow antibodies for CD11b, and CD45 (eBioscience) diluted 1:200 in FACS buffer for 20 minutes at 4°C. Cells were spun down and washed with FACS buffer. Prior to running samples on the cytometer, cells were resuspended in 100 μ l FACS buffer containing DAPI 1:5000. Microglia were gated as live cells (DAPI negative), single cells, and as CD11b^{hi}CD45^{int} cells.

RNA-sequencing analysis

Microglia sorted using MACS isolation were sent to Azenta Next Generation Sequencing. Using splice-aware read aligner HISAT2, FASTQ files were aligned with the UCSC mm10 mouse genome. Quality control filtering was applied using Samtools. Next, HTSeq was used to sort reads into feature counts. DESeq2 (v1.30.0) was utilized to normalize raw counts to read depth and carry out differential expression analysis. The Benjamini-Hochberg procedure was used to correct p-values and limit false positives arising from multiple testing. RNA-seq analyses were performed using Seq2Pathway, fgsea, tidyverse, and dplyr software packages. Heatmaps were produced using the pheatmap R package (<https://github.com/raivokolde/pheatmap>), lattice (<http://lattice.r-forge.r-project.org/>) or ggplot2 (<https://ggplot2.tidyverse.org>) packages.

Intrahippocampal injection

5xFAD and *Card9*^{-/-} 5xFAD mice were anesthetized before receiving a bilateral hippocampal injection of 2 µl of vehicle, 200 µmol of BRD5529, or 5 µmol of Kenpaullone into the right and left hemisphere of the hippocampus (at ±2 mm lateral, -2 mm posterior, and -2 mm ventral relative to the intersection of the coronal and sagittal suture (bregma) at a rate of 200 nl/min) using a stereotaxic frame (51730U, Stoelting) and nanoliter injector (NL2010MC2T, World Precision Instruments). Seven days post injection, mice were euthanized using CO₂ and transcardially perfused before preparing brains for immunofluorescent staining to evaluate Aβ clearance in the hippocampus. Images were acquired using LAS AF software (Leica Microsystems) on a Leica TCS SP8 confocal microscope and analyzed using FIJI software.

Statistics

All statistical analyses were performed using Prism software (GraphPad). Statistical tests include Student's t test (paired and unpaired), one-way ANOVA, and two-way ANOVA. *P* values less than 0.05 were deemed significant: **p* < 0.05, ***p* < 0.01, ****p* < 0.001, *****p* < 0.0001. All data are represented as mean ± SEM.

REFERENCES

1. R. L. Nussbaum, C. E. Ellis, Alzheimer's disease and Parkinson's disease. *N Engl J Med* **348**, 1356-1364 (2003).
2. M. T. Heneka *et al.*, Neuroinflammation in Alzheimer's disease. *The Lancet Neurology* **14**, 388-405 (2015).
3. N. I. o. Aging, What Causes Alzheimer's Disease? (2020).
4. D. P. Perl, Neuropathology of Alzheimer's disease. *Mt Sinai J Med* **77**, 32-42 (2010).
5. Z. He *et al.*, Amyloid-beta plaques enhance Alzheimer's brain tau-seeded pathologies by facilitating neuritic plaque tau aggregation. *Nat Med* **24**, 29-38 (2018).
6. F. M. LaFerla, B. T. Tinkle, C. J. Bieberich, C. C. Haudenschild, G. Jay, The Alzheimer's A beta peptide induces neurodegeneration and apoptotic cell death in transgenic mice. *Nat Genet* **9**, 21-30 (1995).
7. J. Hardy, D. J. Selkoe, The amyloid hypothesis of Alzheimer's disease: progress and problems on the road to therapeutics. *Science* **297**, 353-356 (2002).
8. D. J. Selkoe, J. Hardy, The amyloid hypothesis of Alzheimer's disease at 25 years. *EMBO Mol Med* **8**, 595-608 (2016).
9. E. S. Musiek, D. M. Holtzman, Three dimensions of the amyloid hypothesis: time, space and 'wingmen'. *Nat Neurosci* **18**, 800-806 (2015).
10. C. R. Jack, Jr. *et al.*, Hypothetical model of dynamic biomarkers of the Alzheimer's pathological cascade. *Lancet Neurol* **9**, 119-128 (2010).
11. G. F. Chen *et al.*, Amyloid beta: structure, biology and structure-based therapeutic development. *Acta Pharmacol Sin* **38**, 1205-1235 (2017).
12. S. Chasseigneaux, B. Allinquant, Functions of Abeta, sAPPalpha and sAPPbeta : similarities and differences. *J Neurochem* **120 Suppl 1**, 99-108 (2012).
13. R. Kaye, C. A. Lasagna-Reeves, Molecular mechanisms of amyloid oligomers toxicity. *J Alzheimers Dis* **33 Suppl 1**, S67-78 (2013).
14. N. Katzmarski *et al.*, Abeta oligomers trigger and accelerate Abeta seeding. *Brain Pathol* **30**, 36-45 (2020).
15. A. M. Klein, N. W. Kowall, R. J. Ferrante, Neurotoxicity and oxidative damage of beta amyloid 1-42 versus beta amyloid 1-40 in the mouse cerebral cortex. *Ann N Y Acad Sci* **893**, 314-320 (1999).
16. A. Serrano-Pozo, M. P. Frosch, E. Masliah, B. T. Hyman, Neuropathological alterations in Alzheimer disease. *Cold Spring Harb Perspect Med* **1**, a006189 (2011).
17. K. R. Sadleir *et al.*, Presynaptic dystrophic neurites surrounding amyloid plaques are sites of microtubule disruption, BACE1 elevation, and increased Abeta generation in Alzheimer's disease. *Acta Neuropathol* **132**, 235-256 (2016).
18. R. E. Tanzi, The genetics of Alzheimer disease. *Cold Spring Harb Perspect Med* **2** (2012).
19. C. M. L. LarsBertram, Rudolph E. Tanzi, The Genetics of Alzheimer Disease: Back to the Future. (2010).
20. P. K. Panegyres, H. Y. Chen, Differences between early and late onset Alzheimer's disease. *Am J Neurodegener Dis* **2**, 300-306 (2013).
21. A. T. Isik, Late onset Alzheimer's disease in older people. *Clin Interv Aging* **5**, 307-311 (2010).
22. M. Safieh, A. D. Korczyn, D. M. Michaelson, ApoE4: an emerging therapeutic target for Alzheimer's disease. *BMC Med* **17**, 64 (2019).
23. Y. Huang, R. W. Mahley, Apolipoprotein E: structure and function in lipid metabolism, neurobiology, and Alzheimer's diseases. *Neurobiol Dis* **72 Pt A**, 3-12 (2014).

24. J. Ma, A. Yee, H. B. Brewer, Jr., S. Das, H. Potter, Amyloid-associated proteins alpha 1-antichymotrypsin and apolipoprotein E promote assembly of Alzheimer beta-protein into filaments. *Nature* **372**, 92-94 (1994).
25. Y. Namba, M. Tomonaga, H. Kawasaki, E. Otomo, K. Ikeda, Apolipoprotein E immunoreactivity in cerebral amyloid deposits and neurofibrillary tangles in Alzheimer's disease and kuru plaque amyloid in Creutzfeldt-Jakob disease. *Brain Res* **541**, 163-166 (1991).
26. Q. Tao *et al.*, Association of Chronic Low-grade Inflammation With Risk of Alzheimer Disease in ApoE4 Carriers. *JAMA Netw Open* **1**, e183597 (2018).
27. A. L. Hemonnot, J. Hua, L. Ulmann, H. Hirbec, Microglia in Alzheimer Disease: Well-Known Targets and New Opportunities. *Front Aging Neurosci* **11**, 233 (2019).
28. L. C. Lee, M. Q. L. Goh, E. H. Koo, Transcriptional regulation of APP by apoE: To boldly go where no isoform has gone before: ApoE, APP transcription and AD: Hypothesised mechanisms and existing knowledge gaps. *Bioessays* **39** (2017).
29. T. K. Ulland, M. Colonna, TREM2 - a key player in microglial biology and Alzheimer disease. *Nat Rev Neurol* **14**, 667-675 (2018).
30. H. Konishi, H. Kiyama, Microglial TREM2/DAP12 Signaling: A Double-Edged Sword in Neural Diseases. *Front Cell Neurosci* **12**, 206 (2018).
31. H. Zheng *et al.*, TREM2 in Alzheimer's Disease: Microglial Survival and Energy Metabolism. *Front Aging Neurosci* **10**, 395 (2018).
32. P. Hollingworth *et al.*, Common variants at ABCA7, MS4A6A/MS4A4E, EPHA1, CD33 and CD2AP are associated with Alzheimer's disease. *Nat Genet* **43**, 429-435 (2011).
33. A. C. Naj *et al.*, Common variants at MS4A4/MS4A6E, CD2AP, CD33 and EPHA1 are associated with late-onset Alzheimer's disease. *Nat Genet* **43**, 436-441 (2011).
34. E. M. Bradshaw *et al.*, CD33 Alzheimer's disease locus: altered monocyte function and amyloid biology. *Nat Neurosci* **16**, 848-850 (2013).
35. A. Griciuc *et al.*, Alzheimer's disease risk gene CD33 inhibits microglial uptake of amyloid beta. *Neuron* **78**, 631-643 (2013).
36. J. C. Lambert *et al.*, Genome-wide association study identifies variants at CLU and CR1 associated with Alzheimer's disease. *Nat Genet* **41**, 1094-1099 (2009).
37. E. M. Foster, A. Dangla-Valls, S. Lovestone, E. M. Ribe, N. J. Buckley, Clusterin in Alzheimer's Disease: Mechanisms, Genetics, and Lessons From Other Pathologies. *Front Neurosci* **13**, 164 (2019).
38. R. Sims, M. Hill, J. Williams, The multiplex model of the genetics of Alzheimer's disease. *Nat Neurosci* **23**, 311-322 (2020).
39. W. S. Kim, C. S. Weickert, B. Garner, Role of ATP-binding cassette transporters in brain lipid transport and neurological disease. *J Neurochem* **104**, 1145-1166 (2008).
40. A. W. Jehle *et al.*, ATP-binding cassette transporter A7 enhances phagocytosis of apoptotic cells and associated ERK signaling in macrophages. *J Cell Biol* **174**, 547-556 (2006).
41. M. S. Tan, J. T. Yu, L. Tan, Bridging integrator 1 (BIN1): form, function, and Alzheimer's disease. *Trends Mol Med* **19**, 594-603 (2013).
42. H. F. Wang *et al.*, Bridging Integrator 1 (BIN1) Genotypes Mediate Alzheimer's Disease Risk by Altering Neuronal Degeneration. *J Alzheimers Dis* **52**, 179-190 (2016).
43. X. C. Zhu *et al.*, CR1 in Alzheimer's disease. *Mol Neurobiol* **51**, 753-765 (2015).
44. R. H. Yin, J. T. Yu, L. Tan, The Role of SORL1 in Alzheimer's Disease. *Mol Neurobiol* **51**, 909-918 (2015).
45. R. E. Marioni *et al.*, Correction: GWAS on family history of Alzheimer's disease. *Transl Psychiatry* **9**, 161 (2019).

46. C. Guillonnet, S. Bezie, I. Anegon, Immunoregulatory properties of the cytokine IL-34. *Cell Mol Life Sci* **74**, 2569-2586 (2017).
47. T. Mizuno *et al.*, Interleukin-34 selectively enhances the neuroprotective effects of microglia to attenuate oligomeric amyloid-beta neurotoxicity. *Am J Pathol* **179**, 2016-2027 (2011).
48. J. Ma, J. T. Yu, L. Tan, MS4A Cluster in Alzheimer's Disease. *Mol Neurobiol* **51**, 1240-1248 (2015).
49. Y. Deming *et al.*, The MS4A gene cluster is a key modulator of soluble TREM2 and Alzheimer's disease risk. *Sci Transl Med* **11** (2019).
50. Q. Q. Tao, Y. C. Chen, Z. Y. Wu, The role of CD2AP in the Pathogenesis of Alzheimer's Disease. *Aging Dis* **10**, 901-907 (2019).
51. C. M. Karch, A. M. Goate, Alzheimer's disease risk genes and mechanisms of disease pathogenesis. *Biol Psychiatry* **77**, 43-51 (2015).
52. A. G. Efthymiou, A. M. Goate, Late onset Alzheimer's disease genetics implicates microglial pathways in disease risk. *Mol Neurodegener* **12**, 43 (2017).
53. S. D. Pauls, A. J. Marshall, Regulation of immune cell signaling by SHIP1: A phosphatase, scaffold protein, and potential therapeutic target. *Eur J Immunol* **47**, 932-945 (2017).
54. Y. Asanomi *et al.*, A rare functional variant of SHARPIN attenuates the inflammatory response and associates with increased risk of late-onset Alzheimer's disease. *Mol Med* **25**, 20 (2019).
55. Y. N. Song *et al.*, TREML2 Mutation Mediate Alzheimer's Disease Risk by Altering Neuronal Degeneration. *Front Neurosci* **13**, 455 (2019).
56. I. S. Miguel Tábuas-Pereira, Rita Guerreiro, José Brás, Alzheimer's Disease Genetics: Review of Novel Loci Associated with Disease. *Current Genetic Medicine Reports* (2020).
57. N. Z. Steele *et al.*, Fine-mapping of the human leukocyte antigen locus as a risk factor for Alzheimer disease: A case-control study. *PLoS Med* **14**, e1002272 (2017).
58. M. R. Brier *et al.*, Tau and Abeta imaging, CSF measures, and cognition in Alzheimer's disease. *Sci Transl Med* **8**, 338ra366 (2016).
59. A. Nordberg, PET imaging of amyloid in Alzheimer's disease. *Lancet Neurol* **3**, 519-527 (2004).
60. O. Sabri *et al.*, Florbetaben PET imaging to detect amyloid beta plaques in Alzheimer's disease: phase 3 study. *Alzheimers Dement* **11**, 964-974 (2015).
61. S. M. Landau *et al.*, Amyloid PET imaging in Alzheimer's disease: a comparison of three radiotracers. *Eur J Nucl Med Mol Imaging* **41**, 1398-1407 (2014).
62. N. Okamura *et al.*, Tau PET imaging in Alzheimer's disease. *Curr Neurol Neurosci Rep* **14**, 500 (2014).
63. L. Hamelin *et al.*, Early and protective microglial activation in Alzheimer's disease: a prospective study using 18F-DPA-714 PET imaging. *Brain* **139**, 1252-1264 (2016).
64. M. Mila-Aloma, M. Suarez-Calvet, J. L. Molinuevo, Latest advances in cerebrospinal fluid and blood biomarkers of Alzheimer's disease. *Ther Adv Neurol Disord* **12**, 1756286419888819 (2019).
65. K. Blennow, H. Zetterberg, Cerebrospinal fluid biomarkers for Alzheimer's disease. *J Alzheimers Dis* **18**, 413-417 (2009).
66. K. Blennow, Cerebrospinal fluid protein biomarkers for Alzheimer's disease. *NeuroRx* **1**, 213-225 (2004).
67. H. Hampel *et al.*, Blood-based biomarkers for Alzheimer disease: mapping the road to the clinic. *Nat Rev Neurol* **14**, 639-652 (2018).
68. O. Preische *et al.*, Serum neurofilament dynamics predicts neurodegeneration and clinical progression in presymptomatic Alzheimer's disease. *Nat Med* **25**, 277-283 (2019).
69. S. J. Soscia *et al.*, The Alzheimer's disease-associated amyloid beta-protein is an antimicrobial peptide. *PLoS One* **5**, e9505 (2010).
70. D. K. Kumar *et al.*, Amyloid-beta peptide protects against microbial infection in mouse and worm models of Alzheimer's disease. *Sci Transl Med* **8**, 340ra372 (2016).

71. R. D. Moir, R. Lathe, R. E. Tanzi, The antimicrobial protection hypothesis of Alzheimer's disease. *Alzheimers Dement* **14**, 1602-1614 (2018).
72. D. M. Fowler, A. V. Koulov, W. E. Balch, J. W. Kelly, Functional amyloid--from bacteria to humans. *Trends Biochem Sci* **32**, 217-224 (2007).
73. G. J. Rapsinski *et al.*, Toll-like receptor 2 and NLRP3 cooperate to recognize a functional bacterial amyloid, curli. *Infect Immun* **83**, 693-701 (2015).
74. C. Tukel *et al.*, Responses to amyloids of microbial and host origin are mediated through toll-like receptor 2. *Cell Host Microbe* **6**, 45-53 (2009).
75. A. Salminen, J. Ojala, A. Kauppinen, K. Kaarniranta, T. Suuronen, Inflammation in Alzheimer's disease: amyloid-beta oligomers trigger innate immunity defence via pattern recognition receptors. *Prog Neurobiol* **87**, 181-194 (2009).
76. G. Y. Chen, G. Nunez, Sterile inflammation: sensing and reacting to damage. *Nat Rev Immunol* **10**, 826-837 (2010).
77. T. Guo, W. Noble, D. P. Hanger, Roles of tau protein in health and disease. *Acta Neuropathol* **133**, 665-704 (2017).
78. C. Laurent, L. Buee, D. Blum, Tau and neuroinflammation: What impact for Alzheimer's Disease and Tauopathies? *Biomed J* **41**, 21-33 (2018).
79. M. A. Wozniak, A. L. Frost, R. F. Itzhaki, Alzheimer's disease-specific tau phosphorylation is induced by herpes simplex virus type 1. *J Alzheimers Dis* **16**, 341-350 (2009).
80. W. H. Organization, Globally, an estimated two-thirds of the population under 50 are infected with herpes simplex virus type 1. (2015).
81. M. A. Wozniak, A. L. Frost, C. M. Preston, R. F. Itzhaki, Antivirals reduce the formation of key Alzheimer's disease molecules in cell cultures acutely infected with herpes simplex virus type 1. *PLoS One* **6**, e25152 (2011).
82. N. I. o. Aging, Valacyclovir for Mild Alzheimer's Disease. (2018).
83. K. M. Lenz, L. H. Nelson, Microglia and Beyond: Innate Immune Cells As Regulators of Brain Development and Behavioral Function. *Front Immunol* **9**, 698 (2018).
84. K. R. Wildsmith, M. Holley, J. C. Savage, R. Skerrett, G. E. Landreth, Evidence for impaired amyloid beta clearance in Alzheimer's disease. *Alzheimers Res Ther* **5**, 33 (2013).
85. S. D. Mhatre, C. A. Tsai, A. J. Rubin, M. L. James, K. I. Andreasson, Microglial malfunction: the third rail in the development of Alzheimer's disease. *Trends Neurosci* **38**, 621-636 (2015).
86. H. Sarlus, M. T. Heneka, Microglia in Alzheimer's disease. *J Clin Invest* **127**, 3240-3249 (2017).
87. E. G. Reed-Geaghan, A. L. Croxford, B. Becher, G. E. Landreth, Plaque-associated myeloid cells derive from resident microglia in an Alzheimer's disease model. *J Exp Med* **217** (2020).
88. M. T. H. Darío Tejera, Microglia in Neurodegenerative Disorders. (2019).
89. F. Ginhoux, S. Lim, G. Hoeffel, D. Low, T. Huber, Origin and differentiation of microglia. *Front Cell Neurosci* **7**, 45 (2013).
90. A. Sierra, R. C. Paolicelli, H. Kettenmann, Cien Anos de Microglia: Milestones in a Century of Microglial Research. *Trends Neurosci* **42**, 778-792 (2019).
91. R. Parakalan *et al.*, Transcriptome analysis of amoeboid and ramified microglia isolated from the corpus callosum of rat brain. *BMC Neurosci* **13**, 64 (2012).
92. K. A. Kigerl, J. P. de Rivero Vaccari, W. D. Dietrich, P. G. Popovich, R. W. Keane, Pattern recognition receptors and central nervous system repair. *Exp Neurol* **258**, 5-16 (2014).
93. H. Keren-Shaul *et al.*, A Unique Microglia Type Associated with Restricting Development of Alzheimer's Disease. *Cell* **169**, 1276-1290 e1217 (2017).
94. A. Deczkowska *et al.*, Disease-Associated Microglia: A Universal Immune Sensor of Neurodegeneration. *Cell* **173**, 1073-1081 (2018).
95. R. Guerreiro *et al.*, TREM2 variants in Alzheimer's disease. *N Engl J Med* **368**, 117-127 (2013).

96. T. Jonsson *et al.*, Variant of TREM2 associated with the risk of Alzheimer's disease. *N Engl J Med* **368**, 107-116 (2013).
97. Y. Wang *et al.*, TREM2 lipid sensing sustains the microglial response in an Alzheimer's disease model. *Cell* **160**, 1061-1071 (2015).
98. Y. Zhao *et al.*, TREM2 Is a Receptor for beta-Amyloid that Mediates Microglial Function. *Neuron* **97**, 1023-1031 e1027 (2018).
99. Y. Atagi *et al.*, Apolipoprotein E Is a Ligand for Triggering Receptor Expressed on Myeloid Cells 2 (TREM2). *J Biol Chem* **290**, 26043-26050 (2015).
100. Y. Wang *et al.*, TREM2-mediated early microglial response limits diffusion and toxicity of amyloid plaques. *J Exp Med* **213**, 667-675 (2016).
101. C. Condello, P. Yuan, J. Grutzendler, Microglia-Mediated Neuroprotection, TREM2, and Alzheimer's Disease: Evidence From Optical Imaging. *Biol Psychiatry* **83**, 377-387 (2018).
102. C. Condello, P. Yuan, A. Schain, J. Grutzendler, Microglia constitute a barrier that prevents neurotoxic protofibrillar Abeta42 hotspots around plaques. *Nat Commun* **6**, 6176 (2015).
103. T. K. Ulland *et al.*, TREM2 Maintains Microglial Metabolic Fitness in Alzheimer's Disease. *Cell* **170**, 649-663 e613 (2017).
104. S. Parhizkar *et al.*, Loss of TREM2 function increases amyloid seeding but reduces plaque-associated ApoE. *Nat Neurosci* **22**, 191-204 (2019).
105. S. Krasemann *et al.*, The TREM2-APOE Pathway Drives the Transcriptional Phenotype of Dysfunctional Microglia in Neurodegenerative Diseases. *Immunity* **47**, 566-581 e569 (2017).
106. L. Piccio *et al.*, Cerebrospinal fluid soluble TREM2 is higher in Alzheimer disease and associated with mutation status. *Acta Neuropathol* **131**, 925-933 (2016).
107. L. Zhong *et al.*, Soluble TREM2 ameliorates pathological phenotypes by modulating microglial functions in an Alzheimer's disease model. *Nat Commun* **10**, 1365 (2019).
108. L. Zhao, CD33 in Alzheimer's Disease - Biology, Pathogenesis, and Therapeutics: A Mini-Review. *Gerontology* **65**, 323-331 (2019).
109. A. Varki, Sialic acids in human health and disease. *Trends Mol Med* **14**, 351-360 (2008).
110. D. G. Walker *et al.*, Association of CD33 polymorphism rs3865444 with Alzheimer's disease pathology and CD33 expression in human cerebral cortex. *Neurobiol Aging* **36**, 571-582 (2015).
111. C. M. Karch *et al.*, Expression of novel Alzheimer's disease risk genes in control and Alzheimer's disease brains. *PLoS One* **7**, e50976 (2012).
112. A. Griciuc *et al.*, TREM2 Acts Downstream of CD33 in Modulating Microglial Pathology in Alzheimer's Disease. *Neuron* **103**, 820-835 e827 (2019).
113. J. V. Pluvinage *et al.*, CD22 blockade restores homeostatic microglial phagocytosis in ageing brains. *Nature* **568**, 187-192 (2019).
114. G. D. Brown, Dectin-1: a signalling non-TLR pattern-recognition receptor. *Nat Rev Immunol* **6**, 33-43 (2006).
115. R. Alonso *et al.*, Fungal infection in patients with Alzheimer's disease. *J Alzheimers Dis* **41**, 301-311 (2014).
116. D. Pisa, R. Alonso, A. Juarranz, A. Rabano, L. Carrasco, Direct visualization of fungal infection in brains from patients with Alzheimer's disease. *J Alzheimers Dis* **43**, 613-624 (2015).
117. D. Pisa, R. Alonso, A. Rabano, I. Rodal, L. Carrasco, Different Brain Regions are Infected with Fungi in Alzheimer's Disease. *Sci Rep* **5**, 15015 (2015).
118. M. Watabe-Rudolph *et al.*, Chitinase enzyme activity in CSF is a powerful biomarker of Alzheimer disease. *Neurology* **78**, 569-577 (2012).
119. B. Parady, Innate Immune and Fungal Model of Alzheimer's Disease. *J Alzheimers Dis Rep* **2**, 139-152 (2018).

120. Y. Huang *et al.*, Microglia use TAM receptors to detect and engulf amyloid beta plaques. *Nat Immunol* **22**, 586-594 (2021).
121. C. V. Rothlin, S. Ghosh, E. I. Zuniga, M. B. Oldstone, G. Lemke, TAM receptors are pleiotropic inhibitors of the innate immune response. *Cell* **131**, 1124-1136 (2007).
122. R. S. Scott *et al.*, Phagocytosis and clearance of apoptotic cells is mediated by MER. *Nature* **411**, 207-211 (2001).
123. Z. Yin *et al.*, Immune hyperreactivity of Abeta plaque-associated microglia in Alzheimer's disease. *Neurobiol Aging* **55**, 115-122 (2017).
124. E. Spangenberg *et al.*, Sustained microglial depletion with CSF1R inhibitor impairs parenchymal plaque development in an Alzheimer's disease model. *Nat Commun* **10**, 3758 (2019).
125. D. Doens, P. L. Fernandez, Microglia receptors and their implications in the response to amyloid beta for Alzheimer's disease pathogenesis. *J Neuroinflammation* **11**, 48 (2014).
126. T. Chavakis, A. Bierhaus, P. P. Nawroth, RAGE (receptor for advanced glycation end products): a central player in the inflammatory response. *Microbes Infect* **6**, 1219-1225 (2004).
127. E. J. Lee, J. H. Park, Receptor for Advanced Glycation Endproducts (RAGE), Its Ligands, and Soluble RAGE: Potential Biomarkers for Diagnosis and Therapeutic Targets for Human Renal Diseases. *Genomics Inform* **11**, 224-229 (2013).
128. L. J. Sparvero *et al.*, RAGE (Receptor for Advanced Glycation Endproducts), RAGE ligands, and their role in cancer and inflammation. *J Transl Med* **7**, 17 (2009).
129. F. Fang *et al.*, RAGE-dependent signaling in microglia contributes to neuroinflammation, Abeta accumulation, and impaired learning/memory in a mouse model of Alzheimer's disease. *FASEB J* **24**, 1043-1055 (2010).
130. R. Deane *et al.*, RAGE mediates amyloid-beta peptide transport across the blood-brain barrier and accumulation in brain. *Nat Med* **9**, 907-913 (2003).
131. S. D. Yan *et al.*, RAGE and amyloid-beta peptide neurotoxicity in Alzheimer's disease. *Nature* **382**, 685-691 (1996).
132. D. Walker, L. F. Lue, G. Paul, A. Patel, M. N. Sabbagh, Receptor for advanced glycation endproduct modulators: a new therapeutic target in Alzheimer's disease. *Expert Opin Investig Drugs* **24**, 393-399 (2015).
133. S. Hong *et al.*, Complement and microglia mediate early synapse loss in Alzheimer mouse models. *Science* **352**, 712-716 (2016).
134. D. P. Schafer *et al.*, Microglia sculpt postnatal neural circuits in an activity and complement-dependent manner. *Neuron* **74**, 691-705 (2012).
135. Q. Shi *et al.*, Complement C3-Deficient Mice Fail to Display Age-Related Hippocampal Decline. *J Neurosci* **35**, 13029-13042 (2015).
136. A. H. Stephan *et al.*, A dramatic increase of C1q protein in the CNS during normal aging. *J Neurosci* **33**, 13460-13474 (2013).
137. Q. Shi *et al.*, Complement C3 deficiency protects against neurodegeneration in aged plaque-rich APP/PS1 mice. *Sci Transl Med* **9** (2017).
138. E. Czirr *et al.*, Microglial complement receptor 3 regulates brain Abeta levels through secreted proteolytic activity. *J Exp Med* **214**, 1081-1092 (2017).
139. H. Fu *et al.*, Complement component C3 and complement receptor type 3 contribute to the phagocytosis and clearance of fibrillar Abeta by microglia. *Glia* **60**, 993-1003 (2012).
140. M. I. Fonseca *et al.*, Cell-specific deletion of C1qa identifies microglia as the dominant source of C1q in mouse brain. *J Neuroinflammation* **14**, 48 (2017).
141. B. P. Morgan, Complement in the pathogenesis of Alzheimer's disease. *Semin Immunopathol* **40**, 113-124 (2018).

142. C. Wang *et al.*, Microglia mediate forgetting via complement-dependent synaptic elimination. *Science* **367**, 688-694 (2020).
143. M. Ries, M. Sastre, Mechanisms of Abeta Clearance and Degradation by Glial Cells. *Front Aging Neurosci* **8**, 160 (2016).
144. G. E. Landreth, E. G. Reed-Geaghan, Toll-like receptors in Alzheimer's disease. *Curr Top Microbiol Immunol* **336**, 137-153 (2009).
145. K. L. Richard, M. Filali, P. Prefontaine, S. Rivest, Toll-like receptor 2 acts as a natural innate immune receptor to clear amyloid beta 1-42 and delay the cognitive decline in a mouse model of Alzheimer's disease. *J Neurosci* **28**, 5784-5793 (2008).
146. M. Song *et al.*, TLR4 mutation reduces microglial activation, increases Abeta deposits and exacerbates cognitive deficits in a mouse model of Alzheimer's disease. *J Neuroinflammation* **8**, 92 (2011).
147. R. Arroyo-Espliguero, P. Avanzas, S. Jeffery, J. C. Kaski, CD14 and toll-like receptor 4: a link between infection and acute coronary events? *Heart* **90**, 983-988 (2004).
148. Y. Liu *et al.*, LPS receptor (CD14): a receptor for phagocytosis of Alzheimer's amyloid peptide. *Brain* **128**, 1778-1789 (2005).
149. F. Bard *et al.*, Peripherally administered antibodies against amyloid beta-peptide enter the central nervous system and reduce pathology in a mouse model of Alzheimer disease. *Nat Med* **6**, 916-919 (2000).
150. C. H. van Dyck, Anti-Amyloid-beta Monoclonal Antibodies for Alzheimer's Disease: Pitfalls and Promise. *Biol Psychiatry* **83**, 311-319 (2018).
151. A. Mullard, Anti-amyloid failures stack up as Alzheimer antibody flops. *Nat Rev Drug Discov* 10.1038/d41573-019-00064-1 (2019).
152. I. V. Kurochkin, E. Guarnera, I. N. Berezovsky, Insulin-Degrading Enzyme in the Fight against Alzheimer's Disease. *Trends Pharmacol Sci* **39**, 49-58 (2018).
153. I. Y. Tamboli *et al.*, Statins promote the degradation of extracellular amyloid {beta}-peptide by microglia via stimulation of exosome-associated insulin-degrading enzyme (IDE) secretion. *J Biol Chem* **285**, 37405-37414 (2010).
154. E. Hellstrom-Lindahl, R. Ravid, A. Nordberg, Age-dependent decline of neprilysin in Alzheimer's disease and normal brain: inverse correlation with A beta levels. *Neurobiol Aging* **29**, 210-221 (2008).
155. K. Yasojima, H. Akiyama, E. G. McGeer, P. L. McGeer, Reduced neprilysin in high plaque areas of Alzheimer brain: a possible relationship to deficient degradation of beta-amyloid peptide. *Neurosci Lett* **297**, 97-100 (2001).
156. S. M. Huang *et al.*, Neprilysin-sensitive synapse-associated amyloid-beta peptide oligomers impair neuronal plasticity and cognitive function. *J Biol Chem* **281**, 17941-17951 (2006).
157. E. A. Eckman, M. Watson, L. Marlow, K. Sambamurti, C. B. Eckman, Alzheimer's disease beta-amyloid peptide is increased in mice deficient in endothelin-converting enzyme. *J Biol Chem* **278**, 2081-2084 (2003).
158. S. Oddo, The ubiquitin-proteasome system in Alzheimer's disease. *J Cell Mol Med* **12**, 363-373 (2008).
159. T. Kanekiyo, H. Xu, G. Bu, ApoE and Abeta in Alzheimer's disease: accidental encounters or partners? *Neuron* **81**, 740-754 (2014).
160. J. D. Ulrich *et al.*, ApoE facilitates the microglial response to amyloid plaque pathology. *J Exp Med* **215**, 1047-1058 (2018).
161. L. Yang *et al.*, LRP1 modulates the microglial immune response via regulation of JNK and NF-kappaB signaling pathways. *J Neuroinflammation* **13**, 304 (2016).

162. B. Levine, N. Mizushima, H. W. Virgin, Autophagy in immunity and inflammation. *Nature* **469**, 323-335 (2011).
163. M. H. Cho *et al.*, Autophagy in microglia degrades extracellular beta-amyloid fibrils and regulates the NLRP3 inflammasome. *Autophagy* **10**, 1761-1775 (2014).
164. U. Kruger, Y. Wang, S. Kumar, E. M. Mandelkow, Autophagic degradation of tau in primary neurons and its enhancement by trehalose. *Neurobiol Aging* **33**, 2291-2305 (2012).
165. V. Schaeffer *et al.*, Stimulation of autophagy reduces neurodegeneration in a mouse model of human tauopathy. *Brain* **135**, 2169-2177 (2012).
166. R. Sanchez-Varo *et al.*, Abnormal accumulation of autophagic vesicles correlates with axonal and synaptic pathology in young Alzheimer's mice hippocampus. *Acta Neuropathol* **123**, 53-70 (2012).
167. D. S. Yang *et al.*, Reversal of autophagy dysfunction in the TgCRND8 mouse model of Alzheimer's disease ameliorates amyloid pathologies and memory deficits. *Brain* **134**, 258-277 (2011).
168. O. Butovsky, H. L. Weiner, Microglial signatures and their role in health and disease. *Nat Rev Neurosci* **19**, 622-635 (2018).
169. T. S. Kim *et al.*, Changes in the levels of plasma soluble fractalkine in patients with mild cognitive impairment and Alzheimer's disease. *Neurosci Lett* **436**, 196-200 (2008).
170. M. Fuhrmann *et al.*, Microglial Cx3cr1 knockout prevents neuron loss in a mouse model of Alzheimer's disease. *Nat Neurosci* **13**, 411-413 (2010).
171. S. H. Cho *et al.*, CX3CR1 protein signaling modulates microglial activation and protects against plaque-independent cognitive deficits in a mouse model of Alzheimer disease. *J Biol Chem* **286**, 32713-32722 (2011).
172. N. Lou *et al.*, Purinergic receptor P2RY12-dependent microglial closure of the injured blood-brain barrier. *Proc Natl Acad Sci U S A* **113**, 1074-1079 (2016).
173. S. E. Haynes *et al.*, The P2Y12 receptor regulates microglial activation by extracellular nucleotides. *Nat Neurosci* **9**, 1512-1519 (2006).
174. J. Han, R. A. Harris, X. M. Zhang, An updated assessment of microglia depletion: current concepts and future directions. *Mol Brain* **10**, 25 (2017).
175. N. N. Dagher *et al.*, Colony-stimulating factor 1 receptor inhibition prevents microglial plaque association and improves cognition in 3xTg-AD mice. *J Neuroinflammation* **12**, 139 (2015).
176. H. Asai *et al.*, Depletion of microglia and inhibition of exosome synthesis halt tau propagation. *Nat Neurosci* **18**, 1584-1593 (2015).
177. A. Olmos-Alonso *et al.*, Pharmacological targeting of CSF1R inhibits microglial proliferation and prevents the progression of Alzheimer's-like pathology. *Brain* **139**, 891-907 (2016).
178. E. E. Spangenberg *et al.*, Eliminating microglia in Alzheimer's mice prevents neuronal loss without modulating amyloid-beta pathology. *Brain* **139**, 1265-1281 (2016).
179. M. R. Elmore *et al.*, Colony-stimulating factor 1 receptor signaling is necessary for microglia viability, unmasking a microglia progenitor cell in the adult brain. *Neuron* **82**, 380-397 (2014).
180. J. Bruttger *et al.*, Genetic Cell Ablation Reveals Clusters of Local Self-Renewing Microglia in the Mammalian Central Nervous System. *Immunity* **43**, 92-106 (2015).
181. R. J. Henry *et al.*, Microglial Depletion with CSF1R Inhibitor During Chronic Phase of Experimental Traumatic Brain Injury Reduces Neurodegeneration and Neurological Deficits. *J Neurosci* **40**, 2960-2974 (2020).
182. A. Chodobski, B. J. Zink, J. Szmydynger-Chodobska, Blood-brain barrier pathophysiology in traumatic brain injury. *Transl Stroke Res* **2**, 492-516 (2011).
183. M. D. Sweeney, A. P. Sagare, B. V. Zlokovic, Blood-brain barrier breakdown in Alzheimer disease and other neurodegenerative disorders. *Nat Rev Neurol* **14**, 133-150 (2018).

184. E. F. Willis *et al.*, Repopulating Microglia Promote Brain Repair in an IL-6-Dependent Manner. *Cell* **180**, 833-846 e816 (2020).
185. J. El Khoury *et al.*, Ccr2 deficiency impairs microglial accumulation and accelerates progression of Alzheimer-like disease. *Nat Med* **13**, 432-438 (2007).
186. G. Naert, S. Rivest, Hematopoietic CC-chemokine receptor 2 (CCR2) competent cells are protective for the cognitive impairments and amyloid pathology in a transgenic mouse model of Alzheimer's disease. *Mol Med* **18**, 297-313 (2012).
187. M. J. Moravan, J. A. Olschowka, J. P. Williams, M. K. O'Banion, Brain radiation injury leads to a dose- and time-dependent recruitment of peripheral myeloid cells that depends on CCR2 signaling. *J Neuroinflammation* **13**, 30 (2016).
188. J. C. Cronk *et al.*, Peripherally derived macrophages can engraft the brain independent of irradiation and maintain an identity distinct from microglia. *J Exp Med* **215**, 1627-1647 (2018).
189. T. R. Jay *et al.*, TREM2 deficiency eliminates TREM2+ inflammatory macrophages and ameliorates pathology in Alzheimer's disease mouse models. *J Exp Med* **212**, 287-295 (2015).
190. J. W. Kinney, Inflammation as a central mechanism in Alzheimer's disease. (2018).
191. H. Akiyama *et al.*, Inflammation and Alzheimer's disease. *Neurobiol Aging* **21**, 383-421 (2000).
192. J. W. Kinney *et al.*, Inflammation as a central mechanism in Alzheimer's disease. *Alzheimers Dement (N Y)* **4**, 575-590 (2018).
193. J. M. Taylor, Z. Moore, M. R. Minter, P. J. Crack, Type-I interferon pathway in neuroinflammation and neurodegeneration: focus on Alzheimer's disease. *J Neural Transm (Vienna)* **125**, 797-807 (2018).
194. B. S. Thawkar, G. Kaur, Inhibitors of NF-kappaB and P2X7/NLRP3/Caspase 1 pathway in microglia: Novel therapeutic opportunities in neuroinflammation induced early-stage Alzheimer's disease. *J Neuroimmunol* **326**, 62-74 (2019).
195. K. Bhaskar *et al.*, Microglial derived tumor necrosis factor-alpha drives Alzheimer's disease-related neuronal cell cycle events. *Neurobiol Dis* **62**, 273-285 (2014).
196. H. M. Melo *et al.*, Palmitate Is Increased in the Cerebrospinal Fluid of Humans with Obesity and Induces Memory Impairment in Mice via Pro-inflammatory TNF- α . *Cell Reports* **30**, 2180-2194.e2188 (2020).
197. A. K. Fu *et al.*, IL-33 ameliorates Alzheimer's disease-like pathology and cognitive decline. *Proc Natl Acad Sci U S A* **113**, E2705-2713 (2016).
198. M. S. Tan *et al.*, IL12/23 p40 inhibition ameliorates Alzheimer's disease-associated neuropathology and spatial memory in SAMP8 mice. *J Alzheimers Dis* **38**, 633-646 (2014).
199. M. V. Guillot-Sestier *et al.*, Il10 deficiency rebalances innate immunity to mitigate Alzheimer-like pathology. *Neuron* **85**, 534-548 (2015).
200. W. Swardfager *et al.*, A meta-analysis of cytokines in Alzheimer's disease. *Biol Psychiatry* **68**, 930-941 (2010).
201. E. Polazzi, B. Monti, Microglia and neuroprotection: from in vitro studies to therapeutic applications. *Prog Neurobiol* **92**, 293-315 (2010).
202. K. A. Clayton, A. A. Van Enoo, T. Ikezu, Alzheimer's Disease: The Role of Microglia in Brain Homeostasis and Proteopathy. *Front Neurosci* **11**, 680 (2017).
203. M. Yamamoto *et al.*, Interferon-gamma and tumor necrosis factor-alpha regulate amyloid-beta plaque deposition and beta-secretase expression in Swedish mutant APP transgenic mice. *Am J Pathol* **170**, 680-692 (2007).
204. N. Gorle, R. E. Vandenbroucke, Interferons: A molecular switch between damage and repair in ageing and Alzheimer's disease. *Mech Ageing Dev* **183**, 111148 (2019).
205. E. R. Roy *et al.*, Type I interferon response drives neuroinflammation and synapse loss in Alzheimer disease. *J Clin Invest* 10.1172/JCI133737 (2020).

206. J. Di Domizio *et al.*, Nucleic acid-containing amyloid fibrils potently induce type I interferon and stimulate systemic autoimmunity. *Proc Natl Acad Sci U S A* **109**, 14550-14555 (2012).
207. J. A. Contreras *et al.*, Functional connectivity among brain regions affected in Alzheimer's disease is associated with CSF TNF-alpha in APOE4 carriers. *Neurobiol Aging* **86**, 112-122 (2020).
208. S. Steeland *et al.*, Counteracting the effects of TNF receptor-1 has therapeutic potential in Alzheimer's disease. *EMBO Mol Med* **10** (2018).
209. P. Chakrabarty, A. Herring, C. Ceballos-Diaz, P. Das, T. E. Golde, Hippocampal expression of murine TNFalpha results in attenuation of amyloid deposition in vivo. *Mol Neurodegener* **6**, 16 (2011).
210. S. J. Andrews, A. Goate, Mendelian randomization indicates that TNF is not causally associated with Alzheimer's disease. *Neurobiol Aging* **84**, 241 e241-241 e243 (2019).
211. P. Bossu *et al.*, Interleukin-18, from neuroinflammation to Alzheimer's disease. *Curr Pharm Des* **16**, 4213-4224 (2010).
212. F. Su, F. Bai, Z. Zhang, Inflammatory Cytokines and Alzheimer's Disease: A Review from the Perspective of Genetic Polymorphisms. *Neurosci Bull* **32**, 469-480 (2016).
213. E. M. Sutinen, T. Pirttila, G. Anderson, A. Salminen, J. O. Ojala, Pro-inflammatory interleukin-18 increases Alzheimer's disease-associated amyloid-beta production in human neuron-like cells. *J Neuroinflammation* **9**, 199 (2012).
214. T. C. Tzeng *et al.*, Inflammasome-derived cytokine IL18 suppresses amyloid-induced seizures in Alzheimer-prone mice. *Proc Natl Acad Sci U S A* **115**, 9002-9007 (2018).
215. M. Kitazawa *et al.*, Blocking IL-1 signaling rescues cognition, attenuates tau pathology, and restores neuronal beta-catenin pathway function in an Alzheimer's disease model. *J Immunol* **187**, 6539-6549 (2011).
216. S. Ghosh *et al.*, Sustained interleukin-1beta overexpression exacerbates tau pathology despite reduced amyloid burden in an Alzheimer's mouse model. *J Neurosci* **33**, 5053-5064 (2013).
217. D. F. de Souza *et al.*, S100B secretion is stimulated by IL-1beta in glial cultures and hippocampal slices of rats: Likely involvement of MAPK pathway. *J Neuroimmunol* **206**, 52-57 (2009).
218. J. S. Cristovao, C. M. Gomes, S100 Proteins in Alzheimer's Disease. *Front Neurosci* **13**, 463 (2019).
219. M. L. Chaves *et al.*, Serum levels of S100B and NSE proteins in Alzheimer's disease patients. *J Neuroinflammation* **7**, 6 (2010).
220. Peskind, Cerebrospinal fluid S100B is elevated in the earlier stages of Alzheimer's disease. (2001).
221. T. Mori *et al.*, Overexpression of human S100B exacerbates cerebral amyloidosis and gliosis in the Tg2576 mouse model of Alzheimer's disease. *Glia* **58**, 300-314 (2010).
222. F. Y. Liew, J. P. Girard, H. R. Turnquist, Interleukin-33 in health and disease. *Nat Rev Immunol* **16**, 676-689 (2016).
223. J. Chapuis *et al.*, Transcriptomic and genetic studies identify IL-33 as a candidate gene for Alzheimer's disease. *Mol Psychiatry* **14**, 1004-1016 (2009).
224. D. Gomez-Nicola, N. L. Fransen, S. Suzzi, V. H. Perry, Regulation of microglial proliferation during chronic neurodegeneration. *J Neurosci* **33**, 2481-2493 (2013).
225. D. G. Walker, T. M. Tang, L. F. Lue, Studies on Colony Stimulating Factor Receptor-1 and Ligands Colony Stimulating Factor-1 and Interleukin-34 in Alzheimer's Disease Brains and Human Microglia. *Front Aging Neurosci* **9**, 244 (2017).
226. J. Vom Berg *et al.*, Inhibition of IL-12/IL-23 signaling reduces Alzheimer's disease-like pathology and cognitive decline. *Nat Med* **18**, 1812-1819 (2012).
227. R. Taipa *et al.*, Proinflammatory and anti-inflammatory cytokines in the CSF of patients with Alzheimer's disease and their correlation with cognitive decline. *Neurobiol Aging* **76**, 125-132 (2019).

228. S. Pedrini *et al.*, A blood-based biomarker panel indicates IL-10 and IL-12/23p40 are jointly associated as predictors of beta-amyloid load in an AD cohort. *Sci Rep* **7**, 14057 (2017).
229. P. Eede *et al.*, Interleukin-12/23 deficiency differentially affects pathology in male and female Alzheimer's disease-like mice. *EMBO Rep* 10.15252/embr.201948530, e48530 (2020).
230. M. T. Heneka *et al.*, NLRP3 is activated in Alzheimer's disease and contributes to pathology in APP/PS1 mice. *Nature* **493**, 674-678 (2013).
231. J. Yin *et al.*, NLRP3 Inflammasome Inhibitor Ameliorates Amyloid Pathology in a Mouse Model of Alzheimer's Disease. *Mol Neurobiol* **55**, 1977-1987 (2018).
232. S. Voet *et al.*, A20 critically controls microglia activation and inhibits inflammasome-dependent neuroinflammation. *Nat Commun* **9**, 2036 (2018).
233. P. J. Wu, Y. F. Hung, H. Y. Liu, Y. P. Hsueh, Deletion of the Inflammasome Sensor Aim2 Mitigates A β Deposition and Microglial Activation but Increases Inflammatory Cytokine Expression in an Alzheimer Disease Mouse Model. *Neuroimmunomodulation* **24**, 29-39 (2017).
234. V. A. Rathinam, S. K. Vanaja, K. A. Fitzgerald, Regulation of inflammasome signaling. *Nat Immunol* **13**, 333-342 (2012).
235. S. M. Man, T. D. Kanneganti, Gasdermin D: the long-awaited executioner of pyroptosis. *Cell Res* **25**, 1183-1184 (2015).
236. X. Liu *et al.*, Inflammasome-activated gasdermin D causes pyroptosis by forming membrane pores. *Nature* **535**, 153-158 (2016).
237. I. Mitroulis, P. Skendros, K. Ritis, Targeting IL-1 β in disease; the expanding role of NLRP3 inflammasome. *Eur J Intern Med* **21**, 157-163 (2010).
238. M. Pennisi *et al.*, Inflammasomes, hormesis, and antioxidants in neuroinflammation: Role of NLRP3 in Alzheimer disease. *J Neurosci Res* **95**, 1360-1372 (2017).
239. T. Goldmann, T. L. Tay, M. Prinz, Love and death: microglia, NLRP3 and the Alzheimer's brain. *Cell Res* **23**, 595-596 (2013).
240. M. Saresella *et al.*, The NLRP3 and NLRP1 inflammasomes are activated in Alzheimer's disease. *Mol Neurodegener* **11**, 23 (2016).
241. I. C. Stancu *et al.*, Aggregated Tau activates NLRP3-ASC inflammasome exacerbating exogenously seeded and non-exogenously seeded Tau pathology in vivo. *Acta Neuropathol* **137**, 599-617 (2019).
242. C. Ising *et al.*, NLRP3 inflammasome activation drives tau pathology. *Nature* **575**, 669-673 (2019).
243. M. J. Daniels *et al.*, Fenamate NSAIDs inhibit the NLRP3 inflammasome and protect against Alzheimer's disease in rodent models. *Nat Commun* **7**, 12504 (2016).
244. C. Venegas *et al.*, Microglia-derived ASC specks cross-seed amyloid- β in Alzheimer's disease. *Nature* **552**, 355-361 (2017).
245. L. L. Friker *et al.*, beta-Amyloid Clustering around ASC Fibrils Boosts Its Toxicity in Microglia. *Cell Rep* **30**, 3743-3754 e3746 (2020).
246. C. R. Lammert *et al.*, AIM2 inflammasome surveillance of DNA damage shapes neurodevelopment. *Nature* **580**, 647-652 (2020).
247. P. J. Wu, H. Y. Liu, T. N. Huang, Y. P. Hsueh, AIM 2 inflammasomes regulate neuronal morphology and influence anxiety and memory in mice. *Sci Rep* **6**, 32405 (2016).
248. M. T. Heneka, D. T. Golenbock, E. Latz, Innate immunity in Alzheimer's disease. *Nat Immunol* **16**, 229-236 (2015).
249. R. Guerreiro, J. Bras, The age factor in Alzheimer's disease. *Genome Med* **7**, 106 (2015).
250. D. S. Davies, J. Ma, T. Jegathees, C. Goldsbury, Microglia show altered morphology and reduced arborization in human brain during aging and Alzheimer's disease. *Brain Pathol* **27**, 795-808 (2017).

251. A. Schuitemaker *et al.*, Microglial activation in healthy aging. *Neurobiol Aging* **33**, 1067-1072 (2012).
252. E. C. Koellhoffer, L. D. McCullough, R. M. Ritzel, Old Maids: Aging and Its Impact on Microglia Function. *Int J Mol Sci* **18** (2017).
253. B. Spittau, Aging Microglia-Phenotypes, Functions and Implications for Age-Related Neurodegenerative Diseases. *Front Aging Neurosci* **9**, 194 (2017).
254. S. A. Villeda *et al.*, Young blood reverses age-related impairments in cognitive function and synaptic plasticity in mice. *Nat Med* **20**, 659-663 (2014).
255. J. Rebo *et al.*, A single heterochronic blood exchange reveals rapid inhibition of multiple tissues by old blood. *Nat Commun* **7**, 13363 (2016).
256. K. J. Gan, T. C. Sudhof, Specific factors in blood from young but not old mice directly promote synapse formation and NMDA-receptor recruitment. *Proc Natl Acad Sci U S A* **116**, 12524-12533 (2019).
257. S. A. Villeda *et al.*, The ageing systemic milieu negatively regulates neurogenesis and cognitive function. *Nature* **477**, 90-94 (2011).
258. D. Abraham *et al.*, Exercise and probiotics attenuate the development of Alzheimer's disease in transgenic mice: Role of microbiome. *Exp Gerontol* **115**, 122-131 (2019).
259. M. V. Lourenco *et al.*, Exercise-linked FNDC5/irisin rescues synaptic plasticity and memory defects in Alzheimer's models. *Nat Med* **25**, 165-175 (2019).
260. J. Vukovic, M. J. Colditz, D. G. Blackmore, M. J. Ruitenber, P. F. Bartlett, Microglia modulate hippocampal neural precursor activity in response to exercise and aging. *J Neurosci* **32**, 6435-6443 (2012).
261. L. Forny-Germano, F. G. De Felice, M. Vieira, The Role of Leptin and Adiponectin in Obesity-Associated Cognitive Decline and Alzheimer's Disease. *Front Neurosci* **12**, 1027 (2018).
262. E. Maliszewska-Cyna, M. Lynch, J. J. Oore, P. M. Nagy, I. Aubert, The Benefits of Exercise and Metabolic Interventions for the Prevention and Early Treatment of Alzheimer's Disease. *Curr Alzheimer Res* **14**, 47-60 (2017).
263. G. Neves, S. F. Cooke, T. V. Bliss, Synaptic plasticity, memory and the hippocampus: a neural network approach to causality. *Nat Rev Neurosci* **9**, 65-75 (2008).
264. E. R. Kandel, The molecular biology of memory: cAMP, PKA, CRE, CREB-1, CREB-2, and CPEB. *Mol Brain* **5**, 14 (2012).
265. J. P. Campbell, J. E. Turner, Debunking the Myth of Exercise-Induced Immune Suppression: Redefining the Impact of Exercise on Immunological Health Across the Lifespan. *Front Immunol* **9**, 648 (2018).
266. K. Honjo, R. van Reekum, N. P. Verhoeff, Alzheimer's disease and infection: do infectious agents contribute to progression of Alzheimer's disease? *Alzheimers Dement* **5**, 348-360 (2009).
267. M. Ide *et al.*, Periodontitis and Cognitive Decline in Alzheimer's Disease. *PLoS One* **11**, e0151081 (2016).
268. J. Holmer, M. Eriksdotter, M. Schultzberg, P. J. Pussinen, K. Buhlin, Association between periodontitis and risk of Alzheimer's disease, mild cognitive impairment and subjective cognitive decline: A case-control study. *J Clin Periodontol* **45**, 1287-1298 (2018).
269. P. Sparks Stein *et al.*, Serum antibodies to periodontal pathogens are a risk factor for Alzheimer's disease. *Alzheimers Dement* **8**, 196-203 (2012).
270. A. R. Kamer *et al.*, TNF-alpha and antibodies to periodontal bacteria discriminate between Alzheimer's disease patients and normal subjects. *J Neuroimmunol* **216**, 92-97 (2009).
271. A. R. Kamer *et al.*, Inflammation and Alzheimer's disease: possible role of periodontal diseases. *Alzheimers Dement* **4**, 242-250 (2008).

272. F. B. Teixeira *et al.*, Periodontitis and Alzheimer's Disease: A Possible Comorbidity between Oral Chronic Inflammatory Condition and Neuroinflammation. *Front Aging Neurosci* **9**, 327 (2017).
273. B. J. Balin *et al.*, Identification and localization of Chlamydia pneumoniae in the Alzheimer's brain. *Med Microbiol Immunol* **187**, 23-42 (1998).
274. X. Zhan *et al.*, Gram-negative bacterial molecules associate with Alzheimer disease pathology. *Neurology* **87**, 2324-2332 (2016).
275. D. C. Emery *et al.*, 16S rRNA Next Generation Sequencing Analysis Shows Bacteria in Alzheimer's Post-Mortem Brain. *Front Aging Neurosci* **9**, 195 (2017).
276. R. F. Itzhaki *et al.*, Herpes simplex virus type 1 in brain and risk of Alzheimer's disease. *Lancet* **349**, 241-244 (1997).
277. C. Holmes *et al.*, Systemic inflammation and disease progression in Alzheimer disease. *Neurology* **73**, 768-774 (2009).
278. A. Semmler *et al.*, Persistent cognitive impairment, hippocampal atrophy and EEG changes in sepsis survivors. *J Neurol Neurosurg Psychiatry* **84**, 62-69 (2013).
279. C. H. Chou *et al.*, Septicemia is associated with increased risk for dementia: a population-based longitudinal study. *Oncotarget* **8**, 84300-84308 (2017).
280. V. E. Johnson, W. Stewart, D. H. Smith, Traumatic brain injury and amyloid-beta pathology: a link to Alzheimer's disease? *Nat Rev Neurosci* **11**, 361-370 (2010).
281. H. T. Tran, F. M. LaFerla, D. M. Holtzman, D. L. Brody, Controlled cortical impact traumatic brain injury in 3xTg-AD mice causes acute intra-axonal amyloid-beta accumulation and independently accelerates the development of tau abnormalities. *J Neurosci* **31**, 9513-9525 (2011).
282. N. Tajiri, S. L. Kellogg, T. Shimizu, G. W. Arendash, C. V. Borlongan, Traumatic brain injury precipitates cognitive impairment and extracellular Abeta aggregation in Alzheimer's disease transgenic mice. *PLoS One* **8**, e78851 (2013).
283. D. H. Smith *et al.*, Brain trauma induces massive hippocampal neuron death linked to a surge in beta-amyloid levels in mice overexpressing mutant amyloid precursor protein. *Am J Pathol* **153**, 1005-1010 (1998).
284. B. L. Plassman *et al.*, Documented head injury in early adulthood and risk of Alzheimer's disease and other dementias. *Neurology* **55**, 1158-1166 (2000).
285. S. Fleminger, D. L. Oliver, S. Lovestone, S. Rabe-Hesketh, A. Giora, Head injury as a risk factor for Alzheimer's disease: the evidence 10 years on; a partial replication. *J Neurol Neurosurg Psychiatry* **74**, 857-862 (2003).
286. A. Lobo *et al.*, Prevalence of dementia and major subtypes in Europe: A collaborative study of population-based cohorts. Neurologic Diseases in the Elderly Research Group. *Neurology* **54**, S4-9 (2000).
287. D. H. Smith, V. E. Johnson, W. Stewart, Chronic neuropathologies of single and repetitive TBI: substrates of dementia? *Nat Rev Neurol* **9**, 211-221 (2013).
288. R. Mayeux *et al.*, Synergistic effects of traumatic head injury and apolipoprotein-epsilon 4 in patients with Alzheimer's disease. *Neurology* **45**, 555-557 (1995).
289. J. Ramos-Cejudo *et al.*, Traumatic Brain Injury and Alzheimer's Disease: The Cerebrovascular Link. *EBioMedicine* **28**, 21-30 (2018).
290. G. Edwards, 3rd, J. Zhao, P. K. Dash, C. Soto, I. Moreno-Gonzalez, Traumatic Brain Injury Induces Tau Aggregation and Spreading. *J Neurotrauma* **37**, 80-92 (2020).
291. P. M. Washington, N. Morffy, M. Parsadonian, D. N. Zapple, M. P. Burns, Experimental traumatic brain injury induces rapid aggregation and oligomerization of amyloid-beta in an Alzheimer's disease mouse model. *J Neurotrauma* **31**, 125-134 (2014).
292. A. Louveau *et al.*, Structural and functional features of central nervous system lymphatic vessels. *Nature* **523**, 337-341 (2015).

293. A. Louveau *et al.*, CNS lymphatic drainage and neuroinflammation are regulated by meningeal lymphatic vasculature. *Nat Neurosci* **21**, 1380-1391 (2018).
294. S. Da Mesquita *et al.*, Functional aspects of meningeal lymphatics in ageing and Alzheimer's disease. *Nature* **560**, 185-191 (2018).
295. M. E. H. Ashley C. Bolte, Igor Smirnov, Michael A. Kovacs, Celia A. McKee, Nick Natale, Hannah E. Ennerfelt, Elizabeth L. Frost, Catherine E. Lammert, Jonathan Kipnis, John R. Lukens, Meningeal lymphatic dysfunction exacerbates traumatic brain injury pathogenesis. (2019).
296. V. Braniste *et al.*, The gut microbiota influences blood-brain barrier permeability in mice. *Sci Transl Med* **6**, 263ra158 (2014).
297. M. Carabotti, A. Scirocco, M. A. Maselli, C. Severi, The gut-brain axis: interactions between enteric microbiota, central and enteric nervous systems. *Ann Gastroenterol* **28**, 203-209 (2015).
298. M. E. M. Obrenovich, Leaky Gut, Leaky Brain? *Microorganisms* **6** (2018).
299. K. Kowalski, A. Mulak, Brain-Gut-Microbiota Axis in Alzheimer's Disease. *J Neurogastroenterol Motil* **25**, 48-60 (2019).
300. C. Jiang, G. Li, P. Huang, Z. Liu, B. Zhao, The Gut Microbiota and Alzheimer's Disease. *J Alzheimers Dis* **58**, 1-15 (2017).
301. M. S. Kim *et al.*, Transfer of a healthy microbiota reduces amyloid and tau pathology in an Alzheimer's disease animal model. *Gut* **69**, 283-294 (2020).
302. H. B. Dodiya *et al.*, Sex-specific effects of microbiome perturbations on cerebral A β amyloidosis and microglia phenotypes. *J Exp Med* **216**, 1542-1560 (2019).
303. A. Cattaneo *et al.*, Association of brain amyloidosis with pro-inflammatory gut bacterial taxa and peripheral inflammation markers in cognitively impaired elderly. *Neurobiol Aging* **49**, 60-68 (2017).
304. R. Nagpal, B. J. Neth, S. Wang, S. Craft, H. Yadav, Modified Mediterranean-ketogenic diet modulates gut microbiome and short-chain fatty acids in association with Alzheimer's disease markers in subjects with mild cognitive impairment. *EBioMedicine* **47**, 529-542 (2019).
305. B. A. Mander, J. R. Winer, M. P. Walker, Sleep and Human Aging. *Neuron* **94**, 19-36 (2017).
306. L. Volicer, D. G. Harper, B. C. Manning, R. Goldstein, A. Satlin, Sundowning and circadian rhythms in Alzheimer's disease. *Am J Psychiatry* **158**, 704-711 (2001).
307. O. M. Bubu *et al.*, Sleep, Cognitive impairment, and Alzheimer's disease: A Systematic Review and Meta-Analysis. *Sleep* **40** (2017).
308. E. Shokri-Kojori *et al.*, beta-Amyloid accumulation in the human brain after one night of sleep deprivation. *Proc Natl Acad Sci U S A* **115**, 4483-4488 (2018).
309. B. P. Lucey *et al.*, Effect of sleep on overnight cerebrospinal fluid amyloid beta kinetics. *Ann Neurol* **83**, 197-204 (2018).
310. J. K. Holth *et al.*, The sleep-wake cycle regulates brain interstitial fluid tau in mice and CSF tau in humans. *Science* **363**, 880-884 (2019).
311. J. Holth, T. Patel, D. M. Holtzman, Sleep in Alzheimer's Disease - Beyond Amyloid. *Neurobiol Sleep Circadian Rhythms* **2**, 4-14 (2017).
312. B. W. Patterson *et al.*, Age and amyloid effects on human central nervous system amyloid-beta kinetics. *Ann Neurol* **78**, 439-453 (2015).
313. K. Kaneshwaran *et al.*, Sleep fragmentation, microglial aging, and cognitive impairment in adults with and without Alzheimer's dementia. *Sci Adv* **5**, eaax7331 (2019).
314. M. R. Irwin, M. R. Opp, Sleep Health: Reciprocal Regulation of Sleep and Innate Immunity. *Neuropsychopharmacology* **42**, 129-155 (2017).
315. C. J. Pike, Sex and the development of Alzheimer's disease. *J Neurosci Res* **95**, 671-680 (2017).
316. P. Gaignard *et al.*, Role of Sex Hormones on Brain Mitochondrial Function, with Special Reference to Aging and Neurodegenerative Diseases. *Front Aging Neurosci* **9**, 406 (2017).

317. J. Vina, A. Lloret, Why women have more Alzheimer's disease than men: gender and mitochondrial toxicity of amyloid-beta peptide. *J Alzheimers Dis* **20 Suppl 2**, S527-533 (2010).
318. Y. J. Song *et al.*, The Effect of Estrogen Replacement Therapy on Alzheimer's Disease and Parkinson's Disease in Postmenopausal Women: A Meta-Analysis. *Front Neurosci* **14**, 157 (2020).
319. P. Jadia *et al.*, Impaired mitochondrial calcium efflux contributes to disease progression in models of Alzheimer's disease. *Nat Commun* **10**, 3885 (2019).
320. Y. Chen, Z. Zhou, W. Min, Mitochondria, Oxidative Stress and Innate Immunity. *Front Physiol* **9**, 1487 (2018).
321. M. Aminzadeh, M. Roghani, A. Sarfallah, G. H. Riaz, TRPM2 dependence of ROS-induced NLRP3 activation in Alzheimer's disease. *Int Immunopharmacol* **54**, 78-85 (2018).
322. R. H. Swerdlow, J. M. Burns, S. M. Khan, The Alzheimer's disease mitochondrial cascade hypothesis: progress and perspectives. *Biochim Biophys Acta* **1842**, 1219-1231 (2014).
323. J. S. Kerr *et al.*, Mitophagy and Alzheimer's Disease: Cellular and Molecular Mechanisms. *Trends Neurosci* **40**, 151-166 (2017).
324. X. Wang *et al.*, Oxidative stress and mitochondrial dysfunction in Alzheimer's disease. *Biochim Biophys Acta* **1842**, 1240-1247 (2014).
325. S. Lautrup *et al.*, Microglial mitophagy mitigates neuroinflammation in Alzheimer's disease. *Neurochem Int* **129**, 104469 (2019).
326. E. F. Fang *et al.*, Mitophagy inhibits amyloid-beta and tau pathology and reverses cognitive deficits in models of Alzheimer's disease. *Nat Neurosci* **22**, 401-412 (2019).
327. A. Villa *et al.*, Sex-Specific Features of Microglia from Adult Mice. *Cell Rep* **23**, 3501-3511 (2018).
328. R. Hanamsagar *et al.*, Generation of a microglial developmental index in mice and in humans reveals a sex difference in maturation and immune reactivity. *Glia* **65**, 1504-1520 (2017).
329. T. L. Stephen *et al.*, APOE genotype and sex affect microglial interactions with plaques in Alzheimer's disease mice. *Acta Neuropathol Commun* **7**, 82 (2019).
330. B. D. Trapp, K. A. Nave, Multiple sclerosis: an immune or neurodegenerative disorder? *Annu Rev Neurosci* **31**, 247-269 (2008).
331. J. P. Taylor, J. Hardy, K. H. Fischbeck, Toxic proteins in neurodegenerative disease. *Science* **296**, 1991-1995 (2002).
332. C. G. Chung, H. Lee, S. B. Lee, Mechanisms of protein toxicity in neurodegenerative diseases. *Cell Mol Life Sci* **75**, 3159-3180 (2018).
333. J. C. Vickers *et al.*, Axonopathy and cytoskeletal disruption in degenerative diseases of the central nervous system. *Brain Res Bull* **80**, 217-223 (2009).
334. S. Hickman, S. Izzy, P. Sen, L. Morsett, J. El Khoury, Microglia in neurodegeneration. *Nat Neurosci* **21**, 1359-1369 (2018).
335. A. Lampron *et al.*, Inefficient clearance of myelin debris by microglia impairs remyelinating processes. *J Exp Med* **212**, 481-495 (2015).
336. M. Malik *et al.*, CD33 Alzheimer's risk-altering polymorphism, CD33 expression, and exon 2 splicing. *J Neurosci* **33**, 13320-13325 (2013).
337. C. International Multiple Sclerosis Genetics, Multiple sclerosis genomic map implicates peripheral immune cells and microglia in susceptibility. *Science* **365** (2019).
338. J. Cooper-Knock *et al.*, A data-driven approach links microglia to pathology and prognosis in amyotrophic lateral sclerosis. *Acta Neuropathol Commun* **5**, 23 (2017).
339. S. M. Bemiller *et al.*, TREM2 deficiency exacerbates tau pathology through dysregulated kinase signaling in a mouse model of tauopathy. *Mol Neurodegener* **12**, 74 (2017).
340. A. Mocsai, J. Ruland, V. L. Tybulewicz, The SYK tyrosine kinase: a crucial player in diverse biological functions. *Nat Rev Immunol* **10**, 387-402 (2010).
341. M. S. Lionakis, I. D. Iliev, T. M. Hohl, Immunity against fungi. *JCI Insight* **2** (2017).

342. Y. Kimura *et al.*, Dectin-1-mediated signaling leads to characteristic gene expressions and cytokine secretion via spleen tyrosine kinase (Syk) in rat mast cells. *J Biol Chem* **289**, 31565-31575 (2014).
343. S. Estus *et al.*, Evaluation of CD33 as a genetic risk factor for Alzheimer's disease. *Acta Neuropathol* **138**, 187-199 (2019).
344. S. Lumb *et al.*, Engagement of CD22 on B cells with the monoclonal antibody epratuzumab stimulates the phosphorylation of upstream inhibitory signals of the B cell receptor. *J Cell Commun Signal* **10**, 143-151 (2016).
345. D. M. Underhill, H. S. Goodridge, The many faces of ITAMs. *Trends Immunol* **28**, 66-73 (2007).
346. C. L. Abram, C. A. Lowell, The expanding role for ITAM-based signaling pathways in immune cells. *Sci STKE* **2007**, re2 (2007).
347. J. E. Schweig *et al.*, Alzheimer's disease pathological lesions activate the spleen tyrosine kinase. *Acta Neuropathol Commun* **5**, 69 (2017).
348. D. Paris *et al.*, The spleen tyrosine kinase (Syk) regulates Alzheimer amyloid-beta production and Tau hyperphosphorylation. *J Biol Chem* **289**, 33927-33944 (2014).
349. B. Lawlor *et al.*, Nilvadipine in mild to moderate Alzheimer disease: A randomised controlled trial. *PLoS Med* **15**, e1002660 (2018).
350. B. C. Richard *et al.*, Gene Dosage Dependent Aggravation of the Neurological Phenotype in the 5XFAD Mouse Model of Alzheimer's Disease. *J Alzheimers Dis* **45**, 1223-1236 (2015).
351. D. Gate *et al.*, Clonally expanded CD8 T cells patrol the cerebrospinal fluid in Alzheimer's disease. *Nature* **577**, 399-404 (2020).
352. J. Machhi *et al.*, CD4+ effector T cells accelerate Alzheimer's disease in mice. *J Neuroinflammation* **18**, 272 (2021).
353. S. H. Chen *et al.*, Amyloid-beta uptake by blood monocytes is reduced with ageing and Alzheimer's disease. *Transl Psychiatry* **10**, 423 (2020).
354. U. Munawara *et al.*, Hyperactivation of monocytes and macrophages in MCI patients contributes to the progression of Alzheimer's disease. *Immun Ageing* **18**, 29 (2021).
355. X. Wu, T. Saito, T. C. Saido, A. M. Barron, C. Ruedl, Microglia and CD206(+) border-associated mouse macrophages maintain their embryonic origin during Alzheimer's disease. *Elife* **10** (2021).
356. H. Van Hove *et al.*, A single-cell atlas of mouse brain macrophages reveals unique transcriptional identities shaped by ontogeny and tissue environment. *Nat Neurosci* **22**, 1021-1035 (2019).
357. C. Y. D. Lee *et al.*, Elevated TREM2 Gene Dosage Reprograms Microglia Responsivity and Ameliorates Pathological Phenotypes in Alzheimer's Disease Models. *Neuron* **97**, 1032-1048 e1035 (2018).
358. M. R. Brown, S. E. Radford, E. W. Hewitt, Modulation of beta-Amyloid Fibril Formation in Alzheimer's Disease by Microglia and Infection. *Front Mol Neurosci* **13**, 609073 (2020).
359. L. J. Martin, C. A. Pardo, L. C. Cork, D. L. Price, Synaptic pathology and glial responses to neuronal injury precede the formation of senile plaques and amyloid deposits in the aging cerebral cortex. *Am J Pathol* **145**, 1358-1381 (1994).
360. S. T. Ferreira, M. V. Lourenco, M. M. Oliveira, F. G. De Felice, Soluble amyloid-beta oligomers as synaptotoxins leading to cognitive impairment in Alzheimer's disease. *Front Cell Neurosci* **9**, 191 (2015).
361. L. Gu, Z. Guo, Alzheimer's Aβ₄₂ and Aβ₄₀ peptides form interlaced amyloid fibrils. *J Neurochem* **126**, 305-311 (2013).
362. S. Colie *et al.*, Neuronal p38α mediates synaptic and cognitive dysfunction in an Alzheimer's mouse model by controlling beta-amyloid production. *Sci Rep* **7**, 45306 (2017).

363. S. Jawhar, A. Trawicka, C. Jenneckens, T. A. Bayer, O. Wirths, Motor deficits, neuron loss, and reduced anxiety coinciding with axonal degeneration and intraneuronal Abeta aggregation in the 5XFAD mouse model of Alzheimer's disease. *Neurobiol Aging* **33**, 196 e129-140 (2012).
364. T. Kanno, A. Tsuchiya, T. Nishizaki, Hyperphosphorylation of Tau at Ser396 occurs in the much earlier stage than appearance of learning and memory disorders in 5XFAD mice. *Behav Brain Res* **274**, 302-306 (2014).
365. T. F. Gendron, L. Petrucelli, The role of tau in neurodegeneration. *Mol Neurodegener* **4**, 13 (2009).
366. J. Ha *et al.*, Altered risk-aversion and risk-taking behaviour in patients with Alzheimer's disease. *Psychogeriatrics* **12**, 151-158 (2012).
367. E. Chu, R. Mychasiuk, M. L. Hibbs, B. D. Semple, Dysregulated phosphoinositide 3-kinase signaling in microglia: shaping chronic neuroinflammation. *J Neuroinflammation* **18**, 276 (2021).
368. S. Gabbouj *et al.*, Altered Insulin Signaling in Alzheimer's Disease Brain - Special Emphasis on PI3K-Akt Pathway. *Front Neurosci* **13**, 629 (2019).
369. C. Hooper, R. Killick, S. Lovestone, The GSK3 hypothesis of Alzheimer's disease. *J Neurochem* **104**, 1433-1439 (2008).
370. E. Steen *et al.*, Impaired insulin and insulin-like growth factor expression and signaling mechanisms in Alzheimer's disease--is this type 3 diabetes? *J Alzheimers Dis* **7**, 63-80 (2005).
371. I. Mateo *et al.*, Association between glycogen synthase kinase-3beta genetic polymorphism and late-onset Alzheimer's disease. *Dement Geriatr Cogn Disord* **21**, 228-232 (2006).
372. B. A. Schaffer *et al.*, Association of GSK3B with Alzheimer disease and frontotemporal dementia. *Arch Neurol* **65**, 1368-1374 (2008).
373. B. W. Doble, J. R. Woodgett, GSK-3: tricks of the trade for a multi-tasking kinase. *J Cell Sci* **116**, 1175-1186 (2003).
374. D. E. Hurtado *et al.*, Selectively silencing GSK-3 isoforms reduces plaques and tangles in mouse models of Alzheimer's disease. *J Neurosci* **32**, 7392-7402 (2012).
375. F. Hernandez, J. J. Lucas, J. Avila, GSK3 and tau: two convergence points in Alzheimer's disease. *J Alzheimers Dis* **33 Suppl 1**, S141-144 (2013).
376. B. DaRocha-Souto *et al.*, Activation of glycogen synthase kinase-3 beta mediates beta-amyloid induced neuritic damage in Alzheimer's disease. *Neurobiol Dis* **45**, 425-437 (2012).
377. P. H. Reddy, Amyloid beta-induced glycogen synthase kinase 3beta phosphorylated VDAC1 in Alzheimer's disease: implications for synaptic dysfunction and neuronal damage. *Biochim Biophys Acta* **1832**, 1913-1921 (2013).
378. B. A. Loving *et al.*, Lipoprotein Lipase Regulates Microglial Lipid Droplet Accumulation. *Cells* **10** (2021).
379. J. Marschallinger *et al.*, Lipid-droplet-accumulating microglia represent a dysfunctional and proinflammatory state in the aging brain. *Nat Neurosci* **23**, 194-208 (2020).
380. C. L. Holness, D. L. Simmons, Molecular cloning of CD68, a human macrophage marker related to lysosomal glycoproteins. *Blood* **81**, 1607-1613 (1993).
381. D. G. Walker, L. F. Lue, Immune phenotypes of microglia in human neurodegenerative disease: challenges to detecting microglial polarization in human brains. *Alzheimers Res Ther* **7**, 56 (2015).
382. E. Zotova *et al.*, Microglial alterations in human Alzheimer's disease following Abeta42 immunization. *Neuropathol Appl Neurobiol* **37**, 513-524 (2011).
383. R. A. Drummond, S. Saijo, Y. Iwakura, G. D. Brown, The role of Syk/CARD9 coupled C-type lectins in antifungal immunity. *Eur J Immunol* **41**, 276-281 (2011).
384. M. J. Plastini, H. L. Desu, R. Brambilla, Dynamic Responses of Microglia in Animal Models of Multiple Sclerosis. *Front Cell Neurosci* **14**, 269 (2020).

385. K. Takahashi, M. Prinz, M. Stagi, O. Chechneva, H. Neumann, TREM2-transduced myeloid precursors mediate nervous tissue debris clearance and facilitate recovery in an animal model of multiple sclerosis. *PLoS Med* **4**, e124 (2007).
386. J. G. Weinger *et al.*, Loss of the receptor tyrosine kinase Axl leads to enhanced inflammation in the CNS and delayed removal of myelin debris during experimental autoimmune encephalomyelitis. *J Neuroinflammation* **8**, 49 (2011).
387. F. Cignarella *et al.*, TREM2 activation on microglia promotes myelin debris clearance and remyelination in a model of multiple sclerosis. *Acta Neuropathol* **140**, 513-534 (2020).
388. C. S. Constantinescu, N. Farooqi, K. O'Brien, B. Gran, Experimental autoimmune encephalomyelitis (EAE) as a model for multiple sclerosis (MS). *Br J Pharmacol* **164**, 1079-1106 (2011).
389. R. F. Whittaker Hawkins *et al.*, ICAM1+ neutrophils promote chronic inflammation via ASPRV1 in B cell-dependent autoimmune encephalomyelitis. *JCI Insight* **2** (2017).
390. S. J. Batista *et al.*, Gasdermin-D-dependent IL-1alpha release from microglia promotes protective immunity during chronic *Toxoplasma gondii* infection. *Nat Commun* **11**, 3687 (2020).
391. T. Goldmann *et al.*, A new type of microglia gene targeting shows TAK1 to be pivotal in CNS autoimmune inflammation. *Nat Neurosci* **16**, 1618-1626 (2013).
392. J. Zhan *et al.*, The Cuprizone Model: Dos and Do Nots. *Cells* **9** (2020).
393. V. Gudi, S. Gingele, T. Skripuletz, M. Stangel, Glial response during cuprizone-induced de- and remyelination in the CNS: lessons learned. *Front Cell Neurosci* **8**, 73 (2014).
394. S. A. Back *et al.*, Hyaluronan accumulates in demyelinated lesions and inhibits oligodendrocyte progenitor maturation. *Nat Med* **11**, 966-972 (2005).
395. A. Podlesny-Drabiniok, E. Marcora, A. M. Goate, Microglial Phagocytosis: A Disease-Associated Process Emerging from Alzheimer's Disease Genetics. *Trends Neurosci* **43**, 965-979 (2020).
396. P. Yuan *et al.*, TREM2 Haplodeficiency in Mice and Humans Impairs the Microglia Barrier Function Leading to Decreased Amyloid Compaction and Severe Axonal Dystrophy. *Neuron* **90**, 724-739 (2016).
397. M. Gratuze *et al.*, Activated microglia mitigate Abeta-associated tau seeding and spreading. *J Exp Med* **218** (2021).
398. C. E. G. Leyns *et al.*, TREM2 function impedes tau seeding in neuritic plaques. *Nat Neurosci* **22**, 1217-1222 (2019).
399. C. E. G. Leyns *et al.*, TREM2 deficiency attenuates neuroinflammation and protects against neurodegeneration in a mouse model of tauopathy. *Proc Natl Acad Sci U S A* **114**, 11524-11529 (2017).
400. S. M. Kim *et al.*, TREM2 promotes Abeta phagocytosis by upregulating C/EBPalpha-dependent CD36 expression in microglia. *Sci Rep* **7**, 11118 (2017).
401. E. Gabande-Rodriguez, L. Keane, M. Capasso, Microglial phagocytosis in aging and Alzheimer's disease. *J Neurosci Res* **98**, 284-298 (2020).
402. S. E. Hickman, E. K. Allison, U. Coleman, N. D. Kingery-Gallagher, J. El Khoury, Heterozygous CX3CR1 Deficiency in Microglia Restores Neuronal beta-Amyloid Clearance Pathways and Slows Progression of Alzheimer's Like-Disease in PS1-APP Mice. *Front Immunol* **10**, 2780 (2019).
403. A. Malik *et al.*, SYK-CARD9 Signaling Axis Promotes Gut Fungi-Mediated Inflammasome Activation to Restrict Colitis and Colon Cancer. *Immunity* **49**, 515-530 e515 (2018).
404. S. Latour, M. Fournel, A. Veillette, Regulation of T-cell antigen receptor signalling by Syk tyrosine protein kinase. *Mol Cell Biol* **17**, 4434-4441 (1997).
405. R. J. Cornall, A. M. Cheng, T. Pawson, C. C. Goodnow, Role of Syk in B-cell development and antigen-receptor signaling. *Proc Natl Acad Sci U S A* **97**, 1713-1718 (2000).

406. Y. H. Chung, H. Y. Kim, B. R. Yoon, Y. J. Kang, W. W. Lee, Suppression of Syk activation by resveratrol inhibits MSU crystal-induced inflammation in human monocytes. *J Mol Med (Berl)* **97**, 369-383 (2019).
407. V. Serbulea *et al.*, Macrophages sensing oxidized DAMPs reprogram their metabolism to support redox homeostasis and inflammation through a TLR2-Syk-ceramide dependent mechanism. *Mol Metab* **7**, 23-34 (2018).
408. J. S. Ziegenfuss *et al.*, Draper-dependent glial phagocytic activity is mediated by Src and Syk family kinase signalling. *Nature* **453**, 935-939 (2008).
409. S. Ghosh, R. L. Geahlen, Stress Granules Modulate SYK to Cause Microglial Cell Dysfunction in Alzheimer's Disease. *EBioMedicine* **2**, 1785-1798 (2015).
410. X. C. Ye *et al.*, Dectin-1/Syk signaling triggers neuroinflammation after ischemic stroke in mice. *J Neuroinflammation* **17**, 17 (2020).
411. J. Rosenthal, Nilvadipine: profile of a new calcium antagonist. An overview. *J Cardiovasc Pharmacol* **24 Suppl 2**, S92-107 (1994).
412. R. N. Brogden, D. McTavish, Nilvadipine. A review of its pharmacodynamic and pharmacokinetic properties, therapeutic use in hypertension and potential in cerebrovascular disease and angina. *Drugs Aging* **6**, 150-171 (1995).
413. T. S. Anekonda, J. F. Quinn, Calcium channel blocking as a therapeutic strategy for Alzheimer's disease: the case for isradipine. *Biochim Biophys Acta* **1812**, 1584-1590 (2011).
414. S. V. Ramagopalan, R. Dobson, U. C. Meier, G. Giovannoni, Multiple sclerosis: risk factors, prodromes, and potential causal pathways. *Lancet Neurol* **9**, 727-739 (2010).
415. C. International Multiple Sclerosis Genetics *et al.*, Genetic risk and a primary role for cell-mediated immune mechanisms in multiple sclerosis. *Nature* **476**, 214-219 (2011).
416. C. Mc Guire *et al.*, Paracaspase MALT1 deficiency protects mice from autoimmune-mediated demyelination. *J Immunol* **190**, 2896-2903 (2013).
417. L. L. Molinero, A. Cubre, C. Mora-Solano, Y. Wang, M. L. Alegre, T cell receptor/CARMA1/NF-kappaB signaling controls T-helper (Th) 17 differentiation. *Proc Natl Acad Sci U S A* **109**, 18529-18534 (2012).
418. M. E. Deerhake *et al.*, Dectin-1 limits autoimmune neuroinflammation and promotes myeloid cell-astrocyte crosstalk via Card9-independent expression of Oncostatin M. *Immunity* **54**, 484-498 e488 (2021).
419. H. Yao *et al.*, Distinct Signaling Pathways Regulate TREM2 Phagocytic and NFkappaB Antagonistic Activities. *Front Cell Neurosci* **13**, 457 (2019).
420. J. Wissfeld *et al.*, Deletion of Alzheimer's disease-associated CD33 results in an inflammatory human microglia phenotype. *Glia* **69**, 1393-1412 (2021).
421. E. A. Clark, N. V. Giltiay, CD22: A Regulator of Innate and Adaptive B Cell Responses and Autoimmunity. *Front Immunol* **9**, 2235 (2018).
422. S. Hadas, M. Spira, U. K. Hanisch, F. Reichert, S. Rotshenker, Complement receptor-3 negatively regulates the phagocytosis of degenerated myelin through tyrosine kinase Syk and cofilin. *J Neuroinflammation* **9**, 166 (2012).
423. W. B. Stine, L. Jungbauer, C. Yu, M. J. LaDu, Preparing synthetic Abeta in different aggregation states. *Methods Mol Biol* **670**, 13-32 (2011).
424. G. T. Norris *et al.*, Neuronal integrity and complement control synaptic material clearance by microglia after CNS injury. *J Exp Med* **215**, 1789-1801 (2018).
425. M. A. DeTure, D. W. Dickson, The neuropathological diagnosis of Alzheimer's disease. *Mol Neurodegener* **14**, 32 (2019).
426. M. T. Heneka *et al.*, Neuroinflammation in Alzheimer's disease. *Lancet Neurol* **14**, 388-405 (2015).

427. H. Jahn, Memory loss in Alzheimer's disease. *Dialogues Clin Neurosci* **15**, 445-454 (2013).
428. D. Tejera, M. T. Heneka, Microglia in Neurodegenerative Disorders. *Methods Mol Biol* **2034**, 57-67 (2019).
429. D. V. Hansen, J. E. Hanson, M. Sheng, Microglia in Alzheimer's disease. *J Cell Biol* **217**, 459-472 (2018).
430. T. R. Jay *et al.*, Disease Progression-Dependent Effects of TREM2 Deficiency in a Mouse Model of Alzheimer's Disease. *J Neurosci* **37**, 637-647 (2017).
431. P. J. Cheng-Hathaway *et al.*, The Trem2 R47H variant confers loss-of-function-like phenotypes in Alzheimer's disease. *Mol Neurodegener* **13**, 29 (2018).
432. J. D. Ulrich, T. K. Ulland, M. Colonna, D. M. Holtzman, Elucidating the Role of TREM2 in Alzheimer's Disease. *Neuron* **94**, 237-248 (2017).
433. W. M. Song *et al.*, Humanized TREM2 mice reveal microglia-intrinsic and -extrinsic effects of R47H polymorphism. *J Exp Med* **215**, 745-760 (2018).
434. Y. Zhou, T. K. Ulland, M. Colonna, TREM2-Dependent Effects on Microglia in Alzheimer's Disease. *Front Aging Neurosci* **10**, 202 (2018).
435. X. Xiang *et al.*, The Trem2 R47H Alzheimer's risk variant impairs splicing and reduces Trem2 mRNA and protein in mice but not in humans. *Mol Neurodegener* **13**, 49 (2018).
436. C. B. Lessard *et al.*, High-affinity interactions and signal transduction between Abeta oligomers and TREM2. *EMBO Mol Med* **10** (2018).
437. E. C. Damisah, A. Rai, J. Grutzendler, TREM2: Modulator of Lipid Metabolism in Microglia. *Neuron* **105**, 759-761 (2020).
438. E. R. Roy *et al.*, Type I interferon response drives neuroinflammation and synapse loss in Alzheimer disease. *J Clin Invest* **130**, 1912-1930 (2020).
439. A. Benmamar-Badel, T. Owens, A. Wlodarczyk, Protective Microglial Subset in Development, Aging, and Disease: Lessons From Transcriptomic Studies. *Front Immunol* **11**, 430 (2020).
440. X. Zhong, B. Chen, L. Yang, Z. Yang, Molecular and physiological roles of the adaptor protein CARD9 in immunity. *Cell Death Dis* **9**, 52 (2018).
441. Y. Zhang *et al.*, An RNA-sequencing transcriptome and splicing database of glia, neurons, and vascular cells of the cerebral cortex. *J Neurosci* **34**, 11929-11947 (2014).
442. S. Forner *et al.*, Systematic phenotyping and characterization of the 5xFAD mouse model of Alzheimer's disease. *Sci Data* **8**, 270 (2021).
443. C. Yu, E. Nwabuisi-Heath, K. Laxton, M. J. Ladu, Endocytic pathways mediating oligomeric Abeta42 neurotoxicity. *Mol Neurodegener* **5**, 19 (2010).
444. M. E. Larson, S. E. Lesne, Soluble Abeta oligomer production and toxicity. *J Neurochem* **120 Suppl 1**, 125-139 (2012).
445. B. R. Roberts *et al.*, Biochemically-defined pools of amyloid-beta in sporadic Alzheimer's disease: correlation with amyloid PET. *Brain* **140**, 1486-1498 (2017).
446. Z. Cai, M. D. Hussain, L. J. Yan, Microglia, neuroinflammation, and beta-amyloid protein in Alzheimer's disease. *Int J Neurosci* **124**, 307-321 (2014).
447. N. J. Haughey *et al.*, Disruption of neurogenesis by amyloid beta-peptide, and perturbed neural progenitor cell homeostasis, in models of Alzheimer's disease. *J Neurochem* **83**, 1509-1524 (2002).
448. J. H. Jhoo *et al.*, Beta-amyloid (1-42)-induced learning and memory deficits in mice: involvement of oxidative burdens in the hippocampus and cerebral cortex. *Behav Brain Res* **155**, 185-196 (2004).
449. H. Kadowaki *et al.*, Amyloid beta induces neuronal cell death through ROS-mediated ASK1 activation. *Cell Death Differ* **12**, 19-24 (2005).

450. H. Oakley *et al.*, Intraneuronal beta-amyloid aggregates, neurodegeneration, and neuron loss in transgenic mice with five familial Alzheimer's disease mutations: potential factors in amyloid plaque formation. *J Neurosci* **26**, 10129-10140 (2006).
451. T. Bartsch, J. Dohring, A. Rohr, O. Jansen, G. Deuschl, CA1 neurons in the human hippocampus are critical for autobiographical memory, mental time travel, and autonoetic consciousness. *Proc Natl Acad Sci U S A* **108**, 17562-17567 (2011).
452. F. Ugolini *et al.*, Different Patterns of Neurodegeneration and Glia Activation in CA1 and CA3 Hippocampal Regions of TgCRND8 Mice. *Front Aging Neurosci* **10**, 372 (2018).
453. J. F. Reilly *et al.*, Amyloid deposition in the hippocampus and entorhinal cortex: quantitative analysis of a transgenic mouse model. *Proc Natl Acad Sci U S A* **100**, 4837-4842 (2003).
454. D. R. Thal *et al.*, Sequence of Abeta-protein deposition in the human medial temporal lobe. *J Neuropathol Exp Neurol* **59**, 733-748 (2000).
455. W. A. Eimer, R. Vassar, Neuron loss in the 5XFAD mouse model of Alzheimer's disease correlates with intraneuronal Abeta42 accumulation and Caspase-3 activation. *Mol Neurodegener* **8**, 2 (2013).
456. C. V. Vorhees, M. T. Williams, Morris water maze: procedures for assessing spatial and related forms of learning and memory. *Nat Protoc* **1**, 848-858 (2006).
457. J. Rogers, L. Churilov, A. J. Hannan, T. Renoir, Search strategy selection in the Morris water maze indicates allocentric map formation during learning that underpins spatial memory formation. *Neurobiol Learn Mem* **139**, 37-49 (2017).
458. M. W. Marlatt *et al.*, Proliferation in the Alzheimer hippocampus is due to microglia, not astroglia, and occurs at sites of amyloid deposition. *Neural Plast* **2014**, 693851 (2014).
459. C. Condello *et al.*, Structural heterogeneity and intersubject variability of Abeta in familial and sporadic Alzheimer's disease. *Proc Natl Acad Sci U S A* **115**, E782-E791 (2018).
460. W. Y. Wang, M. S. Tan, J. T. Yu, L. Tan, Role of pro-inflammatory cytokines released from microglia in Alzheimer's disease. *Ann Transl Med* **3**, 136 (2015).
461. E. S. N. M. Lyra *et al.*, Pro-inflammatory interleukin-6 signaling links cognitive impairments and peripheral metabolic alterations in Alzheimer's disease. *Transl Psychiatry* **11**, 251 (2021).
462. B. Parajuli *et al.*, Oligomeric amyloid beta induces IL-1beta processing via production of ROS: implication in Alzheimer's disease. *Cell Death Dis* **4**, e975 (2013).
463. J. Ojala *et al.*, Expression of interleukin-18 is increased in the brains of Alzheimer's disease patients. *Neurobiol Aging* **30**, 198-209 (2009).
464. H. Hara *et al.*, The adaptor protein CARD9 is essential for the activation of myeloid cells through ITAM-associated and Toll-like receptors. *Nat Immunol* **8**, 619-629 (2007).
465. L. Li, X. Zi, D. Hou, Q. Tu, Kruppel-like factor 4 regulates amyloid-beta (Abeta)-induced neuroinflammation in Alzheimer's disease. *Neurosci Lett* **643**, 131-137 (2017).
466. Z. Cheng *et al.*, The Role of KLF4 in Alzheimer's Disease. *Front Cell Neurosci* **12**, 325 (2018).
467. B. Kong *et al.*, microRNA-7 Protects Against 1-Methyl-4-Phenylpyridinium Iodide-Induced Cell Apoptosis in SH-SY5Y Cells by Directly Targeting Kruppel-Like Factor 4. *DNA Cell Biol* **35**, 217-225 (2016).
468. J. Chen *et al.*, Induction of KLF4 contributes to the neurotoxicity of MPP + in M17 cells: a new implication in Parkinson's disease. *J Mol Neurosci* **51**, 109-117 (2013).
469. J. Kwiatek-Majkusiak *et al.*, Relationships between typical histopathological hallmarks and the ferritin in the hippocampus from patients with Alzheimer's disease. *Acta Neurobiol Exp (Wars)* **75**, 391-398 (2015).
470. A. M. Koorts, M. Viljoen, Ferritin and ferritin isoforms I: Structure-function relationships, synthesis, degradation and secretion. *Arch Physiol Biochem* **113**, 30-54 (2007).

471. H. S. Goodridge *et al.*, Activation of the innate immune receptor Dectin-1 upon formation of a 'phagocytic synapse'. *Nature* **472**, 471-475 (2011).
472. H. S. Goodridge *et al.*, Differential use of CARD9 by dectin-1 in macrophages and dendritic cells. *J Immunol* **182**, 1146-1154 (2009).
473. C. Cruchaga *et al.*, GWAS of cerebrospinal fluid tau levels identifies risk variants for Alzheimer's disease. *Neuron* **78**, 256-268 (2013).
474. A. Inc., A Phase 2 Study to Evaluate Efficacy and Safety of AL002 in Participants With Early Alzheimer's Disease (INVOKE-2). (2020).
475. A. Inc., First in Human Study for Safety and Tolerability of AL003. (2020).
476. U. o. Oxford, Microglial Colony Stimulating Factor-1 Receptor (CSF1R) in Alzheimer's Disease (MICAD). (2019).
477. B. Kenkhuis *et al.*, Iron loading is a prominent feature of activated microglia in Alzheimer's disease patients. *Acta Neuropathol Commun* **9**, 27 (2021).
478. A. McIntosh *et al.*, Iron accumulation in microglia triggers a cascade of events that leads to altered metabolism and compromised function in APP/PS1 mice. *Brain Pathol* **29**, 606-621 (2019).
479. M. Colonna, All roads lead to CARD9. *Nat Immunol* **8**, 554-555 (2007).
480. R. B. Rock *et al.*, Role of microglia in central nervous system infections. *Clin Microbiol Rev* **17**, 942-964, table of contents (2004).
481. C. F. Hatton, C. J. A. Duncan, Microglia Are Essential to Protective Antiviral Immunity: Lessons From Mouse Models of Viral Encephalitis. *Front Immunol* **10**, 2656 (2019).
482. R. A. Drummond *et al.*, CARD9(+) microglia promote antifungal immunity via IL-1beta- and CXCL1-mediated neutrophil recruitment. *Nat Immunol* **20**, 559-570 (2019).
483. U. Puntener, S. G. Booth, V. H. Perry, J. L. Teeling, Long-term impact of systemic bacterial infection on the cerebral vasculature and microglia. *J Neuroinflammation* **9**, 146 (2012).
484. R. Alonso, D. Pisa, A. M. Fernandez-Fernandez, L. Carrasco, Infection of Fungi and Bacteria in Brain Tissue From Elderly Persons and Patients With Alzheimer's Disease. *Front Aging Neurosci* **10**, 159 (2018).
485. Y. Wu *et al.*, Microglia and amyloid precursor protein coordinate control of transient *Candida* cerebritis with memory deficits. *Nat Commun* **10**, 58 (2019).
486. P. W. de Groot, O. Bader, A. D. de Boer, M. Weig, N. Chauhan, Adhesins in human fungal pathogens: glue with plenty of stick. *Eukaryot Cell* **12**, 470-481 (2013).
487. N. Shanmugam *et al.*, Microbial functional amyloids serve diverse purposes for structure, adhesion and defence. *Biophys Rev* **11**, 287-302 (2019).
488. D. P. Wightman *et al.*, A genome-wide association study with 1,126,563 individuals identifies new risk loci for Alzheimer's disease. *Nat Genet* **53**, 1276-1282 (2021).
489. M. Chin-Chan, J. Navarro-Yepes, B. Quintanilla-Vega, Environmental pollutants as risk factors for neurodegenerative disorders: Alzheimer and Parkinson diseases. *Front Cell Neurosci* **9**, 124 (2015).
490. H. E. Ennerfelt, J. R. Lukens, The role of innate immunity in Alzheimer's disease. *Immunol Rev* **297**, 225-246 (2020).
491. J. E. Rexach *et al.*, Tau Pathology Drives Dementia Risk-Associated Gene Networks toward Chronic Inflammatory States and Immunosuppression. *Cell Rep* **33**, 108398 (2020).
492. E. Grajchen *et al.*, CD36-mediated uptake of myelin debris by macrophages and microglia reduces neuroinflammation. *J Neuroinflammation* **17**, 224 (2020).
493. J. Cady *et al.*, TREM2 variant p.R47H as a risk factor for sporadic amyotrophic lateral sclerosis. *JAMA Neurol* **71**, 449-453 (2014).

494. C. Pomilio *et al.*, Microglial autophagy is impaired by prolonged exposure to beta-amyloid peptides: evidence from experimental models and Alzheimer's disease patients. *Geroscience* **42**, 613-632 (2020).
495. S. Mandrekar-Colucci, G. E. Landreth, Microglia and inflammation in Alzheimer's disease. *CNS Neurol Disord Drug Targets* **9**, 156-167 (2010).
496. F. Leng, P. Edison, Neuroinflammation and microglial activation in Alzheimer disease: where do we go from here? *Nat Rev Neurol* **17**, 157-172 (2021).
497. G. Devi, P. Scheltens, Heterogeneity of Alzheimer's disease: consequence for drug trials? *Alzheimers Res Ther* **10**, 122 (2018).
498. H. M. Wu, A. M. Goate, P. F. O'Reilly, Heterogeneous effects of genetic risk for Alzheimer's disease on the phenome. *Transl Psychiatry* **11**, 406 (2021).
499. L. Passamonti *et al.*, Neuroinflammation and Functional Connectivity in Alzheimer's Disease: Interactive Influences on Cognitive Performance. *J Neurosci* **39**, 7218-7226 (2019).
500. V. H. Perry, C. Holmes, Microglial priming in neurodegenerative disease. *Nat Rev Neurol* **10**, 217-224 (2014).
501. M. T. Heneka, M. P. Kummer, E. Latz, Innate immune activation in neurodegenerative disease. *Nat Rev Immunol* **14**, 463-477 (2014).
502. E. E. Spangenberg, K. N. Green, Inflammation in Alzheimer's disease: Lessons learned from microglia-depletion models. *Brain Behav Immun* **61**, 1-11 (2017).
503. R. Zhao, W. Hu, J. Tsai, W. Li, W. B. Gan, Microglia limit the expansion of beta-amyloid plaques in a mouse model of Alzheimer's disease. *Mol Neurodegener* **12**, 47 (2017).
504. S. Kiani Shabestari *et al.*, Absence of microglia promotes diverse pathologies and early lethality in Alzheimer's disease mice. *Cell Rep* **39**, 110961 (2022).
505. T. Illouz *et al.*, Maternal antibodies facilitate Amyloid-beta clearance by activating Fc-receptor-Syk-mediated phagocytosis. *Commun Biol* **4**, 329 (2021).
506. S. Bachiller *et al.*, Microglia in Neurological Diseases: A Road Map to Brain-Disease Dependent-Inflammatory Response. *Front Cell Neurosci* **12**, 488 (2018).
507. A. M. Rodriguez, J. Rodriguez, G. H. Giambartolomei, Microglia at the Crossroads of Pathogen-Induced Neuroinflammation. *ASN Neuro* **14**, 17590914221104566 (2022).
508. X. M. Jia *et al.*, CARD9 mediates Dectin-1-induced ERK activation by linking Ras-GRF1 to H-Ras for antifungal immunity. *J Exp Med* **211**, 2307-2321 (2014).
509. S. K. Ryan, Microglia ferroptosis is prevalent in neurodegenerative disease and regulated by SEC24B. *Biorxiv* (2021).
510. X. Liu, B. Jiang, H. Hao, Z. Liu, CARD9 Signaling, Inflammation, and Diseases. *Front Immunol* **13**, 880879 (2022).
511. A. Pozner *et al.*, Intracellular calcium dynamics in cortical microglia responding to focal laser injury in the PC::G5-tdT reporter mouse. *Front Mol Neurosci* **8**, 12 (2015).
512. F. J. Sheedy *et al.*, CD36 coordinates NLRP3 inflammasome activation by facilitating intracellular nucleation of soluble ligands into particulate ligands in sterile inflammation. *Nat Immunol* **14**, 812-820 (2013).
513. A. M. Dobri, M. Dudau, A. M. Enciu, M. E. Hinescu, CD36 in Alzheimer's Disease: An Overview of Molecular Mechanisms and Therapeutic Targeting. *Neuroscience* **453**, 301-311 (2021).
514. I. S. Coraci *et al.*, CD36, a class B scavenger receptor, is expressed on microglia in Alzheimer's disease brains and can mediate production of reactive oxygen species in response to beta-amyloid fibrils. *Am J Pathol* **160**, 101-112 (2002).
515. S. Xu *et al.*, Uptake of oxidized lipids by the scavenger receptor CD36 promotes lipid peroxidation and dysfunction in CD8(+) T cells in tumors. *Immunity* **54**, 1561-1577 e1567 (2021).

516. Y. M. Park, M. Febbraio, R. L. Silverstein, CD36 modulates migration of mouse and human macrophages in response to oxidized LDL and may contribute to macrophage trapping in the arterial intima. *J Clin Invest* **119**, 136-145 (2009).
517. M. E. Deerhake, M. L. Shinohara, Emerging roles of Dectin-1 in noninfectious settings and in the CNS. *Trends Immunol* **42**, 891-903 (2021).
518. O. Gross *et al.*, Card9 controls a non-TLR signalling pathway for innate anti-fungal immunity. *Nature* **442**, 651-656 (2006).
519. A. M. Jurga, M. Paleczna, K. Z. Kuter, Overview of General and Discriminating Markers of Differential Microglia Phenotypes. *Front Cell Neurosci* **14**, 198 (2020).
520. I. Visan, Alzheimer's disease microglia. *Nat Immunol* **18**, 876 (2017).
521. A. Cianciulli *et al.*, Microglia Mediated Neuroinflammation: Focus on PI3K Modulation. *Biomolecules* **10** (2020).
522. J. Benetatos *et al.*, PTEN activation contributes to neuronal and synaptic engulfment by microglia in tauopathy. *Acta Neuropathol* **140**, 7-24 (2020).
523. A. Verkhratsky, M. Olabarria, H. N. Noristani, C. Y. Yeh, J. J. Rodriguez, Astrocytes in Alzheimer's disease. *Neurotherapeutics* **7**, 399-412 (2010).
524. N. Habib *et al.*, Disease-associated astrocytes in Alzheimer's disease and aging. *Nat Neurosci* **23**, 701-706 (2020).
525. R. E. Gonzalez-Reyes, M. O. Nava-Mesa, K. Vargas-Sanchez, D. Ariza-Salamanca, L. Mora-Munoz, Involvement of Astrocytes in Alzheimer's Disease from a Neuroinflammatory and Oxidative Stress Perspective. *Front Mol Neurosci* **10**, 427 (2017).
526. I. Chacon-De-La-Rocha *et al.*, Accelerated Dystrophy and Decay of Oligodendrocyte Precursor Cells in the APP/PS1 Model of Alzheimer's-Like Pathology. *Front Cell Neurosci* **14**, 575082 (2020).
527. I. Vanzulli *et al.*, Disruption of oligodendrocyte progenitor cells is an early sign of pathology in the triple transgenic mouse model of Alzheimer's disease. *Neurobiol Aging* **94**, 130-139 (2020).
528. S. Poyhonen, S. Er, A. Domanskyi, M. Airavaara, Effects of Neurotrophic Factors in Glial Cells in the Central Nervous System: Expression and Properties in Neurodegeneration and Injury. *Front Physiol* **10**, 486 (2019).
529. A. Matejuk, R. M. Ransohoff, Crosstalk Between Astrocytes and Microglia: An Overview. *Front Immunol* **11**, 1416 (2020).
530. S. T. T. Schettters, D. Gomez-Nicola, J. J. Garcia-Vallejo, Y. Van Kooyk, Neuroinflammation: Microglia and T Cells Get Ready to Tango. *Front Immunol* **8**, 1905 (2017).
531. J. M. Fletcher, S. J. Lalor, C. M. Sweeney, N. Tubridy, K. H. Mills, T cells in multiple sclerosis and experimental autoimmune encephalomyelitis. *Clin Exp Immunol* **162**, 1-11 (2010).
532. E. G. Baxi *et al.*, Lineage tracing reveals dynamic changes in oligodendrocyte precursor cells following cuprizone-induced demyelination. *Glia* **65**, 2087-2098 (2017).
533. A. Yazdi, H. Baharvand, M. Javan, Enhanced remyelination following lysolecithin-induced demyelination in mice under treatment with fingolimod (FTY720). *Neuroscience* **311**, 34-44 (2015).
534. E. S. Leshchiner *et al.*, Small-molecule inhibitors directly target CARD9 and mimic its protective variant in inflammatory bowel disease. *Proc Natl Acad Sci U S A* **114**, 11392-11397 (2017).
535. F. Yu *et al.*, Kruppel-like factor 4 (KLF4) is required for maintenance of breast cancer stem cells and for cell migration and invasion. *Oncogene* **30**, 2161-2172 (2011).